THÈSE POUR OBTENIR LE GRADE DE DOCTEUR
DE L'UNIVERSITÉ DE MONTPELLIER

En Biologie des Interactions Symbiotiques et Parasitaires

École doctorale GAIA

Unité de recherche MIVEGEC, Université de Montpellier, IRD, CNRS, Montpellier, France

Titre de la thèse

THE *ANOPHELES* MOSQUITO BRAIN AT SPATIAL AND SINGLE CELL RESOLUTION

Présentée par Irene ROSSI
Le 19 décembre 2025

Sous la direction de Anna COHUET et Arthur TALMAN

Devant le jury composé de

M. Jean-Maurice DURA, Directeur de recherche, IGH, Montpellier	Président du jury
M. Nicolas BLANCHARD, Directeur de recherche, INSERM, INFINITy, Toulouse	Rapporteur
Mme Anna COHUET, Directrice de recherche, IRD, MIVEGEC, Montpellier	Directrice de thèse
Mme Elena LEVASHINA, Professeur, MPIIB, Berlin	Rapporteure

UNIVERSITÉ DE MONTPELLIER

Index

Acknowledgements 3
Résumé détaillé 5
Abstract 14
Résumé 14
Introduction 16
The nervous system of insects 16
Neuroanatomical synopsis 16
The brain of mosquitoes 22
Example of signal integration in mosquito neural system: integration of olfactive stimuli 23
Bridging mosquito brain anatomy to function 27
Mosquito life cycle and malaria transmission biology 28
Mosquito life stages and their influence on disease transmission 29
The life cycle of *Plasmodium* 32
Mosquito-parasite interactions 33
The parasitic manipulation hypothesis 35
Behavioral transcriptomics 42
Connections between transcripts and behavioral phenotypes 43
Advantages and challenges of behavioral transcriptomics 48
NGS for transcriptomics 49
Bulk RNA-seq 52
ScRNA-seq and snRNA-seq 54
Project rationale: insight into the female *An. gambiae* brain structure, composition and function 57
Chapter 1: Optimizing methods to prove mechanisms supporting insect behavior 61
Biological material used in the project 63
An. gambiae mosquitoes 63
P. falciparum cell culture 63
G. m. morsitans flies 63
T. b. brucei cell culture 63
The dissection of a mosquito brain 64
Brain dissection technique 64
Pilot study to scale up snRNA-seq in insects to 1 million nuclei 67
Methods for snRNA-seq 68
Experimental results: attempted small scale snRNA-seq dataset 71
An. gambiae brain scRNA–seq: from pilot data to a 50K cell atlas 76
Methods for scRNA-seq data collection and analysis 76
Pilot scRNA-seq dataset for the female *An. gambiae* brain 76
Preparation of single cell suspensions and sequencing 77
Methods for scRNA-seq preliminary data analysis and tentative homology-based cellular annotation 79

Scaled-up scRNA-seq dataset for the female *An. gambiae* brain_____81
Tentative scRNA-seq on female *An. gambiae* brain after *P. falciparum* infection_____ 82
Experimental infections_____ 82
Experimental results: from pilot data to a 50K cell atlas_____83
Single brain bulk RNA-seq in *An. gambiae* and *G. morsitans*_____ 92
Methods for bulk RNA-seq_____92
Preliminary trials for bulk RNA-seq methods on Tsetse fly_____ 93
Preliminary trials for scRNA-seq methods on Tsetse fly_____ 94
Tsetse fly infection experiments_____95
Experimental results: influence of life cycle and *P. falciparum* infection on the female *An. gambiae* brain_____95
Experimental results: Tsetse fly infections_____ 96
Does a significant cell proliferation happen in the adult *An. gambiae* brain? A click-chemistry approach_____ 101
Methods for cell proliferation assays_____ 101
Experimental results: blood meal does not seem to induce cell proliferation in the *An. gambiae* brain_____ 103
RNAi for behavioral studies_____ 106
Methods for setting up RNAi assays_____ 108
Validation of RNAi methods and targets_____ 111
Optimisation of histological procedures supporting spatial transcriptomics and ISH _____114
Methods for experiments preliminary to ISH_____ 114
Mosquito heads microsectioning_____ 114
House keeping genes (HKGs) identification_____115
Experimental results: optimization of mosquito heads microsectioning____ 116
Chapter 2: The *An. gambiae* brain at spatial and single cell resolution_____119
Submitted manuscript_____ 119
Additional results and discussion_____187
Examples of DEA from single cell data_____ 187
Gaining functional insights in bulk RNA-seq results with scRNA-seq_____ 189
Absence of transcriptional manipulation signatures in the mosquito brain__ 194
Conclusions_____ 195
Bibliography_____202

Acknowledgements

At the end of my PhD journey, I ponder how grateful I am to the people I have met and worked with in the four years of my thesis. They have guided, assisted, advised, and inspired me.

First and foremost, I want to express my heartfelt gratitude to my thesis supervisors, Anna Cohuet and Arthur Talman, for their scientific teaching, for their help and guidance in project management, and for supporting the development of my professional and soft skills. They have advised me across all the research and organization choices we had to make, and I am greatly thankful for their insightful direction. I would also like to thank their research groups and the ESV - TRIAD unit for all the support and scientific exchange. I am grateful to David Carrasco, who showed me how to dissect mosquito brains, for his teaching and help in the project. I thank Cécile Cassan for both directing and helping me at the bench. Also, I am grateful to both Cécile and Johannes Bagnoli for obtaining and analysing data in Montpellier while I was working in Paris. I thank Adeline Valente for the help she has given and is giving in carrying on experiments and advancing the project associated with my thesis. Furthermore, all the bioinformatic analyses I had performed were possible thanks to the advice and help of Quentin Delorme and Johannes, whom I thank for being patient teachers. I am grateful to the MIVEGEC Vectopole facility and to Carole Ginibre for taking care of the insectary and helping in mosquito rearing. I thank Emmanuel Perisse for sharing his knowledge on insect brains.

I want to thank Brice Rotureau, Teun Bousema, Sarah Merkling, and their research groups for hosting me at the Pasteur Institute in Paris and at the Radboudumc in the Netherlands. I am grateful to Brice, Teun, Sarah, Jean-Marc Tsagmo Ngoune, Natalie Petiot, Parul Sharma, Geert-Jan Van Geemert, Chiara Andolina, Wouter Graumans, Richard Bartfai and his group, Sümeyye Özhan, Sarra Loulizi, and Audrey Salles for their help, teaching, and for the scientific exchange we had.

I thank my colleague, mentor and friend Alejandro Marin-Menendez, for all the professional and personal advice and support he has given me, and for involving me and other young colleagues in scientific dissemination projects. I would also like to thank the mentoring program of Femmes et Science, and Anna-Sophie Fiston Lavier for her wise and practical mentoring. In the same way, I am grateful to the members of my CSI, Bernard Duvic, Thierry Lefévre, Sarah Merkling, Emmanuel Perisse, Brice Rotureau and Isabelle Morlais for helping me move through my PhD years both scientifically and personally.

I want to thank the LabEx ParaFrap network, Yvon Sterkers and Patrick Bastien for coordinating the yearly courses and team building activities for us ParaFrap PhD students.

I want to thank my host institution, the IRD - MIVEGEC, and the founding agencies ParaFrap - CNRS, RIVOC, and FRM, for hosting me, providing means and facilities, and funding my experiments and salary.

I thank my friends in Italy and France and the ParaFrap students for always being there, inspiring me and putting me back together even without knowing it. I am happy to have met my colleagues and friends Quentin, Margaux, Ella, Théo, Audric, Noor, Colombine, Silvère, and the others, and value all the moments of fun and exchange we shared.

Most of all, I thank Enrico, who holds my hand and walks with me so gently and fondly. Ringrazio i miei genitori e la mia famiglia, che mi mancano moltissimo e che hanno lasciato che andassi per la mia strada tanti anni fa, quando ne avevo bisogno. Ringrazio i miei nonni per il loro sostegno, sempre.

Résumé détaillé

Contexte

Les insectes constituent la classe la plus diversifiée du règne animal, s'adaptant à une multitude d'environnements grâce à une évolution marquée par une grande diversité morpho-comportementale. Leur succès écologique repose en l'occurrence sur la diversification de leur système nerveux central (SNC) qui contrôle des fonctions cognitives, sensorielles et motrices vitales pour leur survie et leur reproduction dans des environnements variés.

Le SNC des insectes est organisé autour d'un cerveau et d'une chaîne nerveuse ventrale reliant et coordonnant les différentes fonctions corporelles. Le cerveau se divise principalement en trois grandes régions : le protocérébron, le deutocérébron et le tritocérébron. Le protocérébron occupe la partie antérieure du cerveau et intègre des fonctions complexes comme la vision, la mémoire et la plupart des comportements cognitifs avancés. Le deutocérébron, situé derrière le protocérébron, reçoit principalement les informations provenant des organes sensoriels olfactifs, en particulier les antennes. Ces informations olfactives sont souvent fondamentales pour la navigation, la recherche d'hôtes, la détection d'aliments ou encore la reconnaissance de partenaires sexuels. Situé de manière centrale, le tritocérébron joue quant à lui un rôle dans la coordination sensorimotrice, en assurant une interface entre le cerveau et les ganglions moteurs, contrôlant les réponses musculaires réflexes et coordonnées.

Chez les moustiques, la famille des Culicidae, certaines espèces ont des impacts majeurs en terme de santé humaine, notamment *Anopheles gambiae*, le principal vecteur du paludisme humain, une maladie parasitaire majeure à l'échelle mondiale. L'organisation cérébrale des moustiques comprend les grandes structures décrites pour les insectes, mais aussi des spécialisations apparentes, comme un développement accentué des centres olfactifs et visuels, probablement en lien avec les fonctions essentielles nécessaires au cours de leur cycle de vie. En effet, les moustiques ont un cycle de vie complexe, comprenant des stades larvaires aquatiques puis une phase adulte terrestre, au

cours desquels le SNC doit orchestrer avec finesse une palette de comportements spécifiques. Les comportements au stade adulte incluent par exemple pour les femelles la recherche du partenaire sexuel pour l'accouplement, le choix d'hôtes pour les repas sanguins ou la recherche de sites de ponte. Ils impliquent une évaluation sensorielle fine initiée par la détection d'indices environnementaux. Le cerveau intègre donc une masse considérable d'informations multi sensorielles (olfactives, visuelles, thermiques) afin de moduler la prise de décision comportementale en fonction du contexte, qu'il soit physiologique ou environnemental. Cette capacité d'intégration pourrait être le résultat de plasticité neuronale, la capacité du cerveau à s'adapter aux changements externes mais aussi internes, comme les variations hormonales post-accouplement, la prise d'un repas de sang ou le statut d'infection. Ainsi, la structure du cerveau des moustiques vecteurs reflète une adaptation spécifique pour le déroulement de cycles de vie étroitement liés à la transmission des maladies, faisant de l'étude de son organisation neuroanatomique et moléculaire un intérêt scientifique et médical. La connaissance fine des circuits neuronaux et de leurs changements dynamiques dans le cerveau des moustiques vecteurs est aujourd'hui un enjeu en vue de développer des stratégies de lutte ciblée et limiter la propagation du paludisme.

Dans ce contexte, les avancées technologiques dans les neurosciences sont primordiales pour décrypter les mécanismes neuronaux sous-jacents aux comportements des moustiques vecteurs.

Sur le plan cellulaire, le cerveau des moustiques est constitué de divers types cellulaires, notamment neuronaux et gliaux. Les neurones comprennent des populations spécialisées dans la transmission rapide des signaux sensoriels, la modulation de l'activité neuronale et l'intégration des informations complexes. Les cellules gliales sont connues pour leur rôle essentiel dans la protection cérébrale - formant une barrière hémato-encéphalique fonctionnelle - ainsi que dans le métabolisme neuronal et la réponse immunitaire.

L'étude approfondie des structures cérébrales chez les moustiques vecteurs, notamment au moyen de techniques de "next-generation sequencing", telles que

la transcriptomique en cellule unique (scRNA-seq), devrait permettre d'associer l'architecture cérébrale à des profils d'expression génique associés à des conditions spécifiques, produisant une carte détaillée permettant d'éclairer la relation entre anatomie, fonction et comportement.

La transcriptomique en cellule unique permet de définir des profils d'expression et d'identifier des types cellulaires individuels. Elle peut ainsi révéler la complexité et l'hétérogénéité des populations cellulaires, y compris chez les neurones et les cellules gliales du cerveau, précisant les circuits génétiques sous-jacents aux comportements.

Chez les insectes, des modèles bien connus, comme la mouche drosophile *Drosophila melanogaster*, ont bénéficié d'analyses transcriptomiques détaillées, illustrant une diversité cellulaire considérable, notamment au sein des corps pédonculés, centres majeurs d'intégration sensorielle et mémorielle. Ces études ont identifié des sous-types neuronaux spécialisés avec des signatures transcriptionnelles distinctes, associées à des fonctions cognitives comme l'apprentissage, la mémoire et le traitement sensoriel. L'application de la transcriptomique aux insectes vecteurs, notamment les moustiques, en est encore à ses débuts. Jusqu'à récemment, les études transcriptomiques dans ces espèces ciblaient majoritairement la tête entière ou des organes sensoriels isolés, fournissant des données aux niveau de l'organe, certes utiles, mais ne permettant pas la dissociation fine des types cellulaires cérébraux. Le développement d'outils dédiés pour la dissociation cellulaire du cerveau, le séquençage via les plateformes comme 10x Genomics et Smart-seq2, ainsi que les pipelines bioinformatiques avancés, a permis de franchir une étape essentielle vers la cartographie unicellulaire. Les possibilités offertes par la transcriptomique en cellule unique incluent la classification précise des populations neuronales et gliales, la caractérisation des réseaux de régulation génétique, ainsi que l'identification des signatures moléculaires propres aux différentes populations cellulaires. Ces avancées devraient aider à l'identification de gènes qui modulent la plasticité neuronale, la perception sensorielle et la modulation comportementale.

Une autre percée technologique majeure dans la caractérisation de populations cellulaires est représentée par la transcriptomique spatiale, une technologie complémentaire à la transcriptomique en cellule unique qui combine la lecture de l'expression génique à l'échelle tissulaire avec une résolution spatiale fine (de l'ordre du micromètre). En neurobiologie, cette approche permet de localiser précisément dans le cerveau les types cellulaires identifiés en scRNA-seq, fournissant ainsi un contexte anatomique indispensable pour comprendre la fonction des réseaux neuronaux et leurs implications comportementales.

Dans ce contexte, la transcriptomique en cellule unique combinée à la transcriptomique spatiale représente aujourd'hui un levier majeur pour transformer la compréhension neuroscientifique du cerveau des insectes vecteurs. Elle ouvre la perspective de nouveaux modèles intégrant la diversité cellulaire, la dynamique génique et l'organisation anatomique permettant de décrypter la complexité des comportements vecteurs aux regards des variations moléculaires et cellulaires.

Objectifs

L'objectif de ce projet était d'accroître les connaissances sur la biologie moléculaire du cerveau d'A*n. gambiae*, en initiant l'identification de types cellulaires et de leurs marqueurs, en obtenant des informations sur les changements transcriptionnels à différents stades du cycle de vie du moustique, ainsi que la description de la distribution spatiale des transcrits dans le cerveau du moustique. Le développement d'un atlas cérébral détaillé d'A*n. gambiae* repose sur l'intégration de méthodes de pointe en biologie moléculaire, imagerie et bioinformatique. La mise en œuvre de ces méthodes, nouvelles chez A*n. gambiae* exige des mises au point minutieuses pour une dissociation des tissus, une capture précise des ARN messagers, et un traitement analytique adapté pour reconstituer la diversité cellulaire et leur localisation anatomique. Ainsi par l'adaptation et l'utilisation de technologies de pointe dans un système biologique non modèle, ce travail de thèse initie une compréhension fine des populations cellulaires, de leur organisation spatiale dans le cerveau de ce moustique

vecteur et de leur rôle dans l'intégration des signaux physiologiques et environnementaux et l'élaboration des réponses.

Principaux résultats

La première étape cruciale a consisté à extraire les cerveaux de femelles du moustique à différents stades physiologiques, notamment vierge, après accouplement, et après repas sanguin. Ces conditions ont permis d'observer les variations transcriptomiques liées au cycle de vie et à la physiologie du vecteur. Les cerveaux ont été dissociés en cellules individuelles par des protocoles optimisés qui préservent la viabilité et l'intégrité des ARN. Cette dissociation inclut des traitements enzymatiques doux et des manipulations mécaniques minutieuses adaptées à la fragilité des tissus insectes. Pour l'analyse scRNA-seq, la technologie 10x Genomics a été employée. Cette méthode repose sur la capture des cellules uniques, chacune associée à des codes-barres uniques pour individualiser leur transcriptome. Ceci garantit un séquençage multiplexé et à haute résolution, permettant d'identifier des milliers de gènes exprimés et de distinguer des types cellulaires et états spécifiques. La technologie Smart-seq2 est également utilisée pour le séquençage en "bulk", permettant de vérifier et compléter les données en cellule unique au niveau de l'organe.

Parallèlement, des expériences d'infection par le parasite *P. falciparum* ont été menées pour comparer l'expression génique cérébrale chez des moustiques infectés *versus* contrôles non infectés, dans le but d'identifier des signatures transcriptionnelles associées à l'état infectieux ou à la réponse immunitaire cérébrale.

Une fois les données brutes obtenues, elles ont été traitées via des pipelines bioinformatiques robustes. L'annotation des types cellulaires s'est appuyée sur des bases de données existantes, notamment les atlas cellulaires de *D. melanogaster*, via des méthodes d'alignement inter-espèces comme SAMap. Ce processus permet d'attribuer à chaque groupe cellulaire une identité fonctionnelle basée sur l'expression de marqueurs connus, permettant par exemple d'identifier les neurones des corps pédonculés, les lobes optiques, les cellules gliales, ou les populations immunitaires. Aussi, la transcriptomique

spatiale a permis, à partir de coupes histologiques de la tête et du cerveau, de déterminer la position anatomique de groupes cellulaires identifiés par transcriptomique en cellule unique. L'intégration de ces deux types de données offre une cartographie tridimensionnelle précise de l'organisation cérébrale, révélant la distribution anatomique des neurones spécialisés, des couches gliales, des foyers neuronaux circadiens, ainsi que des structures sensorielles et motrices.
La validation expérimentale de cette cartographie du cerveau de moustique a été réalisée par hybridation *in situ* (ISH) ciblée sur les gènes marqueurs, confirmant la localisation spécifique des populations cellulaires et délimitant précisément les régions cérébrales fonctionnelles. Cette démarche expérimentale rigoureuse a permis de garantir la fiabilité des annotations et la contextualisation anatomique des profils transcriptomiques.

L'étude approfondie du transcriptome cérébral de l'A*n. gambiae* a ainsi permis de cataloguer avec une précision sans précédent la diversité cellulaire et fonctionnelle de son cerveau. L'analyse du cerveau de près de 49 000 cellules issues de différentes conditions physiologiques a montré une organisation structurée, avec une quarantaine de clusters neuronaux représentant diverses populations spécialisées. Parmi celles-ci figurent notamment les neurones du corps pédonculé impliqués dans la mémoire et l'apprentissage, les neurones circadiens régulant les rythmes biologiques, des groupes neuronaux des lobes optiques spécialisés dans le traitement visuel, ainsi que plusieurs types de cellules gliales assurant soutien métabolique et protection immunitaire.

L'intégration des données de transcriptomique spatiale a révélé la localisation anatomique précise de ces populations cellulaires dans diverses régions cérébrales, telles que le cortex neuronal, les lobes optiques ou encore les couches gliales. Cette cartographie tridimensionnelle détaillée, confirmée par des ISH, permet désormais de relier les profils transcriptionnels à leur contexte fonctionnel et organisationnel. Les observations ont aussi mis en avant des signatures spécifiques à *An. gambiae*, révélant des neurones et des cellules

gliales probablement associés à des fonctions uniques à ce vecteur de paludisme.

L'analyse comparative des transcriptomes à différents états physiologiques qui peut être effectuée à partir de nos données montre qu'après l'accouplement, les modifications transcriptionnelles sont relativement restreintes mais certains gènes subissent des changements transcriptionnels majeurs. C'est par exemple le cas d'un récepteur de la sérotonine (5HT-1aR), fortement surexprimé après l'accouplement. Ce gène est connu pour un rôle similaire chez des organismes modèles et une étude fonctionnelle plus poussée chez *An. gambiae* devrait déterminer ses modes d'actions.

La comparaison des transcriptomes selon la prise d'un repas sanguin montre que le cerveau manifeste, suite à l'ingestion, une réorganisation globale de l'expression des gènes, notamment une réduction de l'expression des gènes de la machinerie translationnelle et des modifications dans les voies métaboliques, traduisant la phase de repos post-prandial. De plus, réponses transcriptionnelles dans différents types cellulaires, en particulier dans les neurones impliqués dans la mémoire, la signalisation et le remodelage chromatinien, ainsi que dans les cellules gliales à fonctions immunitaires et métaboliques, suggèrent une plasticité adaptative importante liée à cette étape du cycle biologique.

Il est notable que malgré l'infection par *P. falciparum*, les transcriptomes cérébraux des moustiques infectés par *P. falciparum* n'ont pas révélé de changements transcriptionnels majeurs comparés aux moustiques non infectés. Cette absence de régulation visible soulève des questions sur les mécanismes d'interaction entre le parasite et le système nerveux de l'hôte, et sur les mécanismes d'éventuelle manipulation parasitaire. Ceux ci pourraient s'opérer par d'autres voies moléculaires ou cellulaires non détectées par ces analyses, suggérant des modes d'action éventuellement non transcriptionnels, comme des altérations protéomiques, épigénétiques, ou des modifications neuronales plus subtiles non détectables à ce stade. Il est également possible que le phénomène de manipulation parasitaire n'ait pas lieu concernant les souches de moustiques

et parasites utilisés dans cette étude ou qu'ils ne soient pas exprimés dans les conditions de nos laboratoires. De manière intéressante, l'analyse des transcriptomes au cours du développement des parasites dans le moustique a mis en évidence non pas des effets de l'infection mais de l'âge du moustiques, identifiant des signatures transcriptionnelles caractéristiques des moustiques âgés. Sachant que l'espérance de vie d'une population anophélienne est un paramètre majeur dans sa capacité vectorielle pour transmettre les parasites responsables du paludisme, ces signatures transcriptionnelles devront être exploitées pour identifier de potentiels marqueurs de l'âge des individus femelles en vue d'utilisation sur le terrain.

Ainsi l"analyse comparative des transcriptomes entre les cerveaux de moustiques femelles vierges, accouplées, ayant réalisé un repas sanguin et d'âges divers, a montré des changements transcriptionnels importants et spécifiques à certains types cellulaires. Ces modifications correspondent à des régulations de gènes liés à la mémoire, la signalisation neuronale, la modification de la chromatine, ainsi qu'à des ajustements métaboliques chez les neurones. Les cellules gliales montrent notamment des modulations liées à la réponse immunitaire et au métabolisme.

Discussion et perspectives

La discussion de ces résultats met en lumière la complexité des réseaux cellulaires cérébraux des moustiques et leur plasticité en fonction des états biologiques. L'absence de signatures marquées d'infection peut indiquer une forme d'équilibre évolutif entre parasite et vecteur, limitant les coûts neurologiques au bénéfice de la transmission efficace. Par ailleurs, les mosaïques cellulaires identifiées permettent d'envisager des études fonctionnelles ciblées, telles que le knockdown génique, le marquage in vivo, ou l'imagerie calcique, pour décrypter plus finement les circuits neuronaux impliqués dans la modulation des comportements vecteurs.

Les ressources produites par ce projet, notamment la première atlas unicellulaire et spatial détaillé du cerveau d'A*n. gambiae*, sont mises à

disposition de la communauté scientifique. Elles constituent une base de données précieuse pour les chercheurs en neurobiologie, entomologie, et lutte contre le paludisme. Le partage des données brutes, annotées, ainsi que des codes d'analyse et des visualisations offre une plateforme pour accélérer la compréhension des mécanismes neuronaux vecteurs et le développement de stratégies innovantes de contrôle.

Ce travail pionnier apporte une cartographie annotée et exhaustive de la diversité cellulaire cérébrale d'un moustique majeur vecteur de maladie, enrichissant la compréhension fondamentale de la biologie et ouvrant la voie à des approches ciblées pour réduire la transmission du paludisme. Il souligne aussi les défis persistants liés à la détection des interactions parasite-hôte au niveau neuronal et incite à poursuivre les investigations pluridisciplinaires. Dans le futur, des approches expérimentales combinant observation comportementale, imagerie cérébrale et transcriptomique à l'échelle cellulaire devraient permettre de relier les comportements vecteurs aux signatures moléculaires dans le cerveau. La compréhension des mécanismes neurobiologiques et moléculaires responsables de ces interactions devrait ouvrir la voie à une compréhension approfondie du cycle de transmission et à une neurobiologie appliquée au contrôle des maladies vectorielles, enjeu crucial de santé publique mondiale. De manière pragmatique, ces connaissances pourraient être exploitées pour concevoir de nouvelles stratégies de lutte, telles que l'ingénierie génétique des moustiques pour réduire leur capacité à chercher un hôte ou à transmettre *Plasmodium*.

Ainsi, l'infrastructure technique et analytique développée pour cet atlas cérébral d'A*n. gambiae* offre une ressource inédite d'une grande richesse pour la recherche fondamentale en neurobiologie, mais également en perspective d'approches appliquées visant à interférer avec les comportements vecteurs et ainsi réduire la transmission du paludisme.

Abstract

Blood-feeding in *Anopheles* mosquitoes underpins all malaria transmission and relies on a suite of physiological and behavioural adaptations. Yet, the cellular and molecular bases of mosquito behaviour remain largely unexplored. Because behaviour is orchestrated by the central nervous system, we profiled the cellular diversity of the female *Anopheles gambiae* brain. We confirmed tissue localization of some putative markers and applied spatially resolved transcriptomics to reveal how this diversity is organised within the mosquito head. Furthermore, we characterised transcriptional changes linked to key life history events, including mating, blood feeding, *Plasmodium falciparum* infection, and ageing. Beyond representing a major advance in our understanding of the molecular composition and functions of the *An. gambiae* brain, our results also yielded lists of genes putatively involved in disease transmission-related behaviors that are currently under investigation by the means of RNA interference and associated behavioral records. Together, these efforts yield the first comprehensive atlas of the malaria mosquito brain, establishing a foundational resource for investigating non-model insect neurobiology, the neural basis of vector behaviour, and the mechanisms driving malaria transmission.

Résumé

La prise de repas de sang des femelles moustiques *Anopheles* est à la base de toute transmission du paludisme humain et repose sur une série d'adaptations physiologiques et comportementales. Cependant, les bases cellulaires et moléculaires du comportement des moustiques restent largement inexplorées. Le comportement étant orchestré par le système nerveux central, nous avons dressé le profil de la diversité cellulaire du cerveau des moustiques *Anopheles gambiae* femelles. Nous avons confirmé la localisation tissulaire de certains gènes identifiés comme marqueurs de types cellulaires et avons appliqué la

transcriptomique à résolution spatiale pour révéler comment cette diversité est organisée dans la tête du moustique. De plus, nous avons caractérisé les changements transcriptionnels liés à des événements clés du cycle de vie du moustique, notamment l'accouplement, l'alimentation sanguine, l'infection par *Plasmodium falciparum* et le vieillissement. Au-delà d'une avancée majeure dans notre compréhension de la composition moléculaire et des fonctions du cerveau d'*An. gambiae*, nos résultats ont également permis d'établir des listes de gènes présumés impliqués dans les comportements liés à la transmission de maladies, qui font actuellement l'objet d'études par ARN interférence et d'enregistrements comportementaux associés. Ensemble, ces efforts ont abouti au premier atlas complet du cerveau du moustique vecteur du paludisme, établissant une ressource fondamentale pour l'étude de la neurobiologie des insectes non modèles, des bases neuronales du comportement des vecteurs et des mécanismes à l'origine de la transmission du paludisme.

Introduction

The nervous system of insects

The insect class of invertebrates (phylum: Arthropoda) is thought to have originated ~ 480 million years ago (Mya) (Misof et al. 2014). They represent the most diverse animal phylum, counting more than one million described species, with estimates suggesting several million more yet to be identified. Insects make up more than half of all animal species, and a major part of terrestrial biodiversity (Stork 2018). In fact, insects have undergone extensive adaptive radiation and fill a wide array of ecological niches, and can be found in nearly every terrestrial and freshwater habitat. This is reflected in the variety of anatomical traits associated with the most disparate functions across insect orders, such as flight, jump, dig or build nests, make nets, eat leaves or suck lymph or blood. These abilities are supported by specialized morphologies that have arisen through a gradual process of natural selection. Even different life stages of the same species, despite having the exact same genome, can have contrasting features allowing them to occupy different ecological and nutritional niches, and avoid competition to improve fitness.

Anatomical adaptations evolve in response to specific ecological pressures, enabling organisms to perform distinct functions that enhance their survival and reproductive success (Darwin 1859; Mayr 1982; Dawkins 1976). The emergence of new physical traits is often paralleled by the evolution of mechanisms regulating associated behaviors to perform specialised operations and use the newly acquired anatomical structures effectively (Tinbergen 1963). The central nervous system (CNS) is the nexus where stimuli are integrated and behaviors are orchestrated in all bilaterians, and deciphering its structure and functioning is key to understanding the processes leading to the execution of behaviors (Katz 2011; Holland et al. 2013).

Neuroanatomical synopsis

An insect CNS is relatively simple compared to a Mammalian one, and is composed of two major parts: a brain and a ventral nerve cord. Brain size, shape and organization vary across the insect class (Heinze et al. 2021). Nevertheless, a

common structural organization of the insect brain was assessed already in the first half of the 20th century (Hanström 1929), and has recently been delineated in great anatomical detail (Ito et al. 2014).

The different functional areas of the insect brain are constituted by the cerebral ganglia. Ganglia are anatomical structures in which a thinner outer layer of somata, named the “cell body rind” (occasionally referred to as “the cortex”), encloses a synapse-rich region of generally much wider volume made of neural projections, the “neuropil” (Polilov and Makarova 2020). The ganglia are enclosed in a thin sheet of connective tissue under which lies a layer of specialized glial cells, the perineurium, constituting an analogue of the blood brain barrier (BBB) for insects.

Three pairs of fused ganglia are located dorsally within the head; additional nervous structures are located ventrally inside the head, enclosing the first part of the esophagus. These are referred to as subesophageal (or gnathal), while the dorsal ganglia are defined as supraesophageal (or cerebral) (Fig. 1A). The paired brain ganglia constitute three functional regions, containing some main structures that have been associated with specific neurological functions. These are (i) the protocerebrum, which has a cephalic position and is associated with vision (optic lobes), and memory formation (mushroom bodies (MBs)), (ii) the deutocerebrum, rostral, incorporating the olfaction centers (antennal lobes (ALs), lateral horns (LHs)), and (iii) the tritocerebrum, located caudally to the other two, where control of motor function takes place (lateral complex, subesophageal zone). These areas are devoted to subsequent steps of sensory input integration: this involves an initial processing, followed by higher-order processing of unimodal or multimodal information (respectively coming from one or different sensory organs), and final production and control of a motor output. Such a mechanism creates an adequate and concerted behavior regulation in response to stimuli, then nervous signals are transmitted from the brain to the nerve cord for behavior performance (Bouchebti and Arganda 2020). The nerve cord lies ventrally and runs along the midline of both thorax and abdomen. It is made of segmental ganglia, connected to each other through axon bundles. They lay in fused pairs in each metameric body segment, and from which nerves extend bilaterally into the body segment and appendages. The insect thorax encloses three pairs of thoracic ganglia (sometimes fused), which control locomotion thanks to their connection to sensory receptors and by

innervating thoracic muscles, legs and wings. The abdominal ganglia control movements of abdominal muscles in a similar fashion. A terminal pair of abdominal ganglia innervates the anus, internal and external genitalia, and caudal sensory receptors (reviewed in Smarandache-Wellmann 2016).

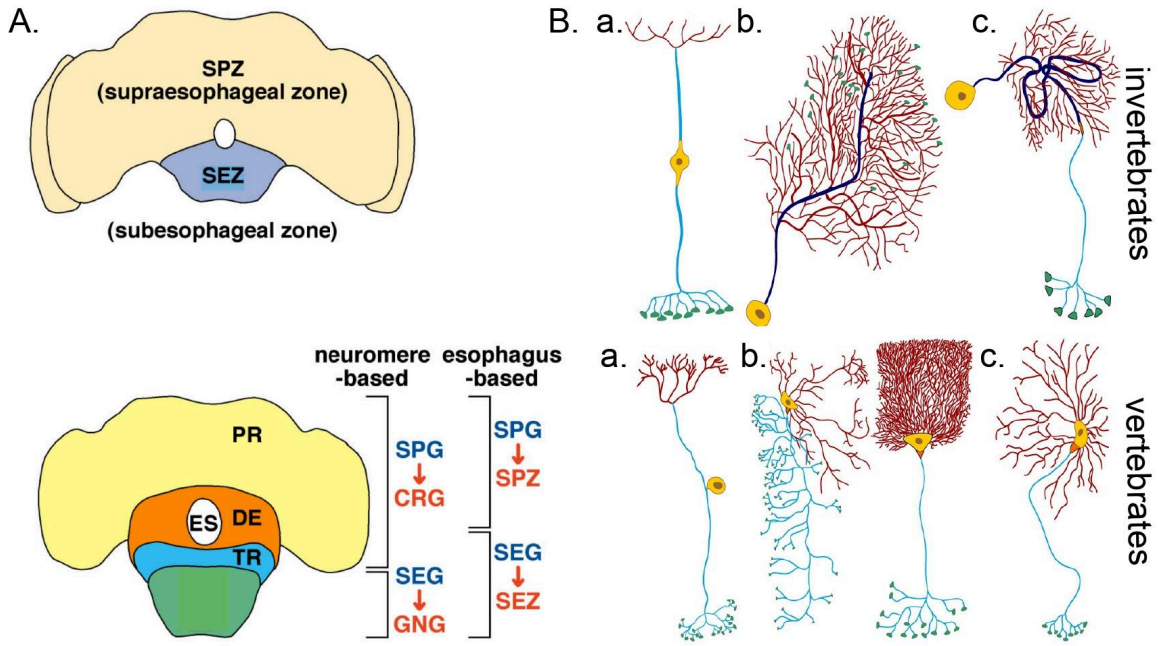


Figure 1. Insects cerebral and neural anatomy. (A) Classification of the insect brain in major regions (*Drosophila melanogaster* brain shown, but the general separation plan is illustrative for all insects). In the top panel the brain is divided in two main compartments based on their spatial relation with the esophagus. In the bottom panel is highlighted the subdivision in protocerebrum, deutocerebrum and tritocerebrum, and how they can be further classified based on their relationship esophagus. Image adapted from Ito and colleagues (Ito et al. 2014). **(B)** Comparison between (a) sensory neurons, (b) interneurons, and (c) motor neurons of invertebrates (e.g. insects) (top), and vertebrates (bottom). Red, dendrites; yellow, soma; cyan, axon; blue, primary neurite; orange, spike initiation zone; green, synaptic boutons. Adapted from Smarandache-Wellmann (Smarandache-Wellmann 2016). SPZ: supraesophageal zone; SEZ: subesophageal zone; PR: protocerebrum; DE: deutocerebrum; TR: tritocerebrum; CRG: cerebral ganglia; GNG: gnathal ganglia; SPG: supraesophageal ganglia; SEG: subesophageal ganglia.

Ganglia are neuronal aggregates formed by networks of interconnected neurons. Insects neurons and their projections share some common features with the vertebrate ones (Fig. 1B). Insects too have both (i) axons, which are long, slender neural projections that carry and deliver efferent signals, converting electric to chemical signals (respectively action potentials and neurotransmitters,

neuromodulators or neurohormones), and (ii) dendrites, which are ramified neural projections that receive afferent signals. Nonetheless, vertebrate and insect neurons have different morphology, cellular compartments, and associated functions. To explore them, we can follow the journey of a sensory signal, from its perception, through its integration, to the moment in which a response is transmitted from the CNS to muscles, referring to Figure 1B as a neuroanatomical guide. Invertebrate sensory neurons are bipolar, with two neurites (i.e. neuronal projections) extending from the cell body. This is different from vertebrate ones which are unipolar or pseudounipolar. Sensory neurons are afferent, they gather sensory information from their dendrites which is then transmitted through their axon to a sensory ganglion in the CNS. Vertebrate axons are typically myelinated, with a consistent diameter across their full extent and are made of a single, continuous projection that terminates in a synaptic bouton. This makes contact with a postsynaptic cell and is the cell compartment from which the chemical messengers are released. Insect axons instead are not myelinated, and possess varicosities all along their length from which chemical messengers are released diffusely, without making any obvious synapse (Spong et al. 2016; Triarhou 2014). Sensory neurons make contact with monopolar interneurons inside the neuropils, initiating the signal integration processes. From each insect interneuron cell body, a single primary neurite projects to the neuropil, where it branches out in dendritic arborizations, the "integrative segments" (Fig. 1B, a). In vertebrates, excitatory or inhibitory postsynaptic potentials, are summed spatially and temporally at the neural soma and shape its integrated membrane potential, which triggers the generation of an action potential at the axon initial segment, leading to neuronal output when crossing a critical threshold. Conversely, the insect soma is seldom involved in integration of synaptic processes: the synaptic information is integrated in the dendrites and adds up to generate an action potential at one of the spike initiation zones (Fig. 1B, b). The interneurons (Fig. 1B, b) and the efferent motor neurons (Fig. 1B, c) make contact within the neuropil through their dendrites, which serve as both sites of signal input and output: they receive excitatory and inhibitory synaptic signals from upstream neurons and can also release neurotransmitters to influence downstream targets (reviewed in Smarandache-Wellmann 2016).

When synaptic transmission is adequate, an action potential is generated at the spike initiation zone of motor neurons, and propagates towards the periphery. While the primary excitatory neurotransmitter of invertebrate motor neurons is glutamate (Glu), vertebrates use acetylcholine (ACh). In addition, invertebrate motor neurons also deliver inhibitory signals able to finely modulate muscle contraction, through the release of γ-amino-butyric acid (GABA), while there is no primary inhibitory neurotransmitter released directly onto muscle fibers by vertebrate motor neurons, and relaxation is controlled by inhibiting the motor neuron itself before it stimulates the muscle (Smarandache-Wellmann 2016; D'Angelo et al. 2011).

Another group of cells is as relevant as neurons in the CNS: glia cells. They comprise a variety of CNS-associated non-neuronal cells, with structural, nutritional support, or immune roles (Kremer et al. 2017). In insects, glia can be classified into a few main populations. Two of them, the astrocyte-like and the ensheathing glia, collectively referred to as neuropil-associated glia, make direct contact with brain nerve processes. They are located at the interface between the cell body rind and the neuropil, forming sheaths around the neuropil, as well as highly branched processes interacting with terminal nerve fibers and synapses (Hoyle 1986). Cortex glia cells ensheath individual neuronal somata, structurally stabilizing them and regulating the nervous system excitability (Melom and Littleton 2013). Two types of surface glia, namely the perineurial and the subperineurial glia, surround the brain and peripheral nerves. Both perineurial and subperineurial glia take part in the BBB. The BBB regulates ionic and hormonal exchanges from the hemolymph to the brain; gaseous exchanges are instead possible thanks to tracheae, which are generally positioned all across the insect body and that penetrate deeply in all tissues, brain included (Nation and Burrows 1997). Subperineurial cells form marked septate junctions, which are equivalent to Mammalian tight junctions, and are thereby primarily important in regulating the molecular exchange between the nervous system and hemolymph. Despite perineurial glial cells being also involved in the BBB, the mechanism by which they participate in this function has not been clarified yet (Limmer et al. 2014).

Despite it has been acknowledged that insect brains share general organization and neural functions (Smarandache-Wellmann 2016), there are differences in homologous neuropils organization and anatomy, divergence in the size of both the organ and the cell populations across species, and even when comparing sexes (Raji and Potter 2021; Li et al. 2022) (Fig. 2A). Morphological and functional comparisons across species like silkmoths, fruit flies, locusts, and crickets indicate neuron type and brain region homologies with conserved circuitry, and underline how homologous nervous structures can arise from homologous developmental processes that can nonetheless differ in timing and progression modalities (Namiki and Kanzaki 2016; Koniszewski et al. 2016; Posnien et al. 2023). Homologous brain regions can have different shapes and sizes in association to the insect needs. The central complex, for example, is a brain region critical for sensory integration, orientation, and navigation, and can vary in size relative to behavioral needs. It is positioned centrally in the protocerebrum region at the midline of the brain, dorsal to the esophagus and tritocerebrum. In some species with complex flight or navigational behaviors, such as migratory moths or foraging ants, the volume of the central complex or its subregions can increase to support those demands (Honkanen et al. 2019) (Fig. 2B).

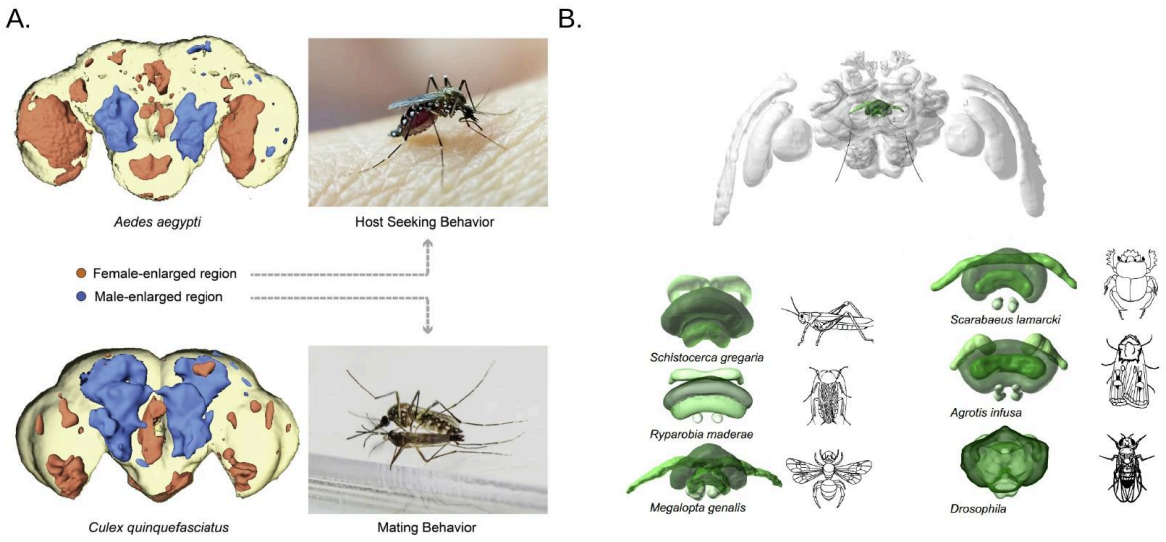


Figure 2. Dimorphism in insect CNS region anatomy. (A) Sexual dimorphisms have been recognized in multiple brain regions in the mosquito *Aedes aegypti*, inferred to be involved in sex-specific behaviors. Image adapted from Ito and colleagues (Li et al. 2022). **(B)** Anatomy of the central complex (CX). Left: (continued)

location of the CX (colour) in the insect brain (the sweat bee *Megalopta genalis*). Right: the CX is conserved across a wide range of insects. All image sources are present in (Honkanen et al. 2019), from which the image was adapted.

The brain of mosquitoes

Mosquitoes are insects belonging to the dipteran order and the Culicidae family. The two main subfamilies of Culicidae are Culicinae and Anophelinae, and are recognized as monophyletic lineages that diverged from a common ancestor early in mosquito evolution, likely during the early Jurassic period (i.e. ~ 190 - 210 Mya). Anophelinae is considered a basal lineage within Culicidae, and it branched off earlier from the root of the mosquito family tree than Culicinae. Culicinae subfamily is more diverse than Anopheline one, and includes many tribes such as Aedini and Culicini, with some lineages adapted to various ecological niches (Foster et al. 2017; Soghigian et al. 2023). Most of the major genera composing the Culicidae family are hematophagous (e.g., *Anopheles*, *Aedes*, *Culex*, *Mansonia*) and transmit pathogens, despite of very different nature (apicomplexans, viruses, nematodes). Despite evident similarities in lifestyles and anatomy, these mosquitoes possess biological variations characterizing their CNS. Indeed, both the anthropophilic mosquito species *Anopheles gambiae* (Anophelinae) and *Aedes aegypti* (Culicinae) show species-specific (and sexual) dimorphism in the anatomy and innervation of ALs glomeruli (Ghaninia et al. 2007; Riabinina et al. 2016; Shankar and McMeniman 2020). These must reflect the different distribution range, rhythmicity of daily behavior and feeding habits specific to each mosquito species, together with other divergent traits arisen in ~ 179 My of evolutionary divergence (Soghigian et al. 2023).

To compare species anatomy, across-species homology assessment is typically performed by focussing on the embryonic primordia of brain structures, rather than on the adult morphology. In fact, developmental stages are less affected by later evolutionary diversification and are more comparable across distant taxa, as suggested by the recapitulation theory (Haeckel 1866). Indeed, genetic communalities exist in distantly related species. *An. gambiae* and *Drosophila melanogaster* phylogenetically diverged 250 million years ago. At the present day, both their genomes have around half of the genes identified as orthologs, showing an average sequence identity of ~ 56%. Despite major chromosomal shuffling and

ortholog genes on average retaining half of their intron/exon structure, chromosomal arms exhibit significant remnants of homology between the two species (Zdobnov et al. 2002). Thus, functional studies can take advantage of the shared information retained among species during the evolutionary timespan, but phylogenetic divergence must be taken into account when comparing distinct species, and their peculiar anatomy and genetics must be acknowledged.

This knowledge has allowed the understanding of key neurological processes in the nervous system of insects. One renowned example is the characterization of the role of olfactory co-receptor (Orco) protein, also known as Or83b in *D. melanogaster*. Top-down studies on insect genomes revealed how this is an odorant receptor protein having a strikingly different DNA sequence compared to the ones of the other members of the same family, but also having homologs in other insect species. Among them, we find *An. gambiae*, showing nearly 70% sequence similarity (Vosshall et al. 1999, 2000; Hill et al. 2002; Krieger et al. 2003; Pitts et al. 2004). With reverse genetics, its role was further characterized and, despite its mechanism of action having not been completely elucidated yet, its major role as general olfactory co-receptor has been proven (Elmore et al. 2003; Larsson et al. 2004).

Example of signal integration in mosquito neural system: integration of olfactive stimuli

Mosquito anatomy and behavior have been long investigated in an attempt to find the key regulators of host-seeking, most often with a focus on response mechanisms to odors (Bowen 1991; Ignell et al. 2005; Konopka et al. 2023). Historically, *An. gambiae* and *Ae. aegypti* have been the most studied mosquito species, as they pose major threats to human health being the main vectors of malaria and arboviruses, respectively. The major odor attractants for mosquitoes present in mammalian hosts exudates and breath have been identified decades ago (Acree et al. 1968; Gillies 1980). This knowledge promoted and directed a somewhat general interest of the scientific community studying mosquitoes towards describing and understanding the functions associated to this insect's sense of smell, with a burgeoning corpus of studies focused on its antennae - the main mosquito olfactory organ - and olfaction centers in its CNS. Since describing the anatomy of a structure is the first step to

understand its function, the neurological olfaction centers were the first areas of a mosquito brain of which the neural architecture was characterized in detail. Indeed, olfactory centers have been comprehensively described in both *Ae. aegypti* and *An. gambiae* (*Childress and McIver 1984*; *Ignell et al. 2005*). In *An. gambiae*, ALs anatomy was elucidated, and it was assessed which glomeruli are subject to olfactory projection neurons innervation coming from different sensory organs of the head (Shankar and McMeniman 2020; Riabinina et al. 2016).

Despite a conserved CNS organizational framework and conserved gene expression across the insect phylogeny (for example, the *orco* gene), mosquito neurobiology reflects highly evolved sensory and neural adaptations characterized by a rich diversity of receptor types and their co-expression in sensory neurons, multisensory integration in the brain, and sophisticated genetic and molecular underpinnings for these processes. These features make mosquitoes highly efficient vectors and also challenging targets for control strategies aimed at disrupting host-seeking and feeding behaviors. In *An. coluzzii*, for example, coupling CRISPR-knock-in of fluorescent markers and pan-neural labeling revealed hundreds of neurons in the head sensory appendages expressing various chemosensory receptors, including odorant, ionotropic, and gustatory receptors. This neural asset allows mosquitoes to detect a wide range of chemical cues mediating host detection and shows signs of redundancy, which makes mosquito olfactory system fault-tolerant, evolutionary resilient and adaptable (Riabinina et al. 2016; Herre et al. 2022; Konopka et al. 2023; Raji et al. 2023).

Chemosensation is the first sense involved in host recognition inducing long-range attraction guiding mosquito behaviors supporting blood-feeding and disease transmission, for which maxillary palps act as activators when perceiving CO_2 sources distant up to 10 meters. This signal is extremely potent in inducing blood feeding-associated behaviors, with a 5 s pulse of fictive carbon dioxide, created by optogenetically activating CO_2-sensitive neurons, inducing a persistent behavioral blood seeking/feeding state in female mosquitoes that lasted for more than 10 minutes. This state is highly specific to females searching for a blood meal and was not induced in recently blood-fed females or in males, which do not feed on blood (Sorrells et al. 2022). Other sensory processing is relevant at the mid-range and at

the short range. Mid-range attraction is mainly guided by odour and visual cues, while heat perception comes into play at the short range (Bernier et al. 2007; van Breugel et al. 2015; Cardé 1996; Morita et al. 2025).

Peripheral inputs, as olfactory stimuli, are directed to the mosquito CNS, and locomotor response is orchestrated in the brain after multimodal integration of information (Fig. 3A, B). The behavioral responses to sensory stimuli that have been most extensively studied are associated with olfaction. Olfactory integration recapitulates many of the main functions and regions currently recognized within the mosquito nervous system.

The primary sensory organs for olfaction are the antennae, on which the olfaction sensory unit is the sensillum. Sensilla are microscopic structures of around 10 μm, decorating the entire surface of the antennae. Each of them houses the dendrites of an olfactory sensory neuron (OSN), which are surrounded by aqueous hemplymph. This is all encased within a thin layer of perforated surface cuticle. Odors can permeate through the cuticle perforations and reach the OSNs. On the surface of mosquitoes' OSNs one or multiple receptor types are expressed, unlike fruit flies, in which each OSN expresses one type of receptor (Herre et al. 2022). This characteristic enables single neurons to respond to diverse and complex odor blends, potentially including hundreds of compounds, such as the one of the human body (Bernier et al. 2007), increasing their olfactory sensitivity and complicating disruption of host-seeking behaviors. Odorant receptors interact with ORCO, and trigger an action potential. OSNs project to the primary brain integration centers, the ALs, where neurites coming from one or multiple OSNs innervate specific glomeruli. Local interneurons allow the first step of integration. The information is then transferred to the Kenyon cells (KCs) of MBs, and then to the LHs, which respectively perform processes leading to learning (KCs) and integrating the multimodal information from both olfaction, vision, mechanosensation, etc. (LHs). LH output neurons then project back to peripheral organs to trigger responses consistent with the integrated stimuli (reviewed in Wolff and Riffell 2018; Konopka et al. 2021).

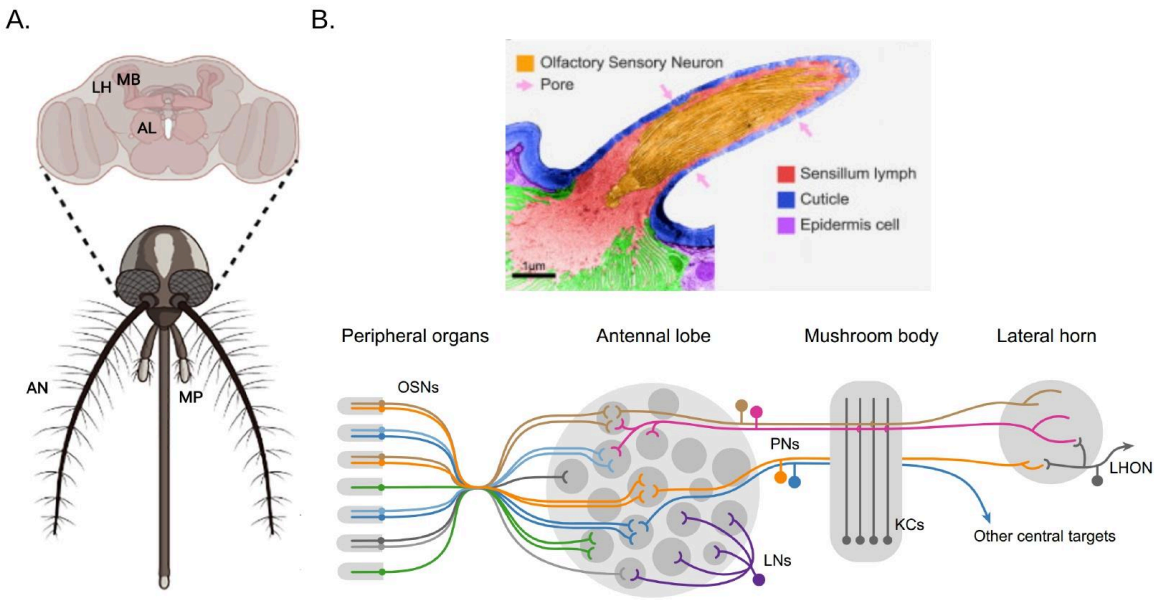


Figure 3. Example of mosquito sensory integration in the brain: olfaction. (A) A mosquito (*Aedes*) head with sensory appendages (e.g. antennae, maxillary palps), and highlighted the areas of the brain involved in sensory integration of olfactory cues (adapted from Coutinho-Abreu et al. 2022). **(B)** On top, a coloured electron scanning microscopy capture of a section of a sensillum (adapted from Hansson and Stensmyr 2011). At the bottom, a schematics of the components of the nervous system involved in olfaction integration and locomotor output (adapted from Zhao and McBride 2020). AN: antenna; MP: maxillary palps; AL: antennal lobe; MB: mushroom bodies; LH: lateral horns; OSNs: olfactory sensory neurons; LNs: local interneurons; PNs: projection neurons; KCs: Kenyon cells; LHON: lateral horn output neurons.

The other main mid-range attraction signals for mosquitoes are visual, and vision brain centers represent preponderant regions in the mosquito brains in terms of mass and volume. In vision, the first signal integration steps happen in the optic lobes. Then, information is transmitted to the LHs where it is integrated with the processed signals coming from the other sensory organs. Optic lobes are constituted by layered glomeruli, namely (from superficial to deep) lamina, medulla, lobula and and lobula plate, integrating visual information coming from the hundreds of ommatidia of the mosquito eyes (Singh and Mohan 2013; Mysore et al. 2014). After approaching a target in search for a blood meal, both the visual cues perceived by the eyes and the odor and heat sensory cues perceived by antennae, proboscis and legs guide the mosquito landing on its host on a short-range (Coutinho-Abreu et al. 2022; Chandel et al. 2024).

The efforts in describing the anatomy of a structure allow us to assess the relationship among specific organ regions, and lay the groundwork to describe their molecular characteristics (such as gene expression, metabolism, etc.), and their physiological response to stimuli. For instance, the knowledge regarding mosquito antennae and AL anatomy established the basis for a more granular description of the molecular patterns of co-expression of odorant receptors, and also for identifying the glomeruli in which neural activity is physiologically elicited by smells of different food sources in *Ae. aegypti* (Herre et al. 2022; Zhao et al. 2022). Considerable knowledge has been gathered about mosquito brains with histological identification of brain structures, fine description of the anatomy of deutocerebrum, and 3D tomography reconstruction of the mosquito brain with recognition of the main functional zones (Ignell et al. 2005; Younger et al. 2014), but a more extensive and deep investigation of the diverse brain centers is scarce, and conducted almost exclusively on *Aedes* species.

Some studies reported classical histological stainings or topographical reconstruction of the whole *Anopheles* body, head structures and soft tissues included, revealing the general, lowly magnified organ architecture (Ishii et al. 2017; Baia-da-Silva et al. 2019; Luna et al. 2023). A few studies have shown the *Anopheles* brain structure with pan-neural stainings, evidenced some of the main neuropils and investigated innervation from peripheral sensory organs, but have not addressed a detailed description and investigation of the CNS structure (Riabinina et al. 2016; Konopka et al. 2023). In addition, most studies mainly focus on brain development and anatomy of sexually dimorphic regions, while a more extensive molecular investigation of cellular types appeared only in a few forward-looking studies in the last five years (Mysore et al. 2011, 2014; Tomchaney et al. 2014; Li et al. 2022; Cui et al. 2022; Gregor et al. 2022; Goldman et al. 2025).

On the other hand, extensive knowledge on brain organization and vast description of cell types is lacking in *Anopheles*, and just two CNS cell type markers have been described to date (Raji and Potter 2021). Instead, more knowledge has been gathered on peripheral neurons. Locating *Anopheles*' olfactory sensory neurons and olfaction integration regions allowed exploring their role, with a particular focus on the associated gene expression (Konopka et al. 2023; Riabinina et al. 2016; Afify and

Potter 2022; Karner et al. 2015; Maguire et al. 2022). For example, it was shown that ectopic expression in non-native OSNs of an odorant receptor activated by human odors did not confer ectopic neuronal functions, but rather dampened the activity of the expressing neuron with a concomitant downregulation of all odorant receptors there expressed in *An. gambiae* (Maguire et al. 2022). Similarly, by combining transgenic lines expressing a QUAS-GCaMP6f, a calcium channel transgene whose transcription is activated by the QF2 transcription factor (TF), and crossing this to an Orco-QF2 driver line, it was possible to assess repellent olfactory responses in all olfactory organs of *An. coluzzii*, and to identify neuron-specific activation mediated by odorants (Afify et al. 2019).

These studies have not yet created a comprehensive knowledge on the CNS of mosquitoes, and effort has still to be made to reach a level of understanding of *Anopheles* CNS comparable or even superior to the one we have for the CNS of *Aedes*, albeit the latter is also limited.

Mosquito life cycle and malaria transmission biology

Malaria is a vector-borne disease caused by *Plasmodium* parasites, transmitted by mosquitoes of the *Anopheles* genus. Of the ~ 500 formally recognized species of *Anopheles*, only ~ 40 of them are capable of transmitting malaria under natural conditions (Autino et al. 2012). The binome *An. gambiae - Plasmodium falciparum* is the vectorial system which is predominantly responsible for malaria cases worldwide nowadays (World Health Organization 2024b). The *An. gambiae* complex includes several closely related species such as *An. gambiae sensu stricto*, *An. coluzzii*, *An. arabiensis*, and others, as well as cryptic subtypes (Riehle et al. 2011; Caputo et al. 2024). These species differ genetically and ecologically but are morphologically almost indistinguishable, such that *An. gambiae* and *An. coluzzii* were recognized as different species only recently, and show only partial reproductive isolation (Coetzee et al. 2013; Thailayil et al. 2018). They represent the major African malaria vectors in wet and dry seasons respectively. Both endemic parasite circulation in tropical regions and malaria epidemics have been oppressing humans for millennia (Michel et al. 2024). The discovery of the etiological agent and the identification of the insect vector were achieved in the second half of the 19th century (Nye 2002; Malpe et al.

2024). Due to the widespread disease prevalence and its strong impact on human health, such discoveries promoted the development of concerted efforts of the scientific community and governments for fighting it. Despite this, the emergence of parasite drug resistance phenotypes, the struggles in obtaining more than moderate protection from vaccines (Li et al. 2025), and practical drawbacks in mosquito elimination (World Health Organization, n.d.), impeded malaria eradication, causing it to still be among the top five most deadly infectious diseases (World Health Organization 2024a). In 2023 its burden was estimated to be 263 million cases and 597,000 deaths in 83 countries, with the African Region carrying a disproportionately high share of the global malaria burden (95% of the cases and 94% of the deaths). In the region, children under 5 accounted for about 76% of all malaria deaths (World Health Organization 2024b).

Mosquito life stages and their influence on disease transmission

Every malaria infection is preceded by the same event: an infected female *Anopheles*, in search of a blood meal, targets a human and uses its sight to approach their skin, attracted by odor plumes and body heat (Coutinho-Abreu et al. 2022). After landing on a human host, the mosquito uses the various structures contained in its proboscis to localize a proper biting site in its own proximity (labella), there burrowing its blood-sucking organs (labrum and hypopharynx) by digging through the host skin (with its maxillae and mandibles). Eventually, the mosquito will quest the skin environment (with the labrum) in search of a capillary from which to obtain blood, allowing the parasites to be transmitted into the human host's skin (Powell 2019). This set of behaviors is fundamental in the completion of the physiological life cycle of the mosquito, aimed to allow sufficient nutrient acquisition to promote proper egg development (Townson 1993). Females of autogenous species can complete the first cycle of egg development without taking blood but require one or more blood meals to complete each subsequent cycle. Females of anautogenous species require one or more blood meals to complete each cycle, including the first. For example, most wild *An. gambiae* would need two blood meals for a complete ovarian development (Townson 1993). Being blood uptake so tightly associated to reproduction success or to a dramatic increase in fitness (respectively for anautogenous and autogenous mosquitoes), this is an inherent trait of the female

mosquito physiology, and all the events and behaviors that can impact a mosquito health or fitness affect the vector competence of an individual or the vectorial capacity of a mosquito population.

The aquatic phase of mosquito life goes from egg to emergence and takes about seven to fourteen days in warm climates. After going through four larval molts, mosquitoes become non-feeding, aquatic, pupae. One to four days after pupation development is complete, the newly emerged adult mosquito splits and climbs out of the pupal case, resting on the surface to allow their wings and cuticle to harden before flying away.

Mating happens only once in a mosquito lifetime, and leads to multiple rounds of oviposition after blood feeding events (Thailayil et al. 2011; Gabrieli et al. 2014). To mate, male mosquitoes aggregate in flying swarms to attract females. In these gatherings, mosquito behavior is guided by both visual and acoustic stimuli, used to track conspecifics, perform courtship and mate, most probably in a polygynous fashion, leading to high variation in male reproductive success and low variation in female reproductive success, with male reproductive success affected by body size and harmonic convergence of male and female wingbeat frequencies (Yuval and Bouskila 1993; Zsemlye et al. 2005; Cator and Zanti 2016; Cator et al. 2021; Gupta et al. 2024).

After adult maturation and mating, floral feeding is the main source of food for the mosquitoes, and only the females of blood-sucking species will feed on blood to accomplish egg development. Female mosquitoes follow cycles of blood feeding, resting and egg laying throughout the course of their lives. Following each blood meal, the females are mostly inactive throughout the period dedicated to ovarian development, and blood feed search follows a dynamic but temporally defined pattern (Edman et al. 1975; Klowden and Lea 1979; Klowden and Briegel 1994; Takken et al. 2001). Flower visiting tends to temporarily cease after a blood meal, mosquitoes tend to rest and nutrients are redirected to vitellogenesis: host seeking behavior is inhibited until egg-laying (Klowden and Lea 1984; Klowden 1994; Christ et al. 2017), while floral seeking is inhibited for up to 48 h (Vargo and Foster 1982; Christ et al. 2017), when pre-oviposition behaviors commence (Klowden and Blackmer 1987).

After mating, and after blood feeding in most cases, mosquito females are poised to lay eggs, and the selection of optimal oviposition sites can influence the offspring's longevity and fitness, even at adult stages. The choice of an appropriate oviposition site is known to be guided by visual and chemical cues revealing the site resource type and availability, and the right amount of conspecific egg-laying in the possible oviposition site (Williams et al. 2008; Wong et al. 2011; Schoelitsz et al. 2020; David et al. 2023). In general, the success of mosquitoes developing from larvae to adults ensures a robust vector population capable of sustaining malaria transmission. Poor or unstable oviposition sites limit larval survival, reducing vector numbers, size and competence of adults (Wong et al. 2012; Suh et al. 2016). In addition to this, larval diet, breeding site temperature, and exposure to environmental bacteria can affect adult life history traits and fitness, and it has also been suggested that mosquito competence for malaria transmission can be affected by larval developmental conditions (Linenberg et al. 2016; Giraud et al. 2022; Mackay et al. 2023). In endemic areas, *Anopheles* breeding sites fill with rainwater seasonally, coinciding with malaria transmission peaks, and the presence of breeding sites closer to human dwellings facilitate more frequent human-mosquito contact, enhancing transmission efficiency (Ndiaye et al. 2020; Woyessa and Yewhalaw 2025).

Evidently, mosquitoes can escape physical threats, such as a human trying to crush them (Cribellier et al. 2024), but this is not the only ability they have to escape threats posed by humans, and to keep biting them and transmitting pathogens. A mosquito biting preferences are never exclusively anthropophilic, and such behavioral plasticity helps in evading insecticides and sustains disease transmission by feeding on alternate hosts and maintaining their populations even when human-targeted control efforts are high (Giglioli 1956; Mlacha et al. 2020; Woyessa and Yewhalaw 2025). Coupled with these facts, mosquitoes can actively detect and avoid insecticides and repellents, developing a behavioral resistance associated to temporal shifts in daily aggressiveness and spatial avoidance of indoor environments (Carrasco et al. 2019; Hubbard and Murillo 2024). Furthermore, learning processes based on sensory information have been shown to guide subsequent host seeking and biting decisions (Vinauger et al. 2014; Vinauger 2019; Coutinho-Abreu et al. 2022).

The life cycle of *Plasmodium*

A few hundred *Plasmodium* parasites are deposited in a human's dermis with a mosquito's saliva during a blood meal. Saliva injection in the skin contributes a local anti-hemostatic and anti-inflammatory effect, facilitating blood meal uptake (Arora et al. 2023). The intensity of infection in the salivary glands (SGs), but also SG architecture important determinant of the number of injected sporozoites, which is, in turn, a key parameter in establishing an infection in the vertebrate host (Andolina et al. 2024; Medica and Sinnis 2005).

Once inside the human circulatory system, a few sporozoites manage to reach the liver and each of them infects one different hepatocyte, undergoing intra-human developmental cycle stages, which lead to both schizogony and gametocyte formation (Fig. 4). The gametocytes can create a zygote inside a mosquito's midgut (MG), which encysts in the MG epithelium, and develops in sporozoites which migrate to the SGs, where they are ready to be transmitted to a new host.

Currently *Plasmodium* parasites have not been detected in other mosquito body districts than the ones of Figure 4. As an example, in contrast to other parasites, *Plasmodium* was never found in mosquito muscles or brain (Mangold et al. 2019; Minetti et al. 2020).

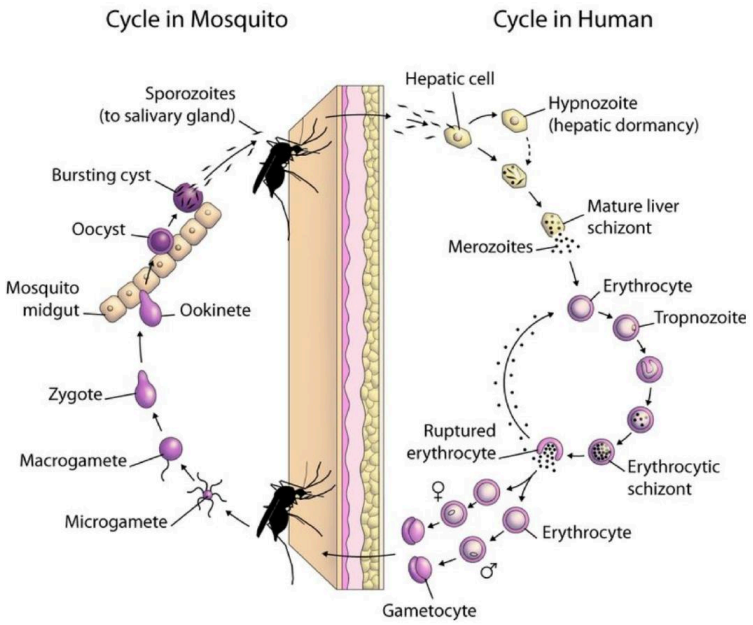


Figure 4. *P. falciparum* life cycle. The parasites deposited by a mosquito into a human host enter the bloodstream and enter liver cells. Here, the parasites undergo liver-stage schizogony, producing

trophozoites, which will then create a syncytium (schizont) containing tens of thousands of nuclei produced with a mitotic replication process. These are then released as daughter cells, called merozoites, which can enter the blood flow. Once there, they will infect red blood cells and replicate inside them producing more merozoites through blood-stage schizogony, which entails a cyclic process of red blood cell lysis and invasion. Erythrocyte egress events happen in a coordinated manner and are associated with the sudden fever typical of the symptomatology of malaria due to exposure of the immune system to thousands of parasites . About 1% to 5% of asexual parasites switch to sexual differentiation and become gametocytes (Ouologuem et al. 2023). Immature gametocytes, preferentially sequestered in the bone marrow and spleen microvasculature, enter the bloodstream once matured (Thomson 1914; Eichner et al. 2001). They now are available to be uptaken and ingested by a mosquito during a blood meal, arriving in the mosquito midgut (MG). There, environmental cues, such as a drop in temperature, an increased pH and the presence of xanthurenic acid, trigger differentiation of sexual cells into gametes, i.e. micro- and macro-gametocytes (respectively male and female sexual cells) (Billker et al. 1997, 1998). Thus, following a blood meal from a malaria-infected host, *Plasmodium* gametogenesis and sexual reproduction take place in the mosquito MG within the first 2 hours after the uptake of the infected blood meal, through the fusion of micro- and macro-gametocytes, which results in the formation of a zygote (McRobert et al. 2008; Lucantoni et al. 2015). To progress into the next life cycle stage, the zygote needs to encyst in the MG epithelium. This is achieved through a maturation into a motile form, the ookinete, which produces chitinases allowing it to traverse the MG peritrophic matrix (Shahabuddin and Kaslow 1994). Despite this transition being accompanied by substantial parasite death (Barillas-Mury and Kumar 2005), the surviving ookinetes can reach the basal lamina of the MG epithelium, where they encyst and differentiate each into one oocyst (Siden-Kiamos et al. 2020).
Over the 10-14 days following encystment, the oocyst undergoes sporogonic development, producing thousands of sporozoites. When mature, the oocyst wall ruptures, and the sporozoites enter the mosquito hemolymph compartment and migrate to the SGs. Once parasites invade the SGs, the mosquito is infectious (~ 14 days after infectious blood meal consumption) and can transmit the parasites during subsequent blood meals. Image source: https://ocw.mit.edu/.

Parasites like *Plasmodium* undergo critical developmental stages within the mosquito vector, ultimately affecting mosquito behavior, physiology, and vector competence.

Mosquito-parasite interactions

Mosquito-parasite interactions start when an infectious blood meal is uptaken, and through each step of infection establishment from gametocyte sexual reproduction to SGs colonization, the mosquito immune system and the parasite defense mechanisms contrast each other (Shahabuddin and Kaslow 1994; Ménard et al. 1997;

Tomas et al. 2001; Thathy et al. 2002; Blandin et al. 2004; Barillas-Mury and Kumar 2005; Baton and Ranford-Cartwright 2005; Wang et al. 2005; Zhu et al. 2022; Barletta et al. 2025). The timespan that goes from infectious blood meal uptake to colonization of the mosquito SGs by sporozoites is called extrinsic incubation period (EIP). Multiple factors affect the likelihood of parasites surviving and completing the EIP. First factor to consider is mosquito age, since older mosquitoes are more likely to be infectious, as they have probably survived long enough for infecting parasites to complete their development. Indeed, in wild mosquito populations the average age is the most important determinant of vectorial capacity, a measure of the transmission potential of a vector borne pathogen within a susceptible population, represented by the daily rate at which new infections could be generated from an existing infectious case. Clearly, older mosquitoes have higher probabilities of consuming an infected blood meal, and a longer lifespan also enables the parasites to complete sporogony, thus a more aged mosquito population would tend to be prone to infect more (Dawes et al. 2009; Johnson et al. 2020). In association to this, while egg laying has been shown to be negatively impacted throughout the mosquito life by both malaria parasite and vector-borne viruses, life span does not seem to be altered (Pigeault and Villa 2018; Gaburro et al. 2018).

Another factor correlated with surviving the EIP is the tradeoff between the positive biting rate effects and the inherent risks for the mosquito and the parasite which come with physical proximity to humans. Frequency, timing (diurnal/nocturnal), and host preference of mosquito biting directly affect malaria transmission risk. Lower transmission is of course associated with low interaction frequency, diurnal activity and a host preference skewed towards animal targets (Sangbakembi-Ngounou et al. 2022; Woyessa and Yewhalaw 2025).

Generally speaking, the behavior of the mosquito vector is greatly influencing transmission success. Mosquito-pathogen interactions are complex biological processes that significantly influence the transmission dynamics of the vector-borne diseases they transmit, and can be guided by both mechanistic and behavioral processes.

As transmissible parasite forms reside in the SGs, multiple studies have explored the interplay between the role of the components of *Anopheles* saliva and the malaria

infection outcomes, leading however to contradictory and inconclusive results when taken all together (Arora et al. 2023). Nonetheless, it was proven that sporozoites in SGs possess heterogeneous developmental features, and it was assessed that sporozoite infection in SGs influences the proteome of the organ, highlighting how the interaction between the parasite and this body compartment is most probably complex and multifaceted (Ruberto et al. 2021; Choumet et al. 2007). In addition, the transcriptome of female SGs presents a daily circadian cycle, most probably associated with supporting the nocturnal activity of the mosquito. This finding was combined with evidence that the gene expression of colonizing sporozoites also possesses a rhythmicity, involving, among others, genes with a role in motility and being potentially implicated in parasite transmission, putatively cross-talking with the daily changes in the SGs environment (Bento et al. 2025).

In *Anopheles* it has been shown that mating increases susceptibility to *P. falciparum* infection (Dahalan et al. 2019), and that the accomplishment of a healthy oogenesis is positively correlated to *P. falciparum* infection intensity due to a regulation of lipid accumulation processes, suggesting that the parasite has evolved a non-competitive strategy for exploiting resources available within its vector (Werling et al. 2019). In addition to this, low *Plasmodium* infection loads have been associated with increased transcript abundance of genes associated with olfactory acuity and a range of synergistic processes that have been suggested to lead to increased fitness based on both anti-aging and reproductive advantages, preserving the mosquito's vectorial capacity (Carr et al. 2021). In disagreement with these results, multiple studies have associated *Plasmodium* infection with a decreased fitness in *Anopheles* species (Hogg and Hurd 1997; Hurd et al. 2005; Alout et al. 2016; Shaw et al. 2022), and the possible conflicts emerging from contrasting fitness needs of the parasite and its vector have been analyzed since the 1980s in the light of the extended phenotype hypothesis.

The parasitic manipulation hypothesis

«Now, here, you see, it takes all the running you can do, to keep in the same place, if you want to get somewhere else, you must run at least twice as fast as that!»

Leigh Van Valen from Lewis Carrol, "Through the Looking-Glass, and What Alice Found There", 1871

«The rabbit runs faster than the fox, because the rabbit is running for his life while the fox is only running for his dinner».
Richard Dawkins and John Krebs, the "life-dinner principle", in "Arms races between and within species", 1979

«An animal's behavior tends to maximize the survival of the genes "for" that behavior, whether or not those genes happen to be in the body of the particular animal performing it».
Richard Dawkins, Central Theorem of "The Extended Phenotype", 1982

In the 1980s, the ethologist Richard Dawkins formulated the concept of "extended phenotype". He stated that it is an extended phenotype of an organism any effect associated with the corresponding DNA sequence that is manifested by an organism whose cells do not contain that gene, or even that simply extends beyond an organism's body to encompass the organism's behavior and the consequences of that behavior (like a beaver's dam is for the beaver). Consequently, each one of such traits that is produced to some extent by an organism, and that enhances such an organism's fitness is to be considered a phenotype of this organism (Dawkins 1982, 1990, 2004).

Extended phenotype effects obviously come into play in parasitic interactions, when parasites and hosts are involved in an "arms race" to increase their own fitness. Multiple examples of extended phenotypes and behavioral manipulations are renowned among parasitic interactions, due to the remarkable ability of parasites to evidently alter the behavior, physiology, or appearance of their hosts in ways that directly benefit the parasite, often at significant cost to the host (Ataev et al. 2013; de Bekker 2019; Mangold et al. 2019; Abdulai-Saiku et al. 2021). When the manipulation phenotypes are not obvious or subtle, behavioral manipulation is particularly tricky to sort out. First it must be proven that a behavioral phenotype, which is a complex phenotype, is the result of the presence of the parasite. Second, it must be proven that this particular phenotype significantly increases parasite fitness (Reeve and Sherman 1993).

Insects' hematophagous behaviors have always been exploited by pathogens as a means to gain access to new hosts (Powell 2019). In the field of vector-borne diseases, the understanding of vector-parasite interactions is pivotal for disease control. The hypothesis that human pathogens can manipulate their vector's

behavior has persisted for decades (Koella and Packer 1996; Moore 2002; Jackson et al. 2012). The most striking manipulation phenotypes currently known are not related to vector-borne diseases, as the ones associated with *Ophiocordiceps* fungi infection or with *Leucochloridium paradoxum*. In these cases, the infection effects and the manipulated behaviors are so evident, and distinctively associated to specific life cycle stages of the parasite, that specific studies could have been designed to observe or infer how these impact parasite fitness (Loreto et al. 2014; Wesołowska and Wesołowski 2014). Conversely, in most cases behavioral studies often lead to ambiguous or conflicting results. This adds up to the fact that studies on such phenomena in wild populations, linking behavioral alteration and actual transmission in the field has yet to be fully demonstrated (Clements 1999; Ferguson and Read 2002; Cator et al. 2012; Robinson et al. 2018). Several factors contribute to this, and may involve the complexity of the examined behavior, the fact that the behavioral response to any insult or cue can be very subtle, and the fact that very subtle cues, difficult to control for, might lead to behavioral responses, a difficulty in foreseeing the behavioral consequences of specific conditions, or a combination of them. In such complicated experimental set ups, the variables influencing experimental outputs can be both the desired ones, of which the consequences are intended to be investigated, but they could also be some under-appreciated environmental factors, intrinsic to the experimental environment, in which hidden variables can linger and influence the experimental results (reviewed in Butler-Struben et al. 2022). However, to my knowledge no specific insect gene related to the onset or performance of manipulated behavior has been identified in the vector-borne parasitic interactions, and no loss-of-function study has been carried out on specific targets to confirm their involvement in increasing the fitness of the parasites.

Whether behaviors specific to infected mosquitoes exist, whether they facilitate disease transmission, and whether the parasites can actively manipulate such behaviors in order to increase their fitness is still a matter of debate (Table 1).

Table 1. Summary of setup and results of studies examining the effects of malaria infection on mosquito behavior. Divided by infected organisms; in chronological order of publication. HMBPP: (E)-4-hydroxy-3-methyl-but- 2-enyl pyrophosphate.

			Infected mosquito			
experimental setup	**mosquito species**	**parasite species**	**mosquito-parasite pair**	**feeding host (target for the parasite)**	**main findings**	**doi**
laboratory	*Ae. aegypti*	*P. gallinaceum*	natural	guinea pig (not natural)	increased intradermal probing time	10.4269/ajtmh.1984.33.17
laboratory	*Ae. aegypti*	*P. gallinaceum*	natural	guinea pig (not natural)	increased biting rate and reduced fertility	10.4269/ajtmh.1986.35.277
laboratory	*An. gambiae*	*P. bergei*	not natural	rat (natural)	no effect on biting behaviour	10.1111/j.1365-2915.1992.tb00036.x
laboratory	*An. gambiae s.l.*, *An. funestus*	*P. falciparum*	natural	hamster (not natural)	increased biting attempts, probing, for longer	10.1017/s0031182000066348
natural environment	*An. punctulatus*	*P. falciparum*, *P. vivax*	natural	human (natural)	increased feeding at night	10.1017/s0031182000066348
laboratory	*An. stephensi*	*P. yoelii*	not natural	human (not natural)	feeding persistence decreased at oocyst and increased at sporozoite infection stage	10.1098/rspb.1999.0839
laboratory	*Ae. aegypti*	*P. gallinaceum*	natural	human (not natural)	blood volume threshold to inhibit host seeking lowered at oocyst and increased at sporozoite infection stage	10.1093/beheco/13.6.816
laboratory	*An. gambiae*	*P. bergei*	not natural	none	12 overrepresented proteins in the infected mosquito brain	10.1002/pmic.200601021
laboratory	*An. gambiae*	*P. falciparum*	natural	human (natural)	increased attraction to human odour	10.1371/journal.pone.0063602
laboratory (but use of sympatric isolates)	*An. coluzzii*	*P. falciparum*	natural	human (natural)	no effect on either long- or short-range attraction	10.3389/fevo.2015.00086

(continued)

			Infected human			
experimental setup	**mosquito species**	**parasite species**	**mosquito-parasite pair**	**feeding host (target for the parasite)**	**main findings**	**doi**
semi-natural	*An. gambiae*	*P. falciparum*	natural	human (natural)	increased attractiveness for children harbouring gametocytes	10.1371/journal.pbio.0030298
laboratory	*An. darlingi*	*P. vivax*	natural	human (natural)	synergistic effect of fever and gametocytes in increased host attractiveness	10.1186/1756-3305-7-251
laboratory	*An. coluzzii*	*P. falciparum*	natural	human (natural)	different skin odour between infected and not infected participants; contrasting results for mosquito attraction	10.1038/s41598-017-08978-9
laboratory	*An. gambiae*	*P. bergei*	not natural	human (not natural)	apyrase activity decreases as the sporozoite load increases; mosquitoes with lower apyrase activity take up less blood, making it more likely that they would feed again	10.1371/journal.pone.0063602
field	*Anopheles* spp.	*Plasmodium* spp.	natural	natural	human blood more present in sporozoite-infected mosquitoes	10.24072/pci.evolbiol.100057
laboratory	*An. gambiae*	*P. falciparum*	natural	human (natural)	in response to human odour mosquitoes carrying sporozoites were more active, shifting activity periods which corresponded with human host availability	10.24072/pci.evolbiol.100057
			Infected bird			
experimental setup	**mosquito species**	**parasite species**	**mosquito-parasite pair**	**feeding host (target for the parasite)**	**main findings**	**doi**
laboratory	*C. pipiens*	*P. relictum*	natural	mice (not natural)	infected birds more attractive	10.1111/ele.12041

(continued)

			No infection			
experimental setup	**mosquito species**	**parasite species**	**mosquito-parasite pair**	**feeding host (target for the parasite)**	**main findings**	**doi**
laboratory	*An. gambiae*	*P. falciparum*	natural	human blood (not natural)	attractiveness of HMBPP produced by *Plasmodium*	10.1126/science.aah4563
laboratory	*An. gambiae*	*P. falciparum*, *P. ovale*, *P. malariae*	natural	human (natural)	*Plasmodium*-induced aldehydes enhanced the attractiveness of a synthetic human odor blend	10.1073/pnas.1721610115
semi-natural	*An. arabiensis and An. pharoensis*	none	none	human (natural)	baits with HMBPP-induced odour blend attracted more mosquitoes	10.1186/s12936-020-03378-3

Multiple studies and meta-analysis showed that establishing firm generalities on the topic is not possible, evidencing that the vector-parasite binome in exam and the organisms' age play a role in the impact of infection on the insect vectors (Ferguson and Read 2002; Lambrechts and Scott 2009). Contrasting results have been gathered on the subject since the 1980s. For example, not surprisingly parasitic infection can lead to reduced mosquito survivorship and/or fertility (Dawes et al. 2009; Pigeault and Villa 2018; Johnson et al. 2020). In other cases, not only it had a low burden in terms of fitness costs for the mosquito caused by infection, but also guided an interplay benefiting both actors (Carr et al. 2021; Shaw et al. 2022).

Cator and colleagues identified clear examples of what can be recognized as parasitic manipulation in infected mosquitoes and what is instead a behavioral output resulting from an ongoing immune response (Cator et al. 2013). For instance, they showed that, compared to mosquitoes challenged with heat-killed bacteria or with injury, oocyst-infected mosquitoes manifested a decreased attraction to one of the main components of human odor (1-octen-3-ol), whilst sporozoite-infected mosquitoes had an increased attraction to this compound. This might have a biological relevance considering that parasites not yet developed to be transmitted (oocyst stage) could profit from reducing behaviors with an inherently high survival risk for the mosquito, later increasing the contacts with humans when infectious (sporozoite stage).

It is important to underline that co-evolution often leads to milder interaction effects in natural vector-pathogen combinations (Frischknecht et al. 2006). Cator and colleagues' study was done on the *P. yoelii - An. gambiae* vectorial binome, which is not considered to be naturally occurring. Multiple other studies have shown modification of *Anopheles* behaviors caused by a *Plasmodium* infection for natural binomes, in ways that increase contacts between vectors, parasites and hosts,, hence favouring parasite transmission (Hurd 2003; Lacroix et al. 2005). Specifically, increased responses to host odors, increased landing and higher volumes of blood intake have been demonstrated, and altered biting rate and duration have been evidenced in the *P. falciparum - An. gambiae* system (Rossignol et al. 1984, 1986; Li et al. 1992; Wekesa et al. 1992; Koella and Packer 1996; Koella et al. 1998; Anderson et al. 1999; Koella et al. 2002; Smallegange et al. 2013). This is not the only parasitic vectorial system in which this was observed. The same has been pointed out in the *Trypanosoma brucei - Glossina morsitans* vectorial system, responsible for the transmission of sleeping sickness (Jenni et al. 1980; Thévenaz and Hecker 1980; Van Den Abbeele et al. 2010). In both cases, it has been suggested that altered biting behavior is the result of reduced anticoagulation activity of the saliva, thus causing feeding impairment (Thiévent et al. 2019; Rossignol et al. 1984; Van Den Abbeele et al. 2010). Comparing and finding similarities between the parasitic infection effects in *An. gambiae* and in *G. moristans* is relevant considering the two vectorial systems are relatively similar, both made by a dipteran and a protozoan. Nonetheless, both insect and parasite species are distant from a phylogenetic point of view, the first belonging to the same order (Diptera) but different families (Culicidae and Brachycera), and the second belonging to different clades (*Plasmodium* belongs to Alveolata, and *Trypanosoma* to Discoba). Comparing them might be interesting considering that many cases of finely regulated manipulation of behavior applied by microorganisms on their arthropod vectors exist, some resulting in convergent behavioral phenotypes in phylogenetically distant species. An example of this are the Acanthocephalans *Polymorphus minutus* and *P. paradoxus*, and the trematode *Microphallus papillorobustus*, all inducing negative geotaxis and positive phototaxis in their crustacean hosts, thus increasing the crustaceans predation by aquatic birds, their definitive hosts (Bethel and Holmes 1973; Helluy 1984).

Multiple experiments evidenced enhanced attraction of *Anopheles* mosquitoes to a vertebrate host and a modified avidity to feed when infected with *Plasmodium* (Lacroix et al. 2005; Cator et al. 2012; Cornet et al. 2013; Batista et al. 2014; Busula et al. 2017; Emami et al. 2017; Stanczyk et al. 2017). Interestingly, a modified host preference skewed towards humans was suggested for the *P. falciparum* - *An. gambiae* combination, with the obvious consideration that mosquitoes that bite humans more frequently (anthropophilic behavior) are more efficient vectors, thus suggesting parasitic manipulation (Vantaux et al. 2015). This must be associated with the consideration that, while the malaria vector host range includes different vertebrate species, the same is not true for malaria parasites, which infect only one or a few vertebrate species (Costantini et al. 1999; Prugnolle et al. 2011; Rayner et al. 2011; Takken and Verhulst 2013; Perkins 2014; Ngoubangoye et al. 2016). In general, these studies showed behavioral alterations with trends compatible with an optimised disease transmission, and an increase of contact with the host, thus increased exposure to host-defensive behaviors, associated with sporozoite-infected mosquitoes, and vice versa to a low responsiveness to stimuli or increased avoidance for oocyst-infected mosquitoes: such behaviors are likely to increase parasite transmission (Schwartz and Koella 2001; Dobson 1988).

Behavioral transcriptomics

In the last decades, novel genetic techniques commonly referred to as “omics” have allowed the untargeted, collective characterization and quantification of pools of biological molecules within a biological system. Among these, the ones which are most directly linked to gene expression characterization are epigenomics, transcriptomics and proteomics.

Transcriptomics is the study of the structure, function, and change in time of the RNA transcript abundance of a given organism, or of a community of organisms, under specific circumstances. Typically, TFs concerted activity guides the activation of specific gene regulatory networks which drive and determine the cellular states (Reilly et al. 2020; Formicola et al. 2021; Pimmett et al. 2025). Gene regulatory networks can be explored with transcriptional approaches, and the cellular states associated with precise transcription profiles can be defined. Thus, currently,

transcriptomics is indispensable for understanding those processes leading from DNA-encoded information to proteins and/or to RNA regulatory particles, which are the main drivers in defining the physiological state of a cell.

The current project applied some of the most recent transcriptomics approaches, more specifically about bulk ribonucleic acid-sequencing (RNA-seq) from whole organ cell lysates, and single cell or single nucleus RNA-seq (scRNA-seq or snRNA-seq), capturing the transcriptional profile of single cells or nuclei, respectively. A detailed overview of these approaches is provided in the section "Next-generation sequencing (NGS) for transcriptomics" (page 49).

Connections between transcripts and behavioral phenotypes

The most prompt responses of an organism to a stimulus are (in order, based on onset timing after the stimulus): neurological (ion fluxes and action potentials, reflexes), cell signaling cascades, post-translational modifications and onset of protein-protein interactions (Qu and Vondriska 2009; D'Angelo et al. 2011). Nonetheless, gene expression can change rapidly and dynamically in response to both exogenous and endogenous stimuli: individual cells can readily tune the expression of thousands of genes, based on a dynamic interplay between epigenetic, transcriptional, and post-transcriptional processes that collectively determine the presence and abundance of messenger RNAs (mRNAs) and proteins (Orphanides and Reinberg 2002). Inside the same cell, some genes can be induced within minutes after a stimulus, while others show delayed expression, in the range of tens of minutes after the stimulus perception. Further, the transcription activation kinetics of a specific gene can vary depending on the ongoing stimulus, thus producing bursts of activity of variable entities across time (Molina et al. 2013; Aymoz et al. 2018).

It is worth emphasizing how the expression of a single gene can be responsible for dramatic changes in the dynamics of responses to a stimulus of a cell once it has been expressed. This is evident from thinking of the functioning and results of the empty-neuron technique, in which the expression of a single protein-coding gene is responsible for the firing of neurons after the perception of a stimulus to which those neurons were not responsive before, providing a clear functional link between a single receptor, its ligand, and animal behavior (Dobritsa et al. 2003; Hallem et al.

2004). The technique that was first used in *D. melanogaster* to "de-orphanize" odorant receptors: some were responsive to multiple compounds of the same chemical class, as for example to aromatic compounds, while some were finely tuned and responded to only one of the odor molecules tested, as Or22a (Hallem and Carlson 2006).

Transcriptional profiles do not respond only to acute stimuli, but can also be concertedly modulated to create a molecular background aiming to shape an organism's functions to satisfy life stage-specific or condition-specific needs which last for relatively long timespans, which can go from a few hours/days cycling processes, to the whole life of an organism. This means that variations in gene expression can have a programmed, defined onset and duration in an organism life cycle, and be long term shaped to make up a transcriptional network different from the one of previous stages, as it happens for growth and development (Wang et al. 2010; Song et al. 2023).

On account of what said above, for sure transcriptional studies allow us to gather a large amount of information and to have an overview of some of the earliest responses an organism produces after a stimulus. In addition to that, multiple studies wanting to get a better insight in behavioral mechanisms, have linked specific transcriptional profiles, or even expression of single genes, to the execution of given behaviors. Indeed, changes in brain gene expression can lead to modified or newly acquired behaviors (Ben-Shahar et al. 2002; Whitfield et al. 2003; Kruse et al. 2004; Burmeister et al. 2007; Cummings et al. 2008; Chandrasekaran et al. 2011; Rittschof et al. 2014; Mukherjee et al. 2018), but not only. Sometimes regulatory gene expression key to behavioral onset has been shown to originate in non-neural tissues. This is the case of *vitellogenin*-2, a gene encoding a glycolipoprotein precursor of egg yolk proteins, which is expressed specifically in the fat body in "young" *Ae. albopictus* after a sugar-meal, or in general after a blood-meal. It was shown that, compared to mosquitoes in which such gene expression was perturbed, sugar-meal and *vitellogenin*-2 physiological upregulation delayed host-seeking. If after being fed, RNA interference (RNAi) against the gene was performed, the mosquito resumed host-seeking behavior as if they did not receive any sugar meal (Klowden et al. 1987; Dittmer et al. 2019).

Transcriptional signatures have even been associated with general behavioral tendencies or personality traits (Sadoul et al. 2022). Similarly, triggering events like the perception of threatening circumstances have been shown to activate homologous gene regulatory networks across Metazoa phyla, programs enriched in TFs and developmental signaling genes (Rittschof et al. 2014; Saul et al. 2017). These fulfill the animals' need to learn and to adapt behavioral responses to adequately face the events of their environment. Involvement of developmental genes in such kinds of processes is intriguing in the light of the fact that gene regulatory networks determine cell states during development, the transition from a transcriptional profile to another being the force inducing the switch to a new cell state and with defined characteristics (Brackston et al. 2018). This means that understanding the gene networks underlying behavioral regulation and flexibility in insects can inform not only on how they adapt to changing environments, but it may also reveal general principles applicable to other animal classes (Harris and Hofmann 2014). Attempting to understand the connections between gene expression and behavior in insects is in fact sensible, considering how they exhibit a plethora of stereotypical interactions, both in solitary life styles and in aggregations with a complex hierarchy. Emerging technologies such as scRNA-seq and spatial transcriptomics allow for unprecedented insights into these processes. Indeed, comparative transcriptomic studies across insect species have revealed how changes in gene regulation contribute to the evolution of complex behaviors, such as sociality and division of labor. For example, brain cells can express genes necessary for caste specification in social insects (Zhang et al. 2022), an event that carries along a collection of well determined associated behaviors, strongly divergent among castes. Moreover, variable composition in cell types and their abundance was described among individuals of the same species not only among different sexes or castes: some data indicated that events triggering switches between life-cycle stages might induce cell type-specific proliferation in the brain of social insects, putatively linked to the organ reshaping and maturation. Indeed, in colonial ants, more than one third of cell types showed variations in abundance after the switch from virgin queens to inseminated queens, an observation based on single nuclei RNA-seq (snRNA-seq) data (Li et al. 2022). Despite indirect evidence, such quantification can be indicative

of processes of neuronal proliferation or death, considering how brain structures possess different shapes in such species when comparing sexes and castes.

Not only cellular composition, but also gene expression is linked to distinct behavioral patterns across Metazoa. For example, individuals belonging to social insects' castes whose life is dedicated to the execution of a determined set of tasks manifest specific gene expression programs in defined brain centers once they start fulfilling a given role (Mu et al. 2025). Similarly to the previous example, this showed how the brain and its gene expression can be linked to maturation through life-cycle stages. These transcriptional changes are foundational for modification of behavioral habits and responses, and influence and are influenced bidirectionally by all those factors contributing to maturation and life cycle progression. Intriguingly, a study on mice brain linked the sex-specific gene expression occurring in a defined cell type in the medial amygdala to opposing behaviors in either sex. The amygdala is particularly relevant in association to behavior since it is downstream in the path to integration of pheromonal detection, and is also involved in innate social behavior, at the same time showing sexual dimorphism. Especially the medial portion of the amygdala drives social behavior, and in males is activated by pup sensory cues or following infanticide (Tachikawa et al. 2013; Kohl et al. 2017). This area has been linked with altered parenting behaviors when damaged since more than half of a century (Fleming et al. 1980; Numan et al. 1993; Sheehan et al. 2001). In their study form 2019, Chen and colleagues showed that, when GABAergic neurons in mice medial amygdala were optogenetically activated at different intensities, males showed opposing behaviors (grooming/infanticide) in association to either low or high intensity activation levels, while females always performed the same behavior (similar levels of pup grooming at any intensity). Indeed, scRNA-seq data revealed a sex-specific transcriptional signature in these cells, and suggest that the differentially expressed genes may be involved in setting nonidentical activation thresholds for infanticidal versus parenting behavior in male or female cells by modulating a cell's excitability (Chen et al. 2019).

Analogously, a more recent study showed that a similar mechanism of transcriptional-behavioral states associations happens for processes involved in circadian control in a cell type-specific fashion in *Drosophila*. ScRNA-seq profiling of adult brains across sleep-wake cycles evidenced the strongest cell type-specific

transcriptomic changes take place in glia, whose gene expression also correlates with sleep homeostat and circadian clock. Eventually, when clock genes were disrupted specifically in glia, this impaired homeostatic sleep rebound, proving their involvement in the physiological functioning of sleep-wake cycles (Dopp et al. 2024). It is evident how transcriptomics is indeed a reliable approach to obtain a large amount of molecular data associated with behavioral performance, without the need of prior knowledge on the system's actors.

A few studies including proteomics and transcriptomics data from mosquito brains were produced in the last decade. They classically entailed obtaining bulk RNA-seq or proteomics data from pooling multiple brains, and mainly focused on working out the different molecular profiles of the brain between male and female mosquitoes, or comparing developmental stages or nutritional states, as these can reveal key features at the basis of mechanisms associated with disease transmission-related behaviors (Lefevre et al. 2007; Dwivedi et al. 2014; Tomchaney et al. 2014; Matthews et al. 2016; Dey et al. 2020; Das De et al. 2022). More recently, it was possible to understand mosquito brain transcriptomics with unprecedented granularity thanks to the development of scRNA-seq techniques. To date this kind of approach was used in two studies on mosquito brains only in *Ae. aegypti*. Cui and colleagues published in 2022 a first investigation of sex-specificity in the cellular transcriptomes of the brain in this species (Cui et al. 2022). In this study the authors manually identified and annotated some cell types in the mosquito brain by analysing the expression patterns of some *Ae. aegypti* genes ortholog to well known *D. melanogaster* genes whose expression characterizes specific cell types (which are also known as "marker" genes). The second study has been published as a pre-print this year by Goldman and colleagues (Goldman et al. 2025). In this work, the authors produced an snRNA-seq atlas obtained from the major body parts and organs of males and females *Ae. aegypti*, among which the brain, and also included data from brains dissected from females at different time intervals after a blood meal, identifying differential expression patterns characterizing specific cell types in the samples.

Advantages and challenges of behavioral transcriptomics

Investigation of transcriptional data from an organism's CNS can uncover the molecular mechanisms driving behavioral plasticity and adaptation, and capture how physiological and environmental factors (e.g., nutrition, hormones, social context, among others) interact with gene expression to shape behavioral outcomes. Understanding the molecular mechanisms underlying complex phenotypes such as behaviors is intricate both on a technical and on a logical basis. Controlling the factors that come into play in inducing the onset and guiding the performance of a given behavior is extremely complex. Elements that can be both exogenous and endogenous to organisms, such as interactions with conspecifics or interindividual genetic variability, can affect the organism's response to an event.

An inherent property of omics technology is to be used for exploratory purposes, gathering a big amount of information with a collective characterization and quantification of molecular constituents of the sample in exam. The molecular bases of behavioral phenotypes are still to be understood and defined almost completely, and untargeted transcriptomics studies are thus suitable for guiding further exploration. Nonetheless, establishing a causality relation between a behavior and specific transcriptional events requires further investigation and experimental validation. Importantly, behavioral information can both influence and be influenced by gene expression, creating feedback loops which can be challenging to disentangle (Robinson et al. 2008). Technical limitations also pose hurdles. RNA-seq techniques purposely aim to capture heterogeneity and temporal dynamics intrinsic in organic matter, a fact that makes the result interpretation laborious: which genes interact, which are the process' master regulators, which factors create inter-individual heterogeneity in the samples?

Nonetheless, transcriptomics allows for a genome-wide analysis of gene expression without the need of prior assumptions, a property that is particularly useful in non-model organisms, for which there is a high percentage of transcripts whose functional annotation is not verified due to lack of existing data, the function of which is, when possible, inferred by orthology. The fact that having precise molecular targets is dispensable in transcriptomics enables the identification of novel regulators and pathways underlying the condition or phenotype in exam. Nowadays, the advances in single-cell and spatial transcriptomics allow researchers

to resolve gene expression at the level of individual cells and/or specific brain regions, revealing how distinct cell populations contribute to behavior.

NGS for transcriptomics

At the beginning of the genetic sequencing era, in the 1970s, low throughput, low sensitivity technologies such as northern blotting were used to study gene expression, revealing target mRNAs with the use of radiolabeled or chemiluminescent probes. This was later replaced by more sensitive quantifications such as reverse transcription quantitative polymerase chain reaction (RT-qPCR), which anyway allowed focus on a low number of genes at the time. In the 1980s-90s, the development of expressed sequence tags libraries, of the serial analysis of gene expression technique, and of Sanger sequencing allowed for a more parallelized elaboration and analysis of untargeted genetic - i.e. DNA or complementary DNA (cDNA) - data, and for the identification and cataloging of expressed genes. Still, even the most modern Sanger sequencers can process only ninetysix DNA fragments of maximum 1 kb in parallel, taking from 20 minutes to up to 3 hours per DNA fragment. The microarray technique expanded the number of different mRNA sequences that could be explored in a given amount of time, but was still supporting a gene expression analysis of the targeted type. Despite not being a sequencing technique, microarrays laid the bases for some aspects of more parallelized and quick NGS approaches developed next. In general, NGS methods entail massive miniaturization and parallelization of the sequencing process, thanks to which millions of sequencing reactions take place in volumes of microliters and are completed in a few hours. Thus, while traditional approaches were limited by being low throughput and hypothesis driven, NGS is high-throughput and more unbiased.
Among NGS techniques, 454 pyrosequencing and Illumina/Solexa are based on the usage of generalistic oligos complementary to specific mRNA sequences, with Illumina being the market leader. Illumina sequencing is done on amplified cDNA fragments of around 300 base-pairs (bp), thanks to an approach that is defined as “sequencing by synthesis” (Fig. 5).

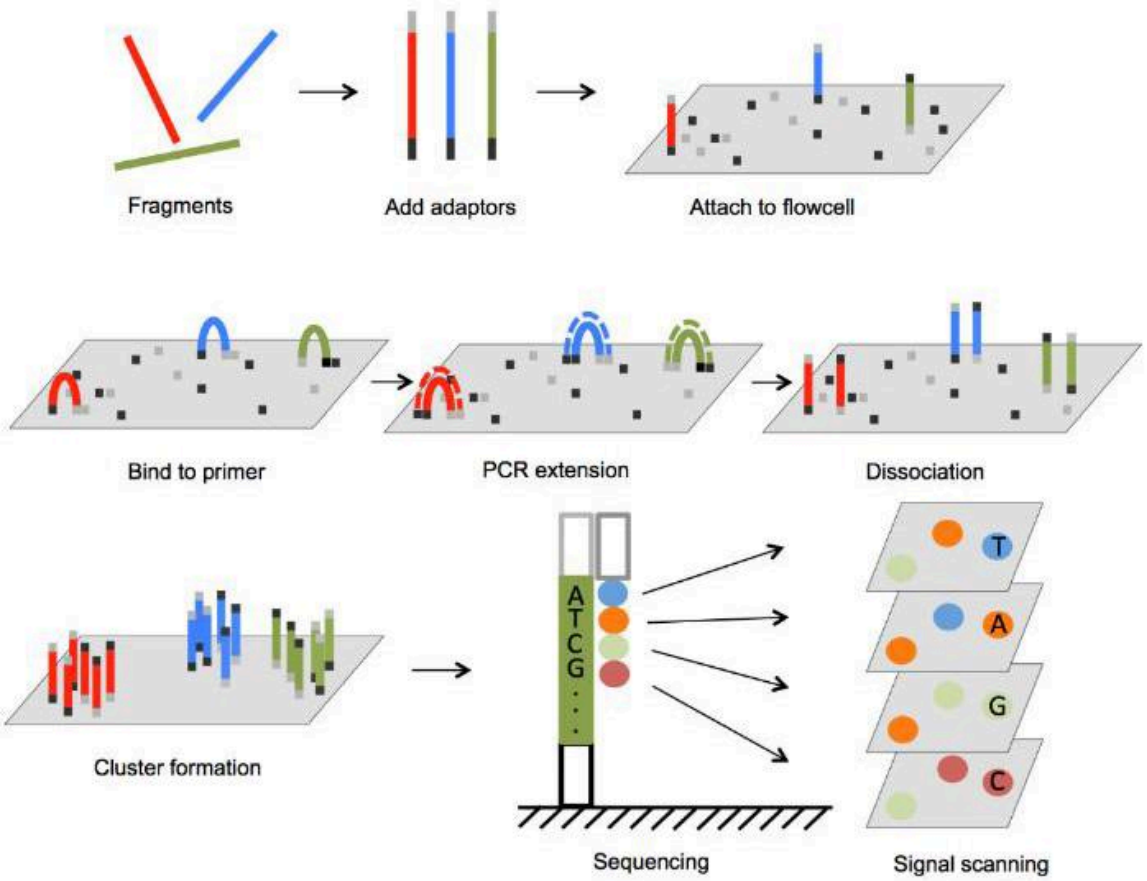


Figure 5. Illumina sequencing. For illumina sequencing, cDNA fragments are first ligated to sequences allowing the addition of sample indexes, synthesis primers and adapters for the binding to the sequencing flowcell. Thanks to initial cycles of amplification reactions of each cDNA fragment while it is still attached to the flowcell and undergoes what is called "bridge amplification", primed by sequences covalently bound to the flowcell, clusters of copies of each of the cDNA fragments form. After bridge denaturation to single nucleic acid chains, all four nucleotides, fluorescently labelled and blocked at their 3'-OH, are added at a time, with only one complementary nucleotide binding to each fragment per cycle. Since each cluster is made of fragments having the same sequence, labelled nucleotide binding creates an amplified, clear signal that can be detected from each cluster of fragments, after which the just-bound nucleotides are unblocked and their fluorophore removed. Image source https://www.bmkgene.com/dnarna-sequencing-illumina-sequencer-product/.

Illumina reads can be sequenced from a single end or from both ends (respectively single and paired-end sequencing), the latter resulting in the most precise information for identifying the expression of the genes captured in the samples during read-mapping on the target genome. Illumina sequencing is fast, reliable and cost-effective, with the sole caveat that only short reads sequencing is possible due to increasing noise-to-signal ratio that increases throughout the sequencing

process due to imperfect nucleotide incorporation, incomplete fluorophore cleavage, fluorescent signal overlapping.
Today, the single molecule real time sequencer of Pacific Biosciences and the Oxford Nanopore sequencer allow for the sequencing of long reads, up to 20,000 nucleotides or 100,000 nucleotides, respectively. They thus enable the acquisition of full-transcript data, and the detection, for example, of multiple transcriptional isoforms arising from the same coding sequence. Compared to them, to this date Illumina maintains high accuracy, cost-effectiveness, throughput, and mature bioinformatics support, thus is still the sequencing method of choice (Lowe et al. 2017; Mohammad et al. 2023).

In the last decades, sequencing technologies have been combined with microfluidics, microbead-based and/or support functionalization approaches to obtain untargeted data from biological samples with the usage of generalistic capture sequences and molecular barcodes allowing discriminating signals coming from single molecules. This is the case of (i) bulk RNA-seq, capturing mRNAs in a sample, mostly using ployT-capture sequences, (ii) scRNA-seq, like 10X technology, combining the use of capture sequence-functionalized microbeads and microfluidics, and (iii) spatial transcriptomics, with a histological support functionalized with tightly packed capture and barcoding molecules.
Compared to bulk RNA-seq, scRNA-seq has more technical noise, dropout events, and data sparsity, which commonly reduce detection power and increase false positives. Bulk RNA-seq, instead, can benefit from higher sequencing depth and larger RNA input, leading to more consistent gene detection and robust expression quantification, while scRNA-seq often experiences low per-cell coverage and higher variance (Nguyen et al. 2023; Mohammad et al. 2023). Because of this, the two techniques can be used to gather complementary information: the high detection power of bulk RNA-seq and the high resolution of scRNA-seq data can reveal a highly detailed and informative picture when they are applied to investigate the same conditions.
Bulk RNA-seq, but also scRNA-seq approach, is well established in insects. Spatial transcriptomics, instead, has been successfully applied multiple times in mammals (Fan et al. 2023; Lebrigand et al. 2023; Russell et al. 2024). A similar approach was

applied by Janssens and colleagues, who performed a highly multiplexed targeted ISH in *Drosophila* (Janssens et al. 2025), but for the moment only one study has been published containing proper spatial transcriptomics performed on insects (this year from Mu and colleagues in honeybees brain) (Mu et al. 2025).

Bulk RNA-seq

Different RNA-seq approaches allow the collection of different types of data, in particular in terms of comprehensiveness and of degree of resolution of the information we obtain. Bulk RNA-seq approaches can measure the average gene expression either across a population of cultured cells, or within a tissue or an organ. This procedure can lead to large amounts of material collected (up to 50-100 mg), to the detriment of recording signal granularity within the tissues in exam. For very small organs as insect brains, those amounts are reached by pooling the same type of tissues or organs from multiple individuals. To give an idea of why this is needed, on average a *Drosophila* weighs around 90-100 mg, and the weight of the brain of a *Drosophila* makes up only a small part of head soft tissue (approximately 14% dry weight) (Karan et al. 1998; Akhund-Zade et al. 2021; Posey et al. 2001). In comparison, the head of *Anopheles* mosquito can be even smaller, with a volume of around 0.7 mm^3, and a head width of around 0.77 mm, while the head width of *Drosophila* is around 0.9 mm (Coetzee et al. 2013; Tsila et al. 2021; Norry et al. 2000; Norry and Gomez 2017).

Fortunately, recent improvements in sensitivity of RNA-seq techniques allowed the application of bulk RNA-seq on very small organs or tissues, as those of insects, or even on single cells (Picelli et al. 2014). In this thesis project, we wanted to obtain single brain transcriptomes from *An. gambiae* females: for this reason, we chose the low-input Smart-seq2 protocol, which will be thoroughly explained in chapter 1 (page 92) and in chapter 2 (page 148). Here, I will give a short overview of the rationale of the molecular mechanisms the techniques entails. Smart-seq2 protocol includes the use of an RNA transcriptase exhibiting terminal transferase activity, such that the enzyme will “fall” once it reaches the 5' end of the transcript, only after adding cytosines to the growing strand. This happens both as the 7-methylguanosine at the cap site is reverse transcribed to cytosine residues, and also during the RT additional nucleotides (predominantly cytosines) are added at the

3' end of the newly synthesized cDNA in an untemplated manner (Fig. 6A). Afterwards, Smart-seq2 implies the use of a primer having ribo-guanosine residues at its 3' that bind to the cytosine overhang at the 3' end of each first-strand cDNA that has just been newly synthesized. In this case, this is a locked nucleic acid template-switching oligonucleotide (LNA-TSO) and allows synthesis of the second-strand cDNA for each transcript in the same reaction as the first-strand. Compared to unlocked nucleic acids, LNA have enhanced annealing strength to the untemplated 3′ extension of the cDNA (Petersen and Wengel 2003; Ballantyne et al. 2008). With this system, an adequate RNA polymerase can jump back on and transcribe the second-strand cDNA when the cytosine overhang has been synthesized and the LNA-TSO has bound to it (meanwhile substituting the original template with DNA) (Hirzmann et al. 1993; Schmidt and Mueller 1999). Such cDNA is then amplified using only one primer (called ISPCR primer), complementary to the edges of both strands (Fig. 6A). During sequencing library creation, the amplified cDNA undergoes enzymatic shotgun tagmentation with the use of a Tn5 transposome. In addition to fragmenting the cDNA in shorter sequences, transposomes inherently insert oligo-tags at the locations where they perform double strand breaks (Goryshin et al. 1998) (Fig. 6A). The tag sequences are used as partial adaptor sequences and can be recognized by index PCR primers, plus work in ligation to Illumina platform for amplification.

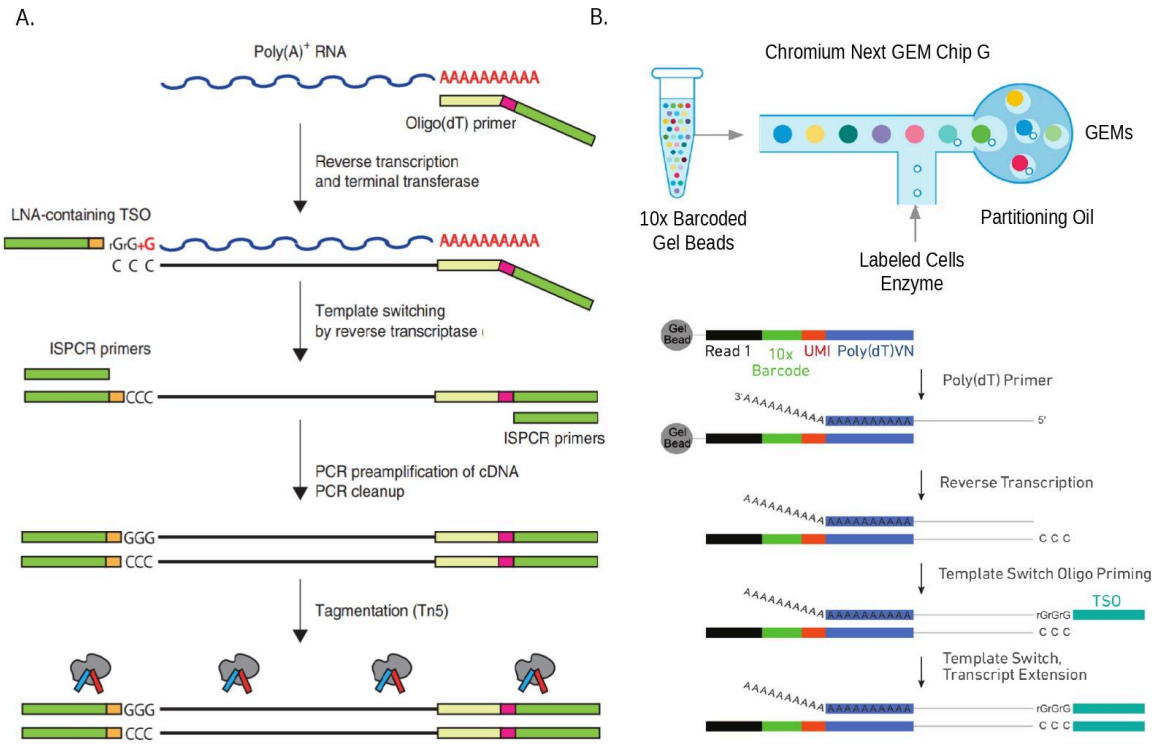


Figure 6. The low input RNA-seq technologies of the current study. (A) Workflow for Smart-seq2 RNA isolation and sample preparation for library processing. Image adapted from Picelli et al., 2014 (Picelli et al. 2014). **(B)** Workflow for 10x Chromium Next GEM Single Cell 3' RNA isolation and sample preparation for library processing. Image adapted from 10x 3' RNA isolation manual.

In the light of the above, applying bulk transcriptomics and scRNA-seq on the same sample types and conditions allows for insightful inferences.

ScRNA-seq and snRNA-seq

The first scRNA-seq approach was developed less than 20 years ago, and since then, wet lab and in silico approaches to obtain and analyze such a type of data have flourished (Tang et al. 2009; Shapiro et al. 2013; Schwartzman and Tanay 2015; Gawad et al. 2016; Tanay and Regev 2017; Stuart and Satija 2019; Labib and Kelley 2020; Tarashansky et al. 2021; Huang et al. 2023). This has happened because scRNA-seq, as well as snRNA-seq, allows the study of transcriptional profiles of individual cells, while bulk RNA-seq provides expression profiles that are averages of those of heterogeneous cell populations. Single-cell methods have been proven to capture specific cell responses and rare cell types, allowing the description of transcriptional signals with unprecedented precision, as it was well proven in cancer research (Guruprasad et al. 2021; Longo et al. 2021; Quek et al. 2021). Also, to some

extent, interacting cells can exhibit transcriptional profile similarities, and scRNA-seq can thus capture the hierarchical organization of organs with complex structures, such as the nervous system, without prior biases (Moffitt et al. 2018; Northcutt et al. 2019).

Different scRNA-seq approaches exist, which can be categorized by core technology: (i) plate-based approaches, both well- (e.g. Smart-seq2, MARS-seq), and microwell-based (e.g. BD rhapsody); (ii) droplet-based, also called emulsion-based, techniques (e.g. Drop-seq, 10x Genomics Chromium); and (iii) combinatorial indexing approaches, based on barcoding without physical isolation (e.g. Parse Biosciences RNA-seq); among others (Jaitin et al. 2014; Kumar et al. 2018; Macosko et al. 2015; Zheng et al. 2017; Cao et al. 2017; Ziegenhain et al. 2017).

Compared to snRNA-seq, scRNA-seq can capture the entire transcriptional profile of a cell, while snRNA-seq is limited to the transcripts that have not been exported from the nucleus yet. In particular, 10x Chromium Next GEM Single Cell 3' protocol workflow allows targeting the transcripts poly-A tail for capture and copying the transcripts into cDNA from the 3' end. While also a newer version of the kit targeting the 5' end is available, the 3' targeting kit is more established for broad gene expression profiling.

Tissue dissociation into single cells can be done by a combination of enzymatic and mechanical means, typically degrading the connective tissue present (e.g. with collagenases and dispases), and by gently shaking/pipetting the sample to aid the process. After dissociation, the cell suspension needs to be filtered to remove clots and debris, and then library preparation can start. 10x library preparation is droplet-based, which means that single cells are partitioned into nanoliter-sized droplets along with barcoded beads and lysis reagents using a microfluidic system (Fig. 6B). In 10x protocols, this is done by partitioning cells into droplets called “Gel Beads-in-emulsion” (GEMs). These statistically contain only one cell, together with RT-PCR reagents and a 10x barcoded bead. The latter are hydrogel beads, each one embedded with large numbers of DNA oligonucleotides with identical sequence setup. These contain a capture sequence (poly-dT for 3' capture) to specifically hybridize with mRNA transcripts, a bead-specific barcode sequence (the “10x barcode”), and unique molecular identifiers (UMIs). UMIs are indeed specific for each

of the sequences attached to a bead, and will later allow the identification of cDNA coming from one specific transcript. 10x barcodes instead, being common to all the sequences attached to a bead, deliver the same, univocal barcode to all the transcripts present in the cell that was included in a given GEM. If cell doublets happen to be captured by GEMs, they could be evidenced and excluded during the downstream bioinformatic processing. After GEMs are formed, these create an isolated in-solution PCR reaction microenvironment, where single cells can be lysed and cDNA produced similarly to how it was explained above for Smart-seq2 (Fig. 6B). Once cDNA is produced, GEMs can be dissolved and cDNA amplified, then fragmented, adapters ligated and library preparation completed for NGS.

Project rationale: insight into the female *An. gambiae* brain structure, composition and function

As of today, there is limited anatomical and functional characterization of the *An. gambiae* brain, and information on cellular composition of the organ is even more scarce. A small number of scRNA-seq datasets has been gathered in *An. gambiae*, and focused mainly on its immunity (Severo et al. 2018; Raddi et al. 2020; Kwon et al. 2021). Indeed, only a few genetic cellular markers have been identified for the nervous system of species, which have been investigated in peripheral organs in the context of olfaction-related studies, and identify subsets of OSNs in head olfactory organs (reported in Giraldo et al. 2024). The few transcriptomics and proteomics studies on the *An. gambiae* head have revealed sex- and life stage-specific molecular profiles, but no study has examined specifically the adult brain transcriptome without including other head organs in the same samples (Lefevre et al. 2007; Dwivedi et al. 2014; Tomchaney et al. 2014; Dey et al. 2020; Carr et al. 2021). This information can not provide sufficient understanding of brain-specific functions related to behaviors, blood-feeding cycles and response to environmental stimuli, despite the molecular tools currently available could be applied for the aim. Indeed, integrated omics such as scRNA-seq and spatial transcriptomics studies have started being used for this purpose in other biological backgrounds in the recent years, and the detailed molecular profile of brain structures in insects and mosquitoes has just started being explored (Davie et al. 2018; Zhang et al. 2022; Li et al. 2022; Cui et al. 2022; Goldman et al. 2025; Mu et al. 2025).

The main purpose of the current project is to describe for the first time the cellular composition of the *An. gambiae* brain. We pursue investigating the contribution of specific cell populations to organ biology across different physiological states. Transcriptomics is our method of election to detect molecular responses triggered in the brain by key life cycle events, namely mating and blood meal. The project envisaged the production of multiple datasets and the application of techniques almost exclusively focused on investigating transcriptional statuses (e.g. bulk and

scRNA-seq, and RNA fluorescence *in situ* hybridization (ISH), among others). The final objective was to establish a brain atlas resource providing a robust foundational reference framework that can pave the path for future investigations into the neural and molecular mechanisms underlying mosquito physiology, behavior, and vectorial capacity.

Integrating *de novo* neuroanatomical, transcriptomic and functional data to reveal brain characteristics was fundamental for us, considering that there is basically no molecular information available on cell lineages of the organ in exam. Instead, separately applying different transcriptomics techniques would have led to weak inferences. For instance, we can rely on the knowledge on *D. melanogaster* cell types to improve scRNA-seq data obtained from *An. gambiae*, but the identification of *An. gambiae* cell types putatively homologous to *D. melanogaster* ones based on transcriptional profiling alone would leave considerable doubts on the reliability of the inferred cellular identity. This deduction would instead gain considerable robustness if coupled with an histological investigation through ISH or spatial transcriptomics, allowing the identification of *bona fide* cellular markers.

Another central point which the study aimed to clarify is how processes related to blood feeding onset and performance are regulated in the mosquitoes' CNS. Mosquito behavioral traits are complex phenotypes with relevant impact on disease transmission levels. The most relevant in this sense are the processes that lead to host recognition and blood feeding, since the latter is the behavior thanks to which female mosquitoes get infected and subsequently transmit the infection. In addition to these, other processes and associated behaviors are linked to the search for a blood meal. As blood uptake is pivotal for egg-laying, this means that blood uptake is strongly connected to the fulfilment of the reproductive function. Mating happens once in a female mosquito's lifetime. For the females of anautogenous species, as *An. gambiae* is, the first blood uptake is tightly bound with the mating event, more strongly than for autogenous females (Townson 1993). Thus, understanding how physiological succession of adult life cycle stages influences brain transcriptional profile, and how genetic programs get switched on and off, either triggering or being triggered by specific key life cycle events, was fundamental for us, especially in relation to the events leading to blood uptake. This meant aiming to collect

information that goes further than identifying the triggering stimuli collected by the peripheral sensory organs and pinpointing the cells that transmit the sensory information guiding mosquitoes towards a host, thus we aimed to gather data to clarify the underlying molecular actors. To date, only one pre-print study associates the expression of two brain neuropeptides to the regulation of blood feeding behavior (Bansal et al. 2024). Our data have the potential to improve the understanding of such processes, for example identifying the expression of genes that can be specifically associated to a blood seeking physiological background (i.e., a mated, blood-deprived mosquito), currently subject of genetic knock-down (KD) assays and associated behavioral studies.

Last, we were curious whether with fine transcriptional approaches we would be able to identify gene expression patterns in the mosquito brains that would help us understand if and how *P. falciparum* can manipulate their behavior. We envisaged that analyzing information coming from different infection stages would have helped recognize putatively manipulated molecular triggers for blood feeding, that could then be proven with further experiments (for example, KD of some candidate genes found to be involved in the process).

In my opinion, all the aforementioned knowledge gaps on behavioral regulation evidence the need to start tackling the study of such processes from an original point of view. Instead of analyzing the influence of some chosen factors or triggers on the animal behavior, we thus chose to expand our background knowledge and to apply a bottom-up approach. We started by associating molecular profiles to specific physiological or pathological states, that could allow inference on which process could putatively guide life stage-associated behavior. After having pinpointed some molecular profiles of interest, we could then have the possibility of interfering with them and see if this affects the animal behavior. We thus planned (i) to describe the influence of the mosquito adult development on the molecular profile of the brain, supported by both bulk, scRNA-seq, and spatial transcriptomics data, and (ii) to investigate whether *P. falciparum* parasites can influence a mosquito brain transcriptional landscape.

In this project multiple experimental approaches were optimised to deal with the mosquito brain organ, maintain its integrity and gather comprehensive molecular data from it.
To have an evolutionary perspective of vector-parasite interaction, the initial planning also envisaged studying the *G. morsitans* - *T. brucei* vectorial system with the same means, and to compare the resulting transcriptional phenotypes to the ones gathered in the *An. gambiae* - *P. falciparum* system. This would have allowed to establish the presence of evolutionary convergence of (putative) proximate manipulation mechanisms in the two vectorial systems mentioned. This attempt that would have brought valuable insights into vector-parasite systems evolution and evolutionary convergence of transmission phenotypes was unfortunately hampered by technical drawbacks (page 93).

In conclusion, by integrating neuroanatomical, transcriptomic, and functional data to reveal brain specialization and plasticity, the project aimed to create a detailed mapping and comparative analysis of an insect vector brain structure and composition. This potentially paves the way to uncover neural correlates of key behaviors influencing vectorial capacity and transmission dynamics that may open the way towards novel vector control strategies targeting neural circuits that mediate host-seeking and feeding in the *An. gambiae* female brain. With our data, we aim to pinpoint neural gene expression regulators linked to brain function and changes in behavioral tendencies (e.g., pre- and post-blood-feeding behaviors), whose role could then be confirmed by coupling gene KD and *ad hoc* behavioral studies to identify molecular pathways underlying attraction to blood sources and sensory processing. The project's ultimate goal is to provide the molecular and biological canvas to which a vector insect's behaviors could be mapped and understood, supported by an extensive data collection and integration of multiple transcriptional datasets and techniques, with a substantial increase in the knowledge about molecular architecture of the brain of insect vectors.

Chapter 1: Optimizing methods to prove mechanisms supporting insect behavior

Mosquito brains are relatively complex organs made of multiple functional regions and inferred containing tens or hundreds of cell types, in a volume of less than 1 mm^3. Anatomical microdissection of this organ is performed manually with the help of sharp steel forceps and a stereomicroscope, practice which requires exercise and extreme precision. As the chitin of the head exoskeleton is exceptionally thin and fragile, and more closely interacting with the underlying soft tissue, compared to insects of comparable size as *Drosophila*, facts that make mosquito brain dissections remarkably difficult (empirical observation), a precise protocol was developed for their dissection. During my thesis studies, I optimised and implemented multiple transcriptomics methods to study the *An. gambiae* brain, encompassing female *An. gambiae* brain dissection, and form this organ produced (i) multiple bulk RNA-seq and scRNA-seq, ISH information from 7 different target genes, (ii) started optimising multiple procedures among which those to investigate cell proliferation, or obtain snRNA-seq data, and (iii) chose targets and performed the initial set up of genetic KD experiments. The study included the integration with spatial transcriptomics data (page 119).
Such methods are either consolidated for decades in multiple systems (e.g. bulk RNA-seq), or have been applied successfully in other species (as scRNA-seq or ISH), with the most relevant data collections gathered from model organisms (among others Croset et al. 2018; Davie et al. 2018; Yao et al. 2023). Thanks to the recent development of algorithms able to compare cellular profiles intra- and inter-species, the knowledge on model organisms could be transferred quickly and collectively to non-model organisms (Kiselev et al. 2018; Tarashansky et al. 2021; Styfhals et al. 2022).

A few scRNA-seq datasets have been collected in *Anopheles*, specifically in *An. gambiae*. They defined the cellular composition of the hemocyte population,

germline cell types and the midgut and its interaction with *P. falciparum* infection (Castillo et al. 2006; Raddi et al. 2020; Kwon et al. 2021; Page et al. 2023; Yan et al. 2024). Data specifically investigating brain transcriptomics of *An. gambiae* were absent. Each organ carries along a peculiar set of technical hurdles when it comes to study it, and we could rely on just a few scRNA-seq studies have been carried out on insect and especially insect and mosquito brains (Croset et al. 2018; Davie et al. 2018; Traniello et al. 2020; Simon and Konstantinides 2021; Cui et al. 2022; Li et al. 2022; Janssens et al. 2022; Ju et al. 2023; Wang et al. 2024; Mu et al. 2025).

The insufficient understanding of how gene expression varies in the *An. gambiae* brain throughout the mosquito life cycle and *Plasmodium* infection stages is a gap that the current study filled. The data presented in this thesis represent a huge leap from the previously poor knowledge about the *An. gambiae* brain. The work performed to obtain and annotate the scRNA-seq brain atlas based on cell type homology with *D. melanogaster*, proved to be robust after confirmation of multiple cellular markers with ISH, and laid the basis for a deeper insight into bulk RNA-seq data, representing the most extensive cell type annotation of a mosquito brain. We applied multiple techniques to perform overall transcriptional profiling of the mosquito brain, successfully obtaining single cell transcriptomes and bulk RNA-seq data from single brains, and produced high quality histological preparations allowing successful ISH and spatial transcriptomics. We also attempted cell proliferation and evaluation of inter-species evolutionary convergence among different vectorial systems, and laid the basis for RNAi coupled to KD essays targeting mating-related events.

Biological material used in the project

An. gambiae mosquitoes

An. gambiae mosquitoes (kisumu strain (Shute 1956)) were reared at 27 °C± 1 °C and 70% ± 20% relative humidity (RH) and photoperiod of 12 h light/12 h dark in the Vectopole insectarium of IRD in Montpellier, France. Larvae were fed with grinded TetraMin (Tetra) powder and adult mosquitoes fed on 10% honey in water *ad libitum*.

P. falciparum cell culture

A *P. falciparum* NF54 strain was cultured in an automated tipper system under a continuous gas flow of 4% CO_2, 3% O2 and 93% N2. For gametocyte production, asynchronous cultures were started at day 0, with 1% parasitemia and 5% red blood cells, and harvested at day 15-16.

G. m. morsitans flies

G. m. morsitans flies were maintained in Roubaud cages at 26 °C and 60% hygrometry and fed every 2-3 days through a silicone membrane with fresh mechanically defibrinated sheep blood.

T. b. brucei cell culture

The *T. b. brucei* RED Tbb AnTat1.1E engineered strain was used (Calvo-Alvarez et al. 2018). It was modified by integrating a plasmid encoding for the chimeric triple reporter which combines the red-shifted firefly luciferase PpyREH9 and the tdTomato red fluorescent protein fused with a TY1 tag. Procyclic forms (PCF) were grown at 27 °C in SDM-79 medium supplemented with 10% (v/v) heat-inactivated foetal calf serum (FCS) and 8 mM glycerol (SDMG).

The dissection of a mosquito brain

The mosquito brain is a small and delicate organ. It has a volume of around 0.5 mm^3, and it is encased within a thin layer of chitinous exoskeleton, to which it is in tight contact (empirical observations). In female mosquitoes, two elongated, rod-like chitinous structures connect the anterior and the posterior part of the head, passing through the brain, which are not found in males (empirical observation for the *An. gambiae* species). These most probably reinforce the integrity of the mouthparts and head structure, which needs to resist the mechanical forces applied by the head muscles allowing blood feeding. These characteristics, associated with the fact that Dipteran esophagus is surrounded by their brain ganglia (Ito et al. 2014), make the dissection of a mosquito brain particularly challenging. This is different from fly brains, with both *Drosophila* and *Glossina* brains being more resistant to mechanical stresses (most probably due to higher presence of connective tissue in the organ), and less tightly in contact with the head exoskeleton (empirical observation).

Both bulk and scRNA-seq data collected in this project required careful dissection of this organ. It was possible for me to develop the know-how to do it not only successfully, but also quickly (5 minutes per brain), for hundreds of mosquitoes.

Brain dissection technique

A mosquito is put asleep by lowering the temperature of its environment to 0-4 °C (in a paper cup on ice). Once asleep, it can be moved from the cup to a glass slide under a stereomicroscope, with the help of entomological forceps. On the glass slide, we placed a droplet of ~ 50 µL of PBS just a few seconds before collecting the mosquito from the cup. The mosquito is put on the glass slide beside the droplet, and the head separated from the neck with the aid of two dissection forceps (Dumont #5), the tips of which must be put in contact to produce a clean cut. The head is then laid on the PBS droplet with the exposed soft tissue of the neck in contact with the PBS, to avoid tissue and cell death due

to lack of hemolymph perfusion. At this point, a small droplet of PBS can be partially separated from the main one with the aid of the side of the tip of the forceps, to create a system in which there is a main droplet, connected with a thin stream of PBS to a smaller one. The radius of the smaller one needs to be slightly bigger than a mosquito head one. This creates a spot where PBS can flow freely, but on which the mosquito head, covered in hydrophobic chitin, will not float. This condition is extremely helpful in maintaining the sample position and facilitating the dissection. The dissected head is thus placed on the smaller droplet by grasping it on the proboscis and palps, to avoid brain damage.

At this point, the brain dissection can start, and is done manually with dissection forceps under a stereomicroscope, for which I personally find the best suited magnification to be 4X. The operation must be performed quickly, in maximum 15 minutes from the first cut to the final isolation of the organ. The best approach is to remove the mouthparts and the clypeus after the entirety of the cheating surrounding the brain has been eliminated, since they are extremely helpful in handling the sample: they are connected to the pharyngeal pump, which passes through the mosquito brain, thus the sample can be held in place, moved, or its position adjusted with the lowest risk of damaging the brain.

As a first step, the antennae can be removed by grasping them with the forceps at the level of the Haller's organ. Then, small nicks can be performed on the top of the head, at the intersection to the brown chitin on the top of the head, and chitin can start to be removed by gently pulling it away. Usually, the posterior part of the head chitin can be removed pretty easily all at once after enough chitin has been removed from the top of the head. Eventually, the two chitinous rod-like structures that pass between the optic lobes and the central brain can be eliminated, the mouthparts, the clypeus, and the pharyngeal pump removed, and the dissection finalized (Fig. 7).

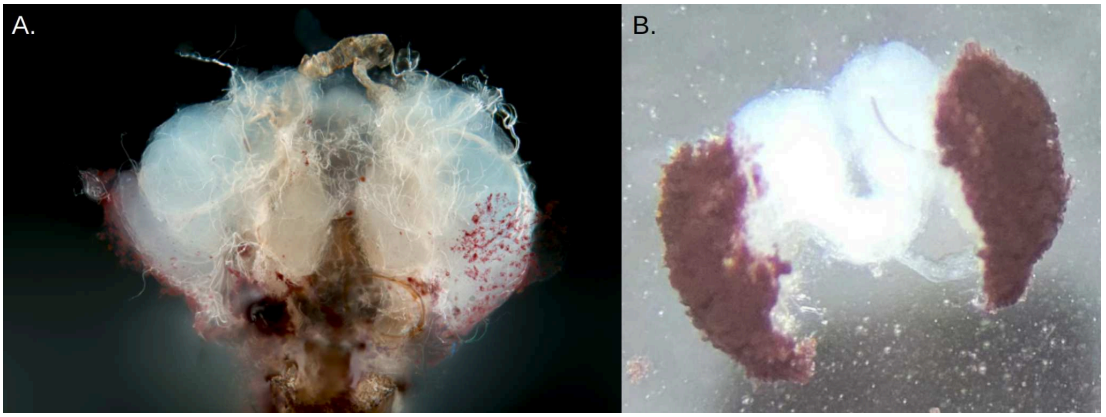


Figure 7. A manually dissected mosquito brain. (A) A high resolution image of a mosquito brain. The dissection is partially incomplete, leaving mouthparts to allow to keep the organ in place for a stack capture. **(B)** A completely dissected mosquito brain. A part of contaminant tissue used to handle the brain for the picture is visible as a white-translucent rod at the bottom of the organ. Images were taken with cameras that did not allow for a scale bar (see Fig. 14 page 104 for brain image with scale).

Pilot study to scale up snRNA-seq in insects to 1 million nuclei

One of the main aims of this project was to create a map of the cellular diversity in the *An. gambiae* brain: in addition to a scRNA-seq approach (page 76), we considered applying an snRNA-seq strategy. Compared to cell dissociation, nuclei extraction usually yields data from a higher number of cells in the samples, since it captures more sensitive and adherent cell types. In addition to this, it tends to induce less dissociation artifacts and can work on frozen and fixed samples. On the other hand, whole cells allow for capturing both cytoplasmic and nuclear RNA, providing a more complete picture of the cell's gene expression profile at the time of sampling. Including cytoplasmic RNA means that more genes per cell and more transcripts are detected overall, improving sensitivity for lowly expressed genes and rare transcripts. Generally speaking, cytoplasmic RNA reflects the current functional state of a cell and its responses to stimuli, stress, or environmental changes, making scRNA-seq more informative for studying active biological processes and cell heterogeneity. Nonetheless, snRNA-seq allows for more homogeneous samples and for a less-biased cell type recovery. Also, nuclear membrane should be more resistant to mechanical stresses than plasma membrane, with a more uniform composition and structure across different cell types and organisms (Agrawal and Lele 2019). This theoretically would make protocols for snRNA-seq optimized in other Eukaryotes to be more easily applied on an insect system.

Considering both single cell and single nucleus RNA-seq have advantages and disadvantages, we decided to attempt optimizing a protocol for single nuclei isolation from different *An. gambiae* body parts, and performed a fixation and a combinatorial barcoding and library preparation based on protocols and kits provided by Parse Biosciences (Seattle, WA, US). The approach allows to have a unique barcoding for samples, cells, and a unique molecular identifier for single transcripts, thus gene expression can be analyzed quantitatively for each of the experimental conditions and sample types in exam (Methods for snRNA-seq, Fig.

9A). This was mainly an attempt of scaling up the process to increase the amount of material retrieved: compared to 10x, Parse Biosciences library preparation would allow for a cheaper and faster way to obtain transcriptomes from hundreds of thousands of cells. We wanted to attempt producing a proof of concept that this snRNA-seq technique worked in our hands on a small scale (10,000 nuclei), with the final aim to then scale it up (up to 1 M nuclei) and obtain a rich dataset from different mosquito sensory organs (i.e., brain, antennae, palps, proboscis, legs), a goal that would be much longer and more expensive with a 10x approach.

Methods for snRNA-seq

Body parts (either heads, legs or antennae) were dissected from sugar-fed female *An. gambiae* of different ages (between 1 day and 4 weeks post-emergence). The difference in age was not accounted as a relevant variable during the protocol optimization, since it was attempted around three times a week for two months. This required large amounts of biological material, and we saw no influence of mosquito age on the number of nuclei retrieved during the experiments: so this approach was suitable for a feasibility study. A different number of mosquitoes was anesthetized on ice in order to obtain an adequate amount of biological material. Depending on body parts size and amount of soft tissue they contain, samples were isolated from: 30-55 individuals for head samples, 50-100 individuals for antennae pairs samples, 55 individuals for legs (all six were kept) samples. To test whether fresh samples can be stored before treatment, a collection of 55 heads was frozen in Sf-900TM III insect cell culture medium (Fisher 12568019) overnight and treated along with another one freshly collected.

Tissues were dissected in Dulbecco's PBS (DPBS) (Fisher 13492609) with the aid of a stereomicroscope and steel dissection forceps Dumont #5, and samples were isolated in a 1.5 µL lo-bind tube in a few hundreds microliters of ice-cold Sf-900TM III. Small chitinous tissues as legs and antennae were grinded with a pellet pestle in Sf-900TM III in the 1.5 µL tube in which they were isolated, then the partly-homogenized sample was transferred to a Dounce homogenizer.

Mosquito heads were directly transferred to a Dounce homogenizer. The tissues were then dissociated with a few tens of pestling and grinding strokes with a tight and/or loose Dounce pestle, followed by ~ 5 minutes of incubation on ice. The buffer used were either 2 mL of nuclei EZ lysis buffer (Nuclei Isolation Kit EZ Prep, Sigma-Aldrich), or 1 mL of homogenation buffer prepared as described by McLaughlin and colleagues for their single-cell transcriptomes of olfactory receptor neurons in *Drosophila* (*McLaughlin et al.* 2021): 250 mM sucrose (Sigma SO389-1KG), 10 mM TrisHCl pH 8.0 (Invitrogen AM9856), 25 mM KCl (Sigma P39M-5004), 5 mM $MgCl_2$ (Invitrogen AM95304), 0.01% Triton x-100 (Sigma 59284-100ML), 0.1 mM DTT (Invitrogen P2325), 0.7 U/µL RNase inhibitor (Sigma 3354012001), complete protease inhibitor (Roche 11697498001), nuclease free water (NFW) (to final volume needed). After centrifugation at 800 rcf at 4 °C for 5 minutes in a swinging bucket rotor, samples were resuspended in 500 µL of an ice-cold nuclei suspension buffer (NSB), consisting in 1X DBPS 1% BSA (Sigma A6003-25G), 20% glycerol (Sigma G7893-1L), 0.2 U/µL RNase inhibitor. During protocol optimization, different centrifugation speeds ranging from 100 rcf to 1000 rcf were tested, with final renderings and nuclei integrity checked with microscopy at the end of the protocol. The homogenate was then filtered through a 20 µm mesh-size strainer (pluriSelect 43-10020-50) into a BSA-coated 15 mL polypropylene tube, and the strainer was washed with additional 3 mL NSB. After a final centrifugation, the samples were then resuspended in 65 µL NSB. Such nuclei suspensions were stained with an equal volume of Vybrant DyeCycle Green (Fisher 10134622) diluted 1:1,000 in NSB to undergo fluorescence activated cell sorting (FACS).

Singlets were sorted out from the samples to separate them from contaminating pieces of connective tissue, cell doublets or aggregates, before final sample processing and sample fixation. Nuclei singlets were sorted thanks to a FACSAria Illu or a CYTEK Aurora sorter (the first used for the sequenced samples) located at the IRMB institute in Montpellier and BD FACSDiva software (v9.0.1). With FACSAria an 85 µm nozzle and a pressure of 45 PSI were used. With CYTEK Aurora a 100 µm nozzle and a 25 PSI pressure were used. Negative FACS controls were made by drawing an aliquot of 2 µL and mixing it with 98 µL of

Lysis EZ Buffer 1% NP40 (ThermoScientific 13434269), then stained with Vybrant DyeCycle Green diluted 1:1,000 in NSB. Positive FACS controls were made by drawing an aliquot of 3 µL and mixing it with 97 µL NSB. Depending on sample type, it was possible to sort from ~ 15,000 (antennae) to ~ 380,000 nuclei (heads). Sort gates were set based on the identification of three populations of increasing green fluorescence, to get singlets, doublets and triplets, and cell aggregates.

Singlets were fixed according to either a Parse Biosciences nuclei fixation protocol carried on in BSA-coated 15 mL tubes, or to a modified Parse Biosciences nuclei fixation protocol, for which samples were treated in a BSA-coated 96 wells cell-culture plate (Corning CLS3896-48EA) after being split in multiple wells. Rendering was much higher when the latter procedure was applied, most probably because of the flatter wells' bottom. Samples were then treated with a nuclei fixation kit (Parse Biosciences WN100): briefly, samples were kept on ice and fixed in Parse Fixation Solution for 10 minutes, then permeabilized in Parse Permeabilization solution for 3 minutes. Eventually, samples were eventually stored at - 80 °C after addition of DMSO (Parse Biosciences), according to the expected cell number in the sample.

Single nuclei barcoding, cDNA amplification and library preparation was performed with Parse Biosciences Evercode WT Mini reagents (barcoding plates SP100, barcoding reagents SB100, cDNA amplification reagents SC100, fragmentation reagents SX100, accessory boxes SA100 and SA200), and according to Parse Biosciences Evercode WT Mini protocols. In substance, nuclei get permeabilized and work as reaction chambers for RT-PCR-associated barcoding, playing the role of droplets in droplet-based approaches. Briefly, samples undergo an initial round of barcoding, kit reagents providing a maximum of twelve different sample barcodes. After this initial RT-PCR and barcoding, all samples can be pooled back together and redistributed in 96 wells with univocal barcodes for another round of barcoding, then the operation is repeated, leading to each nucleus statistically having a unique barcode set, and each transcript a specific UMI (Fig. 10A). Overall, this protocol eliminates the hurdles associated with microfluidic setups for single cell approaches, but

brings in tens of steps in which nuclei are manipulated, which can lead to substantial sample loss.

Two sub-libraries (technical replicates of the library preparation, after barcoding and nuclei lysis) were single indexed and sequenced on an Illumina HiSeq 4000 with PE150.

Sequencing results were aligned to an *An. gambiae* PEST reference genome (assembly: GCA_000005575.2, annotation: AgamP4.14), pre-processed and combined with a Parse Biosciences split-pipe pipeline (v1.0.0p). Data were analyzed in RStudio with Seurat and DoubletFinder packages, setting a lower threshold of 500 UMIs and 250 genes for high quality nuclei. To try to annotate the nuclei, scmap was applied using *D. melanogaster* scRNA-seq brain atlas and our *An. gambiae* scRNA-seq brain atlas as references.

Experimental results: attempted small scale snRNA-seq dataset

In order to obtain technical information about sample preparation procedures and overall comparative quality of the transcriptomes we produced a preliminary library that would have allowed sequencing of transcripts from 10,000 nuclei. Being the aim of our snRNA-seq dataset to provide technical information about the experimental procedures, the protocols applied for single-nuclei isolation were slightly different depending on isolated organs, and also for samples constituted by the same tissue of origin. A total of seven samples were eventually chosen for sequencing: five obtained from heads, one from legs, one from antennae. The highest yield in terms of high quality nuclei singlets was obtained from heads frozen overnight, and with gentle and continuous sample pipetting for aiding the sample filtering process. FACS was performed in order to sort singlets and remove chitin debris, collagen debris and cell doublets or aggregates, and the accuracy of the sorting was always double-checked with fluorescent microscopy (Fig. 10).

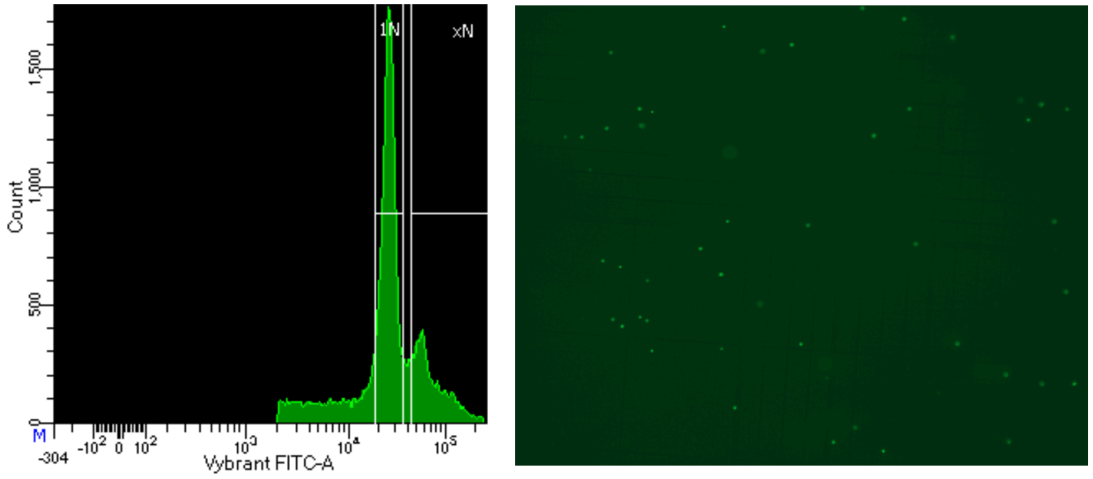


Figure 8. FACS sorted populations. Fluorescence profile of the populations of sorted cells, with number of green fluorescence detection events (counts, Y-axis), and fluorescence intensity of each event (X-axis). In the first panel, the left peak represents lowest fluorescence intensities discriminated from noise, which are isolated cells. The lowest peak on its right and the events of higher fluorescence cell triplets and aggregates. A fluorescent microscopy capture of the singlet population is shown on the right (10X magnification).

Numbers of singlet nuclei obtained after sorting were anyway relatively low considering the numbers of sampled individuals. From 55 heads, our most optimized protocol allowed us to obtain ~ 250,000 singlets, which corresponds to around the total nuclei expected in an *Anopheles* brain (Raji and Potter 2021). During processing, the number of nuclei retained in samples kept plummeting. Despite the starting material being the maximum amount suggested by the protocol to obtain 10,000 nuclei, after barcoding procedure and before library preparation only ~ 1,500 nuclei were counted in the pooled sample (thus containing nuclei from all seven experimental conditions mentioned).

The samples were processed and library sequenced. Data analysis revealed that information had been retained from only 490 high quality nuclei (roughly 50% split in the two sequencing sub-libraries). The dataset was built to contain the 73% of nuclei coming from the 2 samples treated with the protocols we considered the most optimized (sample type: heads), and indeed those made up 81% of the dataset. Just a small number of nuclei could be identified as either neuronal or glia cell types (Fig. 9B). Also, it was not possible to either assign

clusters of nuclei as orthologs to specific *D. melanogaster* cell types, or to clusters of the pilot *An. gambiae* scRNA-seq dataset we had previously produced: the vast majority of cells in all clusters was associated with multiple different cell types, which were almost all not annotated in the *D. melanogaster* data. On top of this, nuclei clustered according to sample and sub-library (Fig. 9C, D). Taken together, this highlighted how variability in the dataset was dictated by sample treatment, without carrying enough biological information or the definition to be resolved in cell types. In addition to this, even the protocols that we considered the most optimized and making up ~ 80% of the dataset clearly failed in yielding the thousands of nuclei we expected.

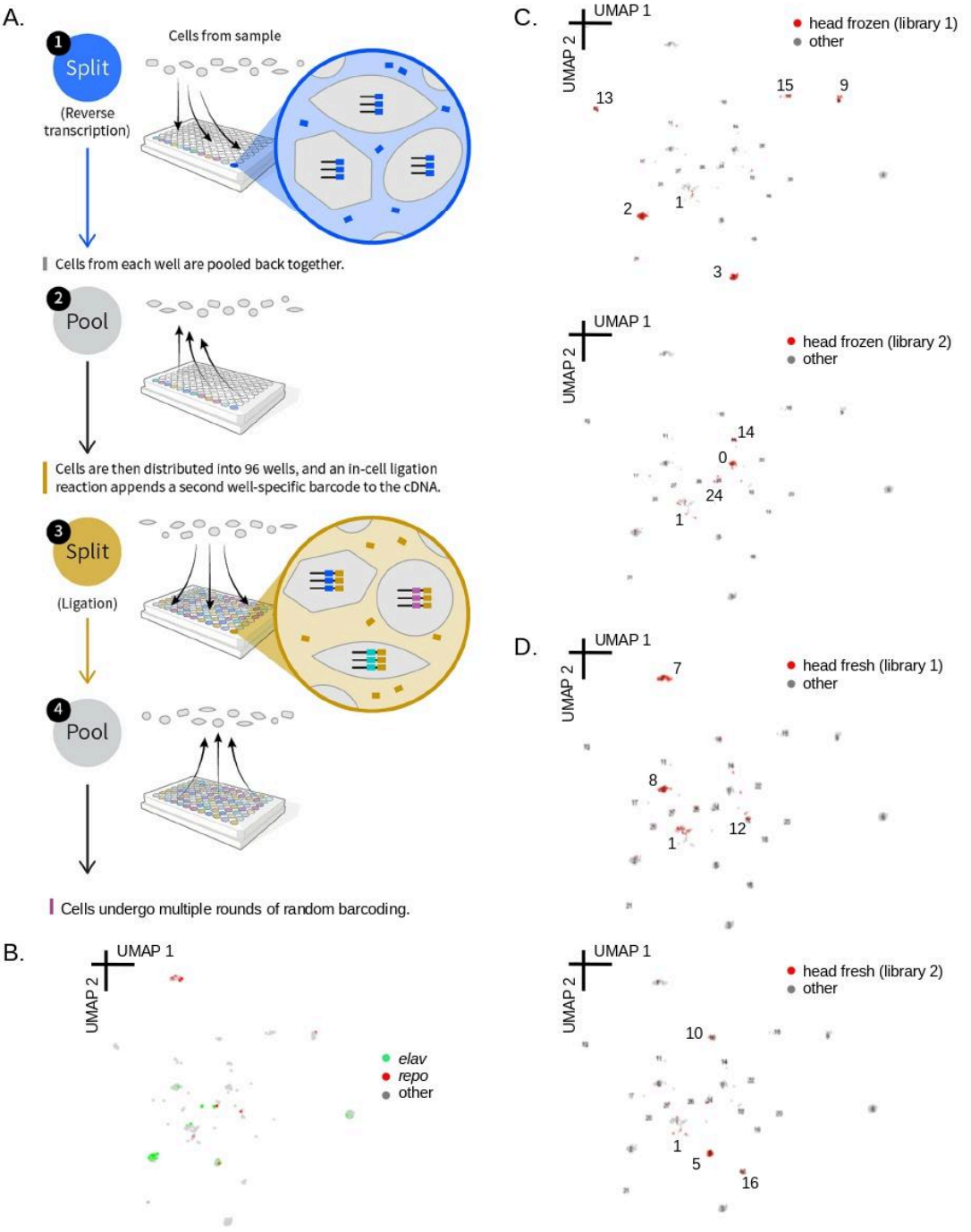


Figure 9. The snRNA-seq pilot dataset data processing and results. (A) Scheme showing the sample combinatorial barcoding process (adapted from Parse Biosciences Manual v1.2.1). **(B)** UMAP showing neuronal (*elav*) and glial (*repo*) gene marker distribution. **(C,D)** UMAPs evidencing how nuclei clustering was influenced by sample treatment for two head samples which made up ~ 60% of the nuclei number in the dataset.

Further testing to improve nuclei retrieval and quality by varying nuclei fixation conditions and cell sorting gating did not lead to better yields in terms of the number of nuclei isolated. A few more attempts for optimizing the protocol were performed with a different cell sorter (CYTEK Aurora), allowing for a lower sorting pressure. This led to the acquisition of even scarcer singlet populations, with a maximum of ~ 13,500 singlets obtained from 141 whole heads.

Considering the unsatisfying output of the snRNA-seq approach, we decided to produce data for the *An. gambiae* brain cell atlas with our optimised 10x scRNA-seq protocol.

An. gambiae brain scRNA–seq: from pilot data to a 50K cell atlas

We sought to collect cell-resolved transcriptional data of the brain of the female mosquitoes while targeting three experimental conditions that would be proxy for transitions among life cycle stages relevant for malaria transmission. This allowed us to both explore transcriptional variation among life cycle stages, but also to sample the cellular complexity of the brain without being restricted to a precise physiological condition. With this goal in mind, we thus attempted to obtain a pilot scRNA-seq dataset of small scale, composed of a few thousands cells, that paved the path that eventually led to produce an *An. gambiae* brain atlas of tens of thousands of cells. In the current section, I will describe the results obtained from the pilot and of the scaled-up scRNA-seq mosquito brain datasets, and the methods used to collect these data. Afterwards, I will present and discuss the results that the two datasets have yielded. I will also present the methods developed for obtaining scRNA-seq data from infected *Anopheles* mosquitoes and Tsetse flies, which had not led to a successful data collection.

Methods for scRNA-seq data collection and analysis

Pilot scRNA-seq dataset for the female *An. gambiae* brain

Brains were dissected from adult, age-matched female mosquitoes which were either virgin, mated or mated and blood-fed, each of these states being characterized by stage-specific behaviors. We reasoned that this sampling and experimental design and workflow allowed us to: (i) establish a protocol that in our hands would work to obtain scRNA-seq data from insect brains, that could also putatively be further applied to explore Tsetse fly brain and infection phenotypes; (ii) assess whether there is transcriptional variation during transitions between life cycle stages in the brain, and whether we are able to detect them; (iii) start collecting molecular insights in the *An. gambiae* brain cells; (iv) start associating gene expression variation along gonotrophic cycle

stages to CNS cell types; (v) with this toolkit in our hands, collect and produce a scaled-up scRNA-seq dataset and obtain the first single cell atlas of the *An. gambiae* brain.

Preparation of single cell suspensions and sequencing

At adult emergence, an adequate number of female *An. gambiae* mosquitoes (~ 20) were put in a separate cage to prevent mating, were and kept as a pool of virgin mosquitoes. The other female and male mosquitoes were left in the same cage to allow mating. On day 6 post-emergence, some mated mosquitoes were allowed to feed on rabbit blood provided at 37 °C through a glass cloche for ~ 30 minutes, after triggering blood-seeking by exposing mosquitoes to human breath. Engorged mosquitoes were then put into a separate cage. In this way, it was possible to study three biological conditions: virgin only sugar-fed, mated only sugar-fed, and mated which were blood-fed 6 days post-emergence. These are reflective of the main events and behaviors that take place during the female mosquitoes' gonotrophic cycle (excluding those related to oviposition): nectar-feeding, mating, host-seeking, blood-feeding.

Mosquito brains were dissected at day 7 post-emergence. Mosquitoes were anesthetized on ice (for a maximum of 30 minutes). The brains were dissected in DPBS (Fisher 10217152) with the aid of a stereomicroscope and steel Dumont #5 dissection forceps; the pharyngeal pump was not removed to avoid damaging subaesophageal brain ganglia. The spermatheca of each mosquito whose brain was isolated was checked under an optical microscope for presence/absence of spermatozoids to ensure that mating state corresponded to the one required for each experimental condition: if so, the brain was kept for further processing. If spermatozoids were present, the organ would appear at 5X magnification lighter in color and opaque, with moving spermatozoids visible both in the whole organ and if broken to release them. Instead, it would appear darker and more transparent if the mosquito had not mated, with no spermatozoid released if broken.

Brains were pooled according to mating and blood-feeding state (i.e. virgin, mated, blood-fed) and kept during tissue isolation procedures in three

separated 1.5 mL lo-bind tubes containing 50 µL of ice-cold Sf-900TM III SFM insect cell culture medium (Fisher 12568019), a suitable isosmotic and isosmolar, nutrient rich medium. These operations were carried out by four people in ~ 3 h. in order to obtain a pool of 12 brains for each of the experimental conditions (i.e. virgin, mated not blood-fed, and mated blood-fed).

The cell dissociation protocol has been adapted by Davie et al., 2018 (Davie et al. 2018). Pools of brains were then dissociated to make a single-cell suspension by being placed in 125 µL of DPBS (Fisher 13492609) containing 60 mg/mL of Gibco collagenase I (Fisher 11500536) and 1.2 mg/mL of dispase I (Sigma D4818-2MG), shaking at 1,000 rcf at 27 °C for 1 h; process was aided by gently pipetting ~ 150 times every 10 minutes with a p200 and a filter tip. Dissociation at room temperature (~ 18 °C), multiple shaking speed (between 500 rpm and 1200 rpm), and mechanical dissociation aid intensities (from 10 to 200 pipetting every 10-15 minutes) were attempted, and the one selected were the ones leading to the best final cell suspensions in terms of cell concentration and numbers (around 100,000-250,000 cells with a concentration ranging from 850 cells/µL to 1,375 cells/µL).

Dissociation reaction was stopped by adding 875 µL DPBS 0.04% bovine serum albumin (BSA) (final volume = 1 mL). Cells were pelletted by centrifugation at 400 rcf for 5 minutes at room temperature. The samples were then treated according to the 10x Cell Multiplexing Oligo Labeling for Single Cell RNA Sequencing Protocol (CG000391, Rev A) using three different Cell Multiplexing Oligos from 10X 3' CellPlex Kit Set A (10x 1000261): after centrifugation, pellets were resuspended each in 100 µL of one among three different Cell Multiplexing Oligo: 10x multiplexing oligo #305 (virgin sample), #307 (mated sample), #309 (blood-fed sample).

Final cell suspensions were prepared by filtering through a 20 µm mesh-size strainer (pluriStrainer 43-50020-03), which removed cell aggregates, debris and chitin leftovers, as the pharyngeal pump bits. Each sample's cell concentration was measured by drawing 5 µL and staining them with an equal volume of Vybrant DyeCycle Green (Fisher 10134622), a membrane-permeable DNA dye diluted 1:1,000 in DPBS. Cells were put in a haemocytometer (Merck Millipore

MDH-2N1-50PK) and counted thanks to a Zeiss Axio Imager 2 microscope under GFP excitation wavelength, and inspected with DIC illumination on a glass slide for shape and integrity. Cells were then pelleted by centrifugation at 800 rcf for 5 minutes at 4 °C. Assuming ~ 60% cell loss, an appropriate volume of chilled 10x Wash & Resuspension buffer was added to obtain a final concentration of 1,300 cells/µL for a targeted cell recovery of 10,000-30,000 cells. Concentration of each sample was measured again as described previously, and an equal amount of cells from each sample was pooled in a single 1.5 µL lo-bind tube. A total of 12,000 cells were measured before the sample was shipped for library preparation. Libraries were obtained with the aid of GemCode Single-Cell Instrument and Single Cell 3' Library & Gel Bead Kit v2. The library was double indexed and sequenced on an Illumina NovaSeq 6000 with paired-end (PE) 150, thanks to which we could generate high-quality sequencing reads with a length of 150 base pairs per read, each one paired with a second read from the opposite end of the cDNA fragment.

Methods for scRNA-seq preliminary data analysis and tentative homology-based cellular annotation

scRNA-seq data was demultiplexed and mapped to the *An. gambiae* PEST genome (assembly: GCA_000005575.2, annotation: AgamP4.14) with CellRanger (v 7.0.0) (Zheng et al. 2017). The downstream analysis of the data was carried out with RStudio environment (v2023.06.1) using R (v4.2.2) and RStudio environment (v2023.06.1) (R Development Core Team, n.d.; RStudio Team 2020). Single cell analysis was conducted with Seurat (v5.0.1) (Satija et al. 2015). For this preliminary inspection on single-cell data, low quality transcriptomes were filtered against if they had fewer than 500 unique transcripts, less than 250 genes and more than 25% mitochondrial genes, and genes were filtered out if expressed in less than 3 cells. Sequencing doublets were identified and removed with DoubletFinder (v2.0.4) (McGinnis et al. 2019). Clustering analysis was performed in the Seurat kNN method based on Jaccard's index with a resolution of 0.8 based on 30 principal components. This means that we first find for each cell its nearest neighbors (cells with most similar gene expression) using a

"k-Nearest Neighbors" graph, where each cell is linked to its closest neighbors based on principal components, where principal components are new variables created by combining the original many variables in the data into fewer variables that capture the most important information (summary features of the data). The Jaccard's index measures how similar two cells are by looking at how many neighbors they share, and helps in refining the graph connections and to better group similar cells. Finally, the clustering resolution parameter controls granularity: higher values yield more clusters, allowing subtypes or cell states to be resolved, whereas lower values produce broader clusters.

Positive cluster marker genes (bioinformatically assigned, not yet annotated) were identified comparing all the clusters against each other using Seurat FindAllMarkers function with a Wilcoxon test, a log fold change (LFC) threshold of 0.25 and a testing only genes that are detected in at least 25% of cells in either of the two populations tested. A preliminary inspection and identification of candidate cell type markers was conducted by checking the top 10 marker genes for each cluster. In addition, an algorithm-based cell annotation was attempted by mapping our scRNA-seq data onto an annotated reference from another species. Cell type mapping was conducted with scmap (v1.18.0) (Kiselev et al. 2018) by selecting the one-to-one orthologs present in our scRNA-seq data and an annotated *D. melanogaster* cellular brain atlas (Davie et al. 2018), and mapping individual *An. gambiae* cells or cellular clusters onto *D. melanogaster* cells or cellular clusters. More specifically, cell identities were determined based on the expression pattern of a set of n = 1,986 *A. gambiae* genes; these genes have been selected since (1) they could be univocally assigned to only one ortholog in the reference *D. melanogaster* dataset, and (2) such *D. melanogaster* ortholog had no other orthologs in the *A. gambiae* dataset. This strict orthologs selection approach was chosen in order to avoid misleading results with genes which were generated by a gene duplication event and are most probably carrying out different functions with the respect to their ortholog in the two organisms.

Scaled-up scRNA-seq dataset for the female *An. gambiae* brain

The pilot scRNA-seq dataset was for us the proof of concept that we could collect scRNA-seq data from mosquito brains, and the results (page 76) served to refine the protocol for a scaled-up study. Methods for preparation of single cell suspensions, data analysis, background noise removal and definitive homology-based cellular annotation of the scaled-up dataset are reported in the submitted manuscript (page 142). For such data analysis, we applied slightly different data collection and processing compared to the ones of the small-scale pilot data. While we still pooled in separated samples brains from virgin, mated and blood-fed *An. gambiae* females, we excluded sample multiplexing during single-cell collection, and collected a total of six independent samples. These were obtained by performing the same experiment twice, thus collecting two independent experimental replicates for each of the three conditions.

Wanting to integrate scRNA-seq data coming from the two experimental replicates, during data analysis we used SCTransform to normalize and transform scRNA-seq data using regularized negative binomial regression. This helped in stabilizing variance, removing technical noise, and improving detection of biologically meaningful patterns for downstream analysis. After SCTransformation we then performed sample data integration, and we further removed background noise with the use of CellBender (Fleming et al. 2023), to improve the quality of the data without losing biological information with a low count threshold of 100.

Finally, we found a more effective tool than scmap for homology-based cell type annotation. In order to use scmap for cross-species comparisons, we reasoned it was rigorous to remove ortholog genes having multiple orthology matches between the species considered. When comparing *An. gambiae* and *D. melanogaster*, these represent the vast majority of the genes detected, accounting for thousands of genes. With scmap we thus had to improve clarity of the signals to interpret, at the expense of failing in leveraging the information coming from entire gene families. To address this issue, we looked for alternative tools and identified the SAMap algorithm. This allows to not only

maintain information from all the ortholog pairs in the datasets we wanted to compare, but also to weight and leverage the information coming from paralogous genes in identifying homologous genetic programs during cross-species comparison (Tarashansky et al. 2021).

Gene Ontology analysis was performed with PANTHER overrepresentation test (release date 2024-08-07), annotation version GO Ontology database DOI: 10.5281/zenodo.15066566 (release date 2025-03-16) Released 2025-03-16. The lists of differentially expressed genes (DEGs) were compared against the An. gambiae gene list present in the database on 2025-08-05, and results obtained using a Fisher's Exact test, with False Discovery Rate (FDR) correction.

Tentative scRNA-seq on female *An. gambiae* brain after *P. falciparum* infection

Experimental infections in *An. gambiae* and scRNA-seq attempts were possible thanks to a collaboration with the groups of Teun Bousema and Richard Bartfai at the Radboud University Medical Center (Radboudumc, Nijmegen, The Netherlands). A colony of *An. gambiae* (kisumu strain) was set up in 2023 from eggs that were produced in the colony hosted in the Vectopole of IRD - MIVEGEC in Montpellier and shipped to Radboudumc.

Experimental infections

Experimental infections took place at the Malaria transmission unit at the Department of Medical Microbiology of Radboudumc. Infectious feeding was performed by using 300 µl of freshly drawn blood kept at 37°C, added to 30 µl of cultured gametocytes and fed by mini-feeders. *An. gambiae* mosquitoes were infected and were kept at 26°C and 80% humidity, with a reversed 12 h light/12 h dark cycle. Mosquitoes from different batches were dissected 6 days later and midguts dissected and stained with 1% mercurochrome for quantification of oocysts by microscopy before proceeding with dissection experiments. In order to allow infection to progress and get infectious mosquitoes, some received a second (not infectious) blood meal on day 8 post-infection, which promotes sporozoite development.

Mosquitoes brains were dissected at day 8 (oocyst stage) and 16 (sporozoite stage) post-infection. Brains were dissected on glass slides with Dumont #5 forceps, from mosquito heads isolated in a drop of PBS for 5 minutes maximum. At the same time, oocysts numbers in midguts were checked after staining with 1% mercurochrome staining in an optical microscope bright field for samples at day 7 post-infection. SGs were checked similarly but without staining for sporozoite presence at day 14 post-infection.
Further details on *P. falciparum* cell culture and experimental infections are present in the Methods section of the submitted manuscript (page 142).

Experimental results: from pilot data to a 50K cell atlas

The raw preliminary dataset was composed of ~ 3,000 cells, and information from 2,245 cells was retained after bioinformatically filtering for high quality cells. Single cell transcriptional profile analysis allowed to identify 23 cell clusters (Fig. 10A). The Seurat clustering process is based on overall similarity in the cells' expression profiles, which we expected was maintained within any given cell population across the mosquito's gonotrophic cycle, thus leading to a cell clustering based on cell type, and not on experimental condition. Indeed, after a literature search for known marker genes, and an unbiased analysis of the expression pattern of cluster markers, we managed to identify cell types in the dataset. The majority of the clusters were marked by the expression and co-expression of *elav* and *very low-density lipoprotein receptor* (*vldlr*) (ortholog to *D. melanogaster lipophorin receptor* 1 and 2), both expressed in neurons (Raji and Potter 2021; Yin et al. 2021; Rojo-Cortés et al. 2022). Instead, glial markers such as *turtle* (ortholog of *D. melanogaster bdl*) and *obp*9 (ortholog or *D. melanogaster obp*44) (Yin et al. 2024; Cameron et al. 2016) were mainly expressed in cell cluster 4 (Fig. 10B). Indeed, scmap helped in confirming the overall identity of cell cluster 4, which was confirmed to be mostly composed of glial cells (Fig. 10C). The other clusters did not have a marker expression profile consistent with the assigned homologous *D. melanogaster* cell type, and anyway most of them were associated with *D. melanogaster* cell types that were not annotated in the reference dataset (Fig. 10D). We attribute the low inter-species

cell type matches obtained with scmap to the fact that using this tool we could consider the expression patterns of only a set of 1,986 ortholog genes (only the one-to-one orthologs present among the two datasets) over the 8,666 present among the two species according to the Orthology MAtrix browser ((Altenhoff et al. 2024) accessed on the 13th of September 2024). Scmap is indeed a valid tool to very quickly annotate single-cell datasets when a reference of the same species is available, as it is based on the comparison of expression levels associated to the same gene ID in two datasets, but the built-in functions are not adequate to handle inter-species comparisons.

Last, unfortunately, the multiplexing process applied during sample preparation was not effective: after experimentally assigning univocal sample barcodes to the cells obtained from brains pooled from either virgin, mated or blood-fed mosquito conditions, just ~ 5% of the high quality cells retained sample barcodes, and it was not possible to assign specific transcriptional variation to any of the experimental conditions tested. In other words, transcriptional information could not be assigned to any of the mosquito life stages (Fig. 10E).

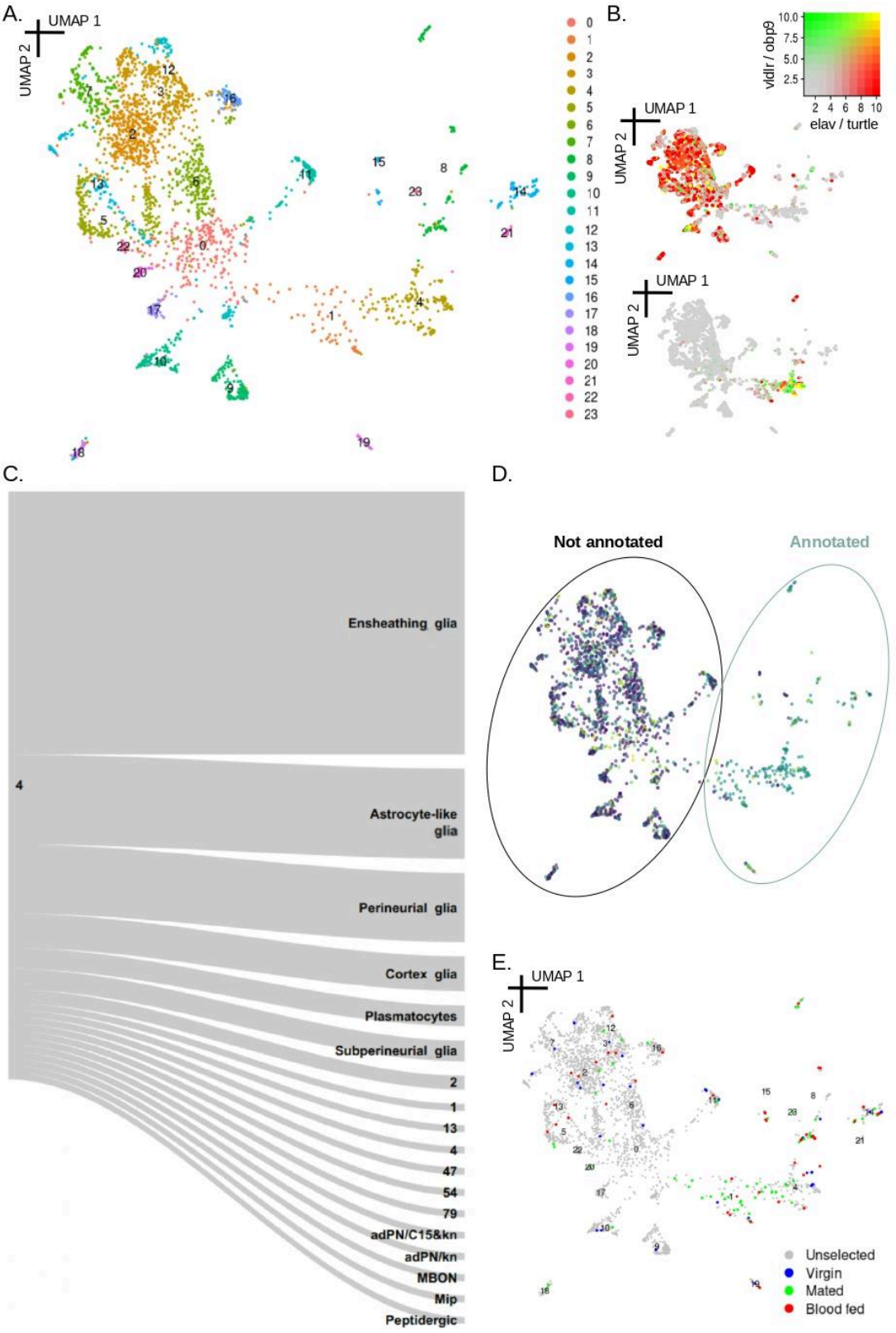


Figure 10. scRNA-seq pilot dataset of the *An. gambiae* female brain. (A) Uniform manifold approximation projection (UMAP) of the 23 cellular clusters grouping the ~ 2.5 K cells of the pilot (continued)

dataset. (B) UMAPs showing gene co-expression: in the top panel *elav* (red gradient) and *vldlr* (green gradient); in the bottom panel *turtle* (red gradient) and *opb9* (green gradient). Maximum expression of both genes is represented in yellow and lack of expression of both in grey. (C) River plot showing how cells of *An. gambiae* cluster 4 are associated with *D. melanogaster* cell types in the reference dataset (Davie et al. 2018). Numbers represent not annotated clusters in the reference dataset. (D) UMAP showing all the cells in the mosquito brain atlas that scmap has mapped to a *D. melanogaster* cell type in the reference dataset. The cells in most clusters have been associated with *D. melanogaster* cell types that have not been annotated in the reference dataset ("Not annotated"); a few clusters, especially *An. gambiae* cluster 4, mapped to known cell types, mainly glial ones ("Annotated"). (E) UMAP showing the distribution of barcoded cells.

Overall, these results made us confident that we could successfully scale-up the whole process and obtain a large single cell dataset from adult *An. gambiae* brain. We thus proceeded to produce a larger scRNA-seq dataset of the organ, with three main goals: (i) create the first scRNA-seq atlas of this species' brain; (ii) explore and identify suitable orthology-based methods for extensive identification of cell types in non-model organisms; (iii) explore the transcriptional events that happen in the *An. gambiae* females' CNS at different gonotrophic cycle stages that display peculiar behaviors, trying to find the first pieces of information that would possibly be connecting given transcriptional programs and cell types to regulation of specific behaviors.

We sought to obtain a dataset of tens of thousands of brain cells, collected from 7 days old *An. gambiae* females that were either virgin only sugar-fed, mated only sugar-fed, and mated which were blood-fed 6 days post-emergence, so the same conditions we aimed to explore with the pilot dataset. This time, we did not perform sample barcoding and pooling, but we removed the barcoding step and opted to process each sample separately, each in a different 10x partition inlet. The resulting dataset was made up of two biological replicates for each of the three conditions, obtained from two different sessions of dissection and following processing. Each of the six samples (two per condition) was obtained by pooling ten brains.

After an initial round of data processing, quality check (QC) and analysis of the resulting dataset with Seurat, we identified unbalanced unique molecular

identifier counts and gene counts among samples, reflected by uneven reads in the six runs (Table 2). The origin of this was the result of a failed attempt of the sequencing facility to load an equal number of cells in the sequencer for the six different samples based on the Illumina pre-MiSeq run results. The Illumina pre-MiSeq run serves as a preliminary sequencing step that evaluates library quality, cluster density, and read output to guide the loading concentration of samples before the main sequencing runs, enabling to estimate and adjust sample input in order to load an equal number of fragments from cells per sample on the sequencer. We identified this analysis as inadequate because it relied on an overly simple definition of number of cells per sample, using the 10x user interface and its spurious elbow method. We therefore decided to carry on an additional round of sequencing to average out this unwanted variation. We aimed to harmonize the read counts of each sample to match the sequencing depth of the sample with the highest coverage from the first sequencing run, i.e. the replicate 1 of the mated condition (Table 2). After this second round of sequencing, each sample was covered by ~ 1 billion reads, and preliminary data inspection confirmed QC parameters improved (Table 2).

Table 2. QC parameters for the brain atlas before and after re-sequencing. Sequencing depth and QC parameters are compared for the 1st sequencing run (1st run) of the brain atlas data and for the re-sequencing (re-seq) results. V1: virgin replicate 1; V2: virgin replicate 2; M1: mated replicate 1; M2: mated replicate 2; B1: mated and blood-fed replicate 1; B2: mated and blood-fed replicate 2; M: millions.

	1st run	re-seq	1st run	re-seq	1st run	re-seq	1st run	re-seq	1st run	re-seq
sample	**reads (total)**	**reads (total)**	**cells per sample**	**cells per sample**	**genes per sample**	**genes per sample**	**genes per cell**	**genes per cell**	**UMIs per cell**	**UMIs per cell**
V1	723 M	1,074 M	13,654	10,917	10,877	10,783	1,160	1,591	2,766	4,358
V2	108 M	1,166 M	9,241	7,902	9,764	10,451	601	1,445	1,044	4,117
M1	936 M	936 M	10,465	11,466	11,242	10,961	1,524	1,662	4,447	4,971
M2	818 M	974 M	11,258	12,520	11,046	10,806	1,418	1,560	3,865	4,323
B1	133 M	913 M	11,941	11,895	10,147	10,802	701	1,470	1,398	4,139

continued

	1st run	re-seq	1st run	re-seq	1st run	re-seq	1st run	re-seq	1st run	re-seq
sample	**reads (total)**	**reads (total)**	**cells per sample**	**cells per sample**	**genes per sample**	**genes per sample**	**genes per cell**	**genes per cell**	**UMIs per cell**	**UMIs per cell**
B2	330 M	971 M	8,885	10,145	10,512	10,654	891	1,489	1,723	4,259
Pilot	13 M	-	2,749	-	10,177	-	1,175	-	3,868	-

The CellRanger inferred fraction of reads per cell after resequencing was above 70% for all samples. Sequencing and alignment metrics were as well optimal, with valid sequencing barcodes ≥ 81%, and ≥ 85% of the reads mapped to the reference genome for all samples.

Encouraged by these results, we attempted scRNA-seq on infected *An. gambiae* brains at Radboudumc. During my stay at the center, infection had a prevalence of ~ 50% for both MG and SG stages, thus it was possible to collect all the biological samples needed for the experiments. Nonetheless, we faced experimental drawbacks related to the protocols to obtain single cell suspensions. Despite trying to replicate the same protocol that allowed us to sequence tens of thousands of cells from non infected mosquitoes, several attempts failed due to the cells' tendency to aggregate in suspension, and the 10x microfluidic chip to obtain a Gel Bead-in-Emulsion partition got clogged twice. We suspect the influence of some hidden variables associated with carrying out the procedures in a different environment impacted negatively on the experimental output.

After the failed attempt to get scRNA-seq data from infected mosquitoes at Radboudumc, we started planning bulk RNA-seq experiments on infected samples to be carried on in Montpellier, and went on analysing the scRNA-seq data on life cycle stages. Despite evident improvement in sample QC parameters, after re-sequencing we noticed signs of high sequencing background in the UMI count distribution in the raw data produced by CellRanger, with a lack of clear separation between cells and empty droplets

data. For this reason, we used the CellBender tool to assess and remove noise associated with background signal and technical artifacts in the data, setting the parameters for identifying empty droplets based on CellRanger outputs (i.e. 100 UMIs per cell corresponded to an empty droplet) (Fig. 11).

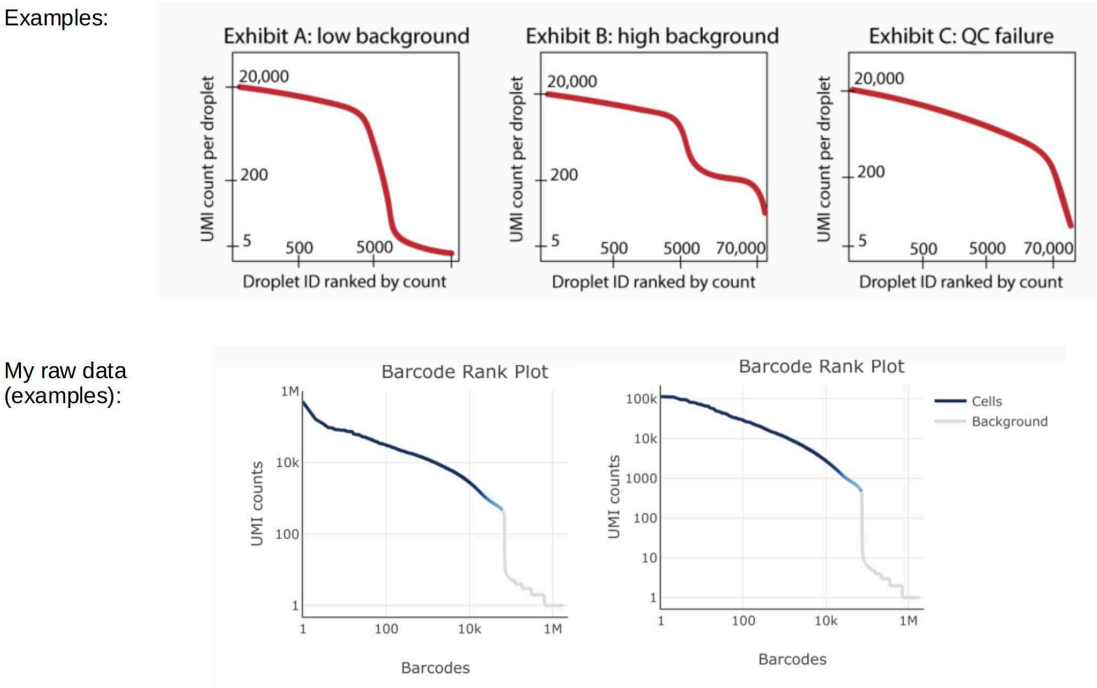


Figure 11. Raw sequencing data counts. Examples of low and high quality elbow plots (top line, image source https://cellbender.readthedocs.io/) with sequencing results of two of my samples (i.e. bottom line, mated replicate 1 and 2, left to right).

This led to a noticeable improvement in the data quality. First, before running CellBender it was not possible to find univocal thresholds for both UMI and gene counts that would lead to reasonable cell counts in all samples. We wanted to maintain the general standard of at least 1,000 UMIs and 800 genes per cell, but in some cases these thresholds led to a number of cells sequenced that would overcome 30,000 per sample, dropping to around 10,000 just slightly increasing the threshold of 150 genes or UMIs per cell. We reasoned that these filtering thresholds applied *post-hoc* would not yield reliable results. For example, we initially set thresholds specifically adjusted for each sample, having the following range: a variable lower UMI counts threshold between 1,000 and

1,150, a very low UMI counts upper threshold of 20,000, and a variable lower threshold for gene counts between 800 and 950. This would lead to a reasonable number of ~ 65,000 cells in the atlas that could be grouped in 55 clusters, with cells pretty much equally distributed among the samples (between ~ 8,000 and ~ 12,500 cells). We thus wanted to compare these data with the results obtained after filtering against background noise.

We selected CellBender as a tool to remove ambient/background RNA from a count matrix. The outputs had QC parameters that were much more uniform among samples. Setting differential QC thresholds was not necessary, as well as setting an upper UMI count threshold, which is an improvement compared to the previous data, since doublets and associated sequencing artifacts get eliminated bioinformatically with a dedicated tool (DoubletFinder), and there should be no need to filter them out using an approximate and generalistic UMI threshold. The number of genes identified in the atlas remained unvaried, being 11,391 before and 11,435 after processing with CellBender (so, it actually slightly increased). Eventually, the atlas was composed of ~ 49,000 cells, distributed in 45 clusters.

A deeper analysis of the two datasets showed they shared 42,137 cellular identifiers. These belonged to all the clusters that could have been identified without running CellBender, suggesting that no information on cell types present in the dataset was lost. While CellBender removed 22,708 cells from the atlas, new information from 6,669 cells, belonging to all the newly identified clusters, was gained with the procedure. General neuronal and glial markers could still be identified with a comparable distribution (Fig. 12A). The expression of the neuronal marker *elav* was marking most of the clusters in both datasets, and *repo* and *turtle* expression, identifying glial cells, was limited to three or four clusters (i.e. clusters 13, 33, 38, and 40 without CellBender; clusters 10, 23 and 25 post-processing with CellBender) (Raji and Potter 2021; Cameron et al. 2016). In addition to this, known marker gene distribution was maintained as expected. As an example, *obp*9 expression was still associated with the clusters that could be related to glia, but the spurious expression that could be initially found in *elav*$^{+}$ clusters was removed (Fig. 12B, C).

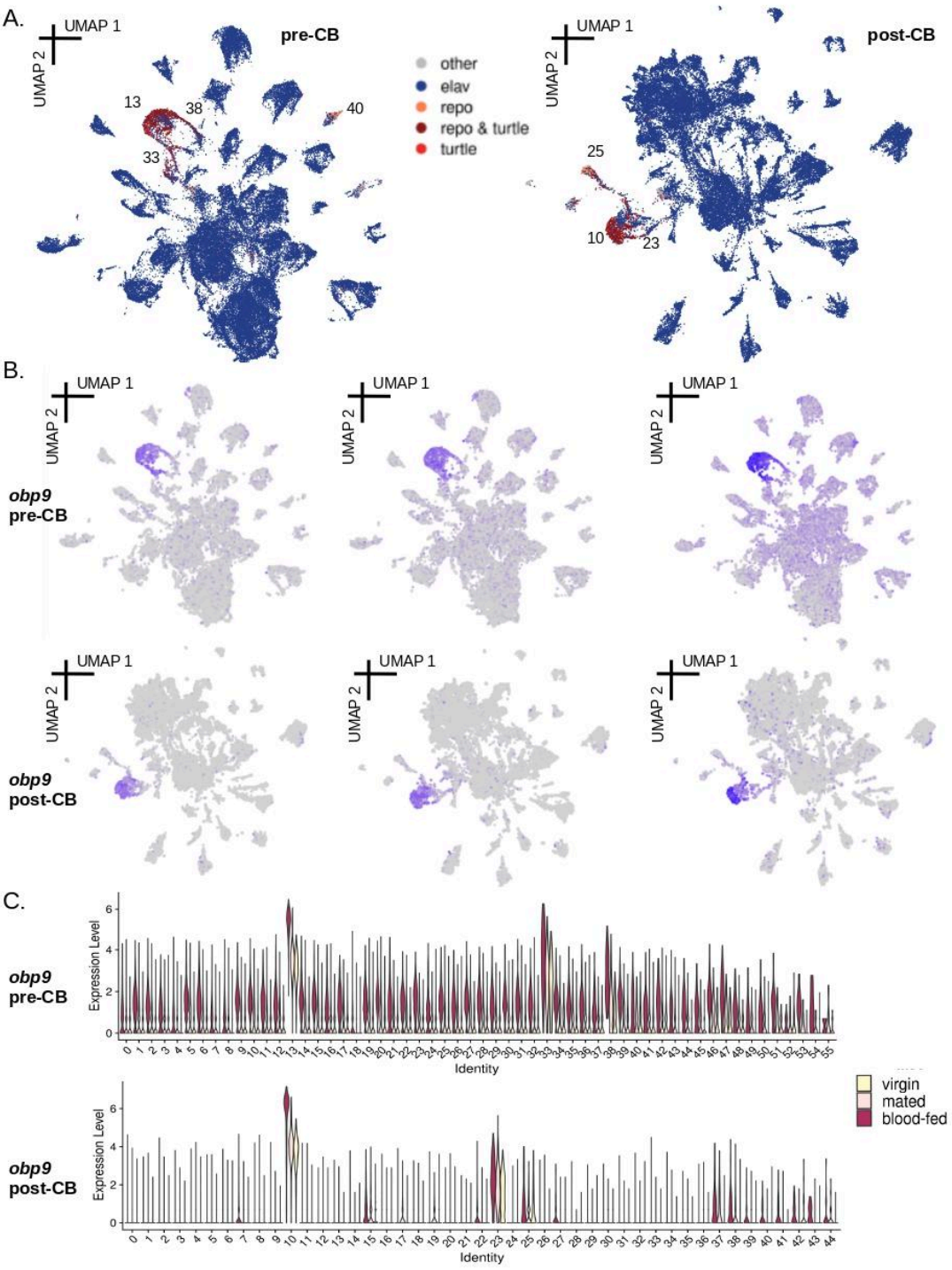


Figure 12. Comparison of atlas data before and after background noise removal. (A) UMAPs showing the expression distribution of neuronal marker *elav* and of the glial markers *repo* and *turtle*. **(B)** UMAPs showing the expression distribution of *obp9*. **(C)** Violin plots showing the expression distribution of *obp9* in the clusters identified in the atlas with (post-CB) and without the application of CellBender pipeline (pre-CB). CB: CellBender.

Single brain bulk RNA-seq in *An. gambiae* and *G. morsitans*

To complement the scRNA-seq data, allowing for a small-scale resolution but lacking an overall vision of the biological context of the brain of the mosquito, we produced a bulk RNA-seq of single brains of *An. gambiae* females to further investigate the changes taking place after mating and after blood feeding. These results were obtained with a low-input Smart-seq2 approach, a technique. The data are integrated in the submitted article and are both complementing and confirming the information brought by the scRNA-seq atlas (page 137). As an example, a strong overexpression of *obp9* after blood meal was confirmed in both datasets, with bulk data showing a log2FC = 2.44 (Benjamini-Hochberg adjusted p-value (BHadj) = 1.77E-26) for mated blood-fed females compared to the virgin condition, and a log2FC = - 0.038 (BHadj p-value = 0.70) for mated not blood-fed females compared to the virgin condition. Such kind of common patterns could be observed both with the pilot and the final scRNA-seq data.

Considering such promising results, in addition to the investigation of gene expression changes across the life cycle, we wanted to apply this method on brains of both *An. gambiae* and *G. morsitans* at different stages of infection with *P. falciparum* and *T. brucei*, respectively. Considered that both these vectors transmit a parasitic disease through haematophagous behavior, but that both parasites and vectors are distantly related phylogenetically, we sought comparing them as a mean to try to infer the molecular background of convergent evolution underlying analogous phenotypes that could influence disease transmission.

Methods for bulk RNA-seq

For life cycle stage studies, experimental conditions and brain dissection were the same as for the scRNA-seq atlas, and we similarly collected brain samples from virgin, mated and blood-fed mosquitoes (page 76).

Experimental infections have been carried out on *An. gambiae* (kisumu) at Radboudumc as described above (page 82). Briefly, female mosquitoes were

infected with cultured cells of *P. falciparum* NF54 strain during a blood meal provided at 6 days post-emergence; some of them received a second, not infectious blood meal 8 days post-infection, to promote sporozoite development. Both infected and control mosquitoes (the latter being age-matched not infected that underwent the same treatments, apart from the infectious blood meal), were sent to our department. During transport (~ 12 hours) hygrometric and temperature parameters of the boxes were recorded in case we needed to troubleshoot infection failures, which fortunately did not happen (TZ-TempU03 logger, TZONE Digital Technology co., Shenzhen, China). Once received, mosquitoes were maintained as described above in the security level 3 of IRD MIVEGEC Vectopole, fed on 10% sugar water. Single brains were obtained from 10 infected mosquitoes at 8 and 16 days post infection (dpi), and the experiment was performed in duplicate for both experimental stages.
Further method details are reported in the submitted manuscript (page 119).

Preliminary trials for bulk RNA-seq methods on Tsetse fly

Bulk RNA-seq methods applied on Tsetse flies were the same as the one described for mosquitoes, with minor optimization needed. If working with Tsetse, just prior dissection each fly needs to be washed thoroughly in a small beaker filled with fresh tap water, to remove dirt. If working with infected flies, first the head was separated and kept in a droplet of clean PBS, while the body was dissected in a separate droplet to check infection state.
Just after dissection, single brains were each placed in a well of a 96-well plate. They were plunged in 41 µL of DPBS (Fisher 13492609) containing 60 mg/mL of Gibco collagenase I (Fisher 11500536) and 1.2 mg/mL of dispase I (Sigma D4818-2MG). The tissues were then dissociated at 28 °C shaking at 1000 rcf for 20 minutes. Tissue dissociation was aided by gently pipetting ~ 150 times at the end of the incubation, with a wide bore and lo-bind filter tip (VWR 613-7089) on a p200 set at 20 uL. Samples were then incubated for additional 10 minutes rocking in the same conditions, and an additional round of pipetting was performed for 20-50 times at the end of the incubation in the same fashion just described. The sample plate was then centrifuged at 800 rcf for 5 minutes at 4

°C, then the dissociation medium was removed without disturbing the pellet. The cells in samples were then lysed and Smart-seq2 protocol was applied with no variation compared to what was done for *An. gambiae* (page 148). More specifically, for Smart-seq2, cells are lysed to release their RNA content in solution. We used a buffer containing lithium dodecylsulfate for dissolving cell membranes, with EDTA and DTT to prevent RNA degradation, and lithium chloride aiding in RNA precipitation. After cell lysis, mRNAs are captured from the crude cell lysate thanks to oligo-dTs covalently ligated to the surface of superparamagnetic beads. These beads have a diameter of around 1 to 5 µm, and can acquire magnetic properties when under the influx of a magnetic field. Applying a magnetic field of around 0.2 to 0.5 Tesla at the magnetic surface, the beads can completely separate from the solution in around 30 seconds. Using an adequate amount of superparamagnetic beads, all the mRNAs in the samples are captured by A-T base pairing on the microbeads surface, and can be cleaned up by separation from the rest of the contaminant cell lysate components. The captured transcripts can be eluted in molecular-grade water and cDNA synthesized simply using PCR reagents and specific primers (Fig. 6A). Initially, the complementary strand of each RNA is formed in a first round of synthesis thanks to oligo-dT priming (with oligo-dTVN: 5'-AAGCAGTGGTATCAACGCAGAGTACTTTTTTTTTTTTTTTTTTTTTTTTTTTV N -3'). In the mix, a LNA-TSO (5'- AAGCAGTGGTATCAACGCAGAGTACATrGrG+G -3') was added to obtain the second-strand cDNA for each transcript in the same reaction. The cDNA can then be amplified using only one primer (ISPCR: 5′- AAGCAGTGGTATCAACGCAGAGT -3′), since the two primers used during RT contain the same sequence at their 5' (Fig. 6A).

The samples eventually undergo cDNA amplification, library preparation and sequencing as described in the submitted manuscript (page 148).

Preliminary trials for scRNA-seq methods on Tsetse fly

The protocol applied for scRNA-seq dissociation tests was the same as described for mosquito brains (page 77), with minor modifications. Tissue dissociation was performed with the same enzymes, and aided by gently

pipetting with a p200 set at 60 uL ~ 150 times every 10' for 1 hour. After the sample was to stop the enzymatic dissociation, filtering and cell counting, the centrifugation before final resuspension was performed at or 500 rcf at 4 °C in a swinging bucket rotor.

Tsetse fly infection experiments

Teneral males (between 24 h and 72 h post-emergence) were allowed to ingest parasites in culture medium during their first meal through a silicone membrane. PCF RED Tbb Trypanosomes were cultured at 10^6 cells/mL in SDM79 medium supplemented with 10% foetal bovine serum and 10 mM glutathione. Flies were starved for at least 24 h before being dissected.
Flies were kept asleep on ice for less than 15 minutes for digestion procedures. The fly head was removed and kept in a separated PBS drop for 5 minutes maximum, while rapid isolation of the SGs and alimentary tract (from proventriculus to posterior gut) was performed. The organs were arranged lengthways in separated PBS drops. Once isolated, infection status was confirmed by checking them in bright field with an optical microscope, and under epifluorescence M165FC stereomicroscope (Leica) at the 10X, 20X and 40X magnification.

Experimental results: influence of life cycle and *P. falciparum* infection on the female *An. gambiae* brain

A first attempt to obtain bulk RNA-seq data from single brains of infected mosquitoes was performed at Radboudumc, in parallel with the aforementioned failed scRNA-seq experiments. For bulk RNA-seq, it was planned to obtain amplified cDNA at Radboudumc and to transport samples to Montpellier to conclude library preparation and perform sequencing. However, some technical issues related to incomplete paramagnetic beads removal from the samples impeded the production of satisfying samples. For further sequencing experiments successfully performed later, we solved the issue by changing the type of magnetic plate holder we used for 96-well plates. We passed from a

holder in which the magnet forms a ring around each well, to one in which magnets are cylinders placed at the center of the space between 4 wells (Magnetic Stand-96, Invitrogen). This completely solved the problem, and it was possible to obtain libraries from brains of infected mosquitoes sent to Montpellier. The data are extensively discussed in the manuscript we submitted for publication (page 119). Interestingly, in this dataset we could detect DE of only one gene, *def1*, the expression of which was increased at the oocyst stage. DEF1 is an antimicrobial peptide proven to be involved in the response against Gram-positive bacteria, but it is not recognized as a major antiparasitic factor in *An. gambiae* in vivo, despite being found overexpressed in concomitance with multiple *Plasmodium* infection stages (at least when infected with *P. bergei*) (Dimopoulos et al. 1997; Richman et al. 1997; Pirahmadi et al. 2025). The expression of *def1* could be associated with the hemocyte clusters An38 and An42 (submitted manuscript Fig. S12). This is consistent with the humoral immune role of these cells, and with previously observed *Anopheles* responses to *Plasmodium* infection (Osta et al. 2004; Pirahmadi et al. 2025).

Experimental results: Tsetse fly infections

Part of our plan to improve understanding on whether and how vector-borne disease parasites manipulate their vectors was to compare infected *An. gambiae* and infected *G. morsitans* females. For this reason, we started Tsetse fly infection experiments in collaboration with our partners in the ParaFrap network from the Trypanosome Transmission group led by Brice Rotureau at the Pasteur Institute of Paris. As for *An. gambiae* infection experiments, the conditions we targeted were represented by infected (but not yet infectious) flies (PCF in the MG at 15 ± 3 dpi), and by infectious flies (metacyclic trypanosome (MT) in the SGs at 28 ± 3 dpi).

To start, it was necessary to assess our ability to dissect Tsetse fly brains and get healthy cellular suspensions, a protocol that we optimised *de novo*. For doing this, we received *Glossina* flies both from Pasteur Institute (*G. m. morsitans* species), and from CIRAD Baillarguet Vectopole Sud of Montpellier (*G. palpalis* species). Tsetse brain dissection revealed to be much easier than for

mosquitoes: the head is larger (~ 3.5 mm^3 (Austen 1911)), the chitin thicker, the brain is well separated from the exoskeleton by layers of muscles and fat body (Fig. 13).

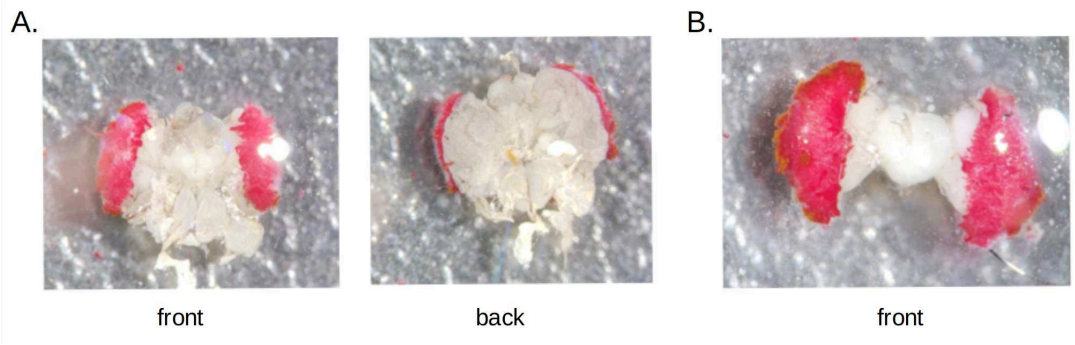


Figure 13. Dissected Tsetse brain. (A) Frontal and posterior views of the soft tissues dissected from a female Tsetse fly head, with the main mass being composed by the brain, being covered by head muscles (grey-translucent tissue). **(B)** Frontal view of an isolated brain. Images were taken with equipment not allowing for scaling.

Tsetse brain poses some additional hurdles associated with cell lysis for bulk RNA-seq compared to the one of mosquitoes, being much bigger and stiffer (empirical observation). Most probably, the Tsetse brain was bulky due to a stiff extracellular matrix (ECM). For this reason, we tested the protocols optimized for *An. gambiae* single brain bulk RNA-seq with just minor modifications, adding a processing step similar to tissue dissociation for scRNA-seq with ECM degrading enzymes just after tissue dissection (page 77).
During these preliminary trials, we also took advantage of the availability of Tsetse specimens and assessed a complete cell dissociation protocol for the organ, from which it was possible to obtain ~ 800,000 healthy cells (concentration 1,190 cells/µL, negligible presence of doublets) from dissociation of five brains, and highly concentrated and good quality cDNA from single brains (an average of ~ 28 ng/µL in 1:10 sample dilutions).

After protocol optimization, infection experiments were carried out at Pasteur Institute, Paris. Initially, four batches were infected to have an adequate number of flies with MTs infecting their SGs (28 ± 3 days post-infection (d.p.i.)), and two

to have an adequate number of flies with PCF MG infection (15 ± 3 d.p.i.). To check infection success, we dissected ~ 350 male flies coming from these six different infection batches. While at 28 dpi we expected a lethality of ~ 75% and SGs infection rate of ~ 20%, mortality was much more variable, and no SG infection could be identified. We could instead score an average of ~ 5% of MG infections in five out of six of the batches. The sixth batch (15 dpi time point) anyway had ~ 62% flies positive for MG infection, and we collected and preserved 7 fly brains for bulk RNA-seq, that we planned to complement with samples coming from SG-infected condition. We indeed realised that the flies belonging to the latter batch received a blood meal 24 hours after infection, while all the others were blood-fed just a few hours after being challenged with the parasite. Considering that this could possibly lower Trypanosomes success in establishing an infection in the flies, we planned a new set of six infection batches for the following month, for which blood feeding was performed 24 hours post-infection and for which infection rates would have been checked in advance. Unfortunately, none of the flies of this second infection experiment had parasites in their SGs at the moment of dissection for brain sampling. This time, though, MG infections were high (details reported in Table 2). Considering that the vectorial system under exam was showing an altered infection progression, and that we aimed to gain insights on alterations associated with different infection stages by comparing MG-infected to SG-infected conditions, we did not process MG samples.

Table 2. Results of the second wave of Tsetse fly infection experiments. Days post-infection dpi; Midgut: MG; salivary glands: SGs; proventriculus: PV.

dpi	Number of dissected flies (all the flies in the batches were dissected)	Percentage of MG infections (number)	Percentage of PV invasion in MG-infected flies (number)	Number of SGs infections
33	25	44.00% (11)	0	0
30	11	72.72% (8)	0	0
27	8	37.50% (3)	33.33% (1) (12.50% of the total)	0

continued

dpi	Number of dissected flies (all the flies in the batches were dissected)	Percentage of MG infections (number)	Percentage of PV invasion in MG-infected flies (number)	Number of SGs infections
29	30	40.00% (12)	50.00% (6) (20.00% of the total)	0
26	43	62.80% (27)	59.26% of the infected (16) (37.21% of the total)	0
18	Not dissected (lacking SGs-infected counterpart)	/	/	(not expected)
14	Not dissected (lacking SGs-infected counterpart)	/	/	(not expected)

Multiple factors have or may have contributed concomitantly to the high variations in lethality and low midgut infection rates observed. *In vivo* infections present a non-neglectable inter-experiment variability, and it is difficult to anticipate what the infection rates could be over successive batches. Tsetse infections are especially sensitive to multiple parameters, such as RH and temperature. Indeed, due to an unexpected technical defect of the insectarium humidifier, which was replaced during the experiments, the infected flies were reared to RH > 90% for probably more than 48 h. Survival rates were low, with only a few or a few tens of flies surviving until the moment of dissection (Table 2). Most of the infected flies, hence those that were more fragile, might have eventually died after an exposure to a high humidity level.

Second, we witnessed infection phenotypes that could be tracked back to a loss of virulence of the RED parasite strain used in this experiment, likely because of a drift over successive passages in cultures. We foresee that amplifying another stored subpopulation of the same clone or using parasites of the wild-type strain would have solved the infection issues. The parasite development *per se* was possibly not impacted, as assessed by the presence of parasites in the cardia of few flies. Indeed, Tsetse flies infected with Trypanosomes often show refractoriness to infection progression. In most cases, only a small fraction of

flies develop full, transmissible infections. The majority either clear the parasites entirely or harbor Trypanosomes only in the midgut, where the infection fails to progress further (reviewed in Geiger et al. 2015). The unsatisfying infection outcomes which were not solved by our attempt to improve the protocol led to abandoning this project line.

Does a significant cell proliferation happen in the adult *An. gambiae* brain? A click-chemistry approach

RNA-seq data obtained from single *An. gambiae* brains highlighted that the biggest transcriptional variation among the conditions in study (virgin sugar-fed, mated sugar-fed, mated blood-fed when 6 days old) happens after blood-feeding (page 137).

Among the DEGs upregulated after blood-feeding, two cathepsin B precursor coding genes (known to enhance matrix metalloproteinases activity), two collagen type IV alpha coding genes, and *sparc* pointed to a possible remodeling of the CNS extracellular matrix (Gregorio et al. 2018; Duncan et al. 2020; Portela et al. 2010). Together with the upregulation of an origin recognition gene (*origin recognition complex subunit 2*), and *nf-x1* gene, involved in neural development and axon guidance (Stroumbakis et al. 1996), these results suggested there could be cell proliferation related to neural networks remodeling that happen in the brain of the adult female after the first blood meal (submitted manuscript Supplementary Table 6, associated to the publication upon acceptance of the manuscript, available on request in the meantime). We also identified putative neuroblast populations in our single cell atlas (page 136). We thus performed a preliminary cell proliferation assay, in which 5-ethynyl-2'-deoxyuridine (EdU), a thymidine analog, was injected in 6 days old female *An. gambiae* mosquitoes 24 hours before providing them with their first blood meal. EdU would reach all tissues and get incorporated in the DNA of proliferating cells during the S phase, and could be revealed by imaging after a click-chemistry cycloaddition reaction linking it to a fluorophore.

Methods for cell proliferation assays

An. gambiae mosquitoes (kisumu strain) were reared as previously described (page 63). For these experiments, all the mosquitoes were kept in the same cage until the day of the injection, and blood feeding was performed as described, at around ~ 20 hours post-EdU injection.

69 nL of either PBS 0.5 mM EdU (test), or PBS (control) solutions were injected in mosquitoes' thorax with a single microinjection using a Drummond Scientific Nanoject II Auto-Nanoliter Injector setup. 60 6-days-old females were injected with EdU 0.5 mM in PBS; of these, 30 would then be provided with a blood meal ~ 20 hours post-injection. 30 6-days-old females were injected with PBS; they would then be provided with a blood meal ~ 20 hours post-injection. For the experiments, 3.5" Drummond Scientific glass capillaries #3-000-203-G/X were pulled at 60 °C with a PC-100 puller. The sealed glass tip was broken with dissection forceps under a stereomicroscope to ensure tip sharpness and narrowness; indeed, carefully breaking the tip was the only parameter that emerged as relevant in order to have proper injection needles, rather than one given pulling setup.

To be injected, mosquitoes were kept on a perforated stone in a 3 L/minute CO 2 flux for 15 minutes maximum. Post-injection survival rates were checked 20 hours and 48 hours post-injection.

Both brains and guts+reproductive tract samples were dissected 48 hours and 96 hours post-injection (i.e. 24 hours and 48 hours post-blood feeding, respectively), The dissections were performed in PBS with the aid of a stereomicroscope and steel Dumont #5 dissection forceps. The brains, ovaries and guts were then kept in 1 mL of ice cold Sf-900 SFM III or RPMI-1640 media for the dissection duration (~ 1 hour).

After dissection, samples were fixed in PBS 4% paraformaldehyde for 2 hours, then washed twice with 1 mL PBS 3% BSA, and left in the second wash for 30 minutes. Samples were permeabilized in PBS 0.5% Triton X-100 for ~ 45 minutes, and washed again twice with PBS 3% BSA. The click reaction was then carried out with the Click-iT EdU Imaging Kit (Alexa Fluor 488 dye) according to manufacturer's protocol, with 5 final washes with PBS 3% BSA. Samples were maintained for the Click-iT EdU protocol in the following setup: each medium was added in a well of a 24-wells plate on ice, and each sample was placed in a sieve made of a cut 2 mL EP tube to which a mosquito net (mesh size: 0.5 mm) was attached. To limit the damage to the tissues of interest, brains were not

separated from the proboscis, so that the samples could be more easily removed from the sieves before imaging by holding the proboscis.
Organ mounts were then prepared by mounting the samples with Fluoromount G with DAPI between two coverglasses, and whole-mount imaging performed with a Zeiss AxioImager 2 optical fluorescent microscope.

Experimental results: blood meal does not seem to induce cell proliferation in the *An. gambiae* brain

96 hours post-injection, both the mosquitoes injected with EdU and blood-fed, and the respective EdU-injected not blood-fed control individuals had a survival rate of ~ 57%, while PBS-injected and blood-fed controls had a survival rate of ~ 91%. Thus, the injection procedure was properly performed, but EdU was toxic for the mosquitoes, to the point that it strongly increased lethality.
We assessed EdU injections and mounting procedures success by inspecting midgut and ovaries. Nuclear staining was evident in the gut cellular monolayer with no signs of cell proliferation (Fig. 14A). It was not completely clear whether high cellular proliferation we expected in the reproductive tract after blood feeding was happening (Laurence and Simpson 1974), or if we just witnessed an accumulation of the EdU nucleotide in ovaries, which is still compatible with post-mating events of resource allocation (Valzania et al. 2019) (Fig. 14A). The brain had a strong concentration of cellular bodies in the outermost layers based on haematoxylin-eosin (HE) stainings (Fig. 14B), which might get damaged during long and laborious processing of the dissected organ. Brain samples had indeed a slightly patchy DAPI staining on the surface of the organ (Fig. 14B, inset).
Just a very small and clustered population of proliferating cells was present in both blood-fed test samples and not blood-fed controls (Fig. 14C). Identifying which was the area of the brain where these cells were located and whether it was the same in the test and control samples was not possible in the prepared tissue squashes without any cell type-specific staining (cell type markers for

specific brain areas were not known until we finalised our scRNA-seq atlas annotation, and confirmed some with ISH).

Some actions to improve the protocol could be taken, such as adding steps for tissue clearing, and avoiding soft tissue dissection performing imaging with an ultramicroscope (Pende et al. 2018).

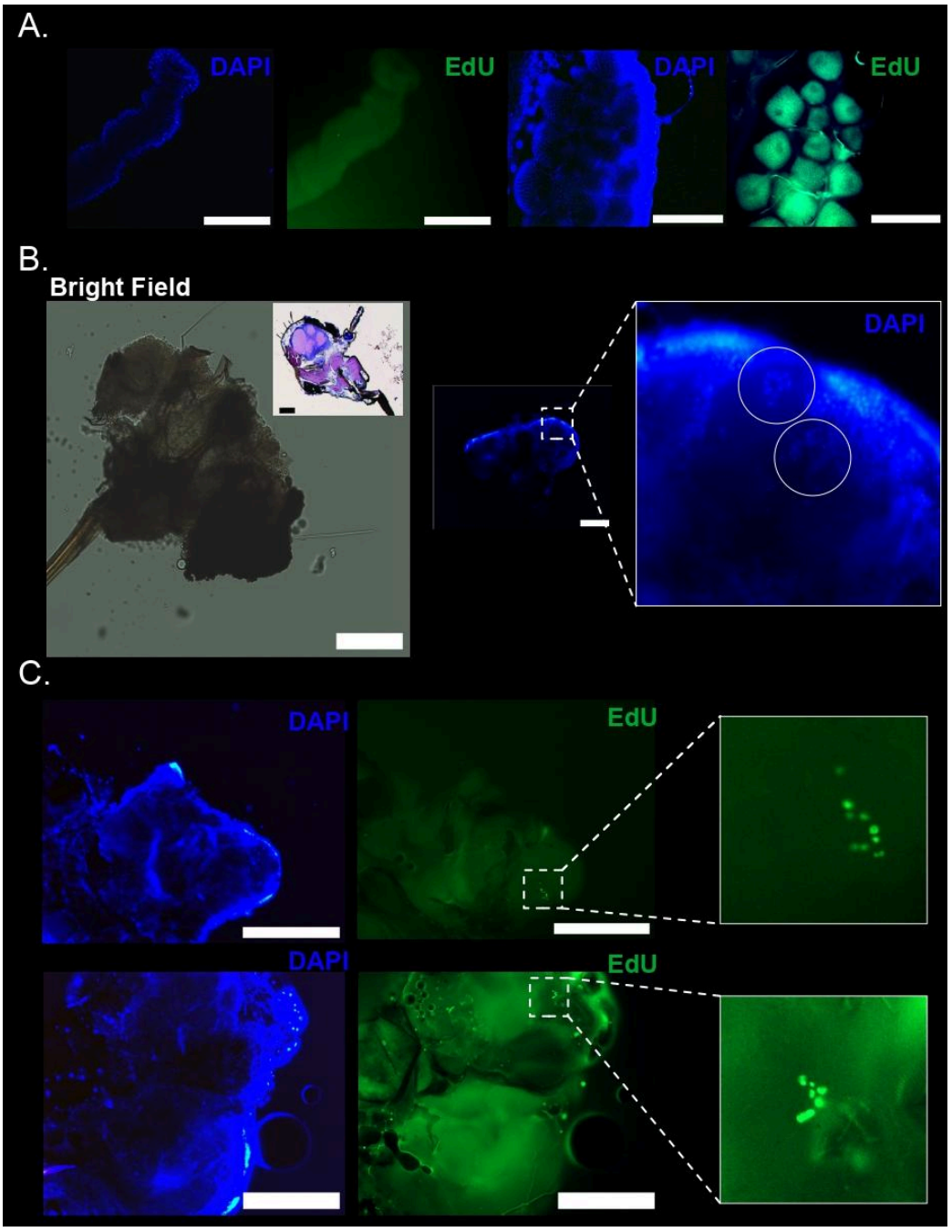


Figure 14. Cell proliferation in adult *An. gambiae* brain. (A) Cell proliferation controls: midgut (continued)

showing no active proliferation (EdU signal) after blood meal (left); ovaries showing EdU accumulation after blood meal (right). **(B)** Signs of tissue damage due to sample handling. Bright Field inset showing HE staining of a sagittal section of an *An. gambiae* head showing nuclei concentration at the surface of the brain. Circled in the DAPI zoom inset, examples of surface brain areas showing signs of damage of the external cell body layer. **(C)** A brain of a mosquito which did (top) and did not (bottom) receive a blood meal. Comparable cell proliferation that takes place in the mosquito brain indicates such a process is independent from blood uptake. White scale bar = 200 μm; black scale bar 10 μm.

RNAi for behavioral studies

The collection of transcriptional data from the brain of female mosquitoes at different life cycle stages was propaedeutical for the set-up of RNAi studies aiming to KD the expression of genes that were found to be differentially expressed in response to events like mating and/or blood meal. In particular, we chose to focus on the identification (RNA-seq data) and the experimental testing (RNAi) of genes that were differentially expressed in the mated condition in our bulk RNA-seq data. We wanted to target those genes whose expression increases (or decreases) in the mated compared to the virgin condition, and that also decreases (or increases) in the post blood-meal compared to the mated condition. We think that such gene expression variation taking place after mating but reversed after blood uptake might be involved in the onset and regulation of blood seeking behaviors, since we expect the mated mosquitoes to be in need of a blood meal for egg development. Bioinformatic analysis of the bulk RNA-seq data, which explore life cycle stages events (page 152), revealed a set of 4 downregulated and 24 upregulated genes that change in their expression after mating, going back to a level of expression similar to the one of the virgin sugar-fed condition after blood meal (i.e. with no significant variation in expression level of these genes between virgin and blood-fed conditions) (Fig. 15).

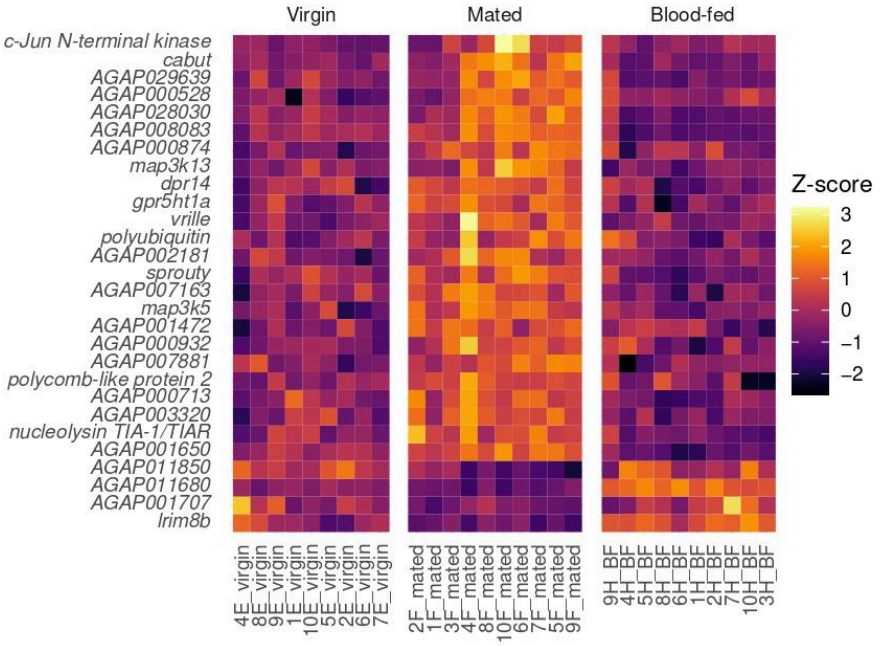


Figure 15. Putative RNAi targets. Heatmap of top DEGs (|log2FC| > 0.25 and FDR < 0.05) associated with the mated condition in the female *An. gambiae* brain (bulk RNA-seq data); samples hierarchically clustered with a complete-distance method.

We are currently targeting with RNAi some of the upregulated genes, and we expect their KD to be associated with a decreased desire of blood. These are *cabut*, the c-Jun N-terminal kinase AGAP009460, AGAP000528, the mitogen-activated protein kinase kinase kinase 13 (*map3k13*) AGAP006461, *dpr14*, *vrille* and *gpr5ht1a*, which caught our attention due to their function.

In particular, the ortholog of *cabut* in *D. melanogaster* regulates circadian behavior and represses the circadian oscillation of a subset of metabolic genes (Bartok et al. 2015). MAP3K13 instead can activate c-Jun N-terminal kinases, and eventually regulate cell proliferation, apoptosis, survival, tumorigenesis and tissue morphogenesis (Ikeda et al. 2001; Masaki et al. 2003; Meng and Xia 2011). The two genes have also been found to be involved in insect behavioral regulation in social insects, and the ortholog of *map3k13* in *D. melanogaster* has a role in synaptic structure regulation (Sommerlandt et al. 2019; Klinedinst et al. 2013; Li et al. 2017). In addition to these, other targets were TFs, as *vrille*, involved in regulation of rhythmic locomotor behaviors in *D. melanogaster* (Gunawardhana and Hardin 2017). AGAP000528 is instead an anopheline-specific

TF (VectorBase, accessed on 22nd January 2025 Giraldo-Calderón et al. 2022). The gene *dpr14* instead might be an immunoglobulin involved in synaptic organization and projection (Scheurer et al. 2021; Wang et al. 2022). To conclude, we sought investigating the putative receptor for serotonin *gpr5ht1a*, which is associated with mating refractoriness in *D. melanogaster*, and seemed particularly relevant in our experimental context (Pooryasin and Fiala 2015).

Methods for setting up RNAi assays

We selected multiple *An. gambiae* genes to be targeted with RNAi: *cabut*, the c-Jun N-terminal kinase AGAP009460, AGAP000528, the mitogen-activated protein kinase kinase kinase 13 AGAP006461, *dpr14*, *vrille* and *gpr5ht1a*. A published interfering double-stranded RNA (dsRNA) sequence targeting *An. gambiae serpin2* was identified as a positive KD control (Michel et al. 2005); *egfp* (then abandoned) and *Escherichia coli lacz* were selected as injection and KD controls. Their coding sequence (CDS) have been locally blasted with NCBI BLAST+ against the A. gambiae PEST genome version AGamP4.14 and against the annotated CDSs (source of all the sequences: Vectorbase, accessed from 2022 to 2025), looking for sequences having at least 90% of similarity with a minimum length of 19 nucleotides. The output allows checking for regions of non-homology suitable for dsRNA and primer design. The CDS of *egfp* gene was similarly checked to assess lack of off-target effects and the possibility to use a dsRNA construct obtained from this gene as an injection control. Eventually, a dsRNA encoding the sequence of E. coli *lacz* from nucleotide 350 to nucleotide 850 included was ordered as an injection and knock-down control.

The primers targeting the genes were designed using Primer-BLAST NCBI online tool, double checked for spurious amplifications with MFEprimer online tool against the *An. gambiae* genome, for correct directionality with EMBOSS online tools (flavour: WATER), and for specificity with Vectorbase online BLAST. The primers targeting *gfp* were designed with the Primer3 online tool and specificity checked against the *An. gambiae* genome with Primer-BLAST. As we initially planned to synthesize the dsRNA sequences in our lab, a T7 promoter

sequence was added at the 5'-end of *cabut* and *egfp* primers to allow for dsRNA amplification.

Primers for quantification of gene expression post-dsRNA injection were designed with PrimerQuest online tool, and specificity checked with Primer-BLAST. Primers were synthesized by Integrated DNA Technologies.

An. gambiae mosquitoes (kisumu strain) were reared as previously described (page 63). For these experiments, all the mosquitoes were kept in the same cage, and blood feeding was not performed.

We started testing primers for dsRNA constructs synthesis on total RNA that was extracted from three whole *An. gambiae* female bodies (each split after pestle homogenization in two technical replicates), with TRizol (ThermoFisher 15596026), DNase treatment performed with Turbo DNA-free kit (ThermoFisher AM1907), and reverse transcription with a High Capacity cDNA Reverse Transcription Kit (ThermoFisher 4368814), following manufacturers' protocols. qPCRs were performed with PowerUP SYBR Green Master Mix (ThermoFisher A25741).

Genomic DNA was purified from *An. gambiae* female whole bodies with NucleoSpin QuickPure columns (Fisher 12770941) according to manufacturers' protocol. PCR amplicons obtained with GoTaq Green master mix 2x (Promega PRM7823) according to the manufacturer's protocol. Primers targeting *cabut* were either: (i) simple: forward 5'-AGCGCAAGAAGAAGGAACCC-3'; reverse 5'-TTGCCACAGTTCGGATGGTC-3'; (ii) T7-linked: forward 5'-TAATACGACTCACTATAGGGAGAAGCGCAAGAAGAAGGAACCC-3'; reverse 5'-TAATACGACTCACTATAGGGAGATTGCCACAGTTCGGATGGTC-3'; and (iii) for qPCR, annealing to an exonic region of the gene other than the one that was targeted to obtain dsRNA constructs: forward 5'-GGAGGACGAAACTACCAAGTC-3'; reverse 5'-ACGAACCGTCCTTGTTGATG-3'; yielding 387 bp, 430 bp and 107 bp, amplicons respectively. We also ordered simple and T7-Linked primers to obtain a longer dsRNA from *cabut* CDS, respectively: (i) forward 5'-AAGCGCAAGAAGAAGGAACCC-3'; reverse 5'-GGGCCACTTGCAGTTGAACG-3'; and (ii) forward

5'-TAATACGACTCACTATAGGGAGAAAGCGCAAGAAGAAGGAACCC-3'; reverse 5'-TAATACGACTCACTATAGGGAGAGGGCCACTTGCAGTTGAACG-3'; yiending a 467 bp and a 510 product, respectively.

Primers for obtaining a dsRNA construct with T7 promoter sequence from *egfp* were: (i) simple: forward 5'-TTTTCAAGAGTGCCATGCCC-3'; reverse 5'-CCATGTGTAATCCCAGCAGC-3'; and (ii) T7-linked: forward 5'-TAATACGACTCACTATAGGGAGATTTTCAAGAGTGCCATGCCC-3'; reverse 5'-TAATACGACTCACTATAGGGAGACCATGTGTAATCCCAGCAGC-3'; yiending a 405 bp and a 448 product, respectively. The melting temperature for each primer was calculated using the formula: Tm = 81.5 °C + 16.6 °C × (log10[[Na^+]+[K^+]]) + 0.41 °C × (%GC) − 675/N

where N = number of nucleotides in the primer. Since PCR is typically conducted in monovalent cation concentration of ~ 50 mM, thus "(log10[0.05])" (Lorenz 2012).

Target DNA was amplified with a PCR program with an initial denaturation step at 90 °C for 2 minutes, followed 10 PCR cycles (95 °C for 30 s, 53 °C for 30 s, 72 °C for 1 minute), followed 35 PCR cycles (95 °C for 30 s, different amplification temperatures depending on the primers for 30 s, 72 °C for 1 minute) and a final extension step at 72 °C for 10 minutes.

PCR products were checked on a Tris-acetate-EDTA 1% agarose gel with 1:10,000 v/v GelRed (Merck SCT123), and a 1:5 dilution of GeneRuler LowRange DNA ladder (ThermoFisher SM1191), with 2 µL to 3 µL of PCR amplificate loaded.

Eventually, we identified a company (Lifeasible, Shirley, NY, US), for production of dsRNAs starting from user-provided genomic sequences. We thus provided sequences suitable for dsRNA synthesis (i.e. checked bioinformatically for absence of off-target effects as described above) for the eight *An. gambiae* genes we wanted to KD. The sequences have lengths ranging from 200 to 600 nucleotides.

To test KD efficiency, 3 days old *An. gambiae* female mosquitoes were injected with 69 uL of either dsRNA for a gene of interest, *lacz* dsRNA, or NFW, at a

concentration of 3 mg/mL. Microinjections were performed as described for EdU experiments (page 101), on ~ 60 mosquitoes per KD construct. Three days later, a total of 15 mosquitoes per injection condition were killed and distributed in 3 biological replicates from which total RNA extracted with a TRIzol protocol. RNA concentration of the samples was measured with Qubit and a dsDNA HS kit (ThermoFisher Q32851).

KD was assessed with RT-qPCR performed with PowerUP SYBR Green Master Mix, with *An. gambiae gapdh* (and sometimes *r7*) as an expression control, and a standardized quantity of 1 µg of RNA. A Pfaffl method was used to calculate KD efficacy and statistical t-test was also used to determine if the mean $2^{-\Delta Ct}$ values differ significantly between the groups.

Validation of RNAi methods and targets

To KD our target genes, we initially planned to synthesize interfering dsRNA with the Megascript kit (Ambion) according to the manufacturer's protocol. Suitable primer pairs have been designed for one of the target genes (*cabut*), and on the CDS of an injection control construct (*egfp*). We ordered primers to obtain products of different lengths from *cabut*, and to allow combinations of primers with and without T7 promoter sequence for the amplification of both *cabut* and *gfp* template DNA and synthesis of dsRNA constructs. Tests to assess the adequate PCR amplification temperature have been carried out and completed, and the optimal temperature has been identified as ~ 57.5 °C for *cabut* T7-linked primers and ~ 66.5 °C for *egfp* T7-linked primers (Fig. 16A, B, C).

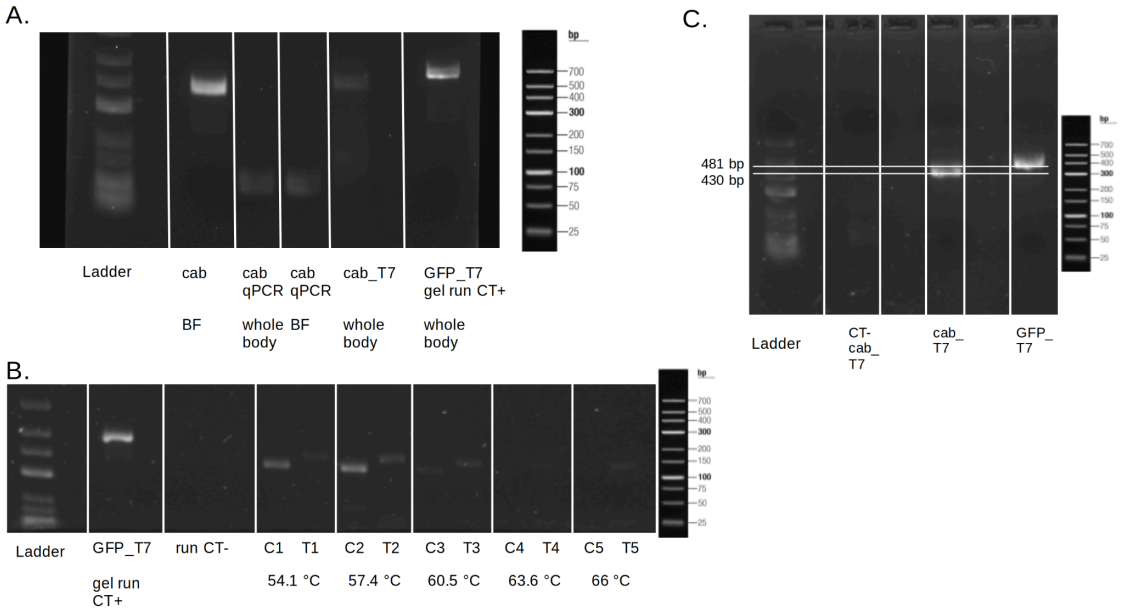


Figure 16. dsRNA and qPCR primer amplification tests. (A) Primers for detection of *cabut* expression with qPCR (cab qPCR) and primers for dsRNA synthesis, created with the same sequence targeting *cabut* both with and without a linked T7 promoter sequence (cab_T7, cab) on either (i) cDNA obtained from the brain of blood-fed female mosquitoes (BF, pooled from 3 different individuals), as a confirmation that the gene is expressed in the brain, and that the sequences chosen to target the gene for both qPCR and dsRNA synthesis work, and on (ii) pooling of DNA obtained from the whole body of 4 different female individuals. The sequences were amplified using 35 PCR cycles with an amplification temperature of: cab 53 °C, cab_T7 66.5 °C, cab qPCR 60 °C. A sample was separately produced with T7-linked primers (GFP_T7) for dsRNA synthesis from *egfp* genomic DNA, as this construct was planned to be used as injection control, and it was loaded in (A) and (B) gels as a positive control (CT+) for the gel runs. The sequence was amplified using 35 PCR cycles with an amplification temperature of 66.5 °C. **(B)** Amplicons obtained with a gradient PCR, cab ("C") and cab_T7 ("T") primers at different amplification temperatures ("1": 54.1 °C; "2": 57.4 °C; "3": 60.5 °C; "4": 63.6 °C; "5": 66 °C), with a negative PCR control (run CT-) run with the same master mix but no genomic DNA. **(C)** Confirmation of the optimal amplification temperature previously observed in (B) for cab_T7 primers, and in (A) for GFP_T7 primers. Amplification temperatures used were 57.7 °C and 66.6 °C, respectively. Negative PCR control (CT- cab_T7) was run with the same master mix as the cab_T7 sample, but in absence of genomic DNA. Bp: base pairs.

Given the length of this process, we interrupted primer testing and charged the dsRNA constructs synthesis for our set of target genes to a specialised company. Our first candidate of interest was *cabut*, due to its function in both circadian rhythm and nutrient metabolism. We microinjected the dsRNA construct

targeting this gene in female mosquitoes, and KD effectiveness was assessed. In two different experimental replicates, using two HKGs (*gapdh* and *rs7*) the gene showed either an irrelevant reduction in abundance (3%) or even an increase, and the mean $2^{-\Delta CT}$ values of injected samples and of injection controls were not significantly different between these two groups.

We thus tested the KD efficiency of a published dsRNA construct shown to successfully target *serpin2* (Michel et al. 2005) to assess whether the material ordered from the company we selected for the dsRNAs synthesis were intrinsically problematic for our experiments. This was not the case, and this time the gene showed a 43% decrease in abundance.

We are proceeding with KD experiments on all the other target genes, and planned associated behavioral tests to assess the impact of these genes on the mosquito behavioral phenotypes. Feeding motivation and double-mating assays on KD individuals are currently in progress.

Optimisation of histological procedures supporting spatial transcriptomics and ISH

In order to obtain consistent information about the spatial distribution of transcripts in mosquito brain tissue, we must complement scRNA-seq data with ISH experiments targeting selected transcripts of interest. We thus started optimizing a protocol for mosquito head microsectioning in parallel to the optimization of our scRNA-seq approach. This eventually led to the acquisition of histological samples that allowed us to both perform ISH and obtain the second ever spatial transcriptomics data in insects, first in literature for insect vectors (Mu et al. 2025).

Methods for experiments preliminary to ISH

Mosquito heads microsectioning

An. gambiae mosquitoes (kisumu strain) were reared as previously described (page 63). For these experiments, all the mosquitoes were kept in the same cage, and blood feeding was not performed.

Heads of female *An. gambiae* mosquitoes were dissected in DPBS with the aid of a stereomicroscope and steel Dumont #5 dissection forceps, and kept in ice-cold Sf-900 SFM III insect cell culture medium for the dissection duration (a few minutes). Three heads were then positioned in MicromMicrotech TFM-5 embedding OCT at room temperature, and oriented with the aid of a stereomicroscope and steel dissection forceps to be cut parallel to the sagittal body plane. Embedded samples were then frozen by submersion in dry ice-cold isopentane, and stored for one day at - 80 °C. An additional sample was obtained by dissecting one mosquito brain in DPBS, eventually embedded in green Epredia Neg-50 Frozen Section Medium (Fisher Scientific 11912365), oriented to be cut parallel to the frontal plane of the sample, slowly frozen by putting the mold in contact with dry ice. Both sample types were cut with the aid of a cryostat-cooled microtome (temperature ~ - 27 °C), obtaining 10 µm

slices. Slices were collected on SuperFrost Plus glass slides (FisherScientific 10149870), fixed via submersion in methanol and stained with an HE protocol; the samples were then dried and cover slides mounted on ProLong Gold Antifade Mountant medium (Thermo Fisher, P10144). The sample slides obtained this way were kept at room temperature and inspected under visible light in a Zeiss AxioImager 2 optical microscope.

After these first optimization steps, a final protocol for tissue sectioning has been successfully applied for ISH, and the methods and results have been reported in our submitted manuscript (page 119).

House keeping genes (HKGs) identification

A literature search was performed in order to identify putative HKGs suitable for ISH on female *An. gambiae* brain: the two top candidates were *gapdh* and *s7*. Both bulk RNA-seq dataset sequencing data and backup cDNA kept from the bulk RNA-seq experiments stored at - 20 °C (obtained as described at page 92) were used to evaluate *gapdh* and *s7* transcription levels stability across four different experimental conditions (i.e. virgin, mated not blood-fed, and mated blood-fed female mosquitoes). Coefficient of variation (CV) and |log2FC| were evaluated in Rstudio using the bulk RNA-seq dataset sequencing data. Additionally, the backup cDNA from the bulk RNA-seq samples was used to perform a qPCR as follows: 0.5 µL of cDNA suspension was pooled from each of the 10 replicates for the same biological condition, and diluted 1:5 in Ultrapure water. This resulted in four samples, each made up by a mixture of the same cDNA volume coming from 10 biological replicates for each of the three experimental conditions considered, reflecting the transcriptional state of *An. gambiae* brain at different steps of the mosquito gonotrophic cycle. Pooled cDNA concentration was assessed thanks to Qubit and a dsDNA HS kit (ThermoFisher Q32851). qPCR reaction was prepared with a PowerUp SYBR Green Master Mix (ThermoFisher A25741) with a standardized [cDNA] = 100 pg/µL. Each of the three samples was run in triplicates with primers for either *gapdh* (forward: 5'-AGATTGCCGTGTTCCAGGAG-3'; reverse: 5'-CTTCTCGGTCGTGGTGAACA-3') or *s7* (forward:

5'-AGAACCAGCAGACCACCATC-3'; reverse: 5'-GCTGCAAACTTCGGCTATTC-3'). The expression variance for the two HKG candidates was calculated among conditions based on the mean Ct values of the triplicates.

Experimental results: optimization of mosquito heads microsectioning

Preparing insect brains for imaging without causing tissue damage or distortion is complex. Classical preparation involves steps of dissection, fixation, inclusion in slicing media and microsectioning. At any point of this processing, the tissue can undergo shrinkage, deformation, or partial destruction, all leading to biased measurements. We thus applied inclusion and slicing methods that we optimised to maintain natural 3D structure and morphology of the mosquito brain within its head. Flash-freezing in OCT inclusion medium is a quick and easy, widely used tissue preparation approach for histopathological analysis, and for cryopreservation of various tissues for a long period (Solanki et al. 2020; Li et al. 2021; Lin et al. 2021). Female *An. gambiae* mosquito heads were embedded in OCT and tissues were cut in cryostat. Slices having a thickness of more than 14 µm were damaged by the cutting procedure, probably due to the mechanical resistance the microtome blade encountered during the cutting process. Best slicing results were obtained for the 10 µm thick tissue slices embedded in MicromMicrotech TFM-5 OCT medium. It was possible to assess autofluorescence of head tissues at multiple excitation/emission wavelengths, showing either absent or negligible autofluorescence in all cases.

We also attempted slicing dissected brains after inclusion in coloured (green) OCT, but we could not identify the slices in which the brain tissue was present, so this direction was abandoned. We also attempted performing fixation in PFA 4% of whole heads for times that ranged from 1 hour to 24 hours before inclusion in OCT, but histological results after HE staining showed poor tissue preservation.

Eventually, we optimized a protocol improving tissue adhesion to the glass slides by keeping the glass slides at room temperature for a few hours before

tissue collection, and then keeping them for 2 hours at - 20 °C, before storage at - 80 °C. With this approach, we obtained the ISH results reported in the submitted research article manuscript (page 119).

Probes targeting HKGs are sometimes used in ISH experiments for evaluation of relative gene expression variation. Thus, we selected two genes among known HKGs and tested their expression parameters in the *An. gambiae* brain, in case we would then decide they could be useful during ISH experiments. These were *gapdh* and 40S ribosomal protein S7 gene (*s7*): their expression stability across our experimental conditions was tested both experimentally and bioinformatically, and we assessed adequate Ct, CV and FC. Both HKG candidates showed a very low variance comparing their mean qPCR Ct values across the considered biological conditions (i.e. virgin, mated not blood-fed, mated to which a blood meal was offered but did not eat, and mated blood-fed female mosquitoes), being the variance of $gapdh_{Ct}$ = 0.064, and the variance of $s7_{Ct}$ = 0.054. Additionally, both genes are widely expressed in the cells of the pilot scRNA-seq dataset. This is relevant because it indicates that most regions of the brain would express the HKGs: this implies that localised ISH fluorescence associated to the expression of target genes would most probably lay in close proximity to fluorescence associated to the HKGs, allowing for image-based quantifications.

According to literature, proper HKGs must have a CV < 0.3 and a |log2FC| < 0.2 across the experimental conditions examined (Liang et al. 2020). When comparing their expression for the bulk RNA-seq experimental conditions with each other, *gapdh* expression showed a CV < 0.3 and a |log2FC| < 0.2. On the other hand, *s7* has a log2FC = - 0.207 for blood-fed mated mosquitoes compared to the virgin ones, and a more relevant log2FC = 0.277 for blood-fed mated mosquitoes compared to the mated not blood-fed ones, so it does not respect the parameters for being an HKG in the project experiments. Thus, we currently consider *gapdh* as the best HKG candidate that could be used for quantitative ISH on the female *An. gambiae* brain.

This toolset of analytical and biological knowledge gathered in the course of my PhD allowed finalizing robust annotation of mosquito brain cell types and investigating its functions in association to both physiological and pathological conditions. We set up an experimental workflow that can allow extensive cell type investigation on organs and organisms in which cellular composition is uncharted, that includes scRNA-seq and the use of orthology-based algorithms, spatial transcriptomics, and ISH. The molecular and histological know-how described above allowed us to integrate multiple techniques to reach this aim. The collection and interpretation of bulkRNA-seq data in parallel with scRNA-seq data allowed us to show how our atlas encloses information that might provide indications on cell type of origin of relevant signals obtained with less resolute techniques (bulk RNA-seq), providing a relevant tool for the community to improve inferences obtained with the quick, established and cost-effective bulk RNA-seq, with the potential to enhance and speed up data interpretation and project progression.

Chapter 2: The *An. gambiae* brain at spatial and single cell resolution

Submitted manuscript

Title-

The *Anopheles* mosquito brain at spatial and single-cell resolution

Authors-

Irene Z. Rossi [1], Cécile Cassan [1]†, Johannes W. Bagnoli [1]†, Sümeyye Özhan [2,3], Adeline Valente [1], Quentin J. Delorme [1], Geert-Jan van Gemert [4], Chiara Andolina [4], Wouter Graumans [4], Richard Bártfai [5], Avinash R. Shenoy [6], David Carrasco [1], Emmanuel Perisse [7], Teun Bousema [4], Sarah H. Merkling [2], Anna Cohuet [1,*‡], Arthur M. Talman [1,*‡]

[1] MIVEGEC, Université de Montpellier, IRD, CNRS, Montpellier, France

[2] Institut Pasteur, Université Paris Cité, CNRS UMR2000, Insect Infection & Immunity group, Insect-Virus Interactions Unit, Paris, France

[3] Sorbonne Université, Collège Doctoral, 75005 Paris, France

[4] Department of Medical Microbiology, Radboud University Medical Center, Nijmegen, the Netherlands

[5] Department of Molecular Biology, Radboud University, 6525 GA Nijmegen, the Netherlands

[6] Department of Infectious Disease, Imperial College, London, UK

[7] Institute of Functional Genomics, University of Montpellier, CNRS, Inserm, 141 rue de la Cardonille, 34094 Montpellier Cedex 5, France

†These authors contributed equally to this work

‡These authors contributed equally to this work

*Corresponding authors. Email: anna.cohuet@ird.fr, arthur.talman@ird.fr

Abstract-

Blood-feeding in *Anopheles* mosquitoes is at the root of all malaria infections and is supported by a range of physiological and behavioural adaptations. However, the cellular and molecular mechanisms underlying mosquito behavior are almost uncharted. Since behavior is orchestrated at the level of the central nervous system, we surveyed the cellular diversity in the female *Anopheles gambiae* brain. We further leveraged spatially-resolved transcriptomics to understand how this cellular diversity is organised in the mosquito head. Finally, we describe transcriptional changes associated with mosquito life history events (mating, blood-feeding, *Plasmodium falciparum* infection, age). Our atlas provides the first map of the malaria mosquito brain, a resource which will enable the study of non-model insect neurobiology, the neural basis of vector behavior and mechanisms underlying malaria transmission.

Introduction-

The nervous system is responsible for perception and integration of both endogenous and environmental cues, enabling decision-making and the generation of appropriate responses. The cellular diversity and neuroanatomy supporting this network are mostly uncharted in insects, and most of the knowledge on the insect brain has been derived in *Drosophila melanogaster* [1,2]. In such model systems, cellular diversity can be interpreted in the light of decades of studies on cell lineages and developmental processes. However, highly diverse behaviors and distinct anatomical structures are found amongst insect species [3,4]. In mosquitoes, blood-feeding has evolved as an essential trait for nutrient acquisition supporting egg development, but has also been exploited by pathogens as a means to gain access to new hosts. *Anopheles* females are the sole vectors of human *Plasmodium* parasites, and long term ecological interactions have shaped their coevolution [5]. *Plasmodium falciparum* is also suspected to manipulate the host-seeking and biting behavior of its vector to enhance transmission success, albeit with conflicting evidence [6–8].

The organization and diversity of cell types in the central nervous system (CNS) of non-model organisms and insect vectors has just started to be explored and

contrasted to model organisms by means of cell type taxonomy methods and cross-species cellular annotation [9–11]. In *Anopheles*, very little information exists on the structure and composition of the CNS in spite of the central role of behavior in determining vectorial capacity [12–14]. Here, we determine the cellular diversity of the female *An. gambiae* brain, spatially-resolve the organisation of the CNS within mosquito heads, and establish transcriptional signatures of mosquito life history events associated with malaria parasite transmission.

Results and discussion-

A cellular atlas of the female *An. gambiae* brain

We dissociated brains from six pools of *An. gambiae* female mosquitoes and analyzed them using single cell RNA-seq (10X genomics) (Fig. S1A). After quality control, the *Anopheles* brain atlas consisted of 48,806 cells (~ 20% of the number of expected cells in a single brain [13], with an average of 5,350 unique molecular identifiers (UMIs) and 1,678 genes per cell (Fig. S2A, B, C and D). We first performed dimensionality reduction analyses and mapped the expression of cellular markers for neurons (*elav-like*) and glia (*repo*) as these markers are widely conserved across the animal kingdom [15,16] including in dipterans [13] (Fig. 1A). Using a conservative approach, we identified 45 cell clusters, (hereafter An clusters). All cell clusters were present in all experimental replicates indicating their consistent representation in the mosquito brain (Fig. S2E and F). As expected a large majority of cells expressed *elav-like* and lacked significant expression of *repo*, and were grouped in 41 neuronal cell clusters (Fig. 1A and B). In contrast, *repo* was expressed in a minority of cells belonging to 3 clusters (An10, An23, An25) (Fig. 1A and B). Cluster An42 showed a highly differentiated transcriptome and did not show expression of *elav-like* or *repo*, but expressed *collagen type IV alpha* (*col4a*) (Fig. 1A), an ortholog of the *D. melanogaster* (Dm) hemocyte marker *col4a1* [17]. Notable marker genes and neurotransmitter profiling allowed us to further classify clusters into main cell types (Fig. 1B, Table S1). We next combined a cross-species cell type mapping (SAMap) [11] against a *D. melanogaster* dataset [18] with a comprehensive conserved marker gene survey to annotate the atlas (Fig. 1C). All clusters were

computationally assigned to at least one *D. melanogaster* cluster with a permissive SAMap alignment score > 0.1, except An29 and An43 (Table S2). Although the SAMap approach accounts for evolutionary divergence between *D. melanogaster* and *An. gambiae* (~250 M years [19]) by including gene-gene paralogy in homolog gene program identification, we cannot outrightly assign cell type based on SAMap results, however, we leveraged them to guide our manual cluster annotation. We concomitantly identified marker genes for each cluster, with an emphasis on genes with orthologs with known functions in other systems and combined these results with the SAMap cell type assignment (Table S1, Table S2). As a result, we confidently ascribed an identity to 30/45 cell clusters, showing a large overlap in cellular composition in the CNS of *D. melanogaster* and *An. gambiae*. We observed a high concordance of our marker-based cell type assignment with the algorithm-predicted clusters (Fig. S3, Table S2, Table S3). For instance, An41 was assigned with high confidence to Poxn neurons (alignment score = 0.89, Fig. S3, Table S2) and consistently was marked by expression of *poxn* [20] (Fig. 1B). For the clusters for which we could not confidently assign an identity we postulate that this could arise from technological limitations of cell state capture, biological divergence between cell types and perhaps point to the existence of *Anopheles*-specific cell types (*i.e.* An29 and An43). Altogether, our brain atlas provides the first comprehensive map of the cellular diversity in the *An. gambiae* brain.

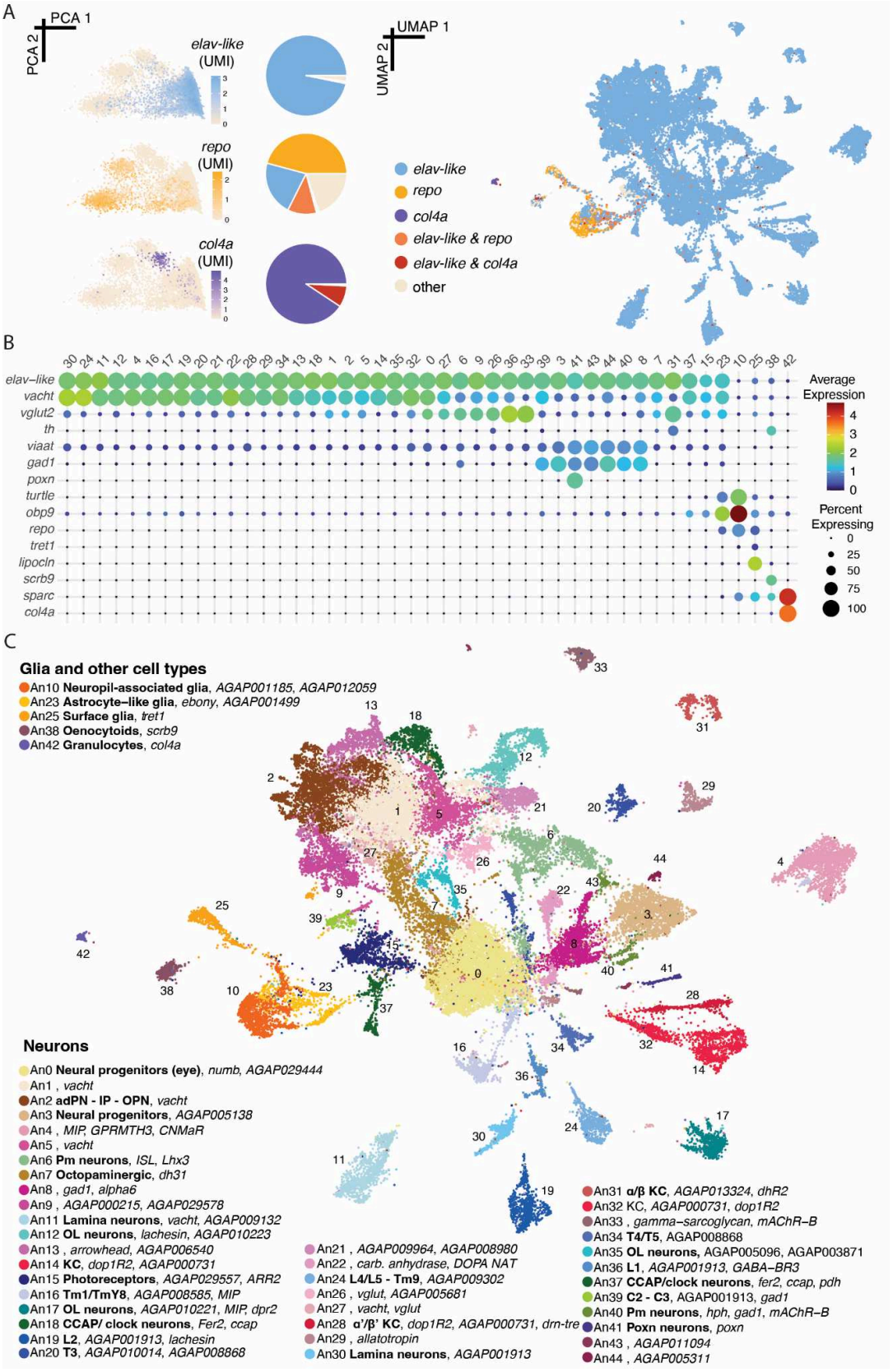


Figure 1. A cellular atlas of the female *An. gambiae* mosquito brain. (A) Left panel: PCA of the

(continued)

48,806 transcriptomes in the atlas highlighting expression levels of *elav-like*, *repo* and *col4a*. Right panel: the pie charts show the percentage of cells expressing these marker genes in 41 putative neuronal clusters, three putative glial clusters (An10, An23 and An25) and the putative hemocyte cluster (An42), alongside expression of these markers in a UMAP representation of the atlas. **(B)** Notable marker gene and neurotransmitter scaled average expression (z-score) in the 45 clusters of the atlas (cluster ID on top). **(C)** UMAP of the brain atlas displaying consensus annotation of the clusters (**bold**) and notable gene markers in each cluster (*italics*).

Spatial organisation of the female *An. gambiae* head

We next sought to define the spatial organisation of the brain within the head of *An. gambiae* female, as its neuro-anatomy has not been investigated yet. We initially used confocal microscopy with a general marker on dissected brains to understand and contrast the anatomy of the *Anopheles* brains compared to other dipterans (namely *D. melanogaster* and *Aedes aegypti*). We observed classical insect brain structures, as described earlier [14,21], such as the optic lobes, the subesophageal zone, the mushroom body or the central complex. However, we noted minor differences compared to the *Drosophila* brain such as the different substructures of the central complex, the number of antennal glomeruli [22] or the different lobes of the mushroom body (Fig. S4). In the mushroom body, we observed classical vertical and horizontal lobes subdivided into different subclasses of Kenyon cells (KCs) [23,24] and subcompartments likely innervated by different subtypes of neuromodulatory neurons (e.g. dopaminergic neurons [25,26]). We next performed histological sections followed by hematoxylin and eosin (H&E) staining, and observed hematoxylin-stained cell body rind regions as well as eosin-stained neuropils (Fig. 2A). Brain regions were more readily observed in the axial sections and this orientation was selected for further experiments. We used RNAScope *in situ* hybridisation (ISH) on head sections and observed a wide distribution of the neuronal marker *elav-like* in soma-rich regions of the brain (Fig. 2B), marking the optic lobe underlying the eye region as well as deeper cell body rind regions. To systematically understand the composition of these regions in the brain, we generated a Slide-seq spatial transcriptomic dataset of 8 female heads from two arrays (10 μm resolution) [27] (Fig. S5A). After quality control, we recovered 9,914 high quality

spatially-resolved transcriptomes (Fig. S5B), grouped in 14 spatial clusters (hereafter Sp clusters) (Fig. S5C and D). To facilitate annotation, we subsetted, oriented, and aligned transcriptomes of five high quality heads using the consecutive H&E stained slices as a guide (Fig. S5A). Using a consensus classification approach combining (i) marker gene analysis (Table S2), (ii) mapping of the spatial clusters onto the cell atlas (Fig. S5E) with 66% of the spots matching to one or more single cell clusters, (iii) an inter-spatial cluster distance metric (Fig. S5F), and (iv) spatial distribution of the clusters (Fig. S6), we were able to assign a tissue and cell composition to most spatial clusters (Fig. 2C, Table S2). Sp1 and Sp4 were associated with glia, while Sp10 was assigned a hemocyte ontology. Neurons were grouped in Sp2 and Sp12, marked by expression of *elav-like* and situated within the cell body rind region (Fig. 2C). Sp11 and Sp13 were located outside the head (Fig. S5D), could not be associated to a single cell cluster and were marked by expression of *salivary gland protein 2-like* and *odorant binding protein 48*, and they were therefore respectively assigned to salivary gland and antennae tissue. Two other clusters positioned in the anterior and posterior parts of the head sections were not associated to any An cluster and were marked by expression of multiple myosins (Table S3). Consequently these were assigned to head-associated muscle tissue (Sp3 and Sp6). Sp9 was consistently situated at the front of the heads and was assigned to clypeus (Fig. 2C, Fig. S6). Finally, the eye region was defined by several clusters (Sp5, Sp7, Sp0, Sp8), which corresponded to eye-associated/lamina single cell clusters and were situated in proximity to spots with expression of vision-associated genes, such as *arrestin 2* (Fig. 2C).

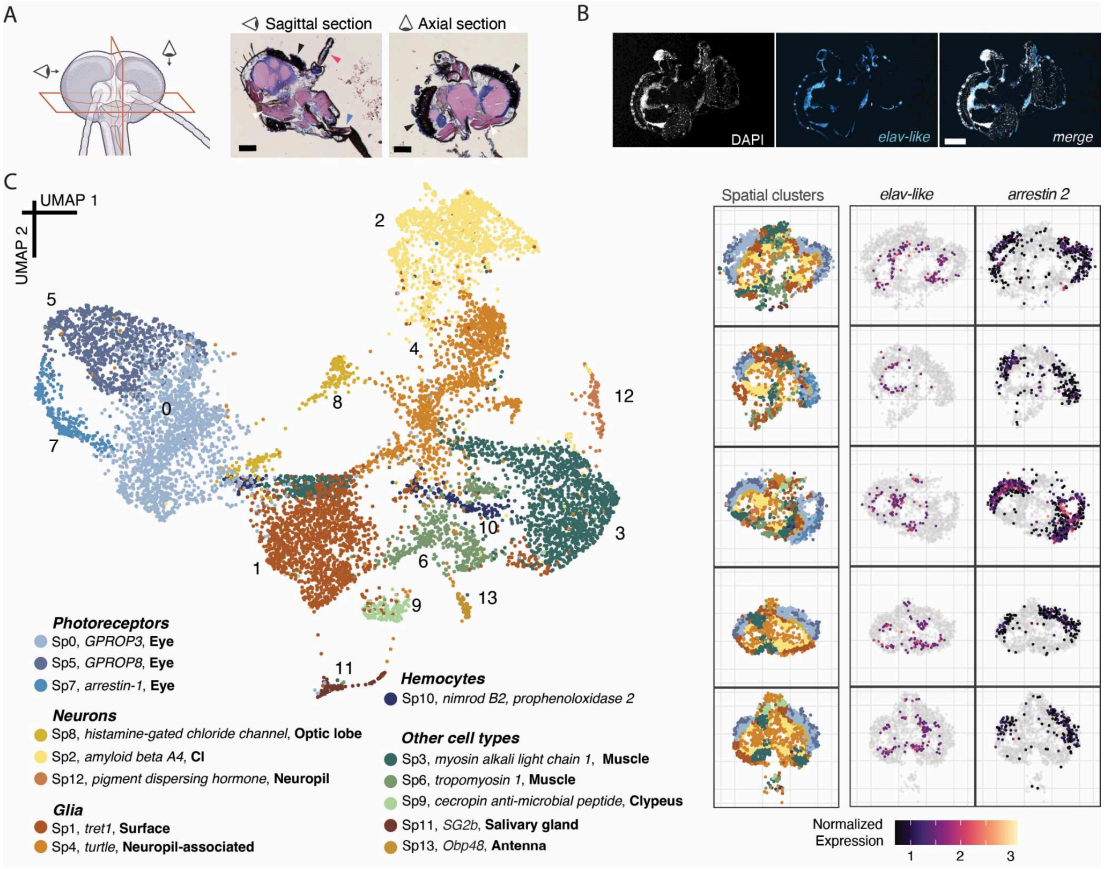


Figure 2. Spatial organisation of the female *An. gambiae* head. (A) Schematic of sectioning orientation of mosquito heads. H&E staining of a sagittal and an axial cut of *An. gambiae* female heads; eye (black arrows), muscle (white arrows), antenna (magenta arrow), and proboscis (blue arrow) are annotated (scale bar = 10 μm). **(B)** ISH imaging of axial histological sections of a mosquito head (front of the head on the top, scale bar = 100 μm), highlighting nuclei (DAPI) and the neuronal marker *elav-like* (oriented with the front of the head on top and the right side of the head on the right). **(C)** Left panel: UMAP representation of 9,914 high quality spatially-resolved transcriptomes. The transcriptomes were clustered and grouped by the predicted major cell types (***bold italics***). For each Sp cluster, notable marker genes (*italics*) and likely tissue of origin (**bold**) are indicated. Right panel: Sp clusters displayed in their spatial context in 5 high quality aligned head regions (oriented with the front of the head on top and the right side of the head on the right). Normalized expression of the neuronal marker *elav-like* and the eye-associated marker *arrestin 2* are displayed.

A spatially-resolved map of cellular diversity in the *An. gambiae* brain

We next sought to combine our cell atlas and our spatially-resolved data to determine the ontology of different cell populations within the brain, understand marker conservation and diversity, and identify important

structures in the female *Anopheles* central nervous system (CNS), thereby providing the first comprehensive transcriptomic cartography of the female *Anopheles* brain.

Glia. Glia are pivotal for neuronal development and function and have been shown to be at the root of behavioural responses [28]. The three *repo*-expressing clusters An10, An23 and An25 were all strongly associated with glial cell types in the reference dataset (Fig. S7A). All glia clusters expressed *threonine 3-dehydrogenase* (AGAP011948) (Fig. 3A), an ortholog of Dm *CG5955*, which is involved in sleep regulation in the brain, a function strongly associated with glia [29,30]. Notably, all glial clusters expressed genes involved in lipid mobilization, a well established glial function which fuels neural metabolism: they included *obp9*, an ortholog of Dm *obp44a* with a role in lipid trafficking in the astrocytes of the fly [31], and *lipocln* (AGAP005223), an ortholog of Dm *glaz*, known to work as a glia-neuron lipid shuttle [32] (Fig. S7B, C and D).

Surface glia have a unique role of insulating the brain from the hemolymph forming a blood-brain barrier. An25 was associated to both perineurial and subperineurial glia and expressed surface glia markers *tret1*, an ortholog of Dm *tret1-1*, a marker of perineurial glia in the CNS [33], as well as *ABC transporter (Family B member 2)* (AGAP005639), an ortholog of Dm *mdr65*, a marker of sub-perineurial glia [34] (Fig. 3A, Fig. S7D). We used ISH to determine the distribution of *tret1*-expressing cells. Our probe panel measured RNA signals from *elav-like*, *repo* and *tret1* transcripts. We identified a dense neuronal cell body rind using the *elav-like* signal, and observed that *repo*-expressing cells were broadly distributed. In contrast, *tret1* had a continuous distribution on the surface of the cell body rind (Fig. 3B), suggesting that the *Anopheles* brain is insulated by surface glia expressing *tret1*. Interestingly, the Sp1 spatial cluster partially matched An25 and was marked by surface glia markers (Table S2). Sp1 was distributed peripherally within the mosquito heads (Fig. 3C), and located at the immediate proximity and at the surface of the cell body rind Sp2 (Fig. S5F and S6). We concluded that An25 and Sp1 confirm the presence and distribution of surface glia in the *Anopheles* brain. Interestingly, we could not differentiate

within An25 between perineurial and subperineurial glia with more than a third of An25 cells expressing both *tret1* and AGAP005639. This suggests a possible divergence in functional sub-compartmentalization between mosquito and fly surface glia.

The ISH distribution of *repo* confirmed the presence of glial cells within the cell body rind and the neuropil (Fig. 3B). Concordantly, Sp4 was associated with An10 and was distributed within both cell body rind and neuropil regions, like AGAP001185 (*smct1*) (Fig. 3B and C), an ortholog of the neuropil-associated glia marker Dm *rumpel* [35]. An10 was most strongly associated with *D. melanogaster* ensheathing, cortex and astrocyte-like glia, whilst An23 was mapped to astrocyte-like glia (Fig. S7, Table S2). In addition, both of these single cell clusters expressed known glial markers (Fig. 1B, Fig. S7B,C and D, Table S1). However, they did not align with specific glia cell type markers in *D. melanogaster*, and displayed co-expression of markers in the same cell thought to be exclusive of specific cell types in *D. melanogaster*. For instance, we observe co-expression of orthologs of Dm *ebony* and *rumpel in* 45% of the cells in An10 and An23, which are respectively markers of astrocyte-like glia [36] and ensheathing glia [35]. Another example is provided by the wide expression of *turtle* in An10, an ortholog of Dm *bdl*, a marker of wrapping glia [37], contrasting with the restricted expression of the ortholog of another wrapping glia marker Dm *wrapper* [38](AGAP012059) in only a small subset of An10 cells (Fig. S7D). This suggests that functional markers of *D. melanogaster* internal glia are not conserved in *An. gambiae*. However, we capture a rich diversity of internal glia cell types within An10 and An23 and identify markers of these different cell types (Table S1, Table S3), which may be leveraged to understand unique glia biology in the mosquito CNS.

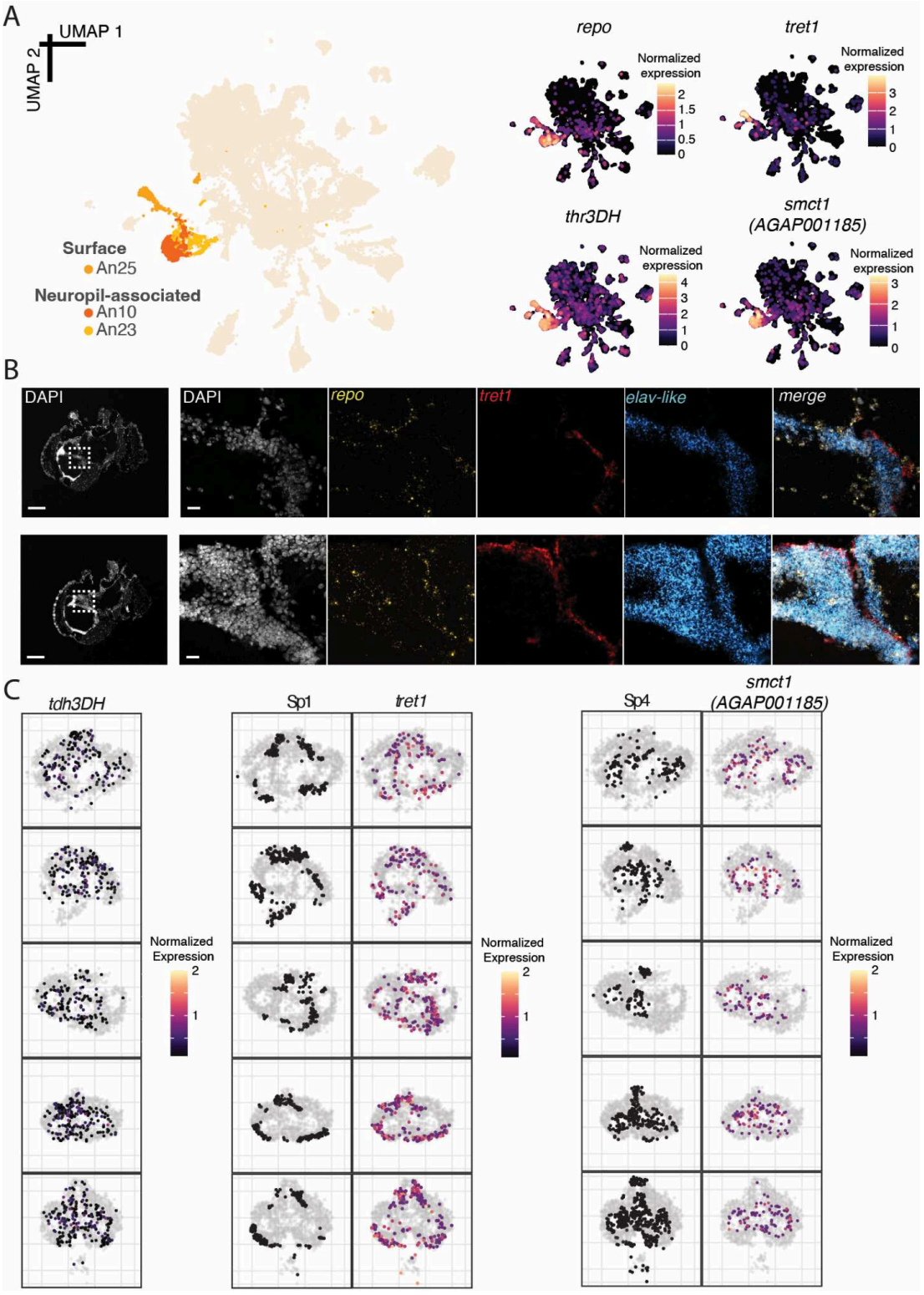


Figure 3. Diversity of glial cell types within the *An. gambiae* CNS. (A) Annotated glia clusters and expression of generalist glia markers (*repo* and *thr3DH*), as well as surface glia (*tret1*) and neuropil-associated glia marker genes (*smct1*). **(B)** ISH images of histological sections of mosquito heads. The whole section is shown on the left with nuclear staining and highlights the position of

(continued)

the inset that is displayed on the right (scale bar = 100 µm, front of the head on top); transcripts of glial marker genes (*repo* and *tret1*) are stained alongside those of the neuronal marker elav-like and nuclear staining (scale bar = 10 µm). **(C)** Five high quality spatial sections (axial cuts, front of the head on top) highlighting the expression of generalist glial marker *thr3DH*, as well as the position of Sp glia clusters and reporter marker expressions associated with surface glia (Sp1 and *tret1*) and neuropil-associated glia (Sp4 and *smct1*).

Vision and circadian neurons. The insect visual system occupies a big volume in the brain (Fig. 4A) and consists of well defined regions (photoreceptors, lamina, medulla, lobula complex), that are composed of distinct cell types [39,40]. Our single cell atlas identified many putative vision-associated cell types (Fig. S8A), which could be grouped in broad categories, including photoreceptors (An15), optic lobe-associated neurons comprising (i) lamina monopolar (An11, An19, An24, An30, and An36), (ii) posterior-medial neurons (Pm) (An6 and An40), (iii) C2/C3 cells (An39), (iv) trans-medullary TmY1/TmY8 (An16), and (v) bushy T neurons T3, T4/T5 (An20, An34). We also associated An17 and An35 to the vision since they showed robust expression of eye-related genes, namely AGAP010221 (Dm *dip ε*, *θ*, *κ*) and *dpr2* [41,42], and AGAP005096 (Dm *optix*) [41,42] (Fig. 4B, S8A-C, Table S2). For example, we annotated An6 and An40 as Pm since these clusters are GABAergic (Fig. 1B) and expressed *LIM/homeobox protein Lhx3* (Dm *lim3*), *nuclear receptor subfamily 2 group F member 3* (Dm *svp*), and *homeobox protein homeothorax* (Dm *hth*) (Fig. S8B, Table S1), which are markers of *D. melanogaster* Pm [43]. We also determined that the expression of either one of two markers identifies different subpopulations of the optic lobe neurons: *adcy8* (Dm *rut*) (An11, 19, 30, 36) and *D1-like dopamine R2* (An17, 20, 24) (Fig. 4B). We performed multiplex ISH of these two markers in regions where both the ommatidia and the cell body rind (*elav-like* positive) were discernible and showed that both markers were present in the lamina with distinct expression patterns, confirming them as appropriate markers of these cell populations and the annotation as optic lobe cell types (Fig. 4C). Interestingly, our spatial transcriptomic dataset captured the expression pattern of the whole eye from photoreception (Sp0, 5, 7) to signal integration in the lamina (Sp8) (Fig. 2C), and displayed a highly structured pattern (Fig. 4D). We reasoned that we

could use these data to identify genes related to vision and signal integration. We therefore selected 3 regions where the tissue sectioning captured the full transition from the lens through the ommatidia and to the optic lobe neurons soma in the cell body rind, and performed an expression-by-distance analysis to identify and contextualise vision-associated genes (Fig. 4D). Using this approach, we identified 103 candidate genes linked to the eye region (Table S4). These ranged from eye-specialised cuticular protein (*e.g. cpr132*) [44], peripheral opsins in the photoreceptor cell (*e.g. gprop8*) [45], through signal transduction factor (*e.g. arr2*) [46] to signal integration in the lamina (*e.g. histamine-gated chloride channel*, *elav-like*) (Fig. 4D and E). Opsins are key to photoreception and have been shown to have expanded in different dipterans [45] but their specific role is unclear in *Anopheles* [47]. Here, we detected five dominantly expressed opsins (*gprop1*, 3, 4, 6, 8) in An15 (Table S3) and within the ommatidia (Table S4). Amongst those there are three representatives of the *Rh6* (long wavelength sensitive) that are responsive to green light in *Drosophila* species but have been shown to have undergone diversification in *Anopheles* [45], and a single putative *Rh3/4* ultraviolet wavelength-sensing opsin. This particular opsin repertoire is likely tailored to the dusk-dawn and night conditions in which adult female *Anopheles* mosquitoes are active for mating and seeking their host.

Vision is intimately linked to circadian rhythm and is usually controlled by specialized inter-regional neurons with projections spanning across multiple neuropils. Interestingly, An11 and An30 were characterized by AGAP001726, an ortholog of Dm *wake*, a clock gene expressed in latero-ventral neurons (LNvs) [48]. Although lamina and LNvs have different tissue localization and roles, lamina neurons have intimate interaction with LNvs and express clock genes in *D. melanogaster* [49–52]. An37 was assigned an LNv identity (Fig. S8A). Furthermore, An37 and An18 were mapped to a CCAP neuronal identity (Fig. S8A), and showed localised expression of the *cardioacceleratory peptide* (Dm *ccap*) (Fig. 4B), which is involved in regulation of circadian behaviors [53,54]. In addition, both clusters were marked by AGAP003739, an ortholog of Dm *fer2* (Fig. S8B, Table S1), which is expressed in a subset of circadian pacemaker neurons [55]. An37 was marked by *zic* (Dm *opa*) [56] and *pdh* (Dm *pdf*), which in other dipterans are associated with a

small number of circadian pacemaker neurons [57,58]. In our spatial data, Sp12 was annotated as an LNv cluster (Table S2). Only two heads sections displayed the Sp12 focus which was positioned in a lateral anterior focus within the cell body rind, the other heads were likely sectioned in a different plane devoid of Sp12 (Fig. 4E), suggesting that LNv cellular bodies have a spatially restricted distribution in the *Anopheles* brain. In agreement with these observations we noted ISH foci of AGAP003739, one of our clock neuron markers, localized in soma-rich structures, in continuity with those lining the outer optic lobe (Fig. 4F). This location matches the one described for *D. melanogaster* clock neurons [48] (Fig. 4A). Altogether, our data showed two distinct clock neuron populations (Fig. S8B and E), and located LNvs foci within the *An. gambiae* brain.

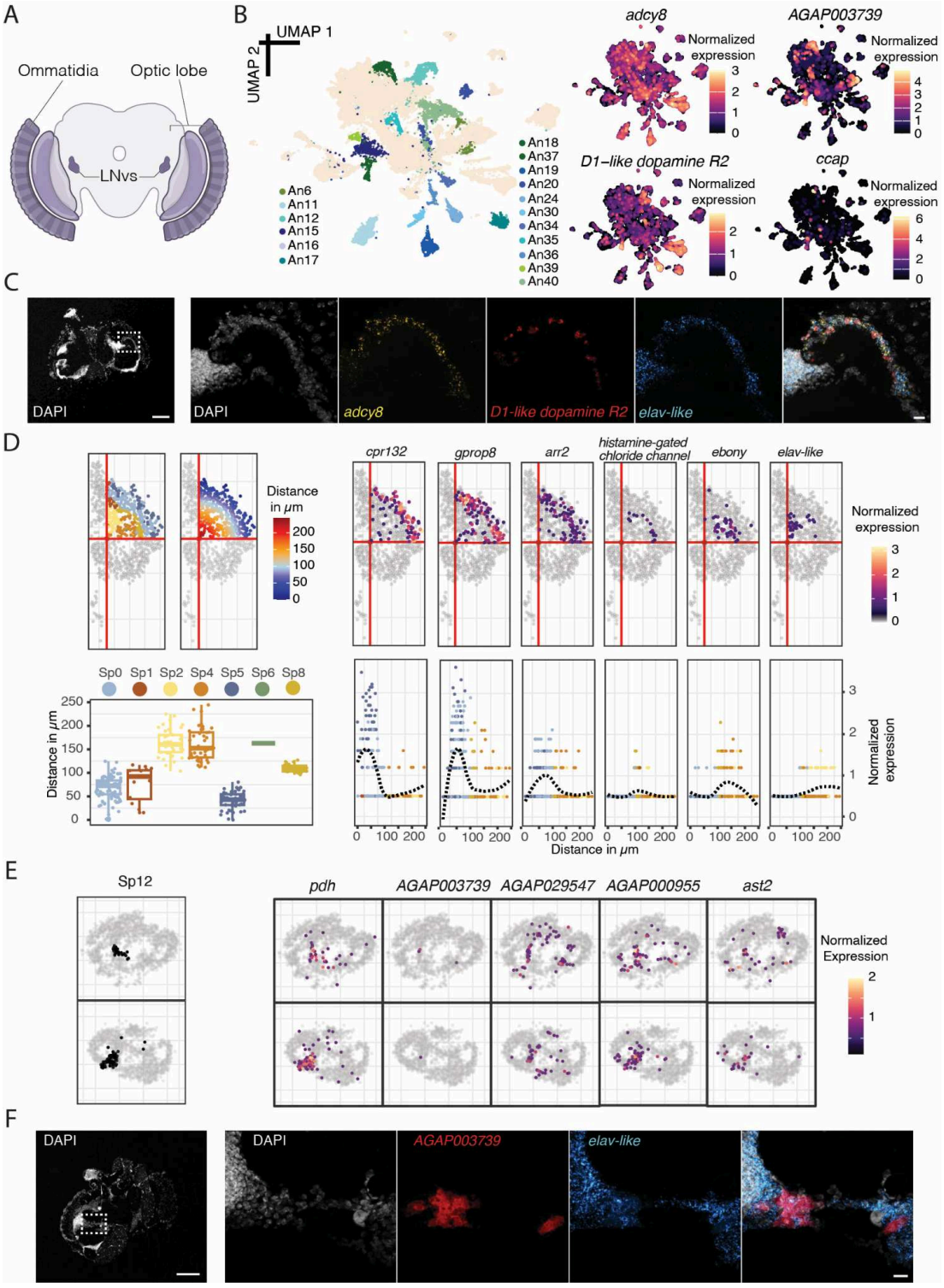


Figure 4. Optic lobe and circadian neurons in the visual system of *An. gambiae*. (A) Schematic of the expected positions of optic lobes and clock neurons in *An. gambiae* brain. **(B)** Annotated optic lobe and clock neuron clusters and expression of optic lobe markers (*adcy8* and *D1-like dopamine R2*), as well as clock neuron markers (*ccap* and AGAP003739). **(C)** ISH images of histological sections of mosquito heads. The whole section is shown on the left with nuclear staining (DAPI) (continued)

and highlights the position of the inset that is displayed on the right (scale bar = 100 μm, front of the head on top); transcripts of optic lobe marker genes (*adcy8* and *D1-like dopamine R2*) are stained alongside those of the neuronal marker *elav-like* and nuclear staining (scale bar = 10 μm). **(D)** One section of a head, showing the distribution of clusters within this section as well as the distance of spots to a centrally-set reference. This reference was used to compute gene expression distribution by distance in the eye structure and the the optic lobe of the mosquito and to identify genes with a distance responsive distribution (from the reference center point(red)) which may be involved in the visual system, example *in situ* gene expression patterns as well as distance computed distribution are displayed in the right panel, the full complement of distance responsive genes is given in Table S4. **(E)** Distribution of Sp12 in two high quality heads as well as normalized expression of five markers of clock neurons (Table S3). **(F)** ISH images on histological sections of mosquito heads. The whole section is shown on the left with nuclear staining and highlights the position of the inset that is displayed on the right (bar = 100 μm, front of the head on top); transcripts of clock neurons marker gene AGAP003739 are stained alongside those of the neuronal marker elav-like and nuclear staining (scale bar = 10 μm).

Kenyon cells. The mushroom bodies (MBs) are paired structures in insect brains, including *Anopheles* (Fig. S4), they are involved in olfactory associative learning, memory and goal-directed behavior [59]. The MBs are primarily composed of intrinsic KCs (Fig. S9A). *D. melanogaster* KC axons typically form horizontal and vertical α/β, α′/β′, and γ lobes, but can be further functionally subdivided into 7 subtypes with a likely unique molecular profile [25]. We identified four distinct KC types of the *Anopheles* MBs. An14, An28, An31 and An32 were associated with one or multiple KC clusters in *D. melanogaster* and expressed multiple KC markers (Fig. S9B-E, Table S1-S3). An28 was assigned to the α′/β′-KC cluster and expressed α′/β′ markers, for instance AGAP000585 the ortholog of Dm *mamo* which specifies a cell's fate in α′/β′-KC [60,61] (Fig. S9B, C, D and E, Table S2). An14 and An32 were associated with both α/β and γ KCs (Fig. S9B). An14, An28 and An32 were marked by expression of genes important for MB development such as as *drn-tre* (Dm *rn-tre*)[62] and for memory formation in MBs, as *nuclear receptor subfamily 2 group E member 3* (Dm *hr51*), *slingshot* (Dm *ssh*), adcy8 and *D1-like dopamine R2* (Dm *dop1R2*) [63–66] (Fig. S9C and E, Table S3). We further noted that An28 and An32 were marked by AGAP029446, an ortholog of Dm *trio*, a marker of α′/β′ and γ KCs [67]. An31 expressed AGAP013324, an ortholog of Dm

TyrR, which is involved in regulation of RNA condensates in MBs [68] (Fig. S9C and E). Although our clusters do not individually align with different KC subtypes in the reference, the transcriptional signature of these clusters suggests conserved KC functions in the *Anopheles* CNS including MB neuroblast proliferation, axon growth and guidance, MB neural network wiring and circadian processes. We further identified a small subcluster of Sp2 that was characterised by the expression of markers of An14, An28, An31 and An32 (Table S3). We isolated these 18 spots (Fig. S9F) and conducted a marker analysis, identifying 11 marker genes, 8 of which were shared with KC single cell clusters (Table S5). These spots clustered in a single focus within the brain's cell body rind, which expressed KC markers and therefore corresponds to an *Anopheles* MB. Altogether, we defined four distinct KC types of the *Anopheles* MBs associated with distinct and *Anopheles*-specific transcriptional profiles.

Immune cells. Three types of hemocytes are described in *Anopheles*: the phagocytic granulocytes, the melanin producing oenocytoids, and the prohemocytes, possible precursor cells of the two mature hemocyte types [69]. An42 was associated with *Drosophila* plasmatocytes and expressed numerous *An. gambiae* granulocyte markers, including *lrim16a*, *lrr8*, *col4a* and *sparc* [70] (Fig. S10A, B, C and D, Table S1). An38 specifically expressed *scrb9*, a univocal marker of *An. gambiae* oenocytoids [70] (Fig. S10B, C and D). We did not identify prohemocytes, suggesting there is no hematopoietic differentiation in the brain. Immune cells were also captured in our spatial data (Sp10) and were distributed throughout the head samples, but showed a preferential proximity to head muscles (Sp3, Sp6) and glia cells-containing foci (Sp1, Sp4) (Fig. 2C, Fig. S5F). We further confirmed granulocyte presence in the *An. gambiae* female head by ISH, which consistently showed *col4a*-positive cells associated with *elav-like*-negative nuclei at the back of the mosquito head (Fig. S10E). Interestingly, the ISH data also suggested that granulocytes can locate between the lamina and the ommatidia (Fig. S10E). Altogether, our results show for the first time mosquito immune cells located in the brain periphery, at the limit of

the insect blood-brain barrier, and are consistent with a recruitment of mature hemocytes from the hemolymph compartment [71, 72].

Other cell types and structures- Other cell types included An0 and An3 which expressed markers suggestive of a progenitor state (Table S1). An0 was marked by expression of *numb*, which in *D. melanogaster* controls asymmetric division in sense organ precursors [73,74] and planar cell polarity establishment in eyes [75], suggesting a possible optic lobe progenitor cell type. In contrast, An3 is marked by the expression of AGAP005138, an ortholog of *lmx1a*, which is associated with neural progenitors in fruit flies and humans [76,77]. While neurogenesis has been shown to take place in the CNS of some adult insects both in physiological conditions and after injury [78–81], to our knowledge this is the first suggestion of this process in an adult mosquito brain.

An2 was associated to 9 *D. melanogaster* olfactory projection neuron subtypes (Fig. S3) suggesting it is composed of cells of the antennal lobe. Interestingly we could identify a subset of 12 cells expressing the multifunctional neuropeptide *allatotropin*, possibly representing a rare cell type amongst antennal lobes neurons [82].

We reasoned that the tight packing of the cell body rind in combination with current technical restriction of spatial transcriptomics could lead to multiple cell types being captured in the Sp2 cell body rind cluster and render the identification of specific structures difficult, especially those composed of a few neurons in each brain. To establish whether we could recover specialized structures within the cell body rind we selected two marker genes of cell clusters captured in the atlas, *Dh31* a top marker of octopaminergic neurons (An7), and *mip* a marker of MIP-neurons (An4). Robust expression of these markers identified sub-clusters within Sp2 (Fig. S11A and B) and had a discrete localisation in the head suggesting octopaminergic and MIP neurons mark discrete structures within the brain of *Anopheles* as in *D. melanogaster* [83,84].

Life history is associated with distinct brain transcriptional states

The different life phases of adult female anophelines are associated with distinct behaviors such as mating or host-seeking, which are likely underlied by distinct neuro-transcriptional states [85–87]. Typically, a virgin female will mate prior to blood feeding and may become infected upon a blood meal on an infectious human. In the case of *An gambiae - P. falciparum* it will then take ~ 10 to 14 days for *P. falciparum* sporozoites to colonize the salivary glands and render the mosquito infectious to another human host, so that only older mosquitoes can transmit parasites [88]. We reasoned that these states may vary significantly amongst individuals, and therefore developed a protocol for single brain RNA-seq (Fig. S1B). We first compared brains from virgin and mated females (Fig. 5A). Most of the 121 differentially expressed genes (DEGs) were upregulated after mating (Table S6). Using our single cell data we determined that DEGs are mainly associated with neurons (Fig. 5B), suggesting a modified neuronal profile after mating. In particular, alterations in expression of transcription factors whose orthologs are involved in circadian rhythm and behavioral regulation, cell fate specification, and axon guidance [89–91], accompanied by chromatin repressors and neural network remodelers [92,93] suggest that mating triggers active rewiring and signaling in the female mosquito brain (Fig. 5C). In addition to that, we identified a post-mating upregulation of a putative receptor for serotonin (GPR5HT1A), a neurotransmitter associated with mating refractoriness in *D. melanogaster* [94].

We then compared brains of age-matched sugar-fed mated females with those of mated females 24 hours after a blood meal (Fig. 5D). We found 1,895 DEGs (Table S6) to which we ascribed a putative cellular type origin (Fig. 5E). Blood feeding induced a profound alteration in genes associated with the translation activity, evidenced by an overall downregulation of genes coding for ribosomal proteins, initiation and elongation factors, and tRNA synthetase, suggesting an overall decrease in translation processes in the brain following blood feeding with an associated increase in transcription of proteasome proteins further pointing to a reshaping of proteostasis (Fig. 5F, Table S6). This is consistent with previous observations in *An. gambiae*, showing a massive uptake

of newly acquired amino acids in reproduction organs after a blood meal, whereas other tissues slow down their translation [95]. A concomitant downregulation of the expression of genes involved in cell proliferation and intracellular signaling (*e.g.* putative GPCR receptors, kinases of the MAPK cascade, Ser/Thr kinases, ion channels) could indicate a lowered response to stimuli, consistent with the refractory/resting interval after a blood meal [96] (Table S6). Switching from sugar to blood digestion corresponds to a massive shift in the amount and type of resources available. Concordantly, we evidenced numerous metabolic alterations, consistent with previous observations in brains of other *Anopheles* species [95]: the expression of enzymes of the purine, pyrimidine, amino acid biosynthesis, glyoxylate and dicarboxylate metabolism, the Krebs cycle, and oxidative phosphorylation increased after blood meal (Table S6, Fig. 5F). This altered metabolic profile contrasts with systemic responses to blood meal [95] and may support highly energy-demanding processes in the brain such as memory consolidation [97,98] during the resting state following a blood meal.

Blood feeding also enhanced immunity genes expression in the brain with upregulation of genes coding for (i) peptidoglycan recognition proteins (*pgrps1*, *pgrps3*) (ii) the Toll-pathway activator *spz1*, pro-inflammatory TNF-α receptor ligand *eiger* [99] (iv) melanization (CLIP domain serine proteases, *srpn2*, *yellow protein*) (v) genes coding for antimicrobial peptides (*cec1*, *def1*) [100] and (vi) extracellular matrix reshaping protein coding genes (Table S6), which are involved in cell migration [101,102]. These genes are predominantly expressed by the hemocyte and the glia clusters in the cell atlas (Fig. 6E, Fig. S12A), suggesting an intrinsic brain immune response to blood-feeding consistent with the presence of immune cells in the brain compartment (Fig. S10). Surprisingly we identified an odorant binding protein *obp9* strongly upregulated following a blood meal (Table S6), this gene is a robust maker of An10 in our atlas (Fig. S7). Together this suggests a non-olfactory role of *obp9*, perhaps associated with metabolic role, as has been hypothesised for its ortholog in *Aedes aegypti* [103].

A recurrent question in malaria transmission biology is whether the parasite manipulates the behaviour of its vector to favor its own transmission [104]. Such a

manipulation would likely have effectors in the CNS of the mosquito. To address this, we generated single brain transcriptomes of *P. falciparum*-infected and uninfected mosquitoes, with a wide range of infection intensities (Fig. S1C, Fig. S13A and B). We compared infected mosquitoes to their non-infected counterparts at (i) 8 days post infection (dpi), when parasites are at the oocyst stage and are not infectious, and (ii) 16 dpi, when parasites are at the infectious sporozoite stage in salivary glands. Our analysis revealed no consistent transcriptional difference at either time point in the brain transcriptional profile, with only *def1* being upregulated at 8 dpi when replicates are combined (Fig. 5G and H, Fig. S13C, Table S6). This could be due either to (i) a transcriptionally-silent parasite manipulation phenotype, (ii) subtle changes below the detection threshold (*e.g.* changes only in a small group of cells), (iii) an ineffective parasitic manipulation in our specific parasite-mosquito strains combination and lab conditions.

All the infected mosquitoes had the same age when challenged with *P. falciparum* (i.e. 6 days old), and were dissected with their non-infected controls either 8 or 14 days later when they were 16 and 22 days old respectively. This window corresponds to the main life period when mosquitoes contribute to malaria transmission in the field [105] and when age-discriminant signals among both field and laboratory reared mosquitoes can be detected by spectrometry methods [106,107]. The median life span of a female *An. gambiae* in optimal conditions is 30 days [108]. Our day 22 time point corresponds to a ~ 30% age-related mortality [108], a proportion where *D. melanogaster* already displays brain aging [18,109]. We therefore explored the influence of aging on the brain and identified a robust transcriptional difference between day 14 and day 22 brains independent of infection status (Fig. 5H, I and J, Table S6). Interestingly we observed signals known to be associated with aging in other systems. For instance, insulin-like-peptides were all upregulated (7/7) (Table S6), these genes have been associated with age-related nutrient sensing [110]. Additionally, immunity impairment with age is well established [111] and we evidence an upregulation of CLIP serine proteases (FDR = 2.92E-07) and serpins (FDR = 3.72E-03) (Fig. S12), which have a role in modulating inflammation [112], and are

likely induced by immune cells and glia (Fig. S12B and C). However, the top upregulated genes with age were mainly linked to oxidative phosphorylation (OxPhos), genes which are expressed in most cell types (Fig. 5K, Fig. S12D). This result contrasts with a usual decline in OxPhos gene expression with age in insects [109,113]. Our observations may reflect an early compensatory mechanism linked to the onset of impaired mitochondrial function in the aging brain [114]. Taken together, these data suggest that aging in the female *Anopheles* brain is initiated by a dysregulation of both mitochondrial function and immunity.

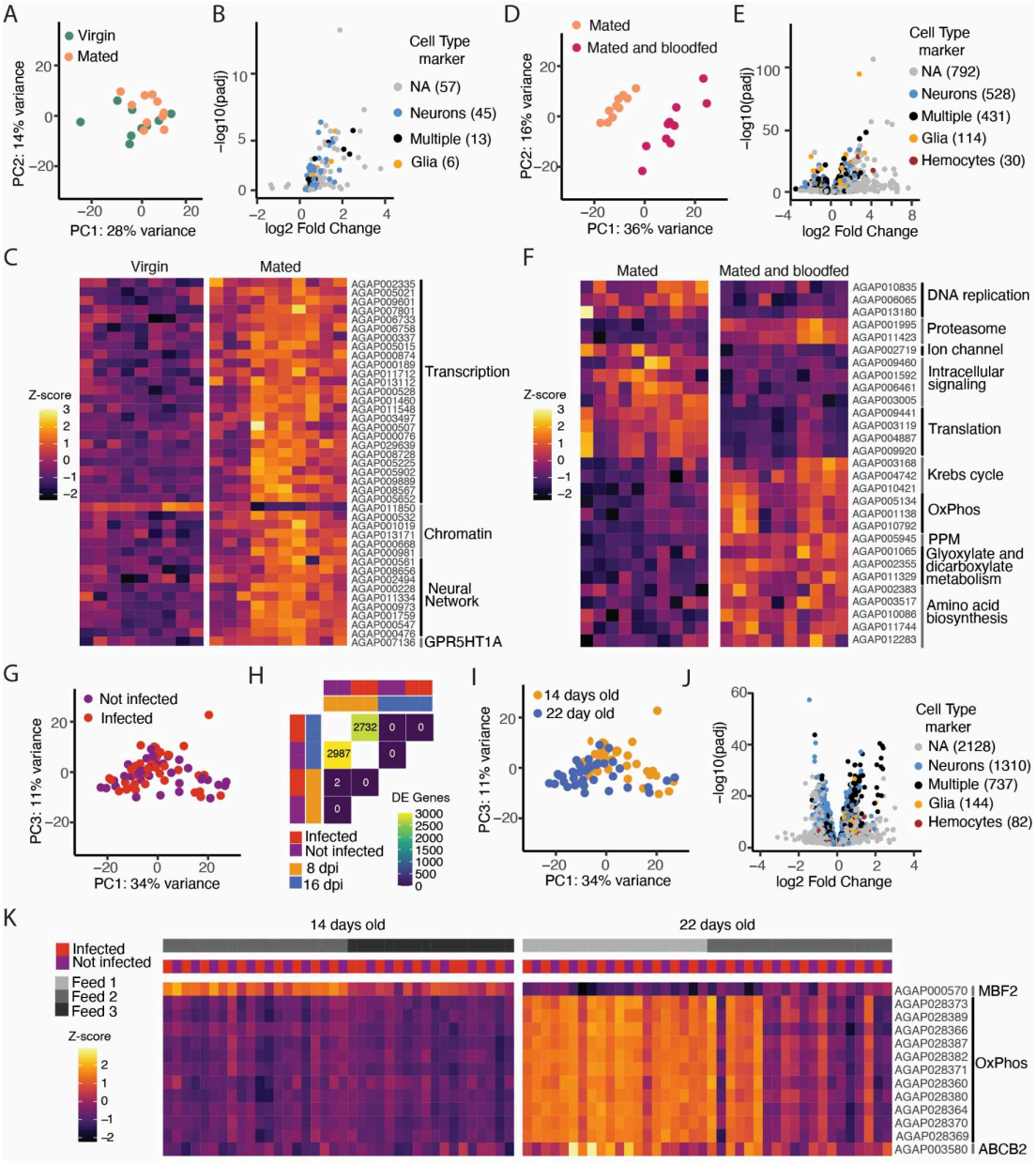


Figure 5. Different biological states in *An. gambiae* females are associated with distinct brain transcriptional states. (A) PCA of single brains transcriptomes from virgin or mated females. **(B)** Volcano plot of DEGs (adjusted p-value < 0.05) between virgin and mated females; genes which are markers of broad cell types present in the atlas are highlighted. **(C)** Heatmap of selected genes from (B), grouped according to broad gene functions curated manually and based on gene ontology and KEGG pathway enrichment. **(D)** PCA of single brains transcriptomes from mated sugar-fed or mated blood-fed females. **(E)** Volcano plot of differentially expressed genes (adjusted p-value < 0.05) between mated sugar-fed or mated blood-fed females. **(F)** Heat map of selected genes from **(**E) grouped according to broad gene functions curated manually and based on gene (continued)

ontology and KEGG pathway enrichment. **(G)** PCA of single brains transcriptomes from infected or non infected females. **(H)** Distance plot showing the number of DEGs found in one-to-one infection condition comparisons (infection status and age) (*ashr* method). **(I)** PCA of single brains transcriptomes from 14 or 22 day old females. **(J)** Volcano plot of differentially expressed genes (adjusted p-value < 0.05) between 14. and 22 day old females. **(K)** Heatmap of top differentially expressed genes from **(J)** ($|\log_2 FC| > 1.5$ and FDR < 1E-20). Putative serotonin 5HT-1a receptor: 5HT-1a R; oxidative phosphorylation: OxPhos; purine and pyrimidine metabolism: PPM; ATP-binding cassette transporter (ABC transporter) family H member 2: ABCB2.

Conclusions

In this study, we present the first survey of cell type composition and tissue organisation of the brain of the primary malaria vector. Specifically, we determined the diversity and spatial organization of glial cell types, optic lobe neurons, MB KCs, circadian neurons and immune cells among others. We showed that despite evolutionary divergence from model organisms, many conserved gene expression patterns persist at the single-cell level and are spatially validated in the *Anopheles* brain. Our data also reveal unique expression patterns and marker genes that likely underlie specific mosquito behaviors. Finally, we integrated developmental stage-resolved single brain transcriptomics and mapped expression changes linked to transmission-related life history. Altogether, our data provides a foundational effort to understand mechanisms supporting mosquito behavior and may help to identify new strategies to disrupt malaria transmission.

Methods

Mosquito rearing

A colony of *An. gambiae* (Kisumu strain [115]) was maintained at 27 °C ± 1 °C and 70% ± 20% relative humidity (RH) and photoperiod of 12 h light/12 h dark in the Vectopole insectarium of IRD in Montpellier, France. Larvae were fed with grinded TetraMin (Tetra) powder and adult mosquitoes fed on 10% honey in water *ad libitum*. A subset of the colony was transferred to Radboudumc (Nijmegen, the Netherlands) for parasite infection. Eggs were

collected in plastic mosquito hatching trays in tap water with a drop of Liquifry (Liquifry No1, Interpet). The larvae were fed with TetraMin baby (Tetra). Larvae were maintained at 27 °C ± 1 °C and 80% ± 10% RH and photoperiod of 12 h light/12 h dark and adult mosquitoes at 21 °C ± 1 °C and 80% ± 10% RH and photoperiod of 12 h light/12 h dark, and fed on 5% glucose (D+ Glucose Monohydrate, Sigma 49159) and 0.4% methylparaben (methyl 4-hydroxybenzoate, Sigma H3647-100G) *ad libitum*.

Single cell transcriptomics

Mosquito sample conditions- In order to capture the diversity of brain cell types along *An. gambiae* females, scRNA-seq experiments included individuals at different stages (i.e. virgin, mated, blood-fed) (FigS1A). Starting from an initial pool of mosquitoes at emergence, a set of females was placed in a cage without males (virgin condition). The other female and male mosquitoes were kept together in a cage (mated condition), reaching a ~70 % prevalence of mated females after 7 days. All cages were fed with 10% honey solution *ad libitum*. On day 6 post-emergence, a subset of the females reared with males were allowed to feed on rabbit blood provided at 37 °C through a glass feeder for 30 minutes. Engorged mosquitoes were then sorted to constitute the pool of blood-fed females. This protocol was applied to two independent sets of mosquitoes. On day seven post emergence, brains of 10 females per condition (virgin, mated, blood-fed) and per replicate were collected. The mosquitoes were anesthetized on ice and brains dissected in a Dulbecco's saline buffer solution (DPBS) (Fisher 10217152) on glass slides with the aid of a stereomicroscope and steel Dumont #5 dissection forceps. The pharyngeal pump was not removed to avoid subesophageal ganglion damage. For each mosquito of which the brain was isolated, the spermatheca was checked under an optical microscope for presence/absence of spermatozoids to ensure that mating state corresponded to the one required for each experimental condition (i.e. virgin = spermatozoids absent; mated/blood-fed = spermatozoids present).

Single cell dissociation and scRNAseq protocol- We adapted a protocol [18] for insect brain cell dissociation. Specifically, pools of dissected brains were placed

into 1.5 mL Protein loBind EP tubes (Eppendorf) in 50 µL of ice-cold Sf-900TM III SFM insect cell culture medium (Fisher 12568019). All the tubes in which biological samples were transferred during the protocol had been Bovine serum albumin (BSA)-coated (Sigma-Aldrich A60003-25G), by incubating them in 1% BSA in sterile Milli-Q water at room temperature (RT) for 30 minutes, and subsequently emptied and dried under a biological cabinet for 30 minutes. Pools of brains were placed in 125 µL of DPBS (Fisher 10217152) containing 60 mg/mL of Gibco collagenase I (Fisher 11500536) and 1.2 mg/mL of dispase I (Sigma D4818-2MG). Samples were kept at 27 °C shaking at 1,000 rcf for 1 h, every 10 minutes the samples were pipetted gently ~ 150 times. Dissociation reactions were stopped by addition of 1 mL of DPBS containing 1% of UltraPure BSA (Invitrogen AM2616). The cell suspensions were filtered through a 40 µm mesh-size cell strainer (PluriStrainer 43-50040-51) into a polypropylene falcon tube. Each sample's cell concentration was measured by staining the cells with an equal volume of Vybrant DyeCycle Green (Fisher 10134622), diluted 1:1,000 in DPBS containing 1% UltraPure BSA. Cells were counted in a MilliCell hemocytometer (Sigma MDH-2N1-50PK) with a Zeiss Axio Imager 2 microscope, and inspected with DIC illumination on a glass slide for shape and integrity.

Cells were then pelleted by centrifugation at 800 rcf for 5 minutes at 4 °C. Assuming a loss of ~ 50% of the counted cells, an adequate volume of chilled DPBS with 1% BSA was added to obtain a concentration of ~ 1,300 cells/µL. The concentration of each sample was measured again and recorded (between 800 cells/ µL and 1,300 cells/ µL). Single cell suspensions were loaded with a target recovery of 10,000 cells per sample. Transcriptomes were obtained with a 10X genomics GemCode Single-Cell Instrument and a Single Cell 3' Library & Gel Bead Kit v3 (10X Genomics) according to manufacturers' recommendations (Single cell 3′ reagent kits v3.1). Amplified cDNA was controlled with High Sensitivity dsDNA quantitation kit (Life technologies Q32851). Libraries were controlled with a Bioanalyzer 2100 (Agilent) and uniquely dual indexed. Sequencing was multiplexed on a NovaSeq 6,000 with paired-end (PE) sequencing (26 and 98 bp) and yielded approximately ~ 1 billion reads per sample.

Spatial transcriptomics

Seven days old *An. gambiae* females were anesthetized on ice, and whole heads from four individuals per inclusion block (complete with mouthparts, antennae and part of the neck to avoid damaging internal structures) were collected and aligned with Dumont #5 dissection forceps, then included in 5 mm x 5 mm plastic molds in optimal cutting temperature compound (OCT) (TFM-C). OCT was solidified by first holding the mold on the surface of isopentane cooled in dry ice, then lowering the whole sample in isopentane for 1 to 2 minutes. Two inclusion blocks were obtained with this procedure. Samples were stored for at least 12 h at - 70 °C before slicing. They were cut axially in a cryostat at - 18 °C to obtain 10 µm thick tissue slices, which were collected on glass slides that were stored at RT. Consecutive slices were alternatively used for spatial transcriptomics or stained with hematoxylin and eosin (H&E) to confirm orientation of the heads and localization of the anatomical structures. For staining, histological samples were plunged for 1 minute in methanol, followed by 1 minute isopropanol. Glass slides are then laid horizontally and covered for 2 minutes with hematoxylin, rinsed in tap water and covered for 30 seconds with eosin. Subsequently the samples were rinsed again in tap water and dried on a heater at 50 °C. Spatial transcriptomics slices were placed on a Curio Seeker 3 x 3 mm tile (Curio bioscience SK004), then covered with a 30 µm section of CryoCube provided by the supplier. The tiles were then processed according to the manufacturer's protocol. Briefly, the tiles were removed from the tile holder and placed into microtubes, and mRNA was captured and hybridized. Reverse transcription was performed *in situ*, then the tissue was cleared and indexed beads were dissociated from the tile and resuspended. The second strand synthesis and cDNA amplification were then performed. Libraries were prepared using the Curio bioscience protocol and were individually indexed with the Curio seeker Dual Indexing Primer kit v1 (Curio bioscience K006). Amplified cDNA and library quality was assessed with High Sensitivity dsDNA kit on a Bioanalyzer 2100 (Agilent) and a Qubit (Thermo Fisher). Libraries were

pooled and sequenced on a NovaSeq 6000 S4 flow cell using PE150, yielding ~ 650 million reads per library.

Confocal microscopy

Female Anopheles were placed in 70% ethanol for five seconds before brain dissection in ice-cold Schneider's Insect Medium (S2). Brains were fixed in 2% paraformaldehyde solution in S2 at room temperature for 60 min. Fixed brains were then washed 10 min in PBS containing 0.5% Triton-X (PBST) , this step was repeated three times. Brains were then incubated in a blocking solution (5% goat serum (Jackson Immunoresearch) in PBST for 90 min at room temperature. Brains were then incubated with a primary antibody, α-Bruchpilot, nc82, (1:30, mouse, DSHB) in PBST containing 5% goat serum for 72 h at 4˚C. Brains were washed for 10 minutes four times in PBST, and subsequently incubated with a secondary antibody, (Alexa Fluor 547-conjugated goat α-mouse; 1:400; Jackson Immunoresearch) overnight at 4˚C. After four 10 min washes in PBS, brains were mounted in Vectashield (Vector Labs) on a glass slide. Anopheles brains were imaged with a Leica SP8-UV confocal microscope. Image resolution was 1024 x 512 with 0.5 µm step size and a frame average of 3 with a 20x objective. All images were analyzed using Fiji [116].

RNA fluorescence *in situ* hybridization

Sections of whole heads of virgin seven days old A*n. gambiae* females were prepared as above, by inclusion in OCT (TBS) and collection of 10 µm tissue slices. Mosquito heads were included in OCT in groups of five per mold, to ensure enough material was available for sample preparation. Seventy six glass slides collecting four to six block slices were prepared from seven different inclusion blocks, and twenty-four of them, obtained from five different inclusion blocks, were used for ISH preliminary tests and main experiments. Glass slides pre-treatment and probe hybridization were carried out according to the ACD manufacturer protocol (UM 323100 Rev B). Samples were fixed for 30 minutes in formaldehyde 4% and subsequently dehydrated with increasing ethanol concentrations. Samples were permeabilized with RNAscope protease IV for 30

minutes. Staining was performed with an RNAscope Multiplex Fluorescent Reagent Kit v2. Hybridized probes consisted of different combinations of three of these probes: (i) ACD Aga-LOC1270460-O1 (ACD 1792161-C1) targeting *elav-like*; (ii) Aga-LOC1274238-O1 (ACD 1792148-C2) targeting *repo*; (iii) Aga-Tret1-1-O1 (ACD 1792131-C3) targeting *tret1*; (iv) Aga-Col4a1-O1 (ACD 1792151-C2) targeting *col4a*; (v) Aga-Fer2 (ACD 1800291-C3) targeting AGAP003739; (vi) Aga-Adcy8 (ACD 1800531-C2) targeting *adenylate cyclase 8*; and (vii) Aga-LOC1272412 (ACD 1800521-C3), targeting *D1-like dopamine R2*. C1, C2, and C3 in the probe codes represent three different fluorescence detection channels associated with three different fluorophores. Chosen fluorophores were Opal620 (Akoya FP1495001KT) for C1, Opal540 (Akoya FP1494001KT) for C2, and Opal650 (Akoya FP1496001KT) for C3. Opal fluorophores were reconstituted in DMSO according to manufacturer's guidelines and diluted at a ratio of 1:1,500 in TSA buffer (ACD 322810). Nuclei were stained with DAPI provided in the RNAscope kit. Glass slides were mounted with Prolong Gold Antifade Mountant (Thermo Fisher, P10144) for 30 minutes at RT. Cryo-slices were kept at - 80 °C or on dry ice until use. Presence of non-specific fluorescence was checked with an RNAscope negative control probe (ACD 320871), fluorophores alone, and with single probe labelling. Not-specific fluorescence associated with opal fluorophore presence was detected in association with ommatidia and keratin in all the negative control conditions and was therefore ignored during the interpretation of the results. Imaging was performed on a Zeiss LSM 780 confocal microscope, with X10 (EC PlnN 10X/0.3 DIC I) and X63 (Pln Apo 63X/1.4 oil DIC III) objectives, and a ZEN 3.11 software. Fluorophores assigned to the different channels were excited with lasers of wavelength 405 nm (30 mW) (DAPI); 512 nm (25 mW) (C2); 561 nm (20 mW) (C1); 633 nm (5 mW) (C3). The context of the whole head slice was captured for each image and insets were subsequently captured at higher resolution. The images shown here are representative of the results obtained from each probe set and chosen among 115 relevant captures. These were elaborated with the ImageJ/FIJI software [116] to produce publication quality images.

Single brain bulk *RNA-seq*

Brains of seven day old mosquitoes that were either virgin (n=9), mated (n=10), or blood-fed and mated (n=10) (as described above) were dissected (Fig. S1B). For *P. falciparum* infections, NF54 asexual and sexual blood stages were cultured in a semi-automated culture system [117,118]. Six days post emergence, *An. gambiae* females were offered either an infectious blood meal or a control uninfected blood meal. Mosquito pots were placed under glass midi-feeders [119] attached to a circulating water bath set at 39 °C, and allowed to feed in the dark for 10 min. The blood was collected in lithium-heparin tubes (BD 367526), obtained from the national blood bank (Sanquin Nijmegen, the Netherlands). The unfed and the partially fed mosquitoes were removed with a suction device, fully-fed mosquitoes were subsequently maintained at 26 °C ± 1 °C with 80% ± 10% RH and a 12 h/12 h light-dark photoperiod. An egg laying bowl was placed in the cage and soaked pads 5% non-sterile glucose solution were placed on top of the cages and changed regularly. Females that were kept until day 22 received a second uninfected blood meal 8 days post-infection (dpi) to accelerate oocyst and sporozoite development. Infected mosquitoes were obtained from 3 different infectious feeding assays, ~ 10 brains (range 8 - 10) were collected for each timepoint and for each of two biological replicates (Fig. S1C). During brain sample collection, we confirmed the infection status at the level of individual mosquitoes by checking for the presence of (i) oocysts in the midguts at 8 dpi, and (ii) sporozoites in salivary glands of individuals at 16 dpi. The midgut of individuals at 16 dpi were also dissected and intact and ruptured oocysts were counted. Dissected midguts were stained with 0.5% mercurochrome and oocyst load assessed by light microscopy. Salivary glands were dissected, ruptured in PBS, and sporozoites were observed by phase contrast microscopy.

Dissected single brains were isolated in 5 µL Sf-900TM III SFM medium (Fisher 11570446) in a well of a 96-well plate kept on ice. RNA was extracted by adding 60 µL volume of a 1.2X ice-cold lysis buffer (120 mM Tris-HCl pH 7.5, 600 mM LiCl, 12 mM EDTA pH 8, 3.6% w/v lithium dodecyl sulfate, 6 mM DTT in nuclease free water (NFW)) to each well. The samples were left at RT for 1 minute under a biological cabinet and subsequently mixed by pipetting up and down ~ 60 times,

before storage at - 70 °C for at least one night. Pulldown of mRNA in solution was performed with oligo-dT(25) Dynabeads (Invitrogen 61002). Dynabeads were equilibrated in a lysis buffer and 20 µl of beads were added to each well, each well was mixed thoroughly by pipetting and incubated for 15 minutes at RT whilst shaking at 1100 rpm. Using a magnet, bead-bound mRNA samples were subsequently washed with two different buffers: first with 10 mM Tris-HCl pH 7.5, 150 mM LiCl, 1 mM EDTA pH 8, LiDS 0.1% w/v in NFW; secondly with 10 mM Tris-HCl pH 7.5, 150 mM LiCl, 1 mM EDTA pH 8 in NFW. The wash buffer was removed and mRNA was eluted by incubation with 10 mM Tris-HCl pH 8 in NFW for 2 minutes. mRNA was reverse transcribed with an oligo dT30VN (5'-AAGCAGTGGTATCAACGCAGAGTACT$_{30}$VN-3'; Integrated DNA Technologies) priming and a template-switching mechanism, using a SmartScribe kit (Takara 639538), with 5X first-strand buffer and 9.2 U/µL of SmartScribe reverse transcriptase, 2.8 µM LNA-oligonucleotide (5′-AGCAGTGGTATCAACGCAGAGTACATrGrG+G-3′; Qiagen), 0.9 U/µL of Superase Inhibitor (Fisher 10085994), 9 µM DTT (Fisher P2325), 1 M betaine (Sigma B0300-1VL), and 0.01 M $MgCl_2$. RT-PCR was carried on with the following program: a 90 minute step at 42 °C, then ten cycles of 2 minutes at 50 °C and 2 minutes at 42 °C, with a final step at 72 °C for 15 minutes. cDNA was then amplified using a KAPA HiFi HS mix (Merck 3736549) and a primer (5'-AAGCAGTGGTATCAACGCAGAGT-3') with a PCR program with an initial incubation step at 98 °C for 3 minutes, followed fourteen PCR cycles (98 °C for 20 s, 67 °C for 15 s, 72 °C for 6 minutes) and a final step at 72 °C for 15 minutes. After a first purification with Agencourt Ampure XP beads (0.8:1), a low-input Nextera protocol including a step for sample dual indexing was used to index each single brain with a specific pair of primers of the Nextera DNA Unique Dual Indexes Set A and C (Illumina 20027213, 20027215). The libraries were again purified with Agencourt Ampure XP beads (0.8:1) and their quality was assessed with High Sensitivity dsDNA kit on a Bioanalyzer 2100 (Agilent) and a Qubit (Thermo Fisher). The libraries were pooled and sequenced on an Illumina HiSeq 4000 with PE150 with ~ 1 million reads per library.

Bioinformatic data processing and analysis

scRNA-seq- Data analysis was carried out with R (v4.2.2) [120] and RStudio environment (v2023.06.1) [121]. The data was demultiplexed and mapped to the *An. gambiae* PEST genome (AgamP4.14) with CellRanger (v 7.0.0) [122] and with an annotation file obtained from VectorBase (v57). Low quality transcriptomes were excluded if they had fewer than 1,000 unique transcripts, less than 800 genes and more than 20% mitochondrial genes; genes were filtered if they were present in less than 5 cells. Background noise from ambient RNA molecules and random barcode swapping was removed with CellBender [123] (v3.0). Downstream analysis of the data was carried out with RStudio environment (v2023.06.1) using R (v4.2.2). Single cell analysis was conducted with Seurat (v5.0.1) [124]. Doublets were identified and removed with DoubletFinder [125] (v2.0.4), and low quality transcriptomes were filtered for if they had fewer than 1000 UMIs or fewer than 800 transcripts. Transcriptomes were normalized and integrated using SCTransform. Clustering analysis was performed in Seurat kNN method based on Jaccard's index with a resolution of 0.7 based on 40 principal components, and positive cluster marker genes were identified comparing all the clusters against each other (Seurat *FindAllMarkers* function with a MAST test [126] and a base-2 logarithmic fold change (LFC) threshold of 0.25). The same approach was used to assess DEGs among conditions for each cluster, without UMI correction. Any significance value inferior to RStudio minimal representable floating number (i.e. < 2.225074E-308) resulted as zeros in the analysis outputs. Cell type mapping was conducted with SAMap mapping on an annotated *D. melanogaster* cellular brain atlas [18 127] (v1.0.15). The threshold was empirically set to 0.1 based on manual cell type assignments to An clusters (*e.g.* lamina monopolar identity assigned to An17 with alignment score = 0.16).

SlideSeq data- Demultiplexed fastq files of each bloc were processed using Curioseekeer Pipeline (v2.0.0) within the Nextflow environment (v24.10.3, build 5933). Star (c2.6.1d) mapping against the *An. gambiae* PEST genome (AgamP4.14) was facilitated by following the pipeline instructions for custom reference genomes using the generate_seeker_reference.sh and pygtftk (v1.6.2) to add missing "gene_names" to the GTF file obtained from VectorBase (v56).

Downstream analysis of the data was carried out with RStudio environment (v2024.12.1) using R (v4.4.3). Data were cleaned from unused spots (selecting only spots > 100 UMIs, > 50 genes, < 40% mitochondrial mapping reads), combined, and analysed using Seurat [124] (v5.3.0). Normalisation and transformation was performed via SCTransform (v0.4.1) regressing out bloc and mitochondrial mapping rates. UMAP dimension reduction was performed on 40 principal components and spots were clustered with the Seurat kNN method based on Jaccard's index with a resolution of 0.5, based on a 50-dimension PCA. Cluster marker genes were identified by comparing all the clusters against each other (Seurat FindAllMarkers function with a MAST test [126] and a LFC threshold = 0.5 and a minimum fraction of 25% of spots in either of the two populations expressing the gene). Annotation of spots to mushroom bodies, MIP cells and octopaminergic neurons was performed by combining marker expression and reclustering of spots assigned to spatial cluster Sp2. Differential expressed genes were obtained from renormalized data of all spots of this cluster by contrasting assigned spots to all other spots within this cluster using the MAST algorithm as implemented in Seurat using the same parameters as before. Functional enrichment analysis of marker genes was performed using richr (v0.0.37). Deconvolution of spots against the single cell dataset was performed using spacexr (v2.2.1). Assignment of spots to single brains was performed visually using the fhs function of gatepoints (v0.1.5) and spot coordinates for each brain were rotated around the center using the rotator function of artpack (v0.1.0) for representation. Five brain slices were selected for further analysis based on their visual integrity. Cluster distance analysis of these 5 slices was performed on non rotated coordinates for each single brain separately by calculating the mean minimal euclidean distance of each cluster to all other clusters. Non-directional distances were then calculated by taking the mean of each combination.

Expression by distance analysis within eye regions was performed by calculating the euclidean distance of each spot within the selected area to the selected point of origin. Gene expression by distance was modeled by fitting a natural cubic spline (splines package, 10 degrees of freedom) per eye area for all genes

in the dataset. To identify genes showing specific spatial expression patterns they were subsequently filtered for a minimum expression range of 1.5 normalised UMIs and a R^2 > 0.1 of the natural cubic spline fit. Cluster abundances within the eye section were estimated by the frequency of assigned spots to each cluster within a given distance bin of 10 pixels. Distributions were modeled by applying a natural cubic spline (10 degrees of freedom) fit over the binned occurrences of clusters.

Single-brain bulk RNA-seq data- Single brain bulk RNA-seq data was aligned to the *An. gambiae* PEST genome (AgamP4.14) with hisat2 [128] (v2.2.1) and read count performed with HTSeq [129] (v2.0) with an annotation file obtained from VectorBase (v56). Downstream analysis of the data was carried out with RStudio environment (v2023.06.1) using R (v4.2.2). For life stage analysis, one virgin condition sample was filtered out as it had a read count that indicated a failed amplification (21,961 reads vs 12,748,569 reads on average in other samples). Data from all samples were pooled, normalized and fit to a linear model, and dispersion was estimated with the DESeq function of DESeq2 [130] (v1.36.0). Differential expression analysis (DEA) was carried out using LFC values shrinkage with the *apeglm* method [131]. Changes in gene expression were considered significant if associated with a Benjamini-Hochberg (FDR) value < 0.05 and an LFC > 0.25.

For infection data, one uninfected sample at day 16 was removed as outlier (9,055 reads vs 5,970,229 reads on average in other samples). For the infection data, the DEA was conducted with different permutations, for instance with DESeq objects containing: (i) individual uninfected vs infected replicate (ii) individual day 16 vs day 22 replicate (iii) pooled samples by either infection status or age. The reference state was set for either infected samples or day 14 samples depending on the test performed.

For all comparisons, data were normalized and fit to a linear model, and dispersion was estimated with the DESeq function of DESeq2 [130] (v1.36.0). DEA was carried out using LFC shrinkage both with the *apeglm* method [131] and with the *ashr* method [132] especially for more complex designs (*i.e.* combining infection and age), the method used is specified in the figure legend. Results of the two

analyses were contrasted to both obtain highly reliable LFC estimates (*apeglm*) and to avoid model over-parameterization (*ashr*). Reasoning that infection could have subtle effects on brain transcriptomes, and that applying DESeq2 shrinkage methods corrects for low counts value dispersion artifacts, LFC threshold was set to zero and results having a FDR value < 0.05 were considered significant.

Gene function information was retrieved from gene annotation present in VectorBase database [133]. Immune gene families enrichment in aging was performed based on categorised gene families in the *An. gambiae* PEST genome annotation GCA_000005575.2, AgamP4.14 (VectorBase Release 68 in May 2025) [134]. To ensure only annotated members were counted, the genes belonging to each immune family were counted based on gene names, and not on gene product description, that could have been automatically assigned without manual curation. The genes considered to be DE for the analysis had a $|\log_2 FC| > 0.25$. Hypergeometric p-values were calculated using the upper-tail (right-tail) probability $P(X \geq a)$. The FDR was adjusted across all known immune families present in the *An. gambiae* PEST genome using the Benjamini-Hochberg method.

Data availability-

All raw sequencing data have been deposited in the European Nucleotide Archive at European Molecular Biology Laboratory European Bioinformatics Institute (www.ebi.ac.uk/ena/) under accession numbers PRJEB90373 or ERP173390. Metadata, raw counts and normalized counts, analysis code and supplementary files are accessible via Github (https://github.com/Parasitedevbio/Agambiae_Brain_Atlas.git).

Expression data matrices are available (https://drive.ird.fr/s/2ZT82yTJmprftfR).

References

1. Janssens, J. *et al.* Decoding gene regulation in the fly brain. *Nature* **601**, 630–636 (2022).
2. Schlegel, P. *et al.* Whole-brain annotation and multi-connectome cell typing of *Drosophila*. *Nature* **634**, 139–152 (2024).

3. Koniszewski, N. D. B. *et al.* The insect central complex as model for heterochronic brain development-background, concepts, and tools. *Dev. Genes Evol.* **226**, 209–219 (2016).
4. Heinze, S. *et al.* A unified platform to manage, share, and archive morphological and functional data in insect neuroscience. *Elife* **10**, (2021).
5. Shaw, W. R., Marcenac, P. & Catteruccia, F. *Plasmodium* development in *Anopheles*: a tale of shared resources. *Trends Parasitol.* **38**, 124–135 (2022).
6. Wekesa, J. W., Copeland, R. S. & Mwangi, R. W. Effect of *Plasmodium falciparum* on blood feeding behavior of naturally infected *Anopheles* mosquitoes in western Kenya. *Am. J. Trop. Med. Hyg.* **47**, 484–488 (1992).
7. Koella, J. C. Malaria as a manipulator. *Behav. Processes* **68**, 271–273 (2005).
8. Vantaux, A. *et al.* Field evidence for manipulation of mosquito host selection by the human malaria parasite, *Plasmodium falciparum*. *Peer Community J.* **1**, 1–None (2021).
9. Goldman, O. V. *et al.* Mosquito Cell Atlas: A single-nucleus transcriptomic atlas of the adult *Aedes aegypti* mosquito. *bioRxiv* 2025.02.25.639765 (2025) doi:10.1101/2025.02.25.639765.
10. Li, Q. *et al.* A single-cell transcriptomic atlas tracking the neural basis of division of labour in an ant superorganism. *Nat. Ecol. Evol.* **6**, 1191–1204 (2022).
11. Tarashansky, A. J. *et al.* Mapping single-cell atlases throughout Metazoa unravels cell type evolution. *Elife* **10**, (2021).
12. Riabinina, O. *et al.* Organization of olfactory centres in the malaria mosquito *Anopheles gambiae*. *Nat. Commun.* **7**, 13010 (2016).
13. Raji, J. I. & Potter, C. J. The number of neurons in *Drosophila* and mosquito brains. *PLoS One* **16**, e0250381 (2021).
14. Konopka, J. K., Task, D., Poinapen, D. & Potter, C. J. Neurogenetic identification of mosquito sensory neurons. *iScience* **26**, 106690 (2023).
15. De Rubeis, S. & Bagni, C. Fragile X mental retardation protein control of neuronal mRNA metabolism: Insights into mRNA stability. *Mol. Cell. Neurosci.* **43**, 43–50 (2010).
16. Khuansuwan, S., Barnhill, L. M., Cheng, S. & Bronstein, J. M. A novel transgenic zebrafish line allows for in vivo quantification of autophagic activity in neurons. *Autophagy* **15**, 1322–1332 (2019).
17. Evans, C. J., Liu, T. & Banerjee, U. *Drosophila* hematopoiesis: Markers and methods for molecular genetic analysis. *Methods* **68**, 242–251 (2014).
18. Davie, K. *et al.* A single-cell transcriptome atlas of the aging *Drosophila* brain. *Cell*

174, 982–998.e20 (2018).

19. Zdobnov, E. M. *et al.* Comparative genome and proteome analysis of *Anopheles gambiae* and *Drosophila melanogaster*. *Science* **298**, 149–159 (2002).
20. Bridi, J. C., Ludlow, Z. N. & Hirth, F. Lineage-specific determination of ring neuron circuitry in the central complex of *Drosophila*. *Biol. Open* **8**, bio045062 (2019).
21. Kwon, H.-W., Lu, T., Rützler, M. & Zwiebel, L. J. Olfactory responses in a gustatory organ of the malaria vector mosquito Anopheles gambiae. *Proc. Natl. Acad. Sci. U. S. A.* **103**, 13526–13531 (2006).
22. Ghaninia, M., Hansson, B. S. & Ignell, R. The antennal lobe of the African malaria mosquito, Anopheles gambiae - innervation and three-dimensional reconstruction. *Arthropod Struct. Dev.* **36**, 23–39 (2007).
23. Tanaka, N. K., Tanimoto, H. & Ito, K. Neuronal assemblies of the Drosophila mushroom body. *J. Comp. Neurol.* **508**, 711–755 (2008).
24. Strausfeld, N. J., Sinakevitch, I., Brown, S. M. & Farris, S. M. Ground plan of the insect mushroom body: functional and evolutionary implications. *J. Comp. Neurol.* **513**, 265–291 (2009).
25. Aso, Y. *et al.* The neuronal architecture of the mushroom body provides a logic for associative learning. *Elife* **3**, e04577 (2014).
26. Pech, U., Pooryasin, A., Birman, S. & Fiala, A. Localization of the contacts between Kenyon cells and aminergic neurons in the Drosophila melanogaster brain using SplitGFP reconstitution. *J. Comp. Neurol.* **521**, 3992–4026 (2013).
27. Rodriques, S. G. *et al.* Slide-seq: A scalable technology for measuring genome-wide expression at high spatial resolution. *Science* **363**, 1463–1467 (2019).
28. Park, A. *et al.* Gliotransmission of D-serine promotes thirst-directed behaviors in Drosophila. *Curr. Biol.* **32**, 3952–3970.e8 (2022).
29. Ki, Y. & Lim, C. Sleep-promoting effects of threonine link amino acid metabolism in *Drosophila* neuron to GABAergic control of sleep drive. *Elife* **8**, (2019).
30. Carvalhas-Almeida, C. & Sehgal, A. Glia: the cellular glue that binds circadian rhythms and sleep. *Sleep* **48**, zsae314 (2025).
31. Yin, J. *et al.* Glia-derived secretory fatty acid binding protein *Obp44a* regulates lipid storage and efflux in the developing *Drosophila* brain. *bioRxivorg* (2024) doi:10.1101/2024.04.10.588417.
32. Yin, J. *et al.* Brain-specific lipoprotein receptors interact with astrocyte derived apolipoprotein and mediate neuron-glia lipid shuttling. *Nat. Commun.* **12**, 2408 (2021).

33. Volkenhoff, A. *et al.* Glial glycolysis is essential for neuronal survival in *Drosophila*. *Cell Metab.* **22**, 437–447 (2015).
34. Mayer, F. *et al.* Evolutionary conservation of vertebrate blood-brain barrier chemoprotective mechanisms in *Drosophila*. *J. Neurosci.* **29**, 3538–3550 (2009).
35. Yildirim, K., Petri, J., Kottmeier, R. & Klämbt, C. *Drosophila* glia: Few cell types and many conserved functions. *Glia* **67**, 5–26 (2019).
36. Suh, J. & Jackson, F. R. *Drosophila* ebony activity is required in glia for the circadian regulation of locomotor activity. *Neuron* **55**, 435–447 (2007).
37. Cameron, S., Chen, Y. & Rao, Y. Borderless regulates glial extension and axon ensheathment. *Dev. Biol.* **414**, 170–180 (2016).
38. Noordermeer, J. N. *et al.* Wrapper, a novel member of the Ig superfamily, is expressed by midline glia and is required for them to ensheath commissural axons in *Drosophila*. *Neuron* **21**, 991–1001 (1998).
39. Li, J. *et al.* Neuroanatomical basis of sexual dimorphism in the mosquito brain. *iScience* **25**, 105255 (2022).
40. Tuthill, J. C., Nern, A., Holtz, S. L., Rubin, G. M. & Reiser, M. B. Contributions of the 12 neuron classes in the fly lamina to motion vision. *Neuron* **79**, 128–140 (2013).
41. Morey, M. Dpr-DIP matching expression in *Drosophila* synaptic pairs. *Fly (Austin)* **11**, 19–26 (2017).
42. Gold, K. S. & Brand, A. H. Optix defines a neuroepithelial compartment in the optic lobe of the *Drosophila* brain. *Neural Dev.* **9**, 18 (2014).
43. Erclik, T. *et al.* Integration of temporal and spatial patterning generates neural diversity. *Nature* **541**, 365–370 (2017).
44. Vannini, L., Augustine Dunn, W., Reed, T. W. & Willis, J. H. Changes in transcript abundance for cuticular proteins and other genes three hours after a blood meal in Anopheles gambiae. *Insect Biochem. Mol. Biol.* **44**, 33–43 (2014).
45. Feuda, R. *et al.* Phylogenomics of opsin genes in Diptera reveals lineage-specific events and contrasting evolutionary dynamics in Anopheles and Drosophila. *Genome Biol. Evol.* **13**, (2021).
46. Dolph, P. J. *et al.* Arrestin function in inactivation of G protein-coupled receptor rhodopsin in vivo. *Science* **260**, 1910–1916 (1993).
47. Montell, C. & Zwiebel, L. J. Mosquito Sensory Systems. in *Advances in Insect Physiology* 293–328 (Elsevier, 2016).
48. Helfrich-Förster, C. Light input pathways to the circadian clock of insects with an emphasis on the fruit fly *Drosophila melanogaster*. *J. Comp. Physiol. A Neuroethol.*

Sens. Neural Behav. Physiol. **206**, 259–272 (2020).

49. Pyza, E. & Meinertzhagen, I. A. Monopolar cell axons in the first optic neuropil of the housefly, *Musca domestica* L., undergo daily fluctuations in diameter that have a circadian basis. *J. Neurosci.* **15**, 407–418 (1995).
50. Weber, P., Kula-Eversole, E. & Pyza, E. Circadian control of dendrite morphology in the visual system of *Drosophila melanogaster*. *PLoS One* **4**, e4290 (2009).
51. Górska-Andrzejak, J. *et al.* Circadian expression of the presynaptic active zone protein Bruchpilot in the lamina of *Drosophila melanogaster*. *Dev. Neurobiol.* **73**, 14–26 (2013).
52. Damulewicz, M. *et al.* Clock and clock-controlled genes are differently expressed in the retina, lamina and in selected cells of the visual system of *Drosophila melanogaster*. *Front. Cell. Neurosci.* **9**, 353 (2015).
53. Park, J. H., Schroeder, A. J., Helfrich-Förster, C., Jackson, F. R. & Ewer, J. Targeted ablation of CCAP neuropeptide-containing neurons of *Drosophila* causes specific defects in execution and circadian timing of ecdysis behavior. *Development* **130**, 2645–2656 (2003).
54. Williams, M. J. *et al.* CCAP regulates feeding behavior via the NPF pathway in *Drosophila* adults. *Proc. Natl. Acad. Sci. U. S. A.* **117**, 7401–7408 (2020).
55. Nagoshi, E. *et al.* Dissecting differential gene expression within the circadian neuronal circuit of *Drosophila*. *Nat. Neurosci.* **13**, 60–68 (2010).
56. Ma, D. *et al.* A transcriptomic taxonomy of *Drosophila* circadian neurons around the clock. *Elife* **10**, (2021).
57. Baik, L. S. *et al.* Circadian regulation of light-evoked attraction and avoidance behaviors in daytime- versus nighttime-biting mosquitoes. *Curr. Biol.* **30**, 3252–3259.e3 (2020).
58. Lee, G. G. *et al.* In vivo characterization of the maturation steps of a pigment dispersing factor neuropeptide precursor in the *Drosophila* circadian pacemaker neurons. *Genetics* **225**, iyad118 (2023).
59. Zars, T. Behavioral functions of the insect mushroom bodies. *Curr. Opin. Neurobiol.* **10**, 790–795 (2000).
60. Liu, L.-Y. *et al. Mamo* decodes hierarchical temporal gradients into terminal neuronal fate. *Elife* **8**, (2019).
61. Croset, V., Treiber, C. D. & Waddell, S. Cellular diversity in the Drosophila midbrain revealed by single-cell transcriptomics. *Elife* **7**, (2018).
62. Nicolaï, M., Lasbleiz, C. & Dura, J.-M. Gain-of-function screen identifies a role of the

Src64 oncogene in *Drosophila* mushroom body development: Mushroom body gain-of-function genetics. *J. Neurobiol.* **57**, 291–302 (2003).

63. Ng, J. & Luo, L. Rho GTPases regulate axon growth through convergent and divergent signaling pathways. *Neuron* **44**, 779–793 (2004).
64. Yaniv, S. P., Issman-Zecharya, N., Oren-Suissa, M., Podbilewicz, B. & Schuldiner, O. Axon regrowth during development and regeneration following injury share molecular mechanisms. *Curr. Biol.* **22**, 1774–1782 (2012).
65. Han, P. L., Levin, L. R., Reed, R. R. & Davis, R. L. Preferential expression of the *Drosophila rutabaga* gene in mushroom bodies, neural centers for learning in insects. *Neuron* **9**, 619–627 (1992).
66. Sayin, S. *et al.* A neural circuit arbitrates between persistence and withdrawal in hungry Drosophila. *Neuron* **104**, 544–558.e6 (2019).
67. Awasaki, T. *et al.* The *Drosophila trio* plays an essential role in patterning of axons by regulating their directional extension. *Neuron* **26**, 119–131 (2000).
68. Formicola, N. *et al.* Tyramine induces dynamic RNP granule remodeling and translation activation in the *Drosophila* brain. *Elife* **10**, e65742 (2021).
69. Raddi, G. *et al.* Mosquito cellular immunity at single-cell resolution. *Science* **369**, 1128–1132 (2020).
70. Kwon, H., Mohammed, M., Franzén, O., Ankarklev, J. & Smith, R. C. Single-cell analysis of mosquito hemocytes identifies signatures of immune cell subtypes and cell differentiation. *Elife* **10**, (2021).
71. Omoto, J. J., Lovick, J. K. & Hartenstein, V. Origins of glial cell populations in the insect nervous system. *Curr Opin Insect Sci* **18**, 96–104 (2016).
72. Contreras, E. G. & Sierralta, J. The fly blood-brain barrier fights against nutritional stress. *Neurosci. Insights* **17**, 26331055221120252 (2022).
73. Spana, E. P., Kopczynski, C., Goodman, C. S. & Doe, C. Q. Asymmetric localization of *numb* autonomously determines sibling neuron identity in the *Drosophila* CNS. *Development* **121**, 3489–3494 (1995).
74. Kraut, R., Chia, W., Jan, L. Y., Jan, Y. N. & Knoblich, J. A. Role of *inscuteable* in orienting asymmetric cell divisions in *Drosophila*. *Nature* **383**, 50–55 (1996).
75. Domingos, P. M. *et al.* Regulation of *Numb* during planar cell polarity establishment in the *Drosophila* eye. *Mech. Dev.* **160**, 103583 (2019).
76. Deng, Q. *et al.* Specific and integrated roles of *Lmx1a*, *Lmx1b* and *Phox2a* in ventral midbrain development. *Development* **138**, 3399–3408 (2011).
77. Cai, J. *et al.* The role of *Lmx1a* in the differentiation of human embryonic stem cells

into midbrain dopamine neurons in culture and after transplantation into a Parkinson's disease model. *Stem Cells* **27**, 220–229 (2009).

78. Cayre, M., Strambi, C. & Strambi, A. Neurogenesis in an adult insect brain and its hormonal control. *Nature* **368**, 57–59 (1994).
79. Scotto-Lomassese, S. *et al.* Suppression of adult neurogenesis impairs olfactory learning and memory in an adult insect. *J. Neurosci.* **23**, 9289–9296 (2003).
80. Crocker, K. L. *et al.* Neurogenesis in the adult *Drosophila* brain. *Genetics* **219**, iyab092 (2021).
81. Casas-Tintó, S., García-Guillen, N. & Losada-Pérez, M. Adult neurogenesis through glial transdifferentiation in a CNS injury paradigm. *eLife* (2024) doi:10.7554/elife.96890.2.
82. Siju, K. P. *et al.* Neuropeptides in the antennal lobe of the yellow fever mosquito, *Aedes aegypti*. *J. Comp. Neurol.* **522**, 592–608 (2014).
83. Jang, Y.-H., Chae, H.-S. & Kim, Y.-J. Female-specific myoinhibitory peptide neurons regulate mating receptivity in Drosophila melanogaster. *Nat. Commun.* **8**, 1630 (2017).
84. Busch, S., Selcho, M., Ito, K. & Tanimoto, H. A map of octopaminergic neurons in the Drosophila brain. *J. Comp. Neurol.* **513**, 643–667 (2009).
85. Dopp, J. *et al.* Single-cell transcriptomics reveals that glial cells integrate homeostatic and circadian processes to drive sleep-wake cycles. *Nat. Neurosci.* **27**, 359–372 (2024).
86. Sinha, S. *et al.* Behavior-related gene regulatory networks: A new level of organization in the brain. *Proc. Natl. Acad. Sci. U. S. A.* **117**, 23270–23279 (2020).
87. Mu, X. *et al.* Single-nucleus and spatial transcriptomics identify brain landscape of gene regulatory networks associated with behavioral maturation in honeybees. *Nat. Commun.* **16**, 3343 (2025).
88. Shaw, W. R. *et al.* Multiple blood feeding in mosquitoes shortens the Plasmodium falciparum incubation period and increases malaria transmission potential. *PLoS Pathog.* **16**, e1009131 (2020).
89. Gunawardhana, K. L. & Hardin, P. E. VRILLE controls PDF neuropeptide accumulation and arborization rhythms in small ventrolateral neurons to drive rhythmic behavior in *Drosophila*. *Curr. Biol.* **27**, 3442–3453.e4 (2017).
90. Stroumbakis, N. D., Li, Z. & Tolias, P. P. A homolog of human transcription factor NF-X1 encoded by the *Drosophila* shuttle craft gene is required in the embryonic central nervous system. *Mol. Cell. Biol.* **16**, 192–201 (1996).

91. Bartok, O. *et al.* The transcription factor Cabut coordinates energy metabolism and the circadian clock in response to sugar sensing. *EMBO J.* **34**, 1538–1553 (2015).
92. Tanaka, K. *et al.* Role of down-regulated neutral ceramidase during all-trans retinoic acid-induced neuronal differentiation in SH-SY5Y neuroblastoma cells. *J. Biochem.* **151**, 611–620 (2012).
93. Taga, Y. *et al.* Identification of a highly stable bioactive 3-hydroxyproline-containing tripeptide in human blood after collagen hydrolysate ingestion. *Npj Sci. Food* **6**, 29 (2022).
94. Pooryasin, A. & Fiala, A. Identified serotonin-releasing neurons induce behavioral quiescence and suppress mating in *Drosophila*. *J. Neurosci.* **35**, 12792–12812 (2015).
95. Marinotti, O., Nguyen, Q. K., Calvo, E., James, A. A. & Ribeiro, J. M. C. Microarray analysis of genes showing variable expression following a blood meal in *Anopheles gambiae*. *Insect Mol. Biol.* **14**, 365–373 (2005).
96. Clements, A. N. *The Biology of Mosquitoes, Volume 2. Development, Nutrition and Reproduction. Oogenesis*, A. N. *Clemets 2000, P. 414*. (1992).
97. Vinauger, C., Lutz, E. K. & Riffell, J. A. Olfactory learning and memory in the disease vector mosquito *Aedes aegypti*. *J. Exp. Biol.* **217**, 2321–2330 (2014).
98. Sgammeglia, N. & Sprecher, S. G. Interplay between metabolic energy regulation and memory pathways in *Drosophila*. *Trends Neurosci.* **45**, 539–549 (2022).
99. Samantsidis, G.-R., Kwon, H., Wendland, M., Fonder, C. & Smith, R. C. TNF signaling mediates cellular immune function and promotes malaria parasite killing in the mosquito *Anopheles gambiae*. *bioRxiv* 2024.05.02.592209 (2024) doi:10.1101/2024.05.02.592209.
100. Osta, M. A., Christophides, G. K., Vlachou, D. & Kafatos, F. C. Innate immunity in the malaria vector *Anopheles gambiae*: comparative and functional genomics. *J. Exp. Biol.* **207**, 2551–2563 (2004).
101. Khokha, R., Murthy, A. & Weiss, A. Metalloproteinases and their natural inhibitors in inflammation and immunity. *Nat. Rev. Immunol.* **13**, 649–665 (2013).
102. Takarada, K., Kinoshita, J. & Inoue, Y. H. Ectopic expression of matrix metalloproteinases and filopodia extension via JNK activation are involved in the invasion of blood tumor cells in *Drosophila* mxc mutant. *Genes Cells* **28**, 709–726 (2023).
103. Wang, J., Murphy, E. J., Nix, J. C. & Jones, D. N. M. *Aedes aegypti* Odorant Binding Protein 22 selectively binds fatty acids through a conformational change in its C-terminal tail. *Sci. Rep.* **10**, 3300 (2020).

104. Cator, L. J., Lynch, P. A., Read, A. F. & Thomas, M. B. Do malaria parasites manipulate mosquitoes? *Trends Parasitol.* **28**, (2012).
105. Brady, O. J. *et al.* Vectorial capacity and vector control: reconsidering sensitivity to parameters for malaria elimination. *Trans. R. Soc. Trop. Med. Hyg.* **110**, 107–117 (2016).
106. Mohammad, N. *et al.* Predicting the age of field Anopheles mosquitoes using mass spectrometry and deep learning. *Sci. Adv.* **10**, eadj6990 (2024).
107. Wagner, I. *et al.* Rapid evaporative ionisation mass spectrometry can age field caught Anopheles gambiae malaria vectors. *Sci. Rep.* **15**, 19342 (2025).
108. Somé, B. M. *et al.* Mosquito ageing modulates the development, virulence and transmission potential of pathogens. *Proc. Biol. Sci.* **291**, 20232097 (2024).
109. Pacifico, R., MacMullen, C. M., Walkinshaw, E., Zhang, X. & Davis, R. L. Brain transcriptome changes in the aging Drosophila melanogaster accompany olfactory memory performance deficits. *PLoS One* **13**, e0209405 (2018).
110. Bartman, S., Coppotelli, G. & Ross, J. M. Mitochondrial dysfunction: A key player in brain aging and diseases. *Curr. Issues Mol. Biol.* **46**, 1987–2026 (2024).
111. Eleftherianos, I. & Castillo, J. C. Molecular mechanisms of aging and immune system regulation in *Drosophila*. *Int. J. Mol. Sci.* **13**, 9826–9844 (2012).
112. Yaron, J. R., Zhang, L., Guo, Q., Haydel, S. E. & Lucas, A. R. Fibrinolytic Serine proteases, therapeutic serpins and inflammation: Fire dancers and firestorms. *Front. Cardiovasc. Med.* **8**, 648947 (2021).
113. Ham, S. & Lee, S.-J. V. Advances in transcriptome analysis of human brain aging. *Exp. Mol. Med.* **52**, 1787–1797 (2020).
114. Giorgi, C. *et al.* Mitochondria and reactive oxygen species in aging and age-related diseases. *Int. Rev. Cell Mol. Biol.* **340**, 209–344 (2018).
115. Shute, G. T. A method of maintaining colonies of East African strains of *Anopheles gambiae*. *Ann. Trop. Med. Parasitol.* **50**, 92–94 (1956).
116. Schindelin, J. *et al.* Fiji: an open-source platform for biological-image analysis. *Nat. Methods* **9**, 676–682 (2012).
117. Ponnudurai, T., Lensen, A. H., Leeuwenberg, A. D. & Meuwissen, J. H. Cultivation of fertile *Plasmodium falciparum* gametocytes in semi-automated systems. 1. Static cultures. *Trans. R. Soc. Trop. Med. Hyg.* **76**, 812–818 (1982).
118. Ponnudurai, T., Lensen, A. H., Meis, J. F. & Meuwissen, J. H. Synchronization of *Plasmodium falciparum* gametocytes using an automated suspension culture system. *Parasitology* **93 (Pt 2)**, 263–274 (1986).
119. Ponnudurai, T. *et al.* Infectivity of cultured *Plasmodium falciparum* gametocytes to

mosquitoes. *Parasitology* **98 Pt 2**, 165–173 (1989).

120. R Development Core Team. R: A *Language and Environment for Statistical Computing*." *Vienna, Austria: R Foundation for Statistical Computing*.
121. RStudio Team. *RStudio: Integrated Development for R*. (2020).
122. Zheng, G. X. Y. *et al.* Massively parallel digital transcriptional profiling of single cells. *Nat. Commun.* **8**, 14049 (2017).
123. Fleming, S. J. *et al.* Unsupervised removal of systematic background noise from droplet-based single-cell experiments using CellBender. *Nat. Methods* **20**, 1323–1335 (2023).
124. Satija, R., Farrell, J. A., Gennert, D., Schier, A. F. & Regev, A. Spatial reconstruction of single-cell gene expression data. *Nat. Biotechnol.* **33**, 495–502 (2015).
125. McGinnis, C. S., Murrow, L. M. & Gartner, Z. J. DoubletFinder: Doublet detection in single-cell RNA sequencing data using artificial nearest neighbors. *Cell Syst* **8**, 329–337.e4 (2019).
126. Finak, G. *et al.* MAST: a flexible statistical framework for assessing transcriptional changes and characterizing heterogeneity in single-cell RNA sequencing data. *Genome Biol.* **16**, 278 (2015).
127. Tarashansky, A. J., Xue, Y., Li, P., Quake, S. R. & Wang, B. Self-assembling manifolds in single-cell RNA sequencing data. *Elife* **8**, (2019).
128. Kim, D., Paggi, J. M., Park, C., Bennett, C. & Salzberg, S. L. Graph-based genome alignment and genotyping with HISAT2 and HISAT-genotype. *Nat. Biotechnol.* **37**, 907–915 (2019).
129. Putri, G. H., Anders, S., Pyl, P. T., Pimanda, J. E. & Zanini, F. Analysing high-throughput sequencing data in Python with HTSeq 2.0. *Bioinformatics* **38**, 2943–2945 (2022).
130. Love, M. I., Huber, W. & Anders, S. Moderated estimation of fold change and dispersion for RNA-seq data with DESeq2. *Genome Biol.* **15**, 550 (2014).
131. Zhu, A., Ibrahim, J. G. & Love, M. I. Heavy-tailed prior distributions for sequence count data: removing the noise and preserving large differences. *Bioinformatics* **35**, 2084–2092 (2019).
132. Stephens, M. False discovery rates: a new deal. *Biostatistics* **18**, 275–294 (2017).
133. Giraldo-Calderón, G. I. *et al.* VectorBase.org updates: bioinformatic resources for invertebrate vectors of human pathogens and related organisms. *Curr Opin Insect Sci* **50**, 100860 (2022).
134. Christophides, G. K. *et al.* Immunity-related genes and gene families in *Anopheles*

gambiae. *Science* **298**, 159–165 (2002).
135. Fei, H. *et al.* Mutation of the *Drosophila* vesicular GABA transporter disrupts visual figure detection. *J. Exp. Biol.* **213**, 1717–1730 (2010).
136. Luque, C. M. & Milán, M. Growth control in the proliferative region of the Drosophila eye-head primordium: the elbow-noc gene complex. *Dev. Biol.* **301**, 327–339 (2007).

Acknowledgements-

This work was supported by a grant from the Parafrap network of excellence awarded to AC (ANR-11-LABX-0024) which supports IR. This work was also funded by the RIVOC program from Région Occitanie awarded to AC and AMT (201555PIRIPPLERV06) and by Fondation pour la Recherche Médicale PhD fellowship awarded to IR (FRM-FDT202404018268). This work was supported by the French National Research Institute for Sustainable Development (IRD). We are very grateful to Carole Ginibre and the Vectopôle team for providing mosquitoes for these experiments. We would like to thank Marga van de Vegte-Bolmer and Rianne Stoter for generating the *P. falciparum* parasites and the mosquito infections. We would also like to thank Jolanda Klaassen, Laura Pelser-Posthumus and Astrid Pouwelsen for breeding mosquitoes for the infection experiments. We acknowledge the support of the MRI core cytometry and imaging facility and the MGX sequencing core facility. We are grateful to Sarrah Loulizi and the HistoPathology platform at Institut Pasteur (Paris) for her help in tissue slicing for the ISH experiments. We are also thankful to Audrey Salles and to the UTechS Photonic BioImaging at Institut Pasteur (Paris) for support in confocal imaging. We are thankful to Julien Marcetteau for producing illustrative material. We thank Adam Dobson and Ana Gomes for critical reading of the manuscript.

Authors contributions-

Conceptualization: AC, AMT. **Data Curation**: IZR, CC, JWB. **Formal Analysis and Methodology:** IZR, CC, JWB, SO, QJD, AV, GJG, CA, WG, RB, ARS, EP, DC, AC,

AMT. **Investigation:** IZR, JWB, AC, AMT. **Visualization:** IZR, CC, EP, JWB, AMT. **Funding acquisition:** TB, SM, AC, AMT. **Project administration:** AC, AMT. **Supervision:** DC, RB, TB, SM, AC, AMT. **Writing – original draft:** IZR, AC, AMT. **Writing – review and editing:** All authors.

Competing interests-

Authors declare that they have no competing interests

Materials & Correspondence-

anna.cohuet@ird.fr, arthur.talman@ird.fr

Supplementary Information-

Figure S1. Experimental design of brain transcriptomics experiments.

Figure S2. Quality control of the brain single cell atlas.

Figure S3. Mapping of the brain single cell atlas to a *D. melanogaster* reference.

Figure S4. Anatomical structures in the *Anopheles* brain.

Figure S5. A spatially-resolved transcriptomic dataset of the female *An. gambiae* head.

Figure S6. Spatial cluster distribution within the five high quality heads.

Figure S7. Characterization of glial cell diversity in the female *Anopheles* brain.

Figure S8. Characterization of optic lobes and clock neurons in the female *Anopheles* brain.

Figure S9. Identification of Kenyon cells and mushroom body in the female *Anopheles* brain.

Figure S10. Characterization immune cell populations in the female *An. gambiae* head.

Figure S11. Spatial support for specialised neuronal foci in the cell body rind.

Figure S12. Differentially expressed genes of the female *Anopheles* brain in different life stages and aging, and association of DEGs to putative cell types of origin.

Figure S13. Impact of *Plasmodium falciparum* infection on the female *Anopheles* brain.

Table S1. Notable cell type marker genes.

Table S2. Cell type annotation and spatial cluster annotation.

Table S3. All marker genes of cell and spatial clusters.

Table S4. Spatially variable genes in eye region.

Table S5. MIP markers, KC markers, Octopaminergic neurons markers.

Table S6. Differentially expressed genes in life history.

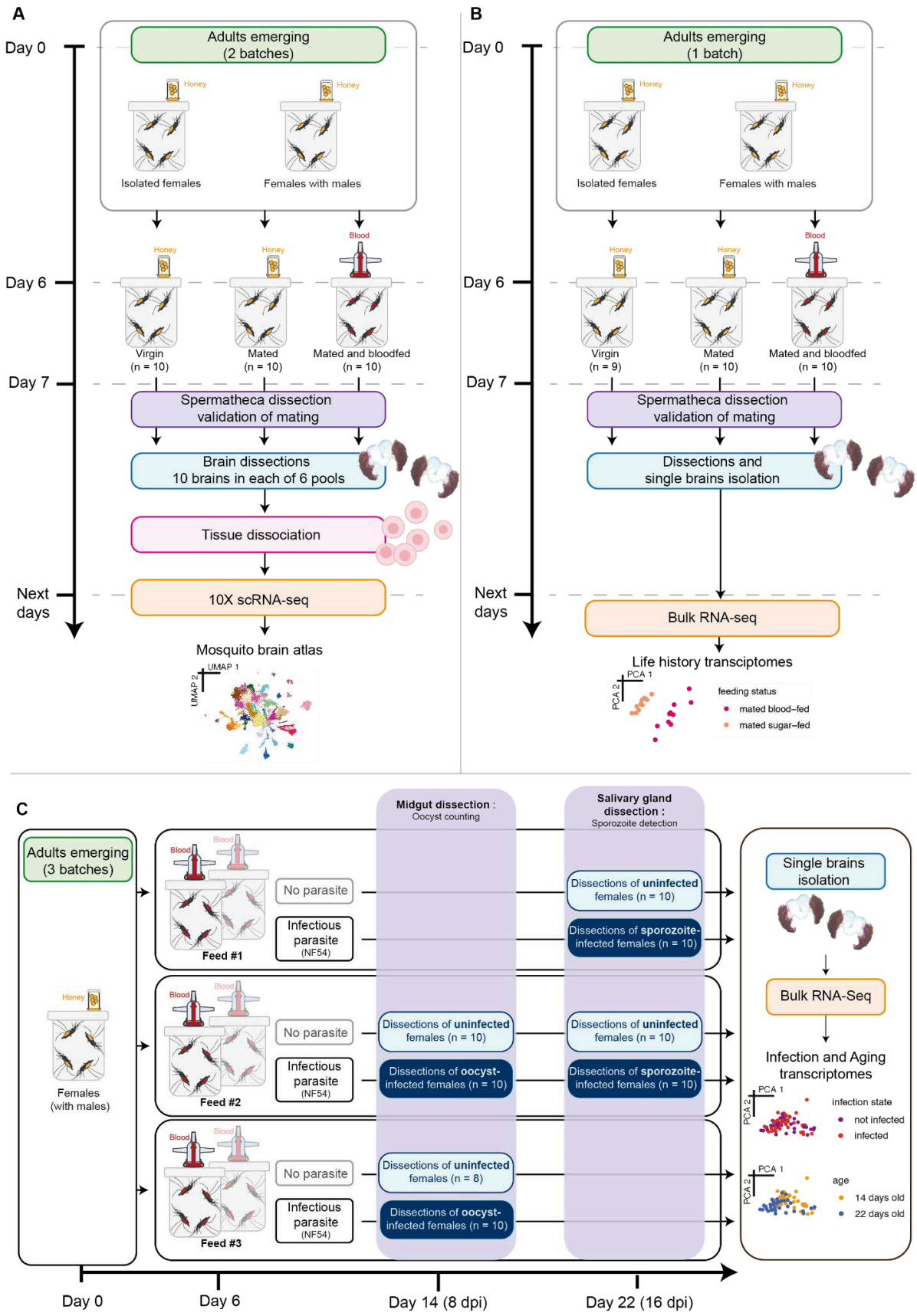


Figure S1. Experimental design of brain transcriptomics experiments. (A) Experimental workflow for sc-RNA-seq data. **(B)** Experimental workflow for single brain bulk RNA-seq of life cycle stages. **(C)** Experimental workflow for single brain bulk RNA-seq of *P. falciparum* infection stages and age.

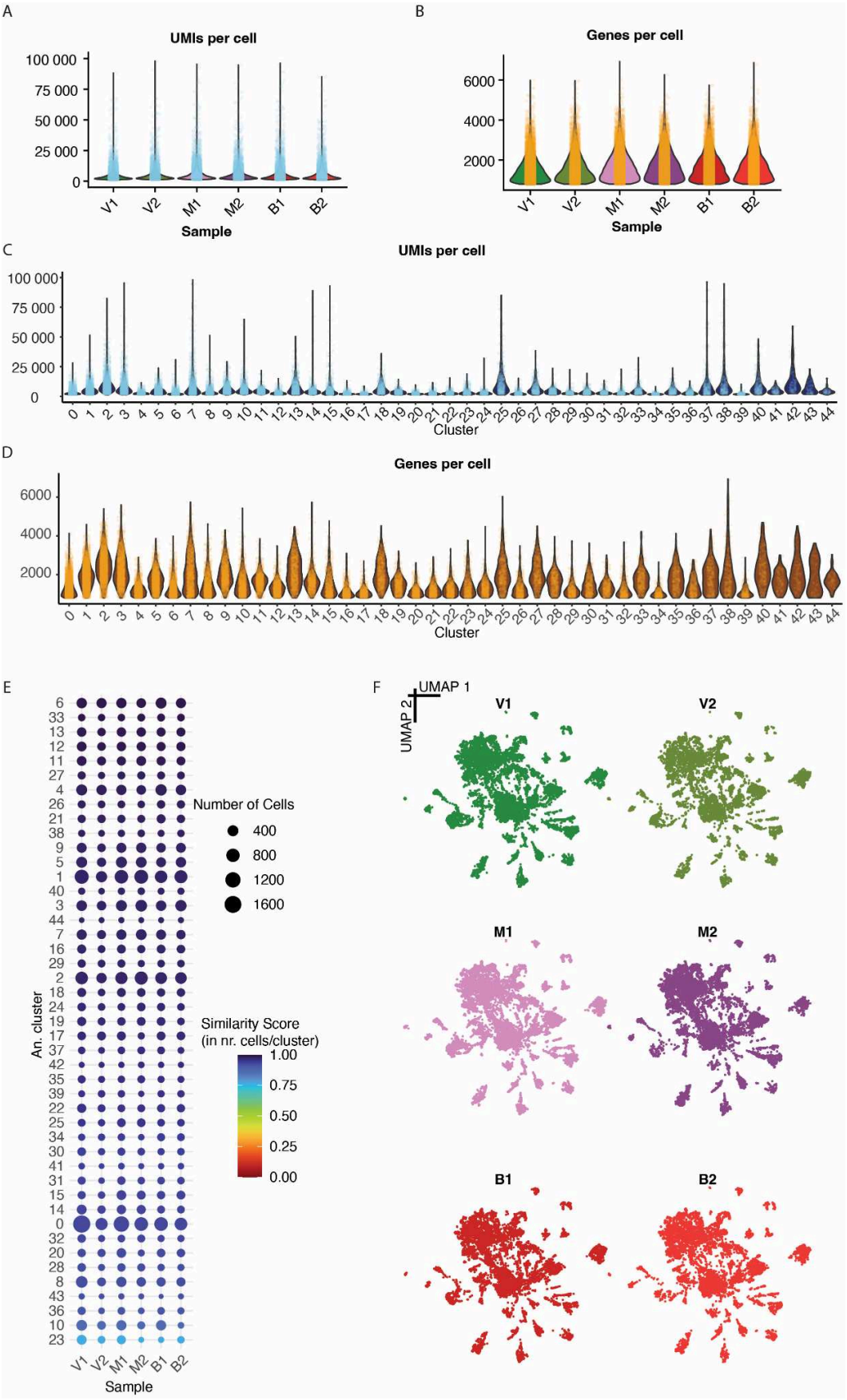


Figure S2. Quality control of the brain single cell atlas. (A) Violin plot of UMI counts in each replicate after

(continued)

QC. Seventeen cells with UMI counts > 100 K UMIs/ are omitted for clarity. **(B)** Violin plot of gene counts in the scRNA-seq replicates after QC. **(C)** Violin plot of UMI counts in each cluster after QC. Seventeen cells with UMI counts > 100 K UMIs/ are omitted for clarity. **(D)** Violin plot of gene counts in each cluster after QC. **(E)** Dotplot showing degree of similarity (cosine similarity) in the number of cells from each replicate and making up a cluster for all of the 45 clusters. Clusters are ordered from the one having the most similar number of cells per experimental replicate (top) to the one that showed the greater differences among sample replicates (bottom). **(F)** UMAPs showing the distribution of cells in the different sample replicates. Virgin sugar-fed replicate #1: V1; virgin sugar-fed replicate #2: V2; mated sugar-fed replicate #1: M1; mated sugar-fed replicate #2: M2; mated blood-fed replicate #1: B1; mated blood-fed replicate #2: B2.



Figure S3. Mapping of the brain single cell atlas to a *D. melanogaster* reference. SAMap results for cell type (continued)

assignment, showing which *D. melanogaster* cell types [18] (y axis) have been assigned as homologous to *An. gambiae* cellular clusters (x axis) by SAMap algorithm. Dot size corresponds to the alignment score value for each*D. melanogaster* cell type - An cluster pair. The strongest matched alignments (alignment score > 0.2) are further highlighted with a color scale to facilitate legibility.

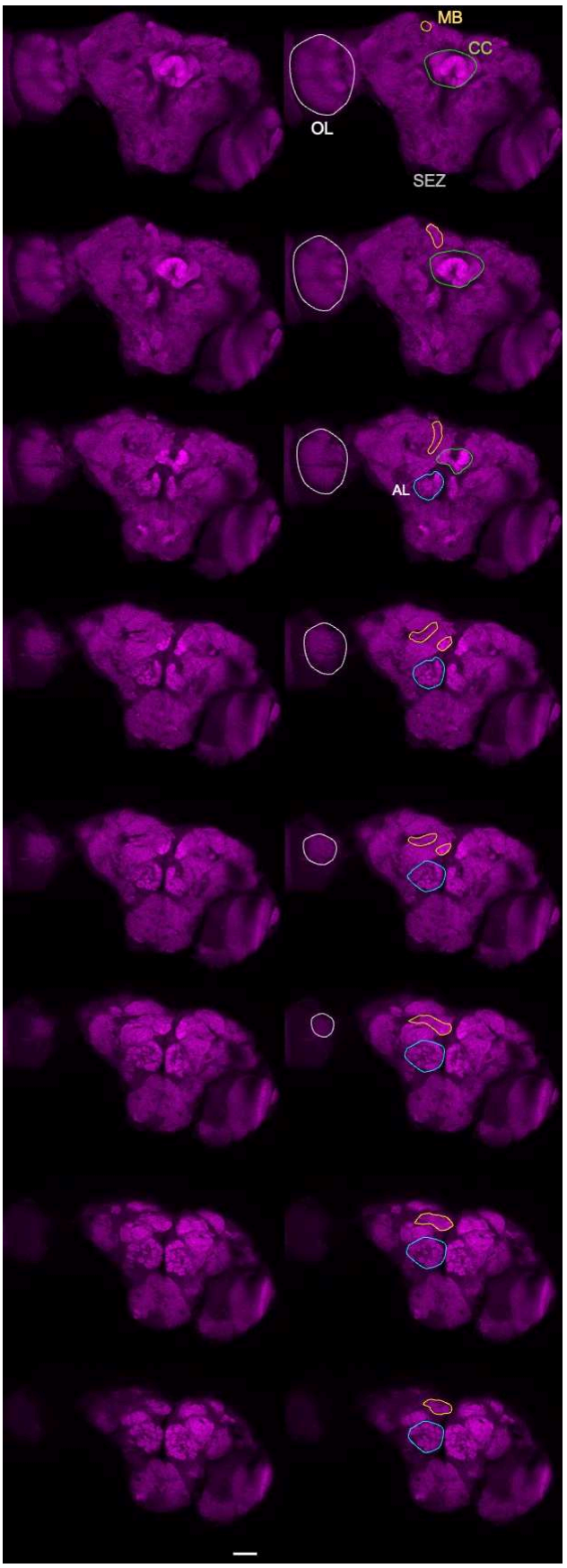


Figure S4. Anatomical structures in the *Anopheles* brain. Representative confocal microscopy image (continued)

showing Z-stacks of a female *Anopheles* brain stained with an anti-Bruchpilot antibody, a component of the presynaptic active zone. The images are displayed bare (left) or with annotation of identifiable structures (right). SEZ: suboesophageal zone; MB: mushroom body; CC: central complex; OL: optic lobe; AL: antennal lobe. Scale bar 50 μm.

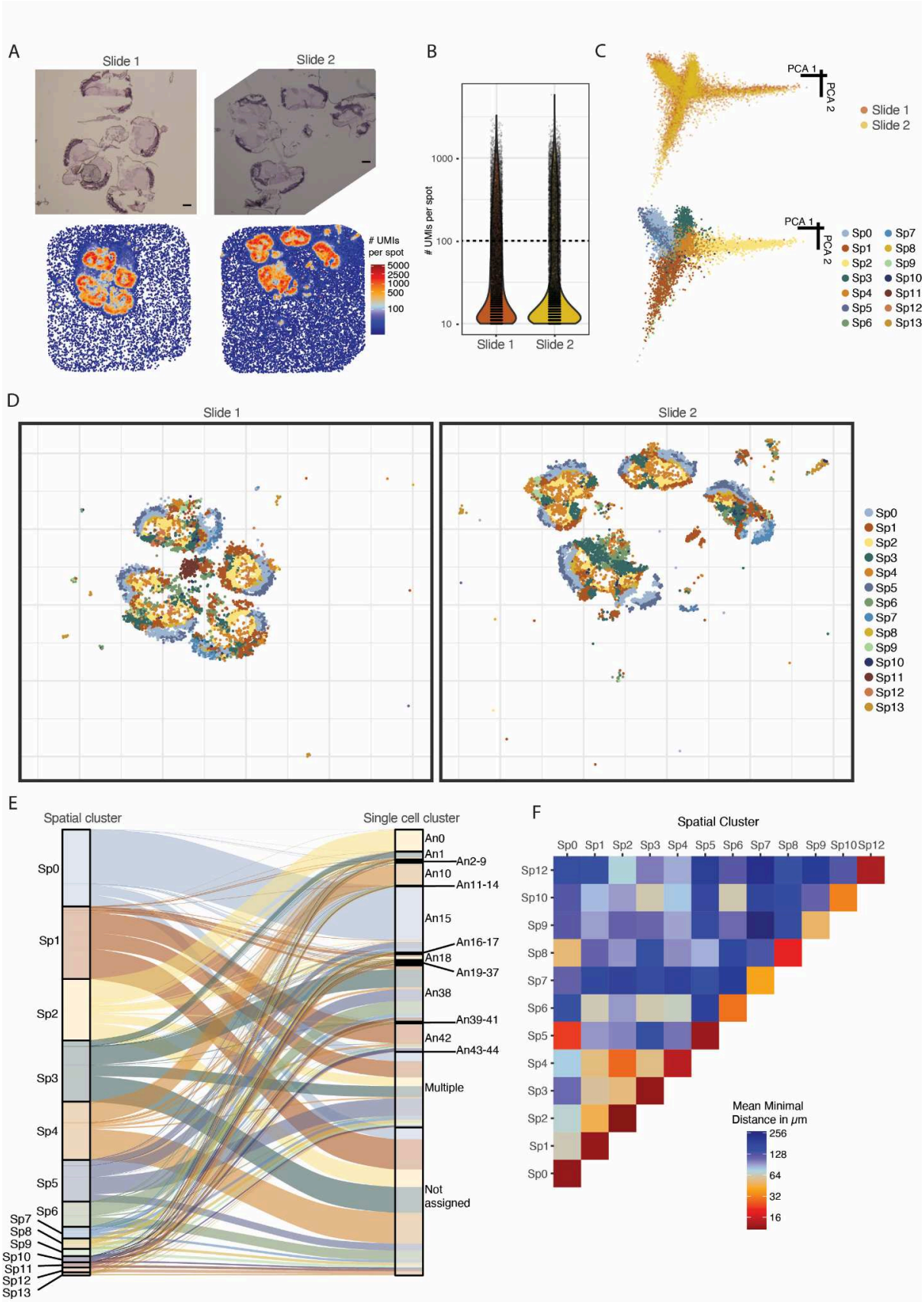


Figure S5. A spatially-resolved transcriptomic dataset of the female *An. gambiae* head. (A) H&E stained sections immediately adjacent sections of the two blocks (top panels) used in spatial transcriptomics (continued)

(bottom panels) depicting the number of UMIs per spot in eight individual brains. **(B)** Distribution of UMIs per spot in both blocks, the cut-off was set to no less than 100 UMIs per spot. **(C)** PCA of the 9,914 high quality spatially-resolved transcriptomes retained in the final dataset, highlighting their block of origin (top panel) and the spatial cluster they belong to (bottom panel). **(D)** Spatial representation of spatial clusters for each block. **(E)** Riverplot of the deconvolution of spatial clusters with the single cell clusters. **(F)** Mean minimal non directional distances between different spatially resolved clusters within the same brains, highlighting the relative proximity of clusters in space.

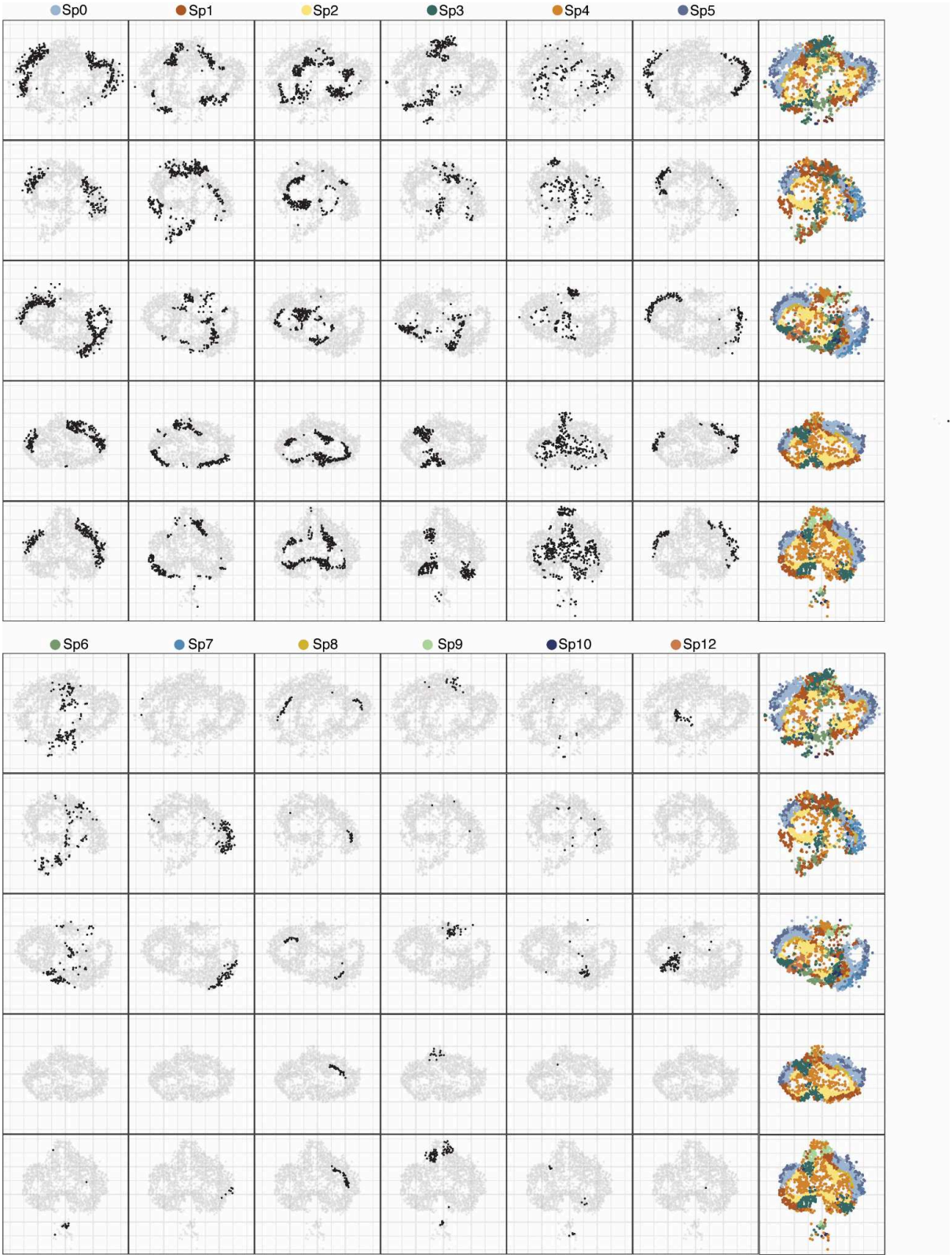


Figure S6. Spatial cluster distribution within the five high quality heads. Sp11 and Sp13 are absent because they were not represented within the head space.

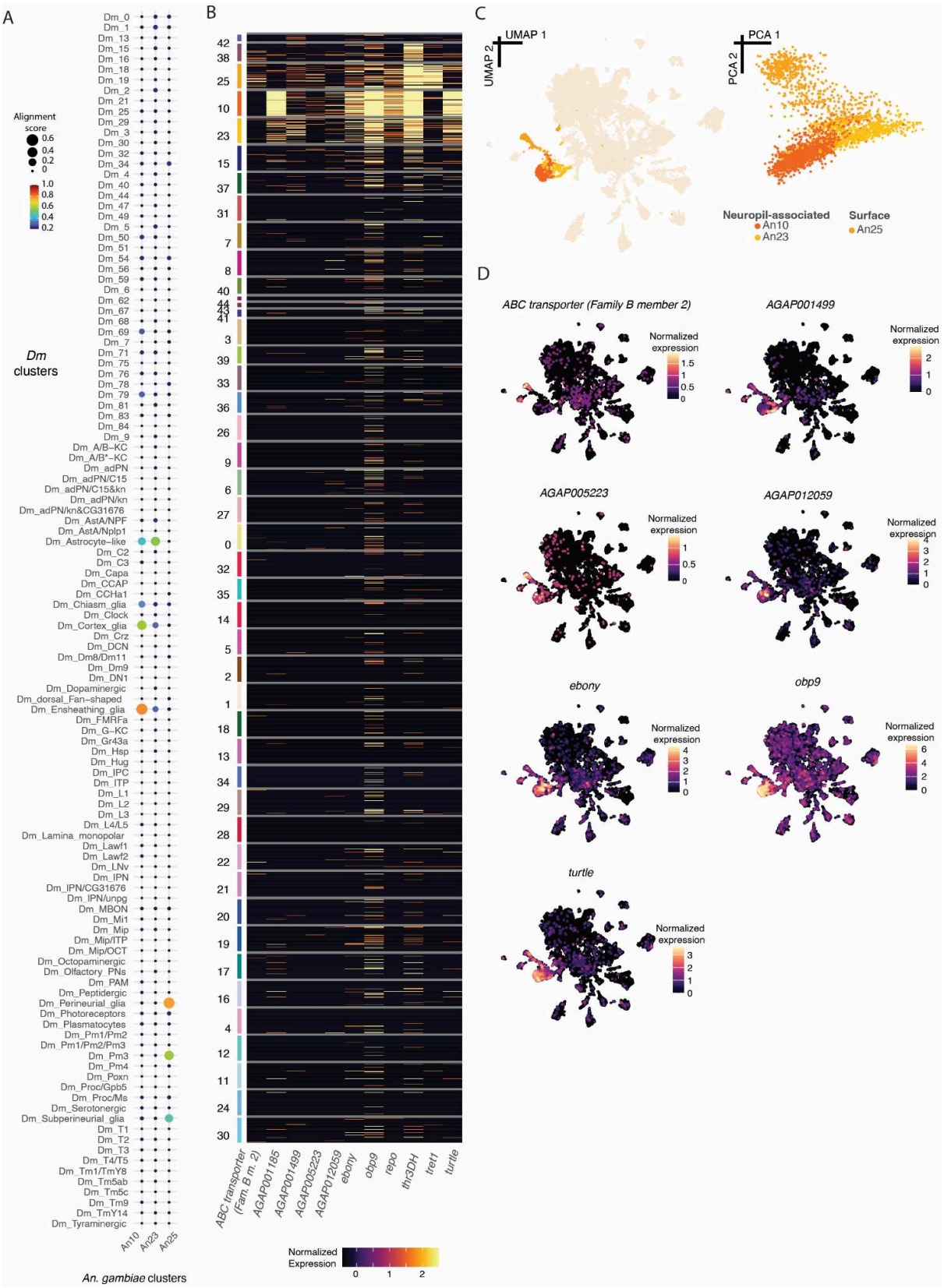


Figure S7. Characterization of glial cell diversity in the female *Anopheles* brain. (A) *D. melanogaster* cell type assignment (SAMap) to An clusters. Dot size and color code correspond to the alignment score value for each *D. melanogaster* cell type - An cluster pair. **(B)** Heatmap of expression data (normalized with

(continued)

SCTransform, scaled with base R scale function) downsampling a maximum of 500 cells per An cluster (y-axis). **(C)** Glia clusters identification in the atlas (UMAP, left panel) and their PCA projection after subsetting and application of SCTransform (right panel). **(D)** UMAPs showing expression distribution of cell markers among cell types, expressing cells in foreground.

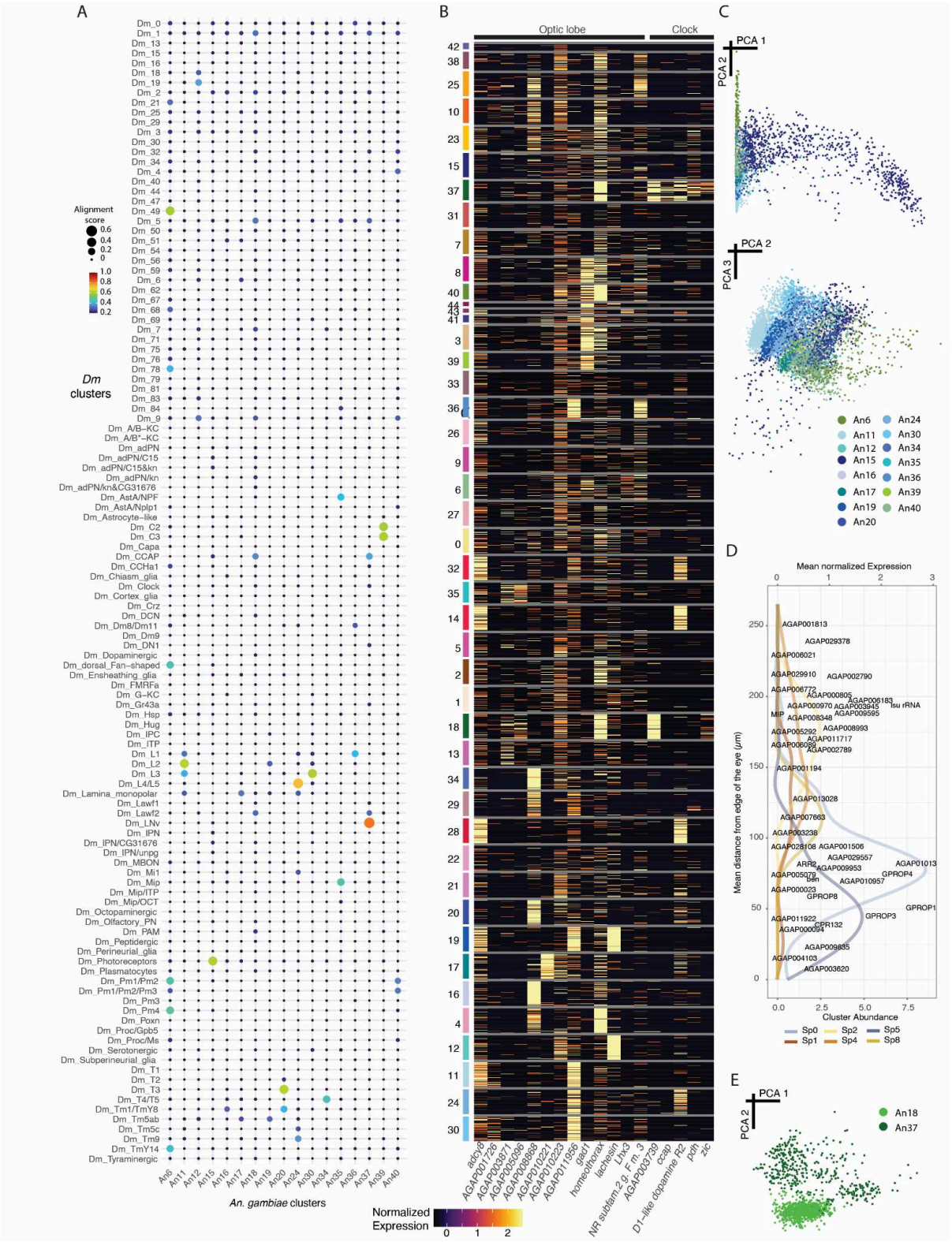


Figure S8. Characterization of optic lobes and clock neurons in the female *Anopheles* brain. (A) *D. melanogaster* cell type assignment (SAMap) to An clusters. Dot size and color code correspond to the alignment score value for each *D. melanogaster* cell type - An cluster pair. **(B)** Heatmap of expression (continued)

data (normalized with SCTransform, scaled with base R scale function) downsampling a maximum of 500 cells per An cluster (y-axis). Dm *drgx* is a marker of TmY1/TmY8 and T4/T5 cells [18], ortholog of AGAP008868; C2/C3 cell are dopaminergic, *gad1* expression [135]; AGAP009132, ortholog of Dm *CG12730* expressed in myelinating oligodendrocytes in eyes [35]; AGAP010223 ortholog of Dm *no ocelli*, crucial for development of adult eye structures [136]; *lachesin* (AGAP010222), ortholog to Dm *dip ε, θ, κ* [43]. **(C)** PCA projections after subsetting and application of SCTransform of optic lobe clusters. **(D)** Abundance of cluster signal shown as lines (lower axis) and mean normalised expression of highly spatially variable genes (upper axis) shown as labels in one eye region of one HQ head depending on the distance in µm to the edge of the head. Line colours correspond to clusters present within the eye section. Position of gene labels correspond to their mean normalised expression as well as the position of peak expression within the region. **(E)** PCA projections of clock neurons after subsetting and application of SCTransform.

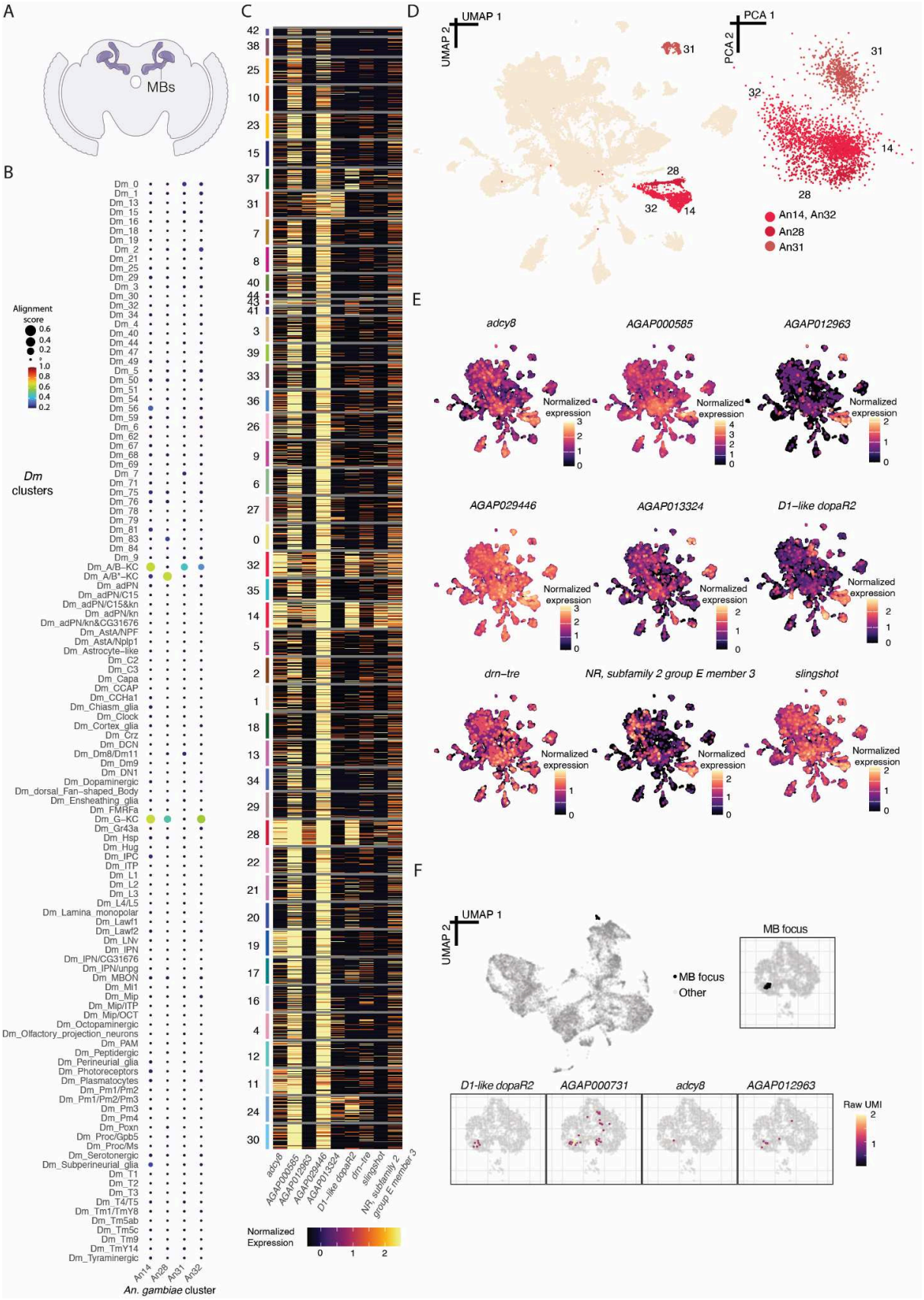


Figure S9. Identification of Kenyon cells and mushroom body in the female *Anopheles* brain. (A) Schematic (continued)

of the expected putative positions of MBs in the *An. gambiae* brain. **(B)** *D. melanogaster* cell type assignment (SAMap) to An clusters. Dot size and color code correspond to the alignment score value for each *D. melanogaster* cell type - An cluster pair. **(C)** Heatmap of expression data (normalized with SCTransform, scaled with base R scale function) downsampling a maximum of 500 cells per An cluster (y-axis). **(D)** KC clusters identification in the atlas (UMAP, left panel) and their PCA projection after subsetting and application of SCTransform (right panel). **(E)** UMAPs showing expression distribution of cell markers among cell types, expressing cells in foreground. **(F)** UMAP showing the MB focus and distribution of this MB focus in one high quality head as well as normalized expression of four markers of MBs.

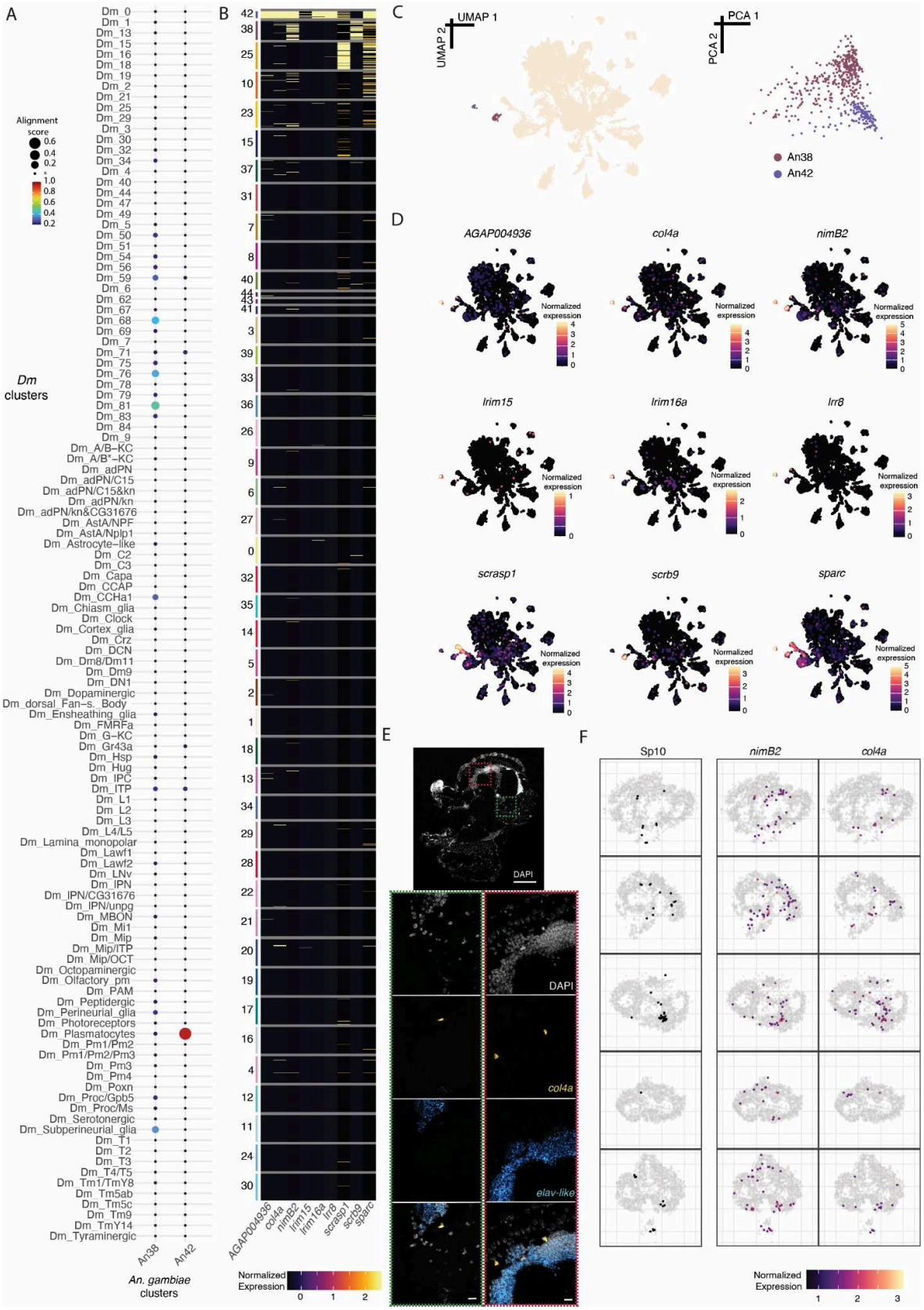


Figure S10. Characterization immune cell populations in the female *An. gambiae* head. (A) *D. melanogaster* (continued)

cell type assignment to An clusters (SAMap). **(B)** Heatmap of expression data (normalized with SCTransform, scaled with base R scale function) downsampling a maximum of 500 cells per An cluster (y-axis). **(C)** Immune cell clusters identification in the atlas (UMAP, left panel) and their PCA projection after subsetting and application of SCTransform (right panel). **(D)** UMAPs showing expression distribution of the oenocytoids marker *scrb9* [70] and of granulocyte marker genes (all the others) [69,70]. **(E)** ISH images on histological sections of mosquito heads. The whole section is shown on the top panel with nuclear staining and highlights the position of the insets below (scale bar = 100 μm, front of the head on top); transcripts of the granulocyte marker gene *col4a* are stained alongside those of the neuronal marker *elav-like* and nuclear staining (scale bar = 10 μm), highlighting granulocyte position in association with muscle (left) and cell body rind surface (right). **(F)** Distribution of Sp10 associated spots in five high quality brains (left) and normalized expression of two immune associated markers (right).

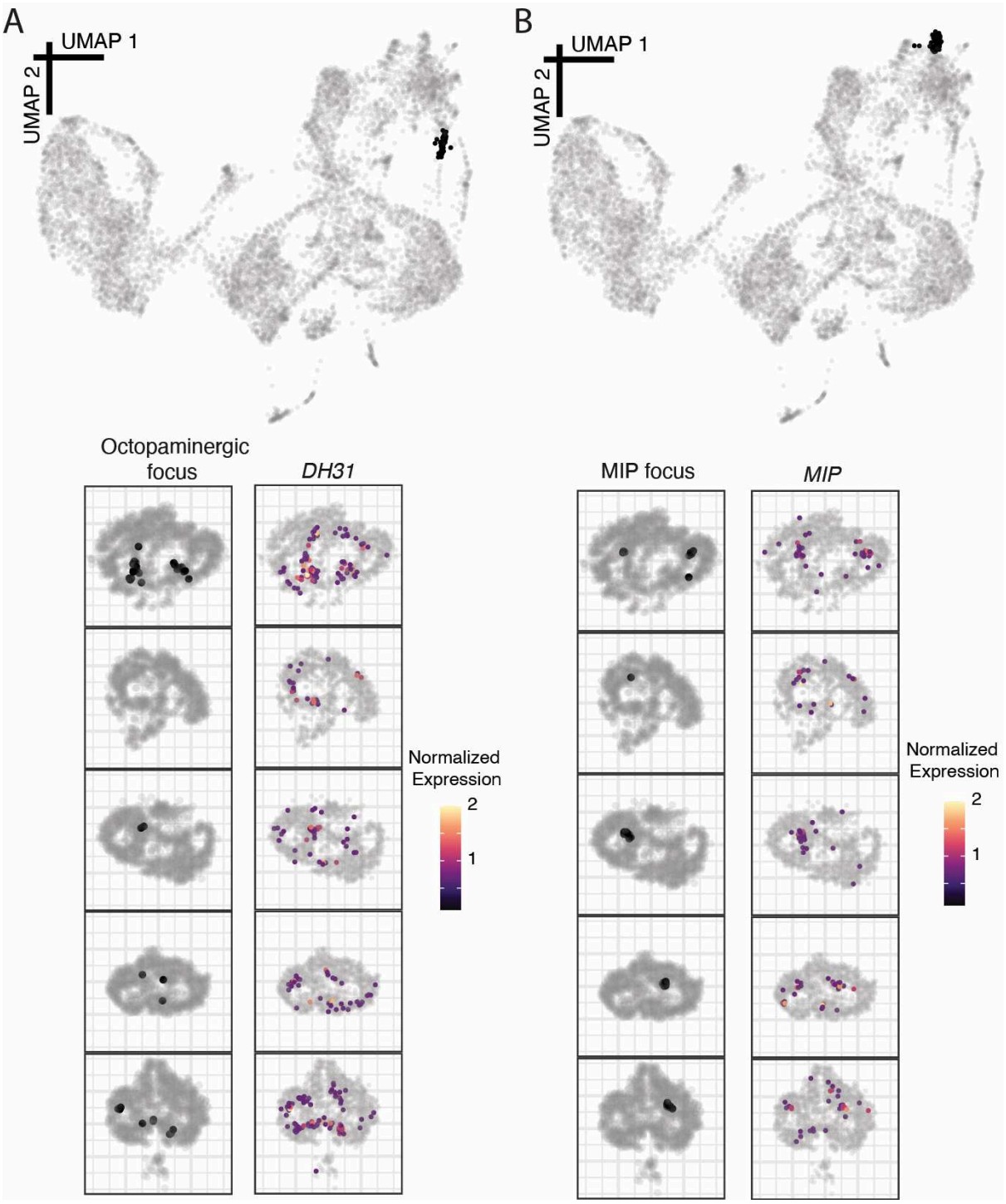


Figure S11. Spatial support for specialised neuronal foci in the cell body rind. (A) UMAP of the spatial transcriptomic dataset highlighting the *DH31*-expressing focus identifying octopaminergic related spots shown in their spatial context**. (B)** *MIP*-expressing focus identifying MIP-related spots shown in their spatial context.

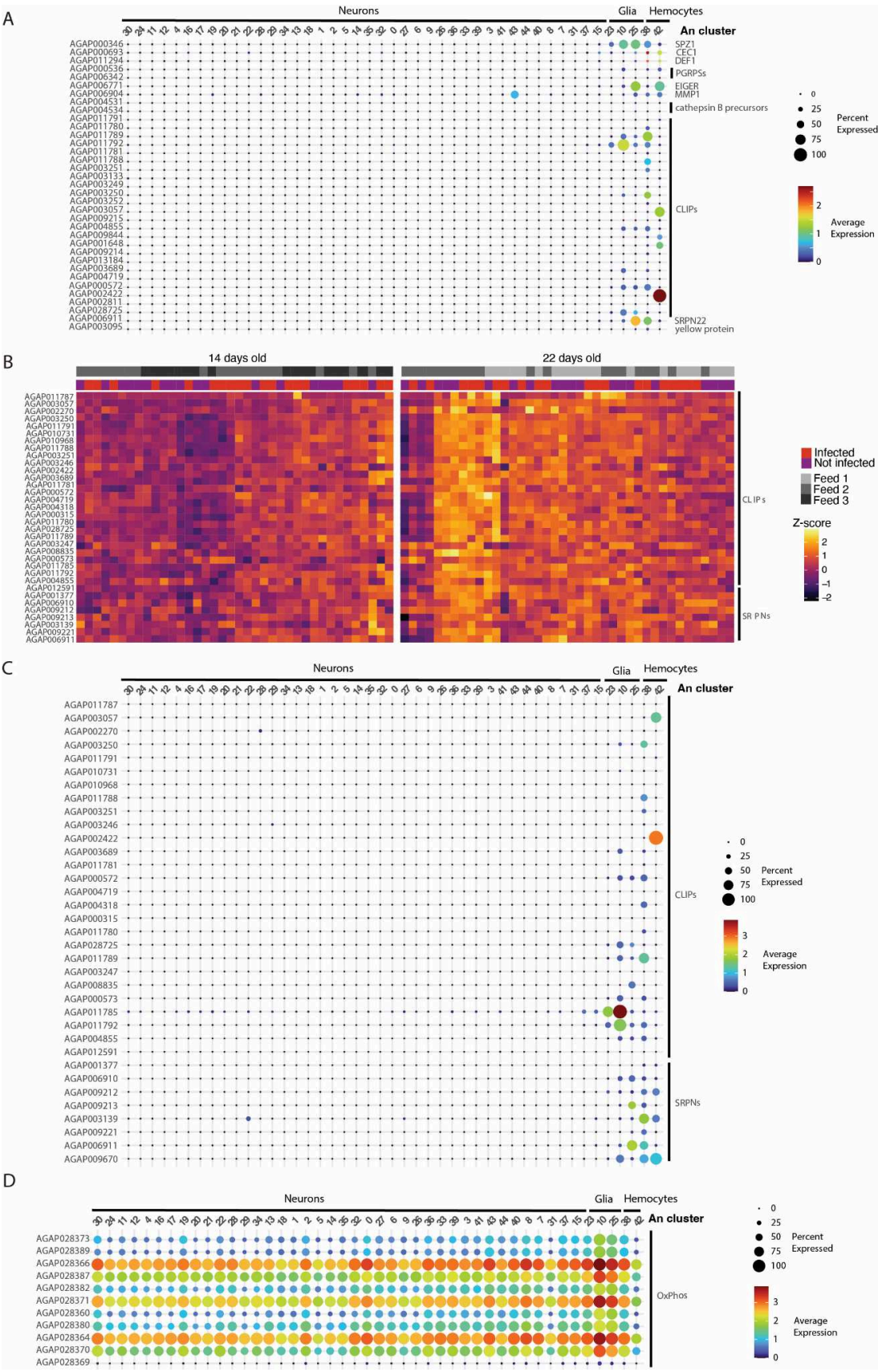


Figure S12. Differentially expressed genes of the female *Anopheles* brain in different life stages and aging, and association of DEGs to putative cell types of origin. (**A**) Mapping of immune genes up-regulated after

(continued)

blood meal to the cell atlas clusters. Scaled average expression (z-score) shown in the 45 An clusters of the atlas (An cluster ID and main cell type classification on the top line); gene annotation showed on the right. **(B)** Heatmap showing the genes belonging to immune gene families (on the right line) enriched in 22 day-old compared to 14 day-old mosquitoes (right and left panels, respectively), samples hierarchically clustered with a complete-distance method. **©** Mapping of immune genes up-regulated with aging (in 22 day-old compared to 14 day-old mosquitoes) to the cell atlas clusters. Scaled average expression (z-score) shown in the 45 An clusters of the atlas (An cluster ID and main cell type classification on the top line); gene annotation showed on the right. **(D)**Mapping of the most up-regulated genes with aging (in 22 day-old compared to 14 day-old mosquitoes) to the cell atlas clusters. Scaled average expression (z-score) shown in the 45 An clusters of the atlas (An cluster ID and main cell type classification on the top line); gene annotation showed on the right.

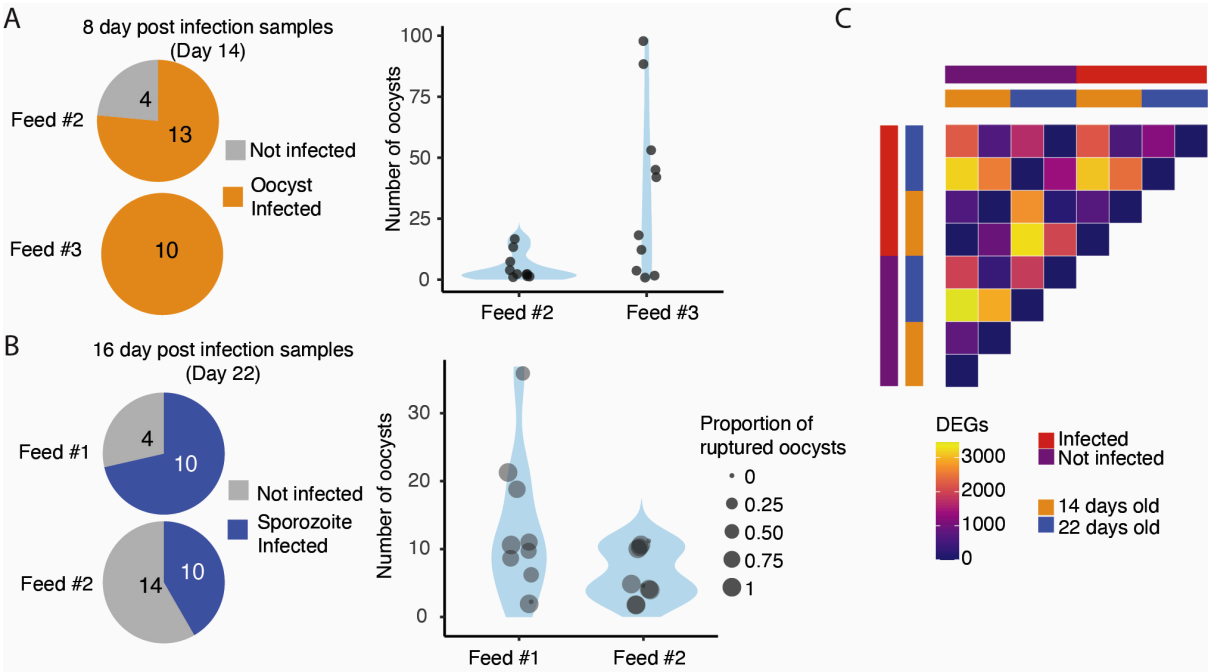


Figure S13. Impact of *Plasmodium falciparum* infection on the female *Anopheles* brain. (A) Prevalence of infection scored during sample dissection in female *An. gambiae* mosquitoes 8 days after the infection challenge (14 day-old individuals). **(B)** Prevalence of infection scored during sample dissection in female *An. gambiae* mosquitoes 16 days after the infection challenge (22 day-old individuals). **(C)** Distance plot showing the number of DEGs (computed with the *ashr* method) among all sample replicates.

Additional results and discussion

Examples of DEA from single cell data

The definitive annotation of the atlas allowed inspection of gene DE for specific cell types of interest. For example, glial cells of An10 are characterized by the expression of *obp*9, which encodes a protein putatively involved in the transport of hydrophobic ligands (Pelosi et al. 2018), the role of which is still unknown. After blood feeding, *obp*9 expression is specifically increased in the cluster (average log2 fold-change (log2FC) = 1.25, Bonferroni adjusted p-value (Bonferroni) < 1E-300), and this finding is consistent our single brain data, and with an in increase of the transcript and protein presence in *Anopheles* head already reported in the literature (Biessmann et al. 2005; Dwivedi et al. 2014). We were thus able to confirm and deconvolute this DE signal, identifying the cellular origin of one of the genes induced most strongly after blood meal in the *An. gambiae* head. In the manuscript, we hypothesized a potential role for *obp*9, and here I will elaborate further on the reasoning of our inference. The gene has been classified as encoding an OBP based on its inferred primary sequence. OBPs are small soluble proteins that have been characterized in insects, later found in vertebrates (Vogt and Riddiford 1981; Tegoni et al. 2000). These proteins are expressed in insect sensory organs, and can be positively or negatively charged at physiological antennal pH. Their role is to deliver hydrophobic odorants to receptor-coreceptor complexes on the OSNs, despite their mechanism of action has not yet been completely understood (Pelletier et al. 2010; Biessmann et al. 2010; Guidobaldi et al. 2014). The primary sequence of OBPs can be highly divergent, and the identity between OBPs of the same species can be lower than 10%. The assignment of a protein into the OBP-family is mainly based on a pattern of six cysteines whose relative positions are well-conserved across all insect orders (Briand et al. 2001; Leal et al. 1999). These proteins are not only found in olfactory organs: *An. gambiae* females express multiple OBPs in non-olfactory tissues (Amenya et al. 2010). This is true

also for *obp9*, the transcript and protein of which can be found both in organs associated with olfaction and in eggs (Biessmann et al. 2005; Mastrobuoni et al. 2013). It was suggested that alternative roles for OBP-like proteins could be hormones and/or lipid binding and transport (Lagarde et al. 2011; Wang et al. 2020). *An. gambiae*'s *obp9* is indeed ortholog to *Ae. aegypti obp22*, to which computational modeling has assigned a putative fatty acid binding role (Wang et al. 2020). Taken together, this evidence suggests that this gene might have a relevant role in glia and in post-blood meal and reproduction physiology, and might be central for lipid transport and nutrient storage or delivery among cells. Further studies are needed to clarify its function: gene KD associated with metabolomics studies, or ISH-immunofluorescence assays on whole body and eggs could reveal more on its role and dynamics of its expression.

We also identified an interesting DEG profile in An14, composed of Kenyon cells (KCs). In our data, they showed post-mating- and post-blood meal-specific transcriptional responses. Their gene expression profile recapitulated a general increase in transcription related to neural activity and excitatory/inhibitory signaling in the *An. gambiae* MBs after mating. Upregulated genes were strongly involved in signaling (Gene Ontology Enrichment (GO) Bonferroni = 7.70E-4). Among them, we could identify *gprdop3*, a dopamine G protein-coupled receptor, and *rdl*, encoding a subunit of a GABA gated chloride channel. The first is ortholog to the *D. melanogaster* gene *dop2R*, involved in reward mechanisms for the creation of long-term olfactory memories in the MBs, a process which also involves projecting GABAergic neurons (Zhou et al. 2019). At the same stage, the glutamate receptor AGAP001434 was upregulated in the cell cluster. In KCs, the glutamatergic function has been related to long-term memory formation in other insect species (Locatelli et al. 2005; Sinakevitch et al. 2010; Strausfeld and Hirth 2013). Taken together, these transcriptional variations delineate a profile that seems to underlie active memory formation processes that are activated after the mating event.

In addition to this, in An14 we could identify a large set of blood-meal induced genes; among these: (i) sixtynine TFs, (ii) nineteen histones and histone

acetylases, deacetylases and methyltransferases, (iii) ten splicing regulators genes (e.g. *muscleblind*), (iv) a few genes associated with cytoskeleton and its remodeling (e.g. tubulins, *actin*-5C, *cofilin*, *spectrin*, *talin*-1), (v) fortyfive initiation and twentyone elongation factors and subunits, (vi) one hundred and twenty ribosomal proteins, and chaperones (e.g. heat shock proteins, *cryab*). We could evidence an increase in abundance of transcripts of genes involved in translation and gene expression regulation after blood feeding (Panther GO FDR = 1.10E-08 and GO FDR = 7.49E-06, respectively), accompanied by a set of ten overexpressed genes associated with a proton-transporting ATP synthase activity (Panther GO FDR = 1.85E-07). This massive switch associated to gene expression processes and energy production once more evidences the fundamental role of KCs in response to life cycle events and putatively indicate ongoing memory formation associated to the post-blood meal rest phase (Su and O'Dowd 2003; Crocker et al. 2016).

Gaining functional insights in bulk RNA-seq results with scRNA-seq

In this project, we took advantage of multiple transcriptomics datasets obtained with various RNA-seq approaches in particular comparing bulk and scRNA-seq data. This was done with two main aims: first, complementing the information obtained from the two different techniques; second, integrating the results obtained with the two types of data and producing stronger inferences on the cellular origin and on the role of specific genes. As an example, we can imagine that the increase in *obp*9 expression after blood meal was revealed only in bulk RNA-seq data, without the support of the same evidence obtained with scRNA-seq. In this case, despite the knowledge about this gene expression in other species and in *An. gambiae* (Dwivedi et al. 2014; Yin et al. 2024), the inferences we could make on its role would have been much weaker, let alone the lingering doubt about putative contamination from surrounding olfactory and gustatory tissues, considering it is classified as having an odorant binding protein (OBP)-like inferred structure.

Being aware that the results of the two techniques could not be completely overlapped, we inferred putative cellular origin for a few thousands of DEGs along life cycle stages utilizing broad categories (neurons, glial cells, hemocytes).

The changes taking place after blood meal are mainly related to metabolism, and are the ones associated with the strongest LFC and showing the highest overlapping expression trends in both bulk and scRNA-seq data (up- or downregulated after blood meal). One gene showing an increased expression after blood meal led to puzzling and intriguing observations. This is the cathepsin B precursor AGAP004534, it is specifically overexpressed after blood meal in the bulk data (manuscript and manuscript Fig. S11), and in three cells in the brain atlas, belonging to the blood-fed condition (Fig. 17A). The three belong to either the surface glia cluster An25 or the hemocyte cluster An38, are positioned in the UMAP bridging between An25 and An38, and are localized amongst *repo*$^{+}$ cells in the data PCA (Fig. 17A, B), despite *repo* not being expressed in the three cells (counts = 0). These initial observations show consistent DE trends associated with blood meal, and hint at the presence of a blood-meal induced immune cell type or cell status associated with the mosquito CNS. Interactions among surface glia and hemocytic cell types are indeed reported in *D. melanogaster* in association with inflammatory responses (Omoto et al. 2016; Winkler et al. 2021). The three cells identified here specifically express five genes (SCTransform log-normalized expression > 1), with peptidase (AGAP004700, AGAP004534) and lipase (triacylglycerol lipase AGAP000211) activity, or involved in immunity functions (protein yellow AGAP007454 and *lrim8a*) (Han et al. 2002; Pirahmadi et al. 2025) (Fig. 17B, C). Of the top twenty genes upregulated in the three cells compared to the rest of the dataset, most showed specific upregulation associated with the three cells (Fig. 18). In this gene list, we can find various lipid transporters, proteases and genes associated with immunity. This profile points to the presence of a cell type that might have specific immunity-related and phagocytic functions, active only after blood meal. Indeed, both phagocytic glia and immune cells use Cathepsin B

for phagocytosis in the context of neural network reshaping, performance of inflammation response mechanisms or antigen/pathogen degradation (Gan et al. 2004; Yadati et al. 2020). Further ISH experiments directed towards AGAP004534 in association with hemocyte markers (as *col4a* and *scrb9*) and general glia or surface glia markers (as *repo* and *tret1*) might help locating the expressing cells in the tissue, show whether they express glia or hemocyte markers, whether they interact with surface glia or whether they intercalate within the brain tissue, and shed light on its role in the post-blood meal brain physiology.

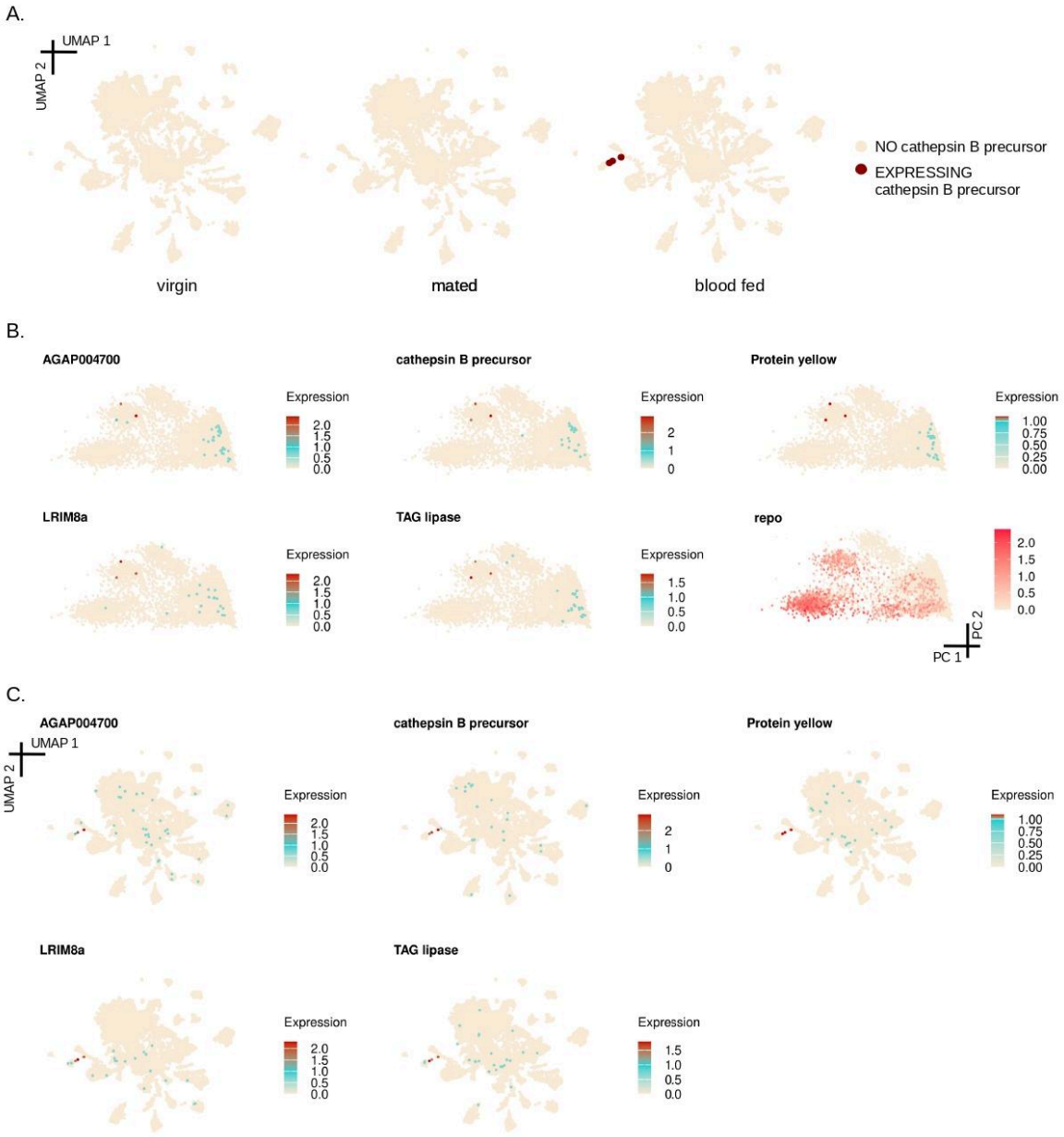


Figure 17. Cathepsin B precursor-expressing cells. (A) UMAPs highlighting the cathepsin B precursor-expressing cells, present only after blood meal. **(B)** PCA plots showing the expression of the five genes univocally expressed in the cathepsin B precursor-expressing cells. Also *repo*$^{+}$ cells are highlighted in the last panel to highlight cell localization. **(C)** UMAPs showing the expression of the five genes univocally expressed in the cathepsin B precursor-expressing cells. LRIM: leucine-rich repeat immune; TAG: triacylglycerol.

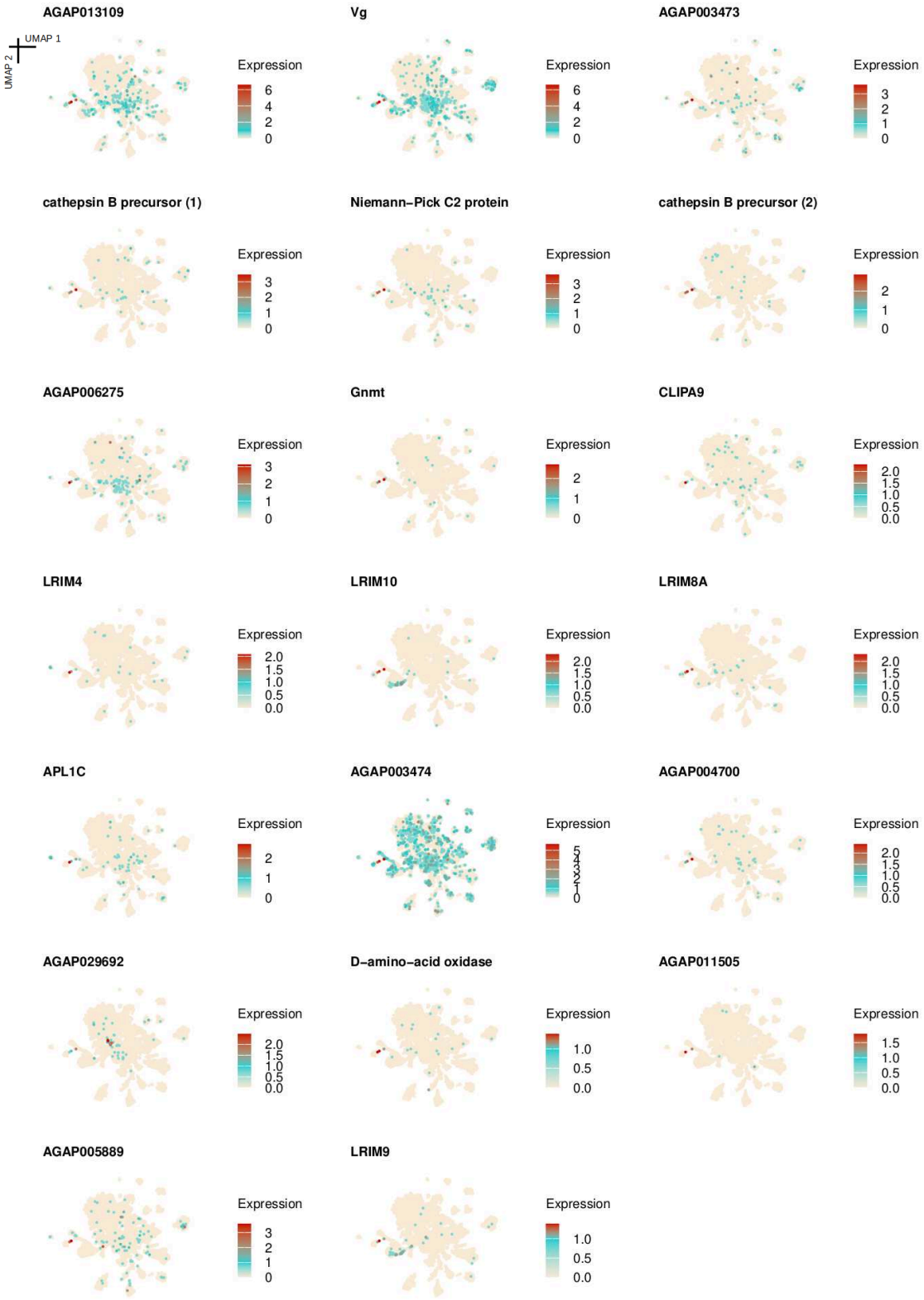


Figure 18. Marker expression for the cathepsin B precursor-expressing cells. UMAPs showing (continued)

the expression of the top 20 marker genes for in the cathepsin B precursor-expressing cells. Vg: vitellogenin; Gnmt: glycine N-methyltransferase; LRIM: leucine-rich repeat immune; APL: *Anopheles Plasmodium*-responsive leucine-rich repeat.

Tracing back information obtained with bulk RNA-seq to the scRNA-seq data provided multiple examples as the ones mentioned above, showing that the brain atlas is a relevant resource to get insights to guide future studies.

Absence of transcriptional manipulation signatures in the mosquito brain

Another focal point, and a surprising result for us, is that infection with *P. falciparum* does not seem to evoke transcriptional shifts in the mosquito brain. Multiple models indicate that malaria sporozoites should attempt to manipulate the mosquito to increase its biting rate, despite a higher risk of dying in the mosquito's attempt to obtain blood (Koella 1999). Nonetheless, previous studies showed that infection costs were associated with larval production and egg hatch rate, but rarely attributed to changes in blood feeding and never to changes in mosquito size, showing that infection might impact resource allocation in the mosquito (Hurd et al. 2005). Intermittent arms race can anyway lead to co-adaptation and accommodation processes in natural host-pathogen interactions, and parasites can benefit from establishing a transmission cycle producing low infection burden in most vectors. This actually appears to have happened for factors influencing mosquito fitness in the *An. gambiae* - *P. falciparum* system (reviewed in Lefèvre et al. 2009; Shaw et al. 2022). Indeed, when clear manipulation phenotypes are present, most of the times a manipulated host gene expression signature can be evidenced, contrary to what we evidenced here (Sadoul et al. 2022). Nonetheless, some parasite factors, maybe even RNAs, might be exported and affect host physiology, as it has been shown for extracellular vesicles content (Mantel and Marti 2014; Kioko et al. 2023). Future analysis on our data to check the presence of *P. falciparum*-specific transcripts in the brain might shed new light on this hypothesis, or prove it false.

Conclusions

The nervous system has long been studied in laboratory animals as a means to understand human neurological processes and diseases, with *D. melanogaster* being one of the favourite models due to its highly conserved inter-species homology with humans, combined with a small size and a fast generation time (Adams et al. 2000; Rubin et al. 2000; Ugur et al. 2016). Understanding which are the general mechanisms underlying Eukaryotes' physiological processes and the multiple homologous molecular actors which are retained across evolution to fulfill the same functions is fundamental for multiple reasons. Identifying the common characteristics of taxa is key for revealing evolutionary history, understanding biological diversity, supporting taxonomy and classification, but also guiding conservation biology and, as stated above, advancing biomedical research. At the same time, the specialized adaptations of some organisms do not find counterparts in model organisms. For example, the need of blood-feeding mosquitoes to alternate blood meals to sugar meals for improving egg nutrient storage is a peculiar trait not found in classical model organisms. This trait can be studied in laboratory conditions, since mosquitoes have similar advantages as fruit flies in terms of rearing procedures.

The fact that blood seeking and feeding behaviors hold intrinsic life-threatening risks to the mosquito itself suggests that their regulatory mechanisms are finely regulated in the insect. Indeed, mosquito sensory perception guiding host seeking and blood feeding has been long studied both in *Aedes* mosquitoes and in human malaria mosquitoes, especially in association to olfactory cues (Wolff and Riffell 2018; Konopka et al. 2021). The reason for this resides largely in the fact that it was soon identified how single odor molecules could guide mosquitoes to a feeding source, which led to further finer and finer dissection of olfactory sensory perception in peripheral organs and peripheral nervous system. Understanding how environmental cues are perceived and which cues drive attraction processes is essential to implement actions aiming to interfere with the mosquito interaction with human hosts, however this does not inform

on the mechanisms associated with the integration of sensory information that guide the decision making processes. Considering the recent discovery of adaptations leading to behavioral resistance to vector control measures (e.g., insecticides, nets, etc.), it is more and more crucial and urgent to understand how processes associated with decisions and learning are performed at the molecular level in the mosquitoes CNS (Hubbard and Murillo 2024).

In *Drosophila*, the molecular nature of the maturation steps along cell lineages progression, the brain anatomy, transcriptional profile, and connectomics have been described with a precision and completeness unmatched in other organisms (Court et al. 2023; Lu et al. 2023; Winding et al. 2023). In addition, thanks to small size, in *Drosophila* it is possible to capture wide interindividual variability, and the intrinsic diversity of cells and tissues of their organs, an aim that is more impractical to reach at larger body scales. In mosquitoes, and especially *Anopheles*, this type of knowledge was lacking. For other mosquito species this is not drastically different: a male and female brain scRNA-seq atlas was obtained for *Ae. aegypti*, some putative cell markers were identified based on literature search of homologous marker genes, but no further algorithm-based or histological investigation has been put in place to confirm the nature and tissue localization of these genes (Cui et al. 2022). This year, a snRNA-seq atlas of multiple organs of *Ae. aegypti*, including the brain, was published as a pre-print. In these data, the authors identified tens of different cell types throughout multiple body tissues, and managed to assign an annotation to Poxn neurons, clock cells, glia and KCs sub-types. They also analysed differential gene expression in multiple conditions in glia and KC populations, but did not go further characterizing the identity of other brain cell types (Goldman et al. 2025). To keep advancing knowledge on the mosquito CNS function, it is necessary to understand what is the detailed structure of the mosquito brain, which cell types make it, which are the functions they carry on, which are the molecular markers that can be used to specifically target cell types of interest in functional studies, and how specialized cell populations express specific sets of genes to guide the mosquito in fulfilling specific tasks.

In the context of this project, we greatly improved the scientific community's knowledge on mosquito brains, and created the first spatial and cellular map of the brain of the main malaria vector. This is the first spatial transcriptomics of an insect vector, second ever example of spatial transcriptomics in insects, the first being published this year describing honeybee brain, an organ much bigger than a mosquito brain (Mu et al. 2025). We collected transcriptional data on the female mosquito brains in order to provide results that would inform on both cellular identities and molecular processes taking place in response to life cycle events or leading characterizing behaviors. We manually curated the annotation of tens of previously uncharacterized cell types crossing the results of cell type taxonomy methods and cross-species cellular annotation with an extensive literature search. Indeed, we confirmed in *An. gambiae* the expression patterns of the two only known brain cell markers for *Anopheles* genus, the generalistic ones for neurons and glia (respectively *elav-like* and *repo*), and described tens of novel brain cell markers. This guided the characterization of tens of cell types, namely the main glia subtypes, antennal lobes cell populations, a wide variety of optic lobes neurons, photoreceptors, KCs subtypes, various circadian rhythm regulatory neurons and LNvs, Poxn neurons and immune cells associated with the CNS.

We went further and characterized the genes we thought being putatively involved in specific functions. We explored the tissue localization of putative cell type markers to confirm their nature, and we attempted the characterization of a cell population putatively proliferating after blood meal with a click-chemistry approach. In addition, we associated cellular annotation and transcriptional profiling with single brain bulk RNA-seq data, which allowed us to understand how the transcriptional landscape varies in the female *An. gambiae* brain in response to essential life cycle or pathological events, and map the cellular origin of such signals thanks to the brain atlas we created. In fact, we investigated the transcriptional variations taking place in the mosquito brain in association with mating and blood feeding, identifying actors supposedly involved in life stage-specific behaviors. We evidenced a profile which could be putatively associated with neural network rewiring and memory formation after

mating, and described a transcriptional state during the resting phase after blood meal suggesting a decrease in translation processes and downregulation of the expression of genes involved in cell proliferation and intracellular signaling, consistent with a decreased mosquito activity and with resource allocation to the reproductive tract. We proceeded showing that there is no influence of *P. falciparum* infection on the transcriptional status of the mosquito brain at any infection stage, in line with the results of some previous studies (reviewed in Lefèvre et al. 2009; Shaw et al. 2022). Such data on infected individuals also allowed us to compare brain transcriptional signatures of aging, detecting a gene expression that we hypothesize to be linked to the earliest inflammaging, with ongoing compensatory mechanisms to delay mitochondrial and immune functions impairment.

Our experimental setup also allowed us to describe the molecular and biological background potentially associated with disease transmission in non-infected individuals, and provided details on the processes taking place in moments of the life cycle that pose risk of malaria infections to the female *An. gambiae*. We identified 28 gene candidates that might be involved in brain regulation of blood-seeking behaviors, which are currently under investigation in an attempt to describe blood-seeking master regulators. If successful, this analysis could lead to the identification of protein/s target/s for pharmacological treatments to be used in combination with the other vector-control measures already in place.

In addition to these aims, the project initially included the exploration of possible evolutionary convergence in parasitic manipulation of insect behavior (reviewed in Lefèvre et al. 2009). We thus attempted to acquire transcriptomics data from Trypanosome-infected Tsetse flies, and planned to compare them with the ones gathered from *Plasmodium*-infected *An. gambiae*, but we faced an unfortunate drawback when infections could not progress to the MT stage for months, a fact that led us to abandon this research line for the project.

Our study is limited to transcriptional signatures, and complementing it with information on other mechanisms that can shape a cell state, such as control of the epigenetic signature, proteomics, phosphoproteomics, or metabolomics, could help delineate a more complete and interpretable picture of the processes under exam. This reasoning grounds on being aware that strong phenotypes can arise from a single molecule factor, with limited impact on other molecular events. This is for example the case of *Toxoplasma gondii* manipulation phenotype exhibited by infected mice: their decreased fear of cats, which are the *T. gondii* definitive hosts, is caused by a single metabolite produced by the parasite and affecting the mouse dopaminergic signalling (reviewed in Abdulai-Saiku et al. 2021). Our data do not favour a *P. falciparum* manipulation phenotype that roots in an altered physiological background state of the mosquito brain, which would probably be impactful on the transcriptional profile of the organ. Nonetheless, they do not exclude the presence of molecular actors influencing neurotransmission. Also, our study does not investigate whether altered transcriptional signatures are present in the infected mosquito brain when they get exposed to a host's cues (e.g. through odors or in the presence of a blood source). Considering that mosquito response to odours and anthropophily are impacted by *P. falciparum* infection (Cator et al. 2013; Vantaux et al. 2015), it is possible that a putative manipulation mechanism could reside in processes which are fastly-triggered by an environmental stimulus, and that can also be quickly switched off, as it happens for the translation of mRNAs included in ribonucleoprotein granules (Chen et al. 2024), or on a metabolite-mediated mechanism.

In addition to these limitations, we investigated through imaging the tissue localization of only a few of the genes we inferred being cellular markers. Although ISH confirmed the role of the marker investigated, and worked as a proof of concept of the reliability of our annotation approach, we explored our inferences just partially with this technique. In this sense, we were limited by the ambitious set up of the project, which aimed to lay the ground for an extensive characterization of the mosquito brain. Indeed, we generated spatial transcriptomics data which, despite lower spatial resolution relative to ISH,

yielded information-rich maps of gene expression localization that complemented and validated our scRNA-seq atlas.
Further to this, we contrasted the outcomes of our bulk RNA-seq with the scRNA-seq data to show how some challenging interpretations of results obtained with bulk RNA-seq could be clarified by comparison with scRNA-seq information. We did not perform an extensive and deep analysis of such data integration, as our aim was to test whether our atlas stands as a resource to gain deeper insights in bulk RNA-seq data. Bulk RNA-seq data can be obtained with a faster and more cost-effective approach than scRNA-seq data: this means that our atlas provides the possibility of obtaining stronger inferences from bulk RNA-seq data in gathered in contexts in which performing scRNA-seq is still challenging (e.g. on field samples).

The information on cell type markers are pivotal in driving the investigation of specific cell lines of interest. Ideally, the information obtained in this study will facilitate and promote research on the mosquito CNS. We are working to have our single-cell atlas publicly available as an interactive website. This would be a ready-to-use source to quickly assess the pattern of expression of genes of interest in the *An. gambiae* brain, overcoming the need of lengthy data analysis, for those cases in which an extensive comparison with our data is not necessary. This resource would allow easy access to the vast amount of data we gathered, otherwise strongly limited if relying just on the description made in the publication manuscript.
Future directions might involve deepening the analysis on the data and characterizing the function of specific cell types in response to defined environmental stimuli. For example, producing lines expressing GCaMP6 calcium indicator under the control of promoters of genes markers of neurons of interest, and studying the response of such cell type to environmental stimuli *in vivo* with two-photon microscopy. For instance, little is known about visual cues perception and integration in the mosquito brain, with information mainly on development and opsin expression patterns (Hu et al. 2009; Mysore et al. 2014; Jenkins and Muskavitch 2015; Giraldo-Calderón et al. 2017). Our spatial and

cellular map might allow dissecting the nature of stimuli that can activate specific optic lobe cell types. As we showed two populations of lamina cells were differentially marked by *adcy8* and *D1-like dopamine R2*: the creation of mosquito lines expressing GCaMP6 under the control of the promoters of these two genes would for example allow the investigation of specific neural activations in response to light stimulation.
Furthermore, multiple genes with unknown functions but interesting expression patterns have been identified (e.g., *obp9*), and their role can be further investigated with ISH, indirect fluorescent antibody labeling, protein purification and crystallography. For example, performing immunoprecipitation on mosquito samples followed by mass spectrometry would possibly reveal *obp9* natural ligand and could elucidate the role of this putative non-chemosensory OBP-like protein.

This in-depth molecular and cellular atlas of the *An. gambiae* brain bridges a critical knowledge gap and establishes a powerful resource for future studies in mosquito neurobiology. By charting the cellular architecture and transcriptional programs across development and infection, we uncovered new opportunities to probe how neural circuits shape vector behavior. This study represents a large leap in the knowledge on insect vector behavioral transcriptomics, and showed how the master organ of behavior regulation undergoes changes in association to life cycle stages with characterizing behaviors. The project has brought a comprehensive body of new data about dozens of cellular types and their involvement in mosquito life cycle stages in which disease transmission-related behaviors are performed, with potential of informing further investigation for the development of targeted field interventions disrupting mosquito behavior at the neural level, and putative cross-applicability to other insects species. We paved the path for extensive in depth characterization of genes involved in the regulation of disease transmission-related behaviors, and laid the foundations for studies on CNS cell lineages and neurobiology in *Anopheles* mosquitoes, unachievable with the previous knowledge.

Bibliography

Abdulai-Saiku, Samira, Wen Han Tong, and Ajai Vyas. 2021. "Behavioral Manipulation by *Toxoplasma Gondii*: Does Brain Residence Matter?" *Trends in Parasitology* 37 (5): 381–390.

Acree, F., Jr, R. B. Turner, H. K. Gouck, M. Beroza, and N. Smith. 1968. "L-Lactic Acid: A Mosquito Attractant Isolated from Humans." *Science (New York, N.Y.)* 161 (3848): 1346–1347.

Adams, M. D., S. E. Celniker, R. A. Holt, et al. 2000. "The Genome Sequence of *Drosophila Melanogaster*." *Science (New York, N.Y.)* 287 (5461): 2185–2195.

Afify, Ali, Joshua F. Betz, Olena Riabinina, Chloé Lahondère, and Christopher J. Potter. 2019. "Commonly Used Insect Repellents Hide Human Odors from *Anopheles Mosquitoes*." *Current Biology: CB* 29 (21): 3669–3680.e5.

Afify, Ali, and Christopher J. Potter. 2022. "Calcium Imaging of *Anopheles Coluzzii* Mosquito Antennae Expressing the Calcium Indicator GCaMP6f." *Cold Spring Harbor Protocols* 2022 (11): Pdb.prot107918.

Agrawal, Ashutosh, and Tanmay P. Lele. 2019. "Mechanics of Nuclear Membranes." *Journal of Cell Science* 132 (14): jcs229245.

Akhund-Zade, Jamilla, Shraddha Lall, Erika Gajda, Denise Yoon, Julien F. Ayroles, and Benjamin L. de Bivort. 2021. "Genetic Basis of Offspring Number-Body Weight Tradeoff in *Drosophila Melanogaster*." *G3 (Bethesda, Md.)* 11 (7): jkab129.

Alout, Haoues, Roch K. Dabiré, Luc S. Djogbénou, et al. 2016. "Interactive Cost of *Plasmodium* Infection and Insecticide Resistance in the Malaria Vector *Anopheles Gambiae*." *Scientific Reports* 6 (1): 29755.

Altenhoff, Adrian M., Alex Warwick Vesztrocy, Charles Bernard, et al. 2024. "OMA Orthology in 2024: Improved Prokaryote Coverage, Ancestral and Extant GO Enrichment, a Revamped Synteny Viewer and More in the OMA Ecosystem." *Nucleic Acids Research* 52 (D1): D513–D521.

Amenya, Dolphine A., Wayne Chou, Jianyong Li, et al. 2010. "Proteomics Reveals Novel Components of the *Anopheles Gambiae* Eggshell." *Journal of Insect Physiology* 56 (10): 1414–1419.

Anderson, R. A., J. C. Koella, and H. Hurd. 1999. "The Effect of Plasmodium Yoelii Nigeriensis Infection on the Feeding Persistence of Anopheles Stephensi Liston throughout the Sporogonic Cycle." *Proceedings of the Royal Society of London. Series B, Containing Papers of a Biological Character. Royal Society* 266. https://doi.org/10.1098/rspb.1999.0839.

Andolina, Chiara, Wouter Graumans, Moussa Guelbeogo, et al. 2024. "Quantification of Sporozoite Expelling by Anopheles Mosquitoes Infected with Laboratory and Naturally Circulating P. Falciparum Gametocytes." *eLife* 12 (RP90989). https://doi.org/10.7554/eLife.90989.

Arora, Gunjan, Yu-Min Chuang, Photini Sinnis, George Dimopoulos, and Erol Fikrig. 2023. “Malaria: Influence of *Anopheles* Mosquito Saliva on *Plasmodium* Infection.” *Trends in Immunology* 44 (4): 256–265.

Ataev, G. L., P. S. Babich, and A. S. Tokmakova. 2013. “The Study of the Sporocyst Broodsacs Coloring in *Leucochloridium Paradoxum* (Trematoda: Brachylaemidae).” *Parazitologiia* 47 (5): 372–379.

Austen, Ernest Edward. 1911. A *Handbook of The Tsetse-Flies*. Order of the Trustees of the British Museum.

Autino, Beatrice, Alice Noris, Rosario Russo, and Francesco Castelli. 2012. “Epidemiology of Malaria in Endemic Areas.” *Mediterranean Journal of Hematology and Infectious Diseases* 4 (1): e2012060.

Aymoz, Delphine, Carme Solé, Jean-Jerrold Pierre, et al. 2018. “Timing of Gene Expression in a Cell-Fate Decision System.” *Molecular Systems Biology* 14 (4): e8024.

Baia-da-Silva, Djane C., Alessandra S. Orfanó, Rafael Nacif-Pimenta, et al. 2019. “Microanatomy of the American Malaria Vector *Anopheles Aquasalis* (Diptera: Culicidae: Anophelinae) Midgut: Ultrastructural and Histochemical Observations.” *Journal of Medical Entomology* 56 (6): 1636–1649.

Ballantyne, K. N., R. A. H. van Oorschot, and R. J. Mitchell. 2008. “Locked Nucleic Acids in PCR Primers Increase Sensitivity and Performance.” *Genomics* 91 (3): 301–305.

Bansal, Prashali, Roshni Pillai, D. B. Pooja, and Sonia Q. Sen. 2024. “Two Neuropeptides That Promote Blood-Feeding in *Anopheles Stephensi* Mosquitoes.” In *bioRxiv*. May 15. https://doi.org/10.1101/2024.05.15.594342.

Barillas-Mury, Carolina, and Sanjeev Kumar. 2005. “*Plasmodium*-Mosquito Interactions: A Tale of Dangerous Liaisons: *Plasmodium*-Mosquito Interactions.” *Cellular Microbiology* 7 (11): 1539–1545.

Barletta, Ana Beatriz F., Carolina Barillas-Mury, and Alvaro Molina-Cruz. 2025. “Mosquito Immune Responses to *Plasmodium* Parasites That Limit Malaria Transmission.” *Cellular and Molecular Life Sciences: CMLS* 82 (1): 143.

Bartok, Osnat, Mari Teesalu, Reut Ashwall-Fluss, et al. 2015. “The Transcription Factor Cabut Coordinates Energy Metabolism and the Circadian Clock in Response to Sugar Sensing.” *The EMBO Journal* 34 (11): 1538–1553.

Batista, E. P., E. F. Costa, and A. A. Silva. 2014. “*Anopheles darlingi* (Diptera: Culicidae) Displays Increased Attractiveness to Infected Individuals with *Plasmodium Vivax* Gametocytes.” *Parasites & Vectors* 7. https://doi.org/10.1186/1756-3305-7-251.

Baton, Luke A., and Lisa C. Ranford-Cartwright. 2005. “Spreading the Seeds of Million-Murdering Death: Metamorphoses of Malaria in the Mosquito.” *Trends in Parasitology* 21 (12): 573–580.

Bekker, Charissa de. 2019. “*Ophiocordyceps*-Ant Interactions as an Integrative Model to Understand the Molecular Basis of Parasitic Behavioral Manipulation.” *Current Opinion in Insect Science* 33 (June): 19–24.

Ben-Shahar, Y., A. Robichon, M. B. Sokolowski, and G. E. Robinson. 2002. “Influence of

Gene Action across Different Time Scales on Behavior." *Science (New York, N.Y.)* 296 (5568): 741–744.

Bento, Inês, Brianna A. Parrington, Rushlenne Pascual, et al. 2025. "Parasite and Vector Circadian Clocks Mediate Efficient Malaria Transmission." *Nature Microbiology* 10 (4): 882–896.

Bernier, Ulrich R., Daniel L. Kline, Sandra A. Allan, and Donald R. Barnard. 2007. "Laboratory Comparison of *Aedes Aegypti* Attraction to Human Odors and to Synthetic Human Odor Compounds and Blends." *Journal of the American Mosquito Control Association* 23 (3): 288–293.

Bethel, William M., and John C. Holmes. 1973. "Altered Evasive Behavior and Responses to Light in Amphipods Harboring Acanthocephalan Cystacanths." *The Journal of Parasitology* 59 (6): 945.

Biessmann, Harald, Evi Andronopoulou, Max R. Biessmann, et al. 2010. "The *Anopheles Gambiae* odorant Binding Protein 1 (AgamOBP1) Mediates Indole Recognition in the Antennae of Female Mosquitoes." *PloS One* 5 (3): e9471.

Biessmann, H., Q. K. Nguyen, D. Le, and M. F. Walter. 2005. "Microarray-Based Survey of a Subset of Putative Olfactory Genes in the Mosquito Anopheles Gambiae." *Insect Molecular Biology* 14 (6): 575–589.

Billker, O., V. Lindo, M. Panico, et al. 1998. "Identification of Xanthurenic Acid as the Putative Inducer of Malaria Development in the Mosquito." *Nature* 392 (6673): 289–292.

Billker, O., M. K. Shaw, G. Margos, and R. E. Sinden. 1997. "The Roles of Temperature, pH and Mosquito Factors as Triggers of Male and Female Gametogenesis of *Plasmodium Berghei* in Vitro." *Parasitology* 115 (Pt 1) (July): 1–7.

Blandin, Stephanie, Shin-Hong Shiao, Luis F. Moita, et al. 2004. "Complement-like Protein TEP1 Is a Determinant of Vectorial Capacity in the Malaria Vector *Anopheles Gambiae*." *Cell* 116 (5): 661–670.

Bouchebti, Sofia, and Sara Arganda. 2020. "Insect Lifestyle and Evolution of Brain Morphology." *Current Opinion in Insect Science* 42 (December): 90–96.

Bowen, M. F. 1991. "The Sensory Physiology of Host-Seeking Behavior in Mosquitoes." *Annual Review of Entomology* 36 (1): 139–158.

Brackston, Rowan D., Eszter Lakatos, and Michael P. H. Stumpf. 2018. "Transition State Characteristics during Cell Differentiation." *PLoS Computational Biology* 14 (9): e1006405.

Breugel, Floris van, Jeff Riffell, Adrienne Fairhall, and Michael H. Dickinson. 2015. "Mosquitoes Use Vision to Associate Odor Plumes with Thermal Targets." *Current Biology: CB* 25 (16): 2123–2129.

Briand, L., C. Nespoulous, J. C. Huet, and J. C. Pernollet. 2001. "Disulfide Pairing and Secondary Structure of ASP1, an Olfactory-Binding Protein from Honeybee (*Apis Mellifera* L): Disulfide Bonds of ASP1, a Honeybee OBP." *The Journal of Peptide Research: Official Journal of the American Peptide Society* 58 (6): 540–545.

Burmeister, Sabrina S., Vinita Kailasanath, and Russell D. Fernald. 2007. "Social Dominance Regulates Androgen and Estrogen Receptor Gene Expression." *Hormones and Behavior* 51 (1): 164–170.

Busula, A. O., T. Bousema, C. K. Mweresa, D. Masiga, J. G. Logan, and R. W. Sauerwein. 2017. "Gametocytemia and Attractiveness of *Plasmodium Falciparum*–infected Kenyan Children to *Anopheles Gambiae* Mosquitoes." *The Journal of Infectious Diseases* 216. https://doi.org/10.1093/infdis/jix214.

Butler-Struben, Hanna M., Amanda C. Kentner, and Brian C. Trainor. 2022. "What's Wrong with My Experiment?: The Impact of Hidden Variables on Neuropsychopharmacology Research." *Neuropsychopharmacology: Official Publication of the American College of Neuropsychopharmacology* 47 (7): 1285–1291.

Calvo-Alvarez, Estefania, Christelle Cren-Travaillé, Aline Crouzols, and Brice Rotureau. 2018. "A New Chimeric Triple Reporter Fusion Protein as a Tool for in Vitro and in Vivo Multimodal Imaging to Monitor the Development of African Trypanosomes and Leishmania Parasites." *Infection, Genetics and Evolution: Journal of Molecular Epidemiology and Evolutionary Genetics in Infectious Diseases* 63 (September): 391–403.

Cameron, Scott, Yixu Chen, and Yong Rao. 2016. "Borderless Regulates Glial Extension and Axon Ensheathment." *Developmental Biology* 414 (2): 170–180.

Cao, Junyue, Jonathan S. Packer, Vijay Ramani, et al. 2017. "Comprehensive Single-Cell Transcriptional Profiling of a Multicellular Organism." *Science (New York, N.Y.)* 357 (6352): 661–667.

Caputo, Beniamino, Carlo M. De Marco, Verena Pichler, et al. 2024. "Population Genomic Evidence of a Putative 'Far-West' African Cryptic Taxon in the *Anopheles Gambiae* Complex." *Communications Biology* 7 (1): 1115.

Cardé, R. T. 1996. "Odour Plumes and Odour-Mediated Flight in Insects." *Ciba Foundation Symposium* 200: 54–66; discussion 66–70.

Carr, Ann L., David C. Rinker, Yuemei Dong, George Dimopoulos, and Laurence J. Zwiebel. 2021. "Transcriptome Profiles of *Anopheles Gambiae* Harboring Natural Low-Level *Plasmodium* Infection Reveal Adaptive Advantages for the Mosquito." *Scientific Reports* 11 (1): 22578.

Carrasco, David, Thierry Lefèvre, Nicolas Moiroux, Cédric Pennetier, Fabrice Chandre, and Anna Cohuet. 2019. "Behavioural Adaptations of Mosquito Vectors to Insecticide Control." *Current Opinion in Insect Science* 34 (August): 48–54.

Castillo, J. C., A. E. Robertson, and M. R. Strand. 2006. "Characterization of Hemocytes from the Mosquitoes Anopheles Gambiae and Aedes Aegypti." *Insect Biochemistry and Molecular Biology* 36 (12): 891–903.

Cator, Lauren J., Justin George, Simon Blanford, et al. 2013. "'Manipulation' without the Parasite: Altered Feeding Behaviour of Mosquitoes Is Not Dependent on Infection with Malaria Parasites." *Proceedings. Biological Sciences / The Royal Society* 280 (1763): 20130711.

Cator, Lauren J., Claudia A. S. Wyer, and Laura C. Harrington. 2021. "Mosquito Sexual Selection and Reproductive Control Programs." *Trends in Parasitology* 37 (4):

330–339.

Cator, Lauren J., and Zacharo Zanti. 2016. “Size, Sounds and Sex: Interactions between Body Size and Harmonic Convergence Signals Determine Mating Success in *Aedes Aegypti*.” *Parasites & Vectors* 9 (1): 622.

Cator, L. J., P. A. Lynch, A. F. Read, and M. B. Thomas. 2012. “Do Malaria Parasites Manipulate Mosquitoes?” *Trends in Parasitology* 28. https://doi.org/10.1016/j.pt.2012.08.004.

Chandel, Avinash, Nicolas A. DeBeaubien, Anindya Ganguly, et al. 2024. “Thermal Infrared Directs Host-Seeking Behaviour in *Aedes Aegypti* Mosquitoes.” *Nature* 633 (8030): 615–623.

Chandrasekaran, Sriram, Seth A. Ament, James A. Eddy, et al. 2011. “Behavior-Specific Changes in Transcriptional Modules Lead to Distinct and Predictable Neurogenomic States.” *Proceedings of the National Academy of Sciences of the United States of America* 108 (44): 18020–18025.

Chen, Patrick B., Rongfeng K. Hu, Ye Emily Wu, et al. 2019. “Sexually Dimorphic Control of Parenting Behavior by the Medial Amygdala.” *Cell* 176 (5): 1206–1221.e18.

Chen, Ruoyu, William Stainier, Jeremy Dufourt, Mounia Lagha, and Ruth Lehmann. 2024. “Direct Observation of Translational Activation by a Ribonucleoprotein Granule.” *Nature Cell Biology* 26 (8): 1322–1335.

Childress, Steven A., and Susan B. McIver. 1984. “Morphology of the Deutocerebrum of Female *Aedes Aegypti* (Diptera: Culicidae).” *Canadian Journal of Zoology* 62 (7): 1320–1328.

Choumet, Valérie, Annick Carmi-Leroy, Christine Laurent, et al. 2007. “The Salivary Glands and Saliva of *Anopheles Gambiae* as an Essential Step in the *Plasmodium* Life Cycle: A Global Proteomic Study.” *Proteomics* 7 (18): 3384–3394.

Christ, Peter, Anna Reifenrath, Jörg Kahnt, et al. 2017. “Feeding-Induced Changes in Allatostatin-A and Short Neuropeptide F in the Antennal Lobes Affect Odor-Mediated Host Seeking in the Yellow Fever Mosquito, Aedes Aegypti.” *PloS One* 12 (11): e0188243.

Clements, A. N. 1999. *The Biology of Mosquitoes. Sensory Reception and Behaviour*. Cambridge University Press.

Coetzee, Maureen, Richard H. Hunt, Richard Wilkerson, Alessandra Della Torre, Mamadou B. Coulibaly, and Nora J. Besansky. 2013. “*Anopheles Coluzzii* and *Anopheles Amharicus*, New Members of the *Anopheles Gambiae* Complex.” *Zootaxa* 3619 (3): 246–274.

Cornet, Stéphane, Antoine Nicot, Ana Rivero, and Sylvain Gandon. 2013. “Malaria Infection Increases Bird Attractiveness to Uninfected Mosquitoes.” *Ecology Letters* 16 (3): 323–329.

Costantini, C., N. Sagnon, A. della Torre, and M. Coluzzi. 1999. “Mosquito Behavioural Aspects of Vector-Human Interactions in the *Anopheles Gambiae* Complex.” *Parassitologia* 41 (1-3): 209–217.

Court, Robert, Marta Costa, Clare Pilgrim, et al. 2023. “Virtual Fly Brain-an Interactive Atlas of the *Drosophila* Nervous System.” *Frontiers in Physiology* 14 (January): 1076533.

Coutinho-Abreu, Iliano V., Jeffrey A. Riffell, and Omar S. Akbari. 2022. “Human Attractive Cues and Mosquito Host-Seeking Behavior.” *Trends in Parasitology* 38 (3): 246–264.

Cribellier, Antoine, Leonardo Honfi Camilo, Pulkit Goyal, and Florian T. Muijres. 2024. “Mosquitoes Escape Looming Threats by Actively Flying with the Bow Wave Induced by the Attacker.” *Current Biology: CB* 34 (6): 1194–1205.e7.

Crocker, Amanda, Xiao-Juan Guan, Coleen T. Murphy, and Mala Murthy. 2016. “Cell-Type-Specific Transcriptome Analysis in the *Drosophila* Mushroom Body Reveals Memory-Related Changes in Gene Expression.” *Cell Reports* 15 (7): 1580–1596.

Croset, Vincent, Christoph D. Treiber, and Scott Waddell. 2018. “Cellular Diversity in the Drosophila Midbrain Revealed by Single-Cell Transcriptomics.” *eLife* 7 (April). https://doi.org/10.7554/eLife.34550.

Cui, Yingjun, Susanta K. Behura, and Alexander W. E. Franz. 2022. “Cellular Diversity and Gene Expression Profiles in the Male and Female Brain of Aedes Aegypti.” *BMC Genomics* 23 (1): 119.

Cummings, Molly E., Jonah Larkins-Ford, Christian R. L. Reilly, Ryan Y. Wong, Mary Ramsey, and Hans A. Hofmann. 2008. “Sexual and Social Stimuli Elicit Rapid and Contrasting Genomic Responses.” *Proceedings. Biological Sciences* 275 (1633): 393–402.

Dahalan, Farah Aida, Thomas S. Churcher, Nikolai Windbichler, and Mara K. N. Lawniczak. 2019. “The Male Mosquito Contribution towards Malaria Transmission: Mating Influences the *Anopheles* Female Midgut Transcriptome and Increases Female Susceptibility to Human Malaria Parasites.” *PLoS Pathogens* 15 (11): e1008063.

D’Angelo, E., A. Peres, and various authors. 2011. *Fisiologia*. Edi.ermes srl.

Darwin, C. R. 1859. *On the Origin of Species by Means of Natural Selection, or the Preservation of Favoured Races in the Struggle for Life*. 1st Edition. London: John Murray.

Das De, Tanwee, Punita Sharma, Sanjay Tevatiya, et al. 2022. “Bidirectional Microbiome-Gut-Brain-Axis Communication Influences Metabolic Switch-Associated Responses in the Mosquito *Anopheles Culicifacies*.” *Cells (Basel, Switzerland)* 11 (11): 1798.

David, Mariana R., Rafael Maciel-de-Freitas, Martha T. Petersen, et al. 2023. “*Aedes Aegypti* Oviposition-Sites Choice under Semi-Field Conditions.” *Medical and Veterinary Entomology* 37 (4): 683–692.

Davie, Kristofer, Jasper Janssens, Duygu Koldere, et al. 2018. “A Single-Cell Transcriptome Atlas of the Aging *Drosophila* Brain.” *Cell* 174 (4): 982–998.e20.

Dawes, Emma J., Thomas S. Churcher, Shijie Zhuang, Robert E. Sinden, and María-Gloria Basáñez. 2009. “Anopheles Mortality Is Both Age- and Plasmodium-Density Dependent: Implications for Malaria Transmission.” *Malaria Journal* 8 (1): 228.

Dawkins, Richard. 1976. *The Selfish Gene*. Oxford University Press.

Dawkins, Richard. 1982. *The Extended Phenotype*. Oxford University Press.

Dawkins, Richard. 1990. "Parasites, Desiderata Lists and the Paradox of the Organism." *Parasitology* 100: S63–S73.

Dawkins, Richard. 2004. "Extended Phenotypes but Not Too Extended. A Reply to Laland, Turner and Jjablonka." *Biology and Phylosophy* 19: 377–396.

Dey, Gourav, Ajeet Kumar Mohanty, Sreelakshmi K. Sreenivasamurthy, Manish Kumar, Ashwani Kumar, and T. S. Keshava Prasad. 2020. "Proteomics Dataset of Adult *Anopheles Stephensi* Female Brain." *Data in Brief* 32 (October): 106243.

Dimopoulos, G., A. Richman, H. M. Müller, and F. C. Kafatos. 1997. "Molecular Immune Responses of the Mosquito *Anopheles Gambiae* to Bacteria and Malaria Parasites." *Proceedings of the National Academy of Sciences of the United States of America* 94 (21): 11508–11513.

Dittmer, Jessica, Ayad Alafndi, and Paolo Gabrieli. 2019. "Fat Body-Specific Vitellogenin Expression Regulates Host-Seeking Behaviour in the Mosquito *Aedes Albopictus*." *PLoS Biology* 17 (5): e3000238.

Dobritsa, Anna A., Wynand van der Goes van Naters, Coral G. Warr, R. Alexander Steinbrecht, and John R. Carlson. 2003. "Integrating the Molecular and Cellular Basis of Odor Coding in the *Drosophila* Antenna." *Neuron* 37 (5): 827–841.

Dobson, A. P. 1988. "The Population Biology of Parasite-Induced Changes in Host Behavior." *The Quarterly Review of Biology* 63 (2): 139–165.

Dopp, Joana, Antonio Ortega, Kristofer Davie, Suresh Poovathingal, El-Sayed Baz, and Sha Liu. 2024. "Single-Cell Transcriptomics Reveals That Glial Cells Integrate Homeostatic and Circadian Processes to Drive Sleep-Wake Cycles." *Nature Neuroscience* 27 (2): 359–372.

Duncan, Sebastian, Samuel Delage, Alexa Chioran, Olga Sirbu, Theodore J. Brown, and Maurice J. Ringuette. 2020. "The Predicted Collagen-Binding Domains of *Drosophila* SPARC Are Essential for Survival and for Collagen IV Distribution and Assembly into Basement Membranes." *Developmental Biology* 461 (2): 197–209.

Dwivedi, Sutopa B., Babylakshmi Muthusamy, Praveen Kumar, et al. 2014. "Brain Proteomics of *Anopheles Gambiae*." *Omics: A Journal of Integrative Biology* 18 (7): 421–437.

Edman, John D., Elaine Cody, and Hilda Lynn. 1975. "Blood-feeding Activity of Partially Engorged *Culex Nigripalpus* (Diptera: Culicidae)." *Entomologia Experimentalis et Applicata* 18 (3): 261–268.

Eichner, M., H. H. Diebner, L. Molineaux, W. E. Collins, G. M. Jeffery, and K. Dietz. 2001. "Genesis, Sequestration and Survival of *Plasmodium Falciparum* Gametocytes: Parameter Estimates from Fitting a Model to Malariatherapy Data." *Transactions of the Royal Society of Tropical Medicine and Hygiene* 95 (5): 497–501.

Emami, S. N., B. G. Lindberg, S. Hua, S. R. Hill, and R. Mozuraitis. 2017. "A Key Malaria Metabolite Modulates Vector Blood Seeking, Feeding, and Susceptibility to

Infection." *Science* 355. https://doi.org/10.1126/science.aah4563.

Fan, Yuhang, Žaneta Andrusivová, Yunming Wu, et al. 2023. "Expansion Spatial Transcriptomics." *Nature Methods* 20 (8): 1179–1182.

Ferguson, Heather M., and Andrew F. Read. 2002. "Why Is the Effect of Malaria Parasites on Mosquito Survival Still Unresolved?" *Trends in Parasitology* 18 (6): 256–261.

Fleming, A. S., F. Vaccarino, and C. Luebke. 1980. "Amygdaloid Inhibition of Maternal Behavior in the Nulliparous Female Rat." *Physiology & Behavior* 25 (5): 731–743.

Fleming, Stephen J., Mark D. Chaffin, Alessandro Arduini, et al. 2023. "Unsupervised Removal of Systematic Background Noise from Droplet-Based Single-Cell Experiments Using CellBender." *Nature Methods* 20 (July): 1323–1335.

Formicola, Nadia, Marjorie Heim, Jérémy Dufourt, et al. 2021. "Tyramine Induces Dynamic RNP Granule Remodeling and Translation Activation in the *Drosophila* Brain." *eLife* 10 (April): e65742.

Foster, Peter G., Tatiane Marques Porangaba de Oliveira, Eduardo S. Bergo, et al. 2017. "Phylogeny of Anophelinae Using Mitochondrial Protein Coding Genes." *Royal Society Open Science* 4 (11): 170758.

Frischknecht, Friedrich, Beatrice Martin, Isabelle Thiery, Catherine Bourgouin, and Robert Menard. 2006. "Using Green Fluorescent Malaria Parasites to Screen for Permissive Vector Mosquitoes." *Malaria Journal* 5 (1): 23.

Gabrieli, Paolo, Evdoxia G. Kakani, Sara N. Mitchell, et al. 2014. "Sexual Transfer of the Steroid Hormone 20E Induces the Postmating Switch in *Anopheles Gambiae*." *Proceedings of the National Academy of Sciences of the United States of America* 111 (46): 16353–16358.

Gaburro, Julie, Prasad N. Paradkar, Melissa Klein, Asim Bhatti, Saeid Nahavandi, and Jean-Bernard Duchemin. 2018. "Dengue Virus Infection Changes *Aedes Aegypti* oviposition Olfactory Preferences." *Scientific Reports* 8 (1): 13179.

Gan, Li, Shiming Ye, Alan Chu, et al. 2004. "Identification of Cathepsin B as a Mediator of Neuronal Death Induced by Abeta-Activated Microglial Cells Using a Functional Genomics Approach." *The Journal of Biological Chemistry* 279 (7): 5565–5572.

Gawad, Charles, Winston Koh, and Stephen R. Quake. 2016. "Single-Cell Genome Sequencing: Current State of the Science." *Nature Reviews. Genetics* 17 (3): 175–188.

Geiger, Anne, Fleur Ponton, and Gustave Simo. 2015. "Adult Blood-Feeding Tsetse Flies, Trypanosomes, Microbiota and the Fluctuating Environment in Sub-Saharan Africa." *The ISME Journal* 9 (7): 1496–1507.

Ghaninia, Majid, Bill S. Hansson, and Rickard Ignell. 2007. "The Antennal Lobe of the African Malaria Mosquito, *Anopheles Gambiae* - Innervation and Three-Dimensional Reconstruction." *Arthropod Structure & Development* 36 (1): 23–39.

Giglioli, G. 1956. "Biological Variations In *Anopheles Darlingi* and *Anopheles Gambiae*; Their Effect on Practical Malaria Control in the Neotropical Region." *Bulletin of the World Health Organization* 15 (3-5): 461–471.

Gillies, M. T. 1980. “The Role of Carbon Dioxide in Host-Finding by Mosquitoes (Diptera: Culicidae): A Review.” *Bulletin of Entomological Research* 70 (4): 525–532.

Giraldo-Calderón, Gloria I., Omar S. Harb, Sarah A. Kelly, Samuel Sc Rund, David S. Roos, and Mary Ann McDowell. 2022. “VectorBase.org Updates: Bioinformatic Resources for Invertebrate Vectors of Human Pathogens and Related Organisms.” *Current Opinion in Insect Science* 50 (April): 100860.

Giraldo-Calderón, Gloria I., Michael J. Zanis, and Catherine A. Hill. 2017. “Retention of Duplicated Long-Wavelength Opsins in Mosquito Lineages by Positive Selection and Differential Expression.” *BMC Evolutionary Biology* 17 (1): 84.

Giraldo, Diego, Andrew M. Hammond, Jinling Wu, Brandon Feole, Noor Al-Saloum, and Conor J. McMeniman. 2024. “An Expanded Neurogenetic Toolkit to Decode Olfaction in the African Malaria Mosquito *Anopheles Gambiae*.” *Cell Reports Methods* 4 (2): 100714.

Giraud, Émilie, Hugo Varet, Rachel Legendre, et al. 2022. “Mosquito-Bacteria Interactions during Larval Development Trigger Metabolic Changes with Carry-over Effects on Adult Fitness.” *Molecular Ecology* 31 (5): 1444–1460.

Goldman, Olivia V., Alexandra E. DeFoe, Yanyan Qi, et al. 2025. “Mosquito Cell Atlas: A Single-Nucleus Transcriptomic Atlas of the Adult *Aedes Aegypti* mosquito.” In *bioRxiv*. February 25. https://doi.org/10.1101/2025.02.25.639765.

Goryshin, I. Y., J. A. Miller, Y. V. Kil, V. A. Lanzov, and W. S. Reznikoff. 1998. “Tn5/IS50 Target Recognition.” *Proceedings of the National Academy of Sciences of the United States of America* 95 (18): 10716–10721.

Gregorio, Ilaria, Paola Braghetta, Paolo Bonaldo, and Matilde Cescon. 2018. “Collagen VI in Healthy and Diseased Nervous System.” *Disease Models & Mechanisms* 11 (6). https://doi.org/10.1242/dmm.032946.

Gregor, Katharina M., Stefanie C. Becker, Fanny Hellhammer, Wolfgang Baumgärtner, and Christina Puff. 2022. “Immunohistochemical Characterization of the Nervous System of Culex Pipiens (Diptera, Culicidae).” *Biology* 11 (1). https://doi.org/10.3390/biology11010057.

Guidobaldi, F., I. J. May-Concha, and P. G. Guerenstein. 2014. “Morphology and Physiology of the Olfactory System of Blood-Feeding Insects.” *Journal of Physiology, Paris* 108 (2-3): 96–111.

Gunawardhana, Kushan L., and Paul E. Hardin. 2017. “VRILLE Controls PDF Neuropeptide Accumulation and Arborization Rhythms in Small Ventrolateral Neurons to Drive Rhythmic Behavior in *Drosophila*.” *Current Biology: CB* 27 (22): 3442–3453.e4.

Gupta, Saumya, Antoine Cribellier, Serge B. Poda, Olivier Roux, Florian T. Muijres, and Jeffrey A. Riffell. 2024. “Mosquitoes Integrate Visual and Acoustic Cues to Mediate Conspecific Interactions in Swarms.” *Current Biology: CB* 34 (18): 4091–4103.e4.

Guruprasad, Puneeth, Yong Gu Lee, Ki Hyun Kim, and Marco Ruella. 2021. “The Current Landscape of Single-Cell Transcriptomics for Cancer Immunotherapy.” *The Journal of Experimental Medicine* 218 (1). https://doi.org/10.1084/jem.20201574.

Haeckel, Ernst. 1866. *Generelle Morphologie Der Organismen*.

Hallem, Elissa A., and John R. Carlson. 2006. “Coding of Odors by a Receptor Repertoire.” *Cell* 125 (1): 143–160.

Hallem, Elissa A., Michael G. Ho, and John R. Carlson. 2004. “The Molecular Basis of Odor Coding in the *Drosophila* Antenna.” *Cell* 117 (7): 965–979.

Han, Qian, Jianmin Fang, Haizhen Ding, Jody K. Johnson, Bruce M. Christensen, and Jianyong Li. 2002. “Identification of *Drosophila Melanogaster* yellow-F and Yellow-f2 Proteins as Dopachrome-Conversion Enzymes.” *The Biochemical Journal* 368 (Pt 1): 333–340.

Hansson, Bill S., and Marcus C. Stensmyr. 2011. “Evolution of Insect Olfaction.” *Neuron* 72 (5): 698–711.

Hanström, Bertil. 1929. “Zur vergleichenden anatomie des zentralnervensystems der opisthobranchier.” *Zeitschrift fur Morphologie und Oekologie der Tiere* 16 (1-2): 101–112.

Harris, Rayna M., and Hans A. Hofmann. 2014. “Neurogenomics of Behavioral Plasticity.” *Advances in Experimental Medicine and Biology* 781: 149–168.

Heinze, Stanley, Basil El Jundi, Bente G. Berg, et al. 2021. “A Unified Platform to Manage, Share, and Archive Morphological and Functional Data in Insect Neuroscience.” *eLife* 10 (August). https://doi.org/10.7554/eLife.65376.

Helluy, S. 1984. “Host-parasite relations of the trematode *Microphallus papillorobustus* (Rankin 1940). III Factors involved in the behavioral changes of the *Gammarus*, intermediate hosts and predator tests.” *Annales de parasitologie humaine et comparee* 59 (1): 41–56. Originally published as *Relations Hôtes-Parasites Du Trématode Microphallus Papillorobustus (Rankin, 1940). III--Facteurs Impliqués Dans Les Modifications Du Comportement Des Gammarus, Hôtes Intermédiaires et Tests de Prédation.*

Herre, Margaret, Olivia V. Goldman, Tzu-Chiao Lu, et al. 2022. “Non-Canonical Odor Coding in the Mosquito.” *Cell* 185 (17): 3104–3123.e28.

Hill, Catherine A., A. Nicole Fox, R. Jason Pitts, et al. 2002. “G Protein-Coupled Receptors in *Anopheles Gambiae*.” *Science (New York, N.Y.)* 298 (5591): 176–178.

Hirzmann, J., D. Luo, J. Hahnen, and G. Hobom. 1993. “Determination of Messenger RNA 5’-Ends by Reverse Transcription of the Cap Structure.” *Nucleic Acids Research* 21 (15): 3597–3598.

Hogg, J. C., and H. Hurd. 1997. “The Effects of Natural *Plasmodium Falciparum* Infection on the Fecundity and Mortality of *Anopheles Gambiae* S. L. in North East Tanzania.” *Parasitology* 114 (Pt 4) (April): 325–331.

Holland, Linda Z., João E. Carvalho, Hector Escriva, et al. 2013. “Evolution of Bilaterian Central Nervous Systems: A Single Origin?” *EvoDevo* 4 (1): 1–20.

Honkanen, Anna, Andrea Adden, Josiane da Silva Freitas, and Stanley Heinze. 2019. “The Insect Central Complex and the Neural Basis of Navigational Strategies.” *The Journal of Experimental Biology* 222 (Pt Suppl 1): jeb188854.

Hoyle, G. 1986. “Glial Cells of an Insect Ganglion.” *The Journal of Comparative Neurology*

246 (1): 85–103.

Huang, Heping, Ce Gao, Shuai Wang, Fen Wu, Jinsong Wei, and Jinrong Peng. 2023. "Bulk RNA-Seq and scRNA-Seq Analysis Reveal an Activation of Immune Response and Compromise of Secretory Function in Major Salivary Glands of Obese Mice." *Computational and Structural Biotechnology Journal* 21 (January): 105–119.

Hubbard, Caleb B., and Amy C. Murillo. 2024. "Behavioral Resistance to Insecticides: Current Understanding, Challenges, and Future Directions." *Current Opinion in Insect Science* 63 (101177): 101177.

Hurd, H. 2003. "Manipulation of Medically Important Insect Vectors by Their Parasites." *Annu Rev Entmol* 48. https://doi.org/10.1146/annurev.ento.48.091801.112722.

Hurd, H., P. J. Taylor, D. Adams, A. Underhill, and P. Eggleston. 2005. "Evaluating the Costs of Mosquito Resistance to Malaria Parasites." *Evolution; International Journal of Organic Evolution* 59 (12): 2560–2572.

Hu, Xiaobang, James H. England, Aaron C. Lani, et al. 2009. "Patterned Rhodopsin Expression in R7 Photoreceptors of Mosquito Retina: Implications for Species-Specific Behavior." *The Journal of Comparative Neurology* 516 (4): 334–342.

Ignell, Rickard, Teun Dekker, Majid Ghaninia, and Bill S. Hansson. 2005. "Neuronal Architecture of the Mosquito Deutocerebrum." *The Journal of Comparative Neurology* 493 (2): 207–240.

Ikeda, A., K. Hasegawa, M. Masaki, et al. 2001. "Mixed Lineage Kinase LZK Forms a Functional Signaling Complex with JIP-1, a Scaffold Protein of the c-Jun NH(2)-Terminal Kinase Pathway." *The Journal of Biochemistry* 130 (6): 773–781.

Ishii, Minehiro, Hirotaka Kanuka, Athanase Badolo, et al. 2017. "Proboscis Infection Route of *Beauveria Bassiana* Triggers Early Death of *Anopheles* Mosquito." *Scientific Reports* 7 (1): 3476.

Ito, Kei, Kazunori Shinomiya, Masayoshi Ito, et al. 2014. "A Systematic Nomenclature for the Insect Brain." *Neuron* 81 (4): 755–765.

Jackson, Bryan T., Carlyle C. Brewster, and Sally L. Paulson. 2012. "La Crosse Virus Infection Alters Blood Feeding Behavior in *Aedes Triseriatus* and *Aedes Albopictus* (Diptera: Culicidae)." *Journal of Medical Entomology* 49 (6): 1424–1429.

Jaitin, Diego Adhemar, Ephraim Kenigsberg, Hadas Keren-Shaul, et al. 2014. "Massively Parallel Single-Cell RNA-Seq for Marker-Free Decomposition of Tissues into Cell Types." *Science (New York, N.Y.)* 343 (6172): 776–779.

Janssens, Jasper, Sara Aibar, Ibrahim Ihsan Taskiran, et al. 2022. "Decoding Gene Regulation in the Fly Brain." *Nature* 601 (7894): 630–636.

Janssens, Jasper, Pierre Mangeol, Nikolai Hecker, et al. 2025. "Spatial Transcriptomics in the Adult *Drosophila* Brain and Body." *eLife* 13 (March). https://doi.org/10.7554/eLife.92618.

Jenkins, A. M., and M. A. T. Muskavitch. 2015. "Crepuscular Behavioral Variation and Profiling of Opsin Genes in Anopheles Gambiae and Anopheles Stephensi (Diptera: Culicidae)." *Journal of Medical Entomology* 52 (3): 296–307.

Jenni, L., D. H. Molyneux, J. L. Livesey, and R. Galun. 1980. “Feeding Behaviour of Tsetse Flies Infected with Salivarian Trypanosomes.” *Nature* 283 (5745): 383–385.

Johnson, Brian J., Leon E. Hugo, Thomas S. Churcher, Oselyne T. W. Ong, and Gregor J. Devine. 2020. “Mosquito Age Grading and Vector-Control Programmes.” *Trends in Parasitology* 36 (1): 39–51.

Ju, Linyang, Karl M. Glastad, Lihong Sheng, et al. 2023. “Hormonal Gatekeeping via the Blood-Brain Barrier Governs Caste-Specific Behavior in Ants.” *Cell* 186 (20): 4289–4309.e23.

Karan, D., J. P. Morin, B. Moreteau, and J. R. David. 1998. “Body Size and Developmental Temperature in *Drosophila Melanogaster*: Analysis of Body Weight Reaction Norm.” *Journal of Thermal Biology* 23 (5): 301–309.

Karner, Tim, Isabelle Kellner, Anna Schultze, Heinz Breer, and Jürgen Krieger. 2015. “Co-Expression of Six Tightly Clustered Odorant Receptor Genes in the Antenna of the Malaria Mosquito Anopheles Gambiae.” *Frontiers in Ecology and Evolution* 3. https://doi.org/10.3389/fevo.2015.00026.

Katz, Paul S. 2011. “Neural Mechanisms Underlying the Evolvability of Behaviour.” *Philosophical Transactions of the Royal Society of London. Series B, Biological Sciences* 366 (1574): 2086–2099.

Kioko, Mwikali, Alena Pance, Shaban Mwangi, et al. 2023. “Extracellular Vesicles Could Be a Putative Posttranscriptional Regulatory Mechanism That Shapes Intracellular RNA Levels In *Plasmodium Falciparum*.” *Nature Communications* 14 (1): 6447.

Kiselev, Vladimir Yu, Andrew Yiu, and Martin Hemberg. 2018. “Scmap: Projection of Single-Cell RNA-Seq Data across Data Sets.” *Nature Methods* 15 (5): 359–362.

Klinedinst, Susan, Xin Wang, Xin Xiong, Jill M. Haenfler, and Catherine A. Collins. 2013. “Independent Pathways Downstream of the Wnd/DLK MAPKKK Regulate Synaptic Structure, Axonal Transport, and Injury Signaling.” *The Journal of Neuroscience: The Official Journal of the Society for Neuroscience* 33 (31): 12764–12778.

Klowden, Marc J., and Jacquelyn L. Blackmer. 1987. “Humoral Control of Pre-Oviposition Behaviour in the Mosquito, *Aedes Aegypti*.” *Journal of Insect Physiology* 33 (10): 689–692.

Klowden, Marc J., Edward E. Davis, and M. F. Bowen. 1987. “Role of the Fat Body in the Regulation of Host-Seeking Behaviour in the Mosquito, *Aedes Aegypti*.” *Journal of Insect Physiology* 33 (9): 643–646.

Klowden, M. J. 1994. “Endogenous Regulation of the Attraction of *Aedes Aegypti* Mosquitoes.” *Journal of the American Mosquito Control Association* 10 (2 Pt 2): 326–332.

Klowden, M. J., and H. Briegel. 1994. “Mosquito Gonotrophic Cycle and Multiple Feeding Potential: Contrasts between *Anopheles* and *Aedes* (Diptera: Culicidae).” *Journal of Medical Entomology* 31 (4): 618–622.

Klowden, M. J., and A. O. Lea. 1979. “Humoral Inhibition of Host-Seeking in *Aedes Aegypti* during Oöcyte Maturation.” *Journal of Insect Physiology* 25 (3): 231–235.

Klowden, M. J., and A. O. Lea. 1984. “Blood Feeding Affects Age-Related Changes in the Host-Seeking Behavior of *Aedes Aegypti* (Diptera: Culicidae) during Oocyte Maturation.” *Journal of Medical Entomology* 21 (3): 274–277.

Koella, Jacob C., Linda Rieu, and Richard E. L. Paul. 2002. “Stage-Specific Manipulation of a Mosquito’s Host-Seeking Behavior by the Malaria Parasite *Plasmodium Gallinaceum*.” *Behavioral Ecology: Official Journal of the International Society for Behavioral Ecology* 13 (6): 816–820.

Koella, J. C. 1999. “An Evolutionary View of the Interactions between Anopheline Mosquitoes and Malaria Parasites.” *Microbes and Infection* 1 (4): 303–308.

Koella, J. C., and M. J. Packer. 1996. “Malaria Parasites Enhance Blood-Feeding of Their Naturally Infected Vector *Anopheles Punctulatus*.” *Parasitology* 113 (Pt 2) (August): 105–109.

Koella, J. C., F. L. Sørensen, and R. A. Anderson. 1998. “The Malaria Parasite, Plasmodium Falciparum, Increases the Frequency of Multiple Feeding of Its Mosquito Vector, Anopheles Gambiae.” *Proceedings of the Royal Society of London. Series B, Containing Papers of a Biological Character. Royal Society* 265. https://doi.org/10.1098/rspb.1998.0358.

Kohl, Johannes, Anita E. Autry, and Catherine Dulac. 2017. “The Neurobiology of Parenting: A Neural Circuit Perspective.” *BioEssays: News and Reviews in Molecular, Cellular and Developmental Biology* 39 (1): 1–11.

Koniszewski, Nikolaus Dieter Bernhard, Martin Kollmann, Mahdiyeh Bigham, et al. 2016. “The Insect Central Complex as Model for Heterochronic Brain Development-Background, Concepts, and Tools.” *Development Genes and Evolution* 226 (3): 209–219.

Konopka, Joanna K., Darya Task, Ali Afify, et al. 2021. “Olfaction in *Anopheles* Mosquitoes.” *Chemical Senses* 46 (January): bjab021.

Konopka, Joanna K., Darya Task, Danny Poinapen, and Christopher J. Potter. 2023. “Neurogenetic Identification of Mosquito Sensory Neurons.” *iScience* 26 (5): 106690.

Kremer, Malte C., Christophe Jung, Sara Batelli, Gerald M. Rubin, and Ulrike Gaul. 2017. “The Glia of the Adult *Drosophila* Nervous System.” *Glia* 65 (4): 606–638.

Krieger, J., O. Klink, C. Mohl, K. Raming, and H. Breer. 2003. “A Candidate Olfactory Receptor Subtype Highly Conserved across Different Insect Orders.” *Journal of Comparative Physiology. A, Neuroethology, Sensory, Neural, and Behavioral Physiology* 189 (7): 519–526.

Kruse, Amy A., Roy Stripling, and David F. Clayton. 2004. “Context-Specific Habituation of the Zenk Gene Response to Song in Adult Zebra Finches.” *Neurobiology of Learning and Memory* 82 (2): 99–108.

Kumar, Manu P., Jinyan Du, Georgia Lagoudas, et al. 2018. “Analysis of Single-Cell RNA-Seq Identifies Cell-Cell Communication Associated with Tumor Characteristics.” *Cell Reports* 25 (6): 1458–1468.e4.

Kwon, Hyeogsun, Mubasher Mohammed, Oscar Franzén, Johan Ankarklev, and Ryan C. Smith. 2021. “Single-Cell Analysis of Mosquito Hemocytes Identifies Signatures of

Immune Cell Subtypes and Cell Differentiation." *eLife* 10 (July). https://doi.org/10.7554/eLife.66192.

Labib, Mahmoud, and Shana O. Kelley. 2020. "Single-Cell Analysis Targeting the Proteome." *Nature Reviews Chemistry* 4 (3): 143–158.

Lacroix, R., W. Mukabana, L. C. Gouagna, and J. Koella. 2005. "Malaria Infection Increases Attractiveness of Humans to Mosquitoes." *PLoS Biology* 3. https://doi.org/10.1371/journal.pbio.0030298.

Lagarde, Amandine, Silvia Spinelli, Mariella Tegoni, et al. 2011. "The Crystal Structure of *odorant Binding Protein* 7 from *Anopheles Gambiae* Exhibits an Outstanding Adaptability of Its Binding Site." *Journal of Molecular Biology* 414 (3): 401–412.

Lambrechts, Louis, and Thomas W. Scott. 2009. "Mode of Transmission and the Evolution of Arbovirus Virulence in Mosquito Vectors." *Proceedings. Biological Sciences* 276 (1660): 1369–1378.

Laurence, B. R., and M. G. Simpson. 1974. "Cell Replication in the Follicular Epithelium of the Adult Mosquito." *Journal of Insect Physiology* 20 (4): 703–715.

Leal, W. S., L. Nikonova, and G. Peng. 1999. "Disulfide Structure of the Pheromone Binding Protein from the Silkworm Moth, *Bombyx Mori*." *FEBS Letters* 464 (1-2): 85–90.

Lebrigand, Kevin, Joseph Bergenstråhle, Kim Thrane, et al. 2023. "The Spatial Landscape of Gene Expression Isoforms in Tissue Sections." *Nucleic Acids Research* 51 (8): e47.

Lefèvre, Thierry, Shelley A. Adamo, David G. Biron, Dorothée Missé, David Hughes, and Frédéric Thomas. 2009. "Invasion of the Body Snatchers: The Diversity and Evolution of Manipulative Strategies in Host-Parasite Interactions." *Advances in Parasitology* 68: 45–83.

Lefevre, Thierry, Frédéric Thomas, Alex Schwartz, et al. 2007. "Malaria *Plasmodium* Agent Induces Alteration in the Head Proteome of Their *Anopheles* Mosquito Host." *Proteomics* 7 (11): 1908–1915.

Liang, Lijun, Zhigui He, Haizheng Yu, et al. 2020. "Selection and Validation of Reference Genes for Gene Expression Studies in *Codonopsis Pilosula* Based on Transcriptome Sequence Data." *Scientific Reports* 10 (1): 1362.

Li, Jiaxing, Yao V. Zhang, Elham Asghari Adib, et al. 2017. "Restraint of Presynaptic Protein Levels by Wnd/DLK Signaling Mediates Synaptic Defects Associated with the Kinesin-3 Motor Unc-104." *eLife* 6 (September). https://doi.org/10.7554/eLife.24271.

Li, Jing, Austin Merchant, Suyue Zhou, Tao Wang, Xuguo Zhou, and Chuan Zhou. 2022. "Neuroanatomical Basis of Sexual Dimorphism in the Mosquito Brain." *iScience* 25 (11): 105255.

Limmer, Stefanie, Astrid Weiler, Anne Volkenhoff, Felix Babatz, and Christian Klämbt. 2014. "The *Drosophila* Blood-Brain Barrier: Development and Function of a Glial Endothelium." *Frontiers in Neuroscience* 8 (November): 365.

Lin, Chen, Meng Jiang, Ling Liu, et al. 2021. "Imaging of Individual Transcripts by

Amplification-Based Single-Molecule Fluorescence *in Situ* Hybridization." *New Biotechnology* 61 (March): 116–123.

Linenberg, Inbar, George K. Christophides, and Mathilde Gendrin. 2016. "Larval Diet Affects Mosquito Development and Permissiveness to Plasmodium Infection." *Scientific Reports* 6 (December): 38230.

Li, Qilong, Tong Liu, Kunying Lv, et al. 2025. "Malaria: Past, Present, and Future." *Signal Transduction and Targeted Therapy* 10 (1): 188.

Li, Qiye, Mingyue Wang, Pei Zhang, et al. 2022. "A Single-Cell Transcriptomic Atlas Tracking the Neural Basis of Division of Labour in an Ant Superorganism." *Nature Ecology & Evolution* 6 (8): 1191–1204.

Li, Xinbei, Sreenivas Eadara, Sangmin Jeon, et al. 2021. "Combined Single-Molecule Fluorescence *in Situ* Hybridization and Immunohistochemistry Analysis in Intact Murine Dorsal Root Ganglia and Sciatic Nerve." *STAR Protocols* 2 (2): 100555.

Li, X., B. Sina, and P. A. Rossignol. 1992. "Probing Behaviour and Sporozoite Delivery by *Anopheles Stephensi* Infected with *Plasmodium Berghei*." *Medical and Veterinary Entomology* 6. https://doi.org/10.1111/j.1365-2915.1992.tb00036.x.

Locatelli, Fernando, Gesine Bundrock, and Uli Müller. 2005. "Focal and Temporal Release of Glutamate in the Mushroom Bodies Improves Olfactory Memory in Apis Mellifera." *The Journal of Neuroscience: The Official Journal of the Society for Neuroscience* 25 (50): 11614–11618.

Longo, Sophia K., Margaret G. Guo, Andrew L. Ji, and Paul A. Khavari. 2021. "Integrating Single-Cell and Spatial Transcriptomics to Elucidate Intercellular Tissue Dynamics." *Nature Reviews. Genetics* 22 (10): 627–644.

Lorenz, Todd C. 2012. "Polymerase Chain Reaction: Basic Protocol plus Troubleshooting and Optimization Strategies." *Journal of Visualized Experiments: JoVE*, no. 63 (May): e3998.

Loreto, Raquel G., Simon L. Elliot, Mayara L. R. Freitas, Thairine M. Pereira, and David P. Hughes. 2014. "Long-Term Disease Dynamics for a Specialized Parasite of Ant Societies: A Field Study." *PloS One* 9 (8): e103516.

Lowe, Rohan, Neil Shirley, Mark Bleackley, Stephen Dolan, and Thomas Shafee. 2017. "Transcriptomics Technologies." *PLoS Computational Biology* 13 (5): e1005457.

Lucantoni, Leonardo, Francesco Silvestrini, Michele Signore, et al. 2015. "A Simple and Predictive Phenotypic High Content Imaging Assay for *Plasmodium Falciparum* Mature Gametocytes to Identify Malaria Transmission Blocking Compounds." *Scientific Reports* 5 (1): 16414.

Luna, Jannat Amrin, Naresh Kumar Ravichandran, Sm Abu Saleah, et al. 2023. "Label-Free Visualization of Internal Organs and Assessment of Anatomical Differences among Adult *Anopheles*, *Aedes*, and *Culex* Mosquito Specimens Using Bidirectional Optical Coherence Tomography." In *SSRN Electronic Journal*. January 1. https://doi.org/10.2139/ssrn.4341704.

Lu, Tzu-Chiao, Maria Brbić, Ye-Jin Park, et al. 2023. "Aging Fly Cell Atlas Identifies Exhaustive Aging Features at Cellular Resolution." *Science* 380 (6650): eadg0934.

Mackay, Andrew J., Jiayue Yan, Chang-Hyun Kim, Antoine M. G. Barreaux, and Chris M. Stone. 2023. “Larval Diet and Temperature Alter Mosquito Immunity and Development: Using Body Size and Developmental Traits to Track Carry-over Effects on Longevity.” *Parasites & Vectors* 16 (1): 434.

Macosko, Evan Z., Anindita Basu, Rahul Satija, et al. 2015. “Highly Parallel Genome-Wide Expression Profiling of Individual Cells Using Nanoliter Droplets.” *Cell* 161 (5): 1202–1214.

Maguire, Sarah E., Ali Afify, Loyal A. Goff, and Christopher J. Potter. 2022. “Odorant-Receptor-Mediated Regulation of Chemosensory Gene Expression in the Malaria Mosquito Anopheles Gambiae.” *Cell Reports* 38 (10): 110494.

Malpe, Medhavi, Sonali G. Choudhari, Nikhilesh Nagtode, and Pramita Muntode Gharde. 2024. “The Legacy of Sir Ronald Ross: From Malaria Research to Multifaceted Achievements.” *Cureus* 16 (8): e65999.

Mangold, Colleen A., Melissa J. Ishler, Raquel G. Loreto, Missy L. Hazen, and David P. Hughes. 2019. “Zombie Ant Death Grip due to Hypercontracted Mandibular Muscles.” *The Journal of Experimental Biology* 222 (Pt 14): jeb200683.

Mantel, Pierre-Yves, and Matthias Marti. 2014. “The Role of Extracellular Vesicles in *Plasmodium* and Other Protozoan Parasites: Extracellular Vesicles in Protozoan Parasites.” *Cellular Microbiology* 16 (3): 344–354.

Masaki, Megumi, Atsushi Ikeda, Eriko Shiraki, Shogo Oka, and Toshisuke Kawasaki. 2003. “Mixed Lineage Kinase LZK and Antioxidant Protein-1 Activate NF-kappaB Synergistically.” *European Journal of Biochemistry* 270 (1): 76–83.

Mastrobuoni, Guido, Huili Qiao, Immacolata Iovinella, et al. 2013. “A Proteomic Investigation of Soluble Olfactory Proteins In *Anopheles Gambiae*.” *PloS One* 8 (11): e75162.

Matthews, Benjamin J., Carolyn S. McBride, Matthew DeGennaro, Orion Despo, and Leslie B. Vosshall. 2016. “The Neurotranscriptome of the *Aedes Aegypti* mosquito.” *BMC Genomics* 17 (1): 32.

Mayr, Ernst. 1982. “The Growth of Biological Thought: Diversity, Evolution, and Inheritance.” https://philpapers.org/rec/MAYTGO-7.

McGinnis, Christopher S., Lyndsay M. Murrow, and Zev J. Gartner. 2019. “DoubletFinder: Doublet Detection in Single-Cell RNA Sequencing Data Using Artificial Nearest Neighbors.” *Cell Systems* 8 (4): 329–337.e4.

McLaughlin, Colleen N., Maria Brbić, Qijing Xie, et al. 2021. “Single-Cell Transcriptomes of Developing and Adult Olfactory Receptor Neurons in *Drosophila*.” *eLife* 10 (February). https://doi.org/10.7554/eLife.63856.

McRobert, Louisa, Cathy J. Taylor, Wensheng Deng, et al. 2008. “Gametogenesis in Malaria Parasites Is Mediated by the cGMP-Dependent Protein Kinase.” *PLoS Biology* 6 (6): e139.

Medica, Darcy L., and Photini Sinnis. 2005. “Quantitative Dynamics of *Plasmodium Yoelii* Sporozoite Transmission by Infected Anopheline Mosquitoes.” *Infection and Immunity* 73 (7): 4363–4369.

Melom, Jan E., and J. Troy Littleton. 2013. “Mutation of a NCKX Eliminates Glial Microdomain Calcium Oscillations and Enhances Seizure Susceptibility.” *The Journal of Neuroscience: The Official Journal of the Society for Neuroscience* 33 (3): 1169–1178.

Ménard, R., A. A. Sultan, C. Cortes, et al. 1997. “Circumsporozoite Protein Is Required for Development of Malaria Sporozoites in Mosquitoes.” *Nature* 385 (6614): 336–340.

Meng, Qinghang, and Ying Xia. 2011. “C-Jun, at the Crossroad of the Signaling Network.” *Protein & Cell* 2 (11): 889–898.

Michel, Kristin, Aidan Budd, Sofia Pinto, Toby J. Gibson, and Fotis C. Kafatos. 2005. “Anopheles Gambiae SRPN2 Facilitates Midgut Invasion by the Malaria Parasite Plasmodium Berghei.” *EMBO Reports* 6 (9): 891–897.

Michel, Megan, Eirini Skourtanioti, Federica Pierini, et al. 2024. “Ancient *Plasmodium* Genomes Shed Light on the History of Human Malaria.” *Nature* 631 (8019): 125–133.

Minetti, Corrado, Nils Pilotte, Michael Zulch, et al. 2020. “Field Evaluation of DNA Detection of Human Filarial and Malaria Parasites Using Mosquito Excreta/feces.” *PLoS Neglected Tropical Diseases* 14 (4): e0008175.

Misof, Bernhard, Shanlin Liu, Karen Meusemann, et al. 2014. “Phylogenomics Resolves the Timing and Pattern of Insect Evolution.” *Science (New York, N.Y.)* 346 (6210): 763–767.

Mlacha, Yeromin P., Prosper P. Chaki, Athuman Muhili, et al. 2020. “Reduced Human-Biting Preferences of the African Malaria Vectors *Anopheles Arabiensis* and *Anopheles Gambiae* in an Urban Context: Controlled, Competitive Host-Preference Experiments in Tanzania.” *Malaria Journal* 19 (1): 418.

Moffitt, Jeffrey R., Dhananjay Bambah-Mukku, Stephen W. Eichhorn, et al. 2018. “Molecular, Spatial, and Functional Single-Cell Profiling of the Hypothalamic Preoptic Region.” *Science (New York, N.Y.)* 362 (6416): eaau5324.

Mohammad, Ajmal Ali, Li Joongku, and various authors. 2023. *Transcriptome Profiling*. London Wall Publishing.

Molina, Nacho, David M. Suter, Rosamaria Cannavo, Benjamin Zoller, Ivana Gotic, and Félix Naef. 2013. “Stimulus-Induced Modulation of Transcriptional Bursting in a Single Mammalian Gene.” *Proceedings of the National Academy of Sciences of the United States of America* 110 (51): 20563–20568.

Moore, J. 2002. *Parasites and the Behavior of Animals*. Oxford University Press.

Morita, Takeshi, Nia G. Lyn, Ricarda K. von Heynitz, et al. 2025. “Cross-Modal Sensory Compensation Increases Mosquito Attraction to Humans.” *Science Advances* 11 (1): eadn5758.

Mukherjee, Diptendu, Bogna Marta Ignatowska-Jankowska, Eyal Itskovits, et al. 2018. “Salient Experiences Are Represented by Unique Transcriptional Signatures in the Mouse Brain.” *eLife* 7 (February). https://doi.org/10.7554/eLife.31220.

Mu, Xiaohuan, Zijing Zhang, Qun Liu, et al. 2025. “Single-Nucleus and Spatial Transcriptomics Identify Brain Landscape of Gene Regulatory Networks Associated with Behavioral Maturation in Honeybees.” *Nature Communications* 16 (1): 3343.

Mysore, Keshava, Ellen Flannery, Matthew T. Leming, et al. 2014. “Role of *semaphorin-1a* in the Developing Visual System of the Disease Vector Mosquito *Aedes Aegypti*.” *Developmental Dynamics: An Official Publication of the American Association of Anatomists* 243 (11): 1457–1469.

Mysore, Keshava, Susanne Flister, Pie Müller, Veronica Rodrigues, and Heinrich Reichert. 2011. “Brain Development in the Yellow Fever Mosquito *Aedes Aegypti*: A Comparative Immunocytochemical Analysis Using Cross-Reacting Antibodies from *Drosophila Melanogaster*.” *Development Genes and Evolution* 221 (5-6): 281–296.

Namiki, Shigehiro, and Ryohei Kanzaki. 2016. “Comparative Neuroanatomy of the Lateral Accessory Lobe in the Insect Brain.” *Frontiers in Physiology* 7 (June): 244.

Nation, James L., and M. Burrows. 1997. “The Neurobiology of an Insect Brain.” *The Florida Entomologist* 80 (3): 418.

Ndiaye, Assane, El Hadji Amadou Niang, Aminata Niang Diène, et al. 2020. “Mapping the Breeding Sites of *Anopheles Gambiae* S. L. in Areas of Residual Malaria Transmission in Central Western Senegal.” *PloS One* 15 (12): e0236607.

Ngoubangoye, Barthélémy, Larson Boundenga, Céline Arnathau, et al. 2016. “The Host Specificity of Ape Malaria Parasites Can Be Broken in Confined Environments.” *International Journal for Parasitology* 46 (11): 737–744.

Nguyen, Hai C. T., Bukyung Baik, Sora Yoon, Taesung Park, and Dougu Nam. 2023. “Benchmarking Integration of Single-Cell Differential Expression.” *Nature Communications* 14 (1): 1570.

Norry, Fabian M., and Federico H. Gomez. 2017. “Quantitative Trait Loci and Antagonistic Associations for Two Developmentally Related Traits in the *Drosophila* Head.” *Journal of Insect Science* 17 (1): 19.

Norry, F. M., J. C. Vilardi, and E. Hasson. 2000. “Negative Genetic Correlation between Traits of the *Drosophila* Head, and Interspecific Divergence in Head Shape.” *Heredity* 85 (Pt 2) (2): 177–183.

Northcutt, Adam J., Daniel R. Kick, Adriane G. Otopalik, et al. 2019. “Molecular Profiling of Single Neurons of Known Identity in Two Ganglia from the Crab *Cancer Borealis*.” *Proceedings of the National Academy of Sciences of the United States of America* 116 (52): 26980–26990.

Numan, M., M. J. Numan, and J. B. English. 1993. “Excitotoxic Amino Acid Injections into the Medial Amygdala Facilitate Maternal Behavior in Virgin Female Rats.” *Hormones and Behavior* 27 (1): 56–81.

Nye, Edwin R. 2002. “Alphonse Laveran (1845-1922): Discoverer of the Malarial Parasite and Nobel Laureate, 1907.” *Journal of Medical Biography* 10 (2): 81–87.

Omoto, Jaison J., Jennifer K. Lovick, and Volker Hartenstein. 2016. “Origins of Glial Cell Populations in the Insect Nervous System.” *Current Opinion in Insect Science* 18 (December): 96–104.

Orphanides, George, and Danny Reinberg. 2002. “A Unified Theory of Gene Expression.” *Cell* 108 (4): 439–451.

Osta, Mike A., George K. Christophides, Dina Vlachou, and Fotis C. Kafatos. 2004. “Innate Immunity in the Malaria Vector *Anopheles Gambiae*: Comparative and Functional Genomics.” *The Journal of Experimental Biology* 207 (Pt 15): 2551–2563.

Ouologuem, Dinkorma T., Antoine Dara, Aminatou Kone, Amed Ouattara, and Abdoulaye A. Djimde. 2023. “*Plasmodium Falciparum* Development from Gametocyte to Oocyst: Insight from Functional Studies.” *Microorganisms* 11 (8): 1966.

Page, Nicole, Chrysanthi Taxiarchi, Daniel Tonge, et al. 2023. “Single-Cell Profiling of *Anopheles Gambiae* Spermatogenesis Defines the Onset of Meiotic Silencing and Premeiotic Overexpression of the X Chromosome.” *Communications Biology* 6 (1): 850.

Pelletier, Julien, Aline Guidolin, Zainulabeuddin Syed, Anthony J. Cornel, and Walter S. Leal. 2010. “Knockdown of a Mosquito Odorant-Binding Protein Involved in the Sensitive Detection of Oviposition Attractants.” *Journal of Chemical Ecology* 36 (3): 245–248.

Pelosi, Paolo, Immacolata Iovinella, Jiao Zhu, Guirong Wang, and Francesca R. Dani. 2018. “Beyond Chemoreception: Diverse Tasks of Soluble Olfactory Proteins in Insects.” *Biological Reviews of the Cambridge Philosophical Society* 93 (1): 184–200.

Pende, Marko, Klaus Becker, Martina Wanis, et al. 2018. “High-Resolution Ultramicroscopy of the Developing and Adult Nervous System in Optically Cleared Drosophila Melanogaster.” *Nature Communications* 9 (1): 4731.

Perkins, Susan L. 2014. “Malaria’s Many Mates: Past, Present, and Future of the Systematics of the Order Haemosporida.” *The Journal of Parasitology* 100 (1): 11–25.

Petersen, Michael, and Jesper Wengel. 2003. “LNA: A Versatile Tool for Therapeutics and Genomics.” *Trends in Biotechnology* 21 (2): 74–81.

Picelli, Simone, Omid R. Faridani, Asa K. Björklund, Gösta Winberg, Sven Sagasser, and Rickard Sandberg. 2014. “Full-Length RNA-Seq from Single Cells Using Smart-seq2.” *Nature Protocols* 9 (1): 171–181.

Pigeault, Romain, and Manon Villa. 2018. “Long-Term Pathogenic Response to Plasmodium Relictum Infection in *Culex Pipiens* Mosquito.” *PloS One* 13 (2): e0192315.

Pimmett, Virginia L., James McGehee, Antonio Trullo, et al. 2025. “Optogenetic Manipulation of Nuclear Dorsal Reveals Temporal Requirements and Consequences for Transcription.” *Development (Cambridge, England)* 152 (6): dev204706.

Pirahmadi, Sakineh, Zahra Sadat Mousavi Shafi, Zeinab Mohammadi Firouz, et al. 2025. “Effects of *Plasmodium Berghei* infection on the Expression of Salivary Gland Immune-Related Genes in the *Anopheles Stephensi* Mosquito.” *Malaria Journal* 24 (1): 180.

Pitts, R. Jason, A. Nicole Fox, and Laurence J. Zwiebel. 2004. “A Highly Conserved Candidate Chemoreceptor Expressed in Both Olfactory and Gustatory Tissues in the Malaria Vector *Anopheles Gambiae*.” *Proceedings of the National Academy of Sciences of the United States of America* 101 (14): 5058–5063.

Polilov, Alexey A., and Anastasia A. Makarova. 2020. “Constant Neuropilar Ratio in the Insect Brain.” *Scientific Reports* 10 (1): 21426.

Pooryasin, Atefeh, and André Fiala. 2015. "Identified Serotonin-Releasing Neurons Induce Behavioral Quiescence and Suppress Mating in *Drosophila*." *The Journal of Neuroscience: The Official Journal of the Society for Neuroscience* 35 (37): 12792–12812.

Portela, Marta, Sergio Casas-Tinto, Christa Rhiner, et al. 2010. "*Drosophila* SPARC Is a Self-Protective Signal Expressed by Loser Cells during Cell Competition." *Developmental Cell* 19 (4): 562–573.

Posey, K. L., L. B. Jones, R. Cerda, et al. 2001. "Survey of Transcripts in the Adult *Drosophila* Brain." *Genome Biology* 2 (3): RESEARCH0008.

Posnien, Nico, Vera S. Hunnekuhl, and Gregor Bucher. 2023. "Gene Expression Mapping of the Neuroectoderm across Phyla - Conservation and Divergence of Early Brain Anlagen between Insects and Vertebrates." *eLife* 12 (September). https://doi.org/10.7554/eLife.92242.

Powell, Jeffrey R. 2019. "An Evolutionary Perspective on Vector-Borne Diseases." *Frontiers in Genetics* 10 (December): 1266.

Prugnolle, Franck, Patrick Durand, Benjamin Ollomo, et al. 2011. "A Fresh Look at the Origin of *Plasmodium Falciparum*, the Most Malignant Malaria Agent." *PLoS Pathogens* 7 (2): e1001283.

Quek, Camelia, Xinyu Bai, Georgina V. Long, Richard A. Scolyer, and James S. Wilmott. 2021. "High-Dimensional Single-Cell Transcriptomics in Melanoma and Cancer Immunotherapy." *Genes* 12 (10): 1629.

Qu, Zhilin, and Thomas M. Vondriska. 2009. "The Effects of Cascade Length, Kinetics and Feedback Loops on Biological Signal Transduction Dynamics in a Simplified Cascade Model." *Physical Biology* 6 (1): 016007.

Raddi, Gianmarco, Ana Beatriz F. Barletta, Mirjana Efremova, et al. 2020. "Mosquito Cellular Immunity at Single-Cell Resolution." *Science* 369 (6507): 1128–1132.

Raji, Joshua I., Joanna K. Konopka, and Christopher J. Potter. 2023. "A Spatial Map of Antennal-Expressed Ionotropic Receptors in the Malaria Mosquito." *Cell Reports* 42 (2): 112101.

Raji, Joshua I., and Christopher J. Potter. 2021. "The Number of Neurons In *Drosophila* and Mosquito Brains." *PloS One* 16 (5): e0250381.

Rayner, Julian C., Weimin Liu, Martine Peeters, Paul M. Sharp, and Beatrice H. Hahn. 2011. "A Plethora of *Plasmodium* Species in Wild Apes: A Source of Human Infection?" *Trends in Parasitology* 27 (5): 222–229.

R Development Core Team. n.d. *R: A Language and Environment for Statistical Computing*." *Vienna, Austria: R Foundation for Statistical Computing*. http://www.R-project.org.

Reeve, H., and P. Sherman. 1993. "Adaptation and the Goals of Evolutionary Research." *The Quarterly Review of Biology* 68 (1): 1–32.

Reilly, Molly B., Cyril Cros, Erdem Varol, Eviatar Yemini, and Oliver Hobert. 2020. "Unique Homeobox Codes Delineate All the Neuron Classes of *C. Elegans*." *Nature* 584 (7822): 595–601.

Riabinina, Olena, Darya Task, Elizabeth Marr, et al. 2016. “Organization of Olfactory Centres in the Malaria Mosquito *Anopheles Gambiae*.” *Nature Communications* 7 (October): 13010.

Richman, A. M., G. Dimopoulos, D. Seeley, and F. C. Kafatos. 1997. “*Plasmodium* Activates the Innate Immune Response of *Anopheles Gambiae* Mosquitoes.” *The EMBO Journal* 16 (20): 6114–6119.

Riehle, Michelle M., Wamdaogo M. Guelbeogo, Awa Gneme, et al. 2011. “A Cryptic Subgroup of Anopheles Gambiae Is Highly Susceptible to Human Malaria Parasites.” *Science (New York, N.Y.)* 331 (6017): 596–598.

Rittschof, Clare C., Syed Abbas Bukhari, Laura G. Sloofman, et al. 2014. “Neuromolecular Responses to Social Challenge: Common Mechanisms across Mouse, Stickleback Fish, and Honey Bee.” *Proceedings of the National Academy of Sciences of the United States of America* 111 (50): 17929–17934.

Robinson, A., A. O. Busula, M. A. Voets, K. B. Beshir, and J. C. Caulfield. 2018. “Plasmodium-Associated Changes in Human Odor Attract Mosquitoes.” *Proceedings of the National Academy of Sciences of the United States of America* 115. https://doi.org/10.1073/pnas.1721610115.

Robinson, Gene E., Russell D. Fernald, and David F. Clayton. 2008. “Genes and Social Behavior.” *Science (New York, N.Y.)* 322 (5903): 896–900.

Rojo-Cortés, Francisca, Nicolás Fuenzalida-Uribe, Victoria Tapia-Valladares, et al. 2022. “Lipophorin Receptors Regulate Mushroom Body Development and Complex Behaviors in *Drosophila*.” *BMC Biology* 20 (1): 198.

Rossignol, P. A., J. M. Ribeiro, and A. Spielman. 1984. “Increased Intradermal Probing Time in Sporozoite-Infected Mosquitoes.” *The American Journal of Tropical Medicine and Hygiene* 33. https://doi.org/10.4269/ajtmh.1984.33.17.

Rossignol, P. A., J. M. Ribeiro, and A. Spielman. 1986. “Increased Biting Rate and Reduced Fertility in Sporozoite-Infected Mosquitoes.” *The American Journal of Tropical Medicine and Hygiene* 35. https://doi.org/10.4269/ajtmh.1986.35.277.

RStudio Team. 2020. *RStudio: Integrated Development for R*. http://www.rstudio.com/.

Ruberto, Anthony A., Caitlin Bourke, Nicolas Merienne, Thomas Obadia, Rogerio Amino, and Ivo Mueller. 2021. “Single-Cell RNA Sequencing Reveals Developmental Heterogeneity among *Plasmodium Berghei* Sporozoites.” *Scientific Reports* 11 (1): 4127.

Rubin, G. M., M. D. Yandell, J. R. Wortman, et al. 2000. “Comparative Genomics of the Eukaryotes.” *Science (New York, N.Y.)* 287 (5461): 2204–2215.

Russell, Andrew J. C., Jackson A. Weir, Naeem M. Nadaf, et al. 2024. “Slide-Tags Enables Single-Nucleus Barcoding for Multimodal Spatial Genomics.” *Nature* 625 (7993): 101–109.

Sadoul, Bastien, Sébastien Alfonso, Conor Goold, et al. 2022. “Transcriptomic Profiles of Consistent Risk-Taking Behaviour across Time and Contexts in European Sea Bass.” *Proceedings. Biological Sciences* 289 (1975): 20220399.

Sangbakembi-Ngounou, Claire, Carlo Costantini, Neil Michel Longo-Pendy, et al. 2022.

"Diurnal Biting of Malaria Mosquitoes in the Central African Republic Indicates Residual Transmission May Be 'out of Control.'" *Proceedings of the National Academy of Sciences of the United States of America* 119 (21): e2104282119.

Satija, Rahul, Jeffrey A. Farrell, David Gennert, Alexander F. Schier, and Aviv Regev. 2015. "Spatial Reconstruction of Single-Cell Gene Expression Data." *Nature Biotechnology* 33 (5): 495–502.

Saul, Michael C., Christopher H. Seward, Joseph M. Troy, et al. 2017. "Transcriptional Regulatory Dynamics Drive Coordinated Metabolic and Neural Response to Social Challenge in Mice." *Genome Research* 27 (6): 959–972.

Scheurer, Louis, Rebecca R. Das Gupta, Annika Saebisch, et al. 2021. "Expression of Immunoglobulin Constant Domain Genes in Neurons of the Mouse Central Nervous System." *Life Science Alliance* 4 (11): e202101154.

Schmidt, W. M., and M. W. Mueller. 1999. "CapSelect: A Highly Sensitive Method for 5' CAP-Dependent Enrichment of Full-Length cDNA in PCR-Mediated Analysis of mRNAs." *Nucleic Acids Research* 27 (21): e31.

Schoelitsz, Bruce, Victor Mwingira, Leonard E. G. Mboera, et al. 2020. "Chemical Mediation of Oviposition by *Anopheles* Mosquitoes: A Push-Pull System Driven by Volatiles Associated with Larval Stages." *Journal of Chemical Ecology* 46 (4): 397–409.

Schwartz, A., and J. C. Koella. 2001. "Trade-Offs, Conflicts of Interest and Manipulation in *Plasmodium*-Mosquito Interactions." *Trends in Parasitology* 17 (4): 189–194.

Schwartzman, Omer, and Amos Tanay. 2015. "Single-Cell Epigenomics: Techniques and Emerging Applications." *Nature Reviews. Genetics* 16 (12): 716–726.

Severo, Maiara S., Jonathan J. M. Landry, Randall L. Lindquist, et al. 2018. "Unbiased Classification of Mosquito Blood Cells by Single-Cell Genomics and High-Content Imaging." *Proceedings of the National Academy of Sciences of the United States of America* 115 (32): E7568–E7577.

Shahabuddin, M., and D. C. Kaslow. 1994. "*Plasmodium*: Parasite Chitinase and Its Role in Malaria Transmission." *Experimental Parasitology* 79 (1): 85–88.

Shankar, Shruti, and Conor J. McMeniman. 2020. "An Updated Antennal Lobe Atlas for the Yellow Fever Mosquito *Aedes Aegypti*." *PLoS Neglected Tropical Diseases* 14 (10): e0008729.

Shapiro, Ehud, Tamir Biezuner, and Sten Linnarsson. 2013. "Single-Cell Sequencing-Based Technologies Will Revolutionize Whole-Organism Science." *Nature Reviews. Genetics* 14 (9): 618–630.

Shaw, W. Robert, Perrine Marcenac, and Flaminia Catteruccia. 2022. "*Plasmodium* Development in *Anopheles*: A Tale of Shared Resources." *Trends in Parasitology* 38 (2): 124–135.

Sheehan, T., M. Paul, E. Amaral, M. J. Numan, and M. Numan. 2001. "Evidence That the Medial Amygdala Projects to the Anterior/ventromedial Hypothalamic Nuclei to Inhibit Maternal Behavior in Rats." *Neuroscience* 106 (2): 341–356.

Shute, G. T. 1956. "A Method of Maintaining Colonies of East African Strains of *Anopheles*

Gambiae." *Annals of Tropical Medicine and Parasitology* 50 (1): 92–94.

Siden-Kiamos, Inga, Lefteris Spanos, and Chiara Currà. 2020. "A Method for Purification of *Plasmodium* Oocysts from Mosquito Midguts." *Scientific Reports* 10 (1): 7262.

Simon, Félix, and Nikolaos Konstantinides. 2021. "Single-Cell Transcriptomics in the Drosophila Visual System: Advances and Perspectives on Cell Identity Regulation, Connectivity, and Neuronal Diversity Evolution." *Developmental Biology* 479 (November): 107–122.

Sinakevitch, Irina, Yves Grau, Nicholas J. Strausfeld, and Serge Birman. 2010. "Dynamics of Glutamatergic Signaling in the Mushroom Body of Young Adult Drosophila." *Neural Development* 5 (April): 10.

Singh, Sandeep, and L. Mohan. 2013. "Variations in the Ommatidia and Compound Eyes of Three Species of Mosquito Vectors." *Journal of Entomology and Zoology Studies* 1 (October): 16–21.

Smallegange, R. C., G. -. J. Gemert, M. Vegte-Bolmer, S. Gezan, and W. Takken. 2013. "Malaria Infected Mosquitoes Express Enhanced Attraction to Human Odor." *PloS One* 8. https://doi.org/10.1371/journal.pone.0063602.

Smarandache-Wellmann, Carmen Ramona. 2016. "Arthropod Neurons and Nervous System." *Current Biology: CB* 26 (20): R960–R965.

Soghigian, John, Charles Sither, Silvia Andrade Justi, et al. 2023. "Phylogenomics Reveals the History of Host Use in Mosquitoes." *Nature Communications* 14 (1): 6252.

Solanki, Shyam, Gazala Ameen, Jin Zhao, Jordan Flaten, Pawel Borowicz, and Robert S. Brueggeman. 2020. "Visualization of Spatial Gene Expression in Plants by Modified RNAscope Fluorescent *in Situ* Hybridization." *Plant Methods* 16 (1): 71.

Sommerlandt, Frank M. J., Axel Brockmann, Wolfgang Rössler, and Johannes Spaethe. 2019. "Immediate Early Genes in Social Insects: A Tool to Identify Brain Regions Involved in Complex Behaviors and Molecular Processes Underlying Neuroplasticity." *Cellular and Molecular Life Sciences: CMLS* 76 (4): 637–651.

Song, Yura, Marco Fioramonti, Gaëlle Bouvencourt, Christine Dubois, Cédric Blanpain, and Alexandra Van Keymeulen. 2023. "Cell Type and Stage Specific Transcriptional, Chromatin and Cell-Cell Communication Landscapes in the Mammary Gland." *Heliyon* 9 (7): e17842.

Sorrells, Trevor R., Anjali Pandey, Adriana Rosas-Villegas, and Leslie B. Vosshall. 2022. "A Persistent Behavioral State Enables Sustained Predation of Humans by Mosquitoes." *eLife* 11 (May). https://doi.org/10.7554/eLife.76663.

Spong, Kristin E., R. David Andrew, and R. Meldrum Robertson. 2016. "Mechanisms of Spreading Depolarization in Vertebrate and Insect Central Nervous Systems." *Journal of Neurophysiology* 116 (3): 1117–1127.

Stanczyk, Nina M., Mark C. Mescher, and Consuelo M. De Moraes. 2017. "Effects of Malaria Infection on Mosquito Olfaction and Behavior: Extrapolating Data to the Field." *Current Opinion in Insect Science* 20 (April): 7–12.

Stork, Nigel E. 2018. "How Many Species of Insects and Other Terrestrial Arthropods Are

There on Earth?" *Annual Review of Entomology* 63 (Volume 63, 2018): 31–45.

Strausfeld, Nicholas J., and Frank Hirth. 2013. "Deep Homology of Arthropod Central Complex and Vertebrate Basal Ganglia." *Science (New York, N.Y.)* 340 (6129): 157–161.

Stroumbakis, N. D., Z. Li, and P. P. Tolias. 1996. "A Homolog of Human Transcription Factor NF-X1 Encoded by the *Drosophila* Shuttle Craft Gene Is Required in the Embryonic Central Nervous System." *Molecular and Cellular Biology* 16 (1): 192–201.

Stuart, Tim, and Rahul Satija. 2019. "Integrative Single-Cell Analysis." *Nature Reviews. Genetics* 20 (5): 257–272.

Styfhals, Ruth, Grygoriy Zolotarov, Gert Hulselmans, et al. 2022. "Cell Type Diversity in a Developing Octopus Brain." *Nature Communications* 13 (1): 7392.

Su, Hailing, and Diane K. O'Dowd. 2003. "Fast Synaptic Currents in *Drosophila* Mushroom Body Kenyon Cells Are Mediated by Alpha-Bungarotoxin-Sensitive Nicotinic Acetylcholine Receptors and Picrotoxin-Sensitive GABA Receptors." *The Journal of Neuroscience: The Official Journal of the Society for Neuroscience* 23 (27): 9246–9253.

Suh, Eunho, Dong-Hwan Choe, Ahmed M. Saveer, and Laurence J. Zwiebel. 2016. "Suboptimal Larval Habitats Modulate Oviposition of the Malaria Vector Mosquito *Anopheles Coluzzii*." *PloS One* 11 (2): e0149800.

Tachikawa, Kashiko S., Yoshihiro Yoshihara, and Kumi O. Kuroda. 2013. "Behavioral Transition from Attack to Parenting in Male Mice: A Crucial Role of the Vomeronasal System." *The Journal of Neuroscience: The Official Journal of the Society for Neuroscience* 33 (12): 5120–5126.

Takken, Willem, and Niels O. Verhulst. 2013. "Host Preferences of Blood-Feeding Mosquitoes." *Annual Review of Entomology* 58: 433–453.

Takken, W., J. J. van Loon, and W. Adam. 2001. "Inhibition of Host-Seeking Response and Olfactory Responsiveness in *Anopheles gambiae* Following Blood Feeding." *Journal of Insect Physiology* 47 (3): 303–310.

Tanay, Amos, and Aviv Regev. 2017. "Scaling Single-Cell Genomics from Phenomenology to Mechanism." *Nature* 541 (7637): 331–338.

Tang, Fuchou, Catalin Barbacioru, Yangzhou Wang, et al. 2009. "mRNA-Seq Whole-Transcriptome Analysis of a Single Cell." *Nature Methods* 6 (5): 377–382.

Tarashansky, Alexander J., Jacob M. Musser, Margarita Khariton, et al. 2021. "Mapping Single-Cell Atlases throughout Metazoa Unravels Cell Type Evolution." *eLife* 10 (May). https://doi.org/10.7554/eLife.66747.

Tegoni, M., P. Pelosi, F. Vincent, et al. 2000. "Mammalian Odorant Binding Proteins." *Biochimica et Biophysica Acta* 1482 (1-2): 229–240.

Thailayil, Janis, Paolo Gabrieli, Beniamino Caputo, et al. 2018. "Analysis of Natural Female Post-Mating Responses of Anopheles Gambiae and Anopheles Coluzzii Unravels Similarities and Differences in Their Reproductive Ecology." *Scientific Reports* 8 (1): 6594.

Thailayil, Janis, Kalle Magnusson, H. Charles J. Godfray, Andrea Crisanti, and Flaminia Catteruccia. 2011. "Spermless Males Elicit Large-Scale Female Responses to Mating in the Malaria Mosquito *Anopheles Gambiae*." *Proceedings of the National Academy of Sciences of the United States of America* 108 (33): 13677–13681.

Thathy, Vandana, Hisashi Fujioka, Soren Gantt, Ruth Nussenzweig, Victor Nussenzweig, and Robert Ménard. 2002. "Levels of Circumsporozoite Protein in the Plasmodium Oocyst Determine Sporozoite Morphology." *The EMBO Journal* 21 (7): 1586–1596.

Thévenaz, P., and H. Hecker. 1980. "Distribution and Attachment of *Trypanosoma* (Nannomonas) Congolense in the Proximal Part of the Proboscis of *Glossina Morsitans Morsitans*." *Acta Tropica* 37 (2): 163–175.

Thiévent, K., G. Zilio, G. Hauser, and J. C. Koella. 2019. "Malaria Load Affects the Activity of Mosquito Salivary Apyrase." *Journal of Insect Physiology* 116. https://doi.org/10.1016/j.jinsphys.2019.04.003.

Thomson, David. 1914. "The Origin and Development of Gametes (crescents) in Malignant Tertian Malaria: Some Observations on Flagellation, Etc." *Annals of Tropical Medicine and Parasitology* 8 (1): 85–104.

Tinbergen, N. 1963. *On Aims and Methods of Ethology*. 20:410–433.

Tomas, A. M., G. Margos, G. Dimopoulos, et al. 2001. "P25 and P28 Proteins of the Malaria Ookinete Surface Have Multiple and Partially Redundant Functions." *The EMBO Journal* 20 (15): 3975–3983.

Tomchaney, Michael, Keshava Mysore, Longhua Sun, et al. 2014. "Examination of the Genetic Basis for Sexual Dimorphism in the *Aedes Aegypti* (dengue Vector Mosquito) Pupal Brain." *Biology of Sex Differences* 5 (1): 10.

Townson, H. 1993. "The Biology of Mosquitoes. Volume 1. Development, Nutrition and Reproduction. By A.N. Clements. (London: Chapman & Hall, 1992). ISBN 0-412-40180-0." *Bulletin of Entomological Research* 83 (2): 307–308.

Traniello, Ian M., Syed Abbas Bukhari, Jessica Kevill, et al. 2020. "Meta-Analysis of Honey Bee Neurogenomic Response Links Deformed Wing Virus Type A to Precocious Behavioral Maturation." *Scientific Reports* 10 (1): 3101.

Triarhou, Lazaros C. 2014. "Axons Emanating from Dendrites: Phylogenetic Repercussions with Cajalian Hues." *Frontiers in Neuroanatomy* 8 (November): 133.

Tsila, H. G., P. A. Ntonga, Elono A. L. M., T. Tchuinkam, and M. Mbida. 2021. "Laboratory Growth of *Anopheles Gambiae* (Diptera: Culicidae) and Morphological Determinism of Moulting." *Advances in Entomology* 9 (4): 176–185.

Ugur, Berrak, Kuchuan Chen, and Hugo J. Bellen. 2016. "Drosophila Tools and Assays for the Study of Human Diseases." *Disease Models & Mechanisms* 9 (3): 235–244.

Valzania, Luca, Melissa T. Mattee, Michael R. Strand, and Mark R. Brown. 2019. "Blood Feeding Activates the Vitellogenic Stage of Oogenesis in the Mosquito *Aedes Aegypti* through Inhibition of Glycogen Synthase Kinase 3 by the Insulin and TOR Pathways." *Developmental Biology* 454 (1): 85–95.

Van Den Abbeele, Jan, Guy Caljon, Karin De Ridder, Patrick De Baetselier, and Marc

Coosemans. 2010. "*Trypanosoma Brucei* Modifies the Tsetse Salivary Composition, Altering the Fly Feeding Behavior That Favors Parasite Transmission." *PLoS Pathogens* 6 (6): e1000926.

Vantaux, A., D. F. Sales Hien, B. Yameogo, K. R. Dabiré, and T. Lefèvre. 2015. "Host-Seeking Behaviors of Mosquitoes Experimentally Infected with Sympatric Field Isolates of the Human Malaria Parasite Plasmodium Falciparum: No Evidence for Host Manipulation." *Front Ecol Evol* 3. https://doi.org/10.3389/fevo.2015.00086.

Vargo, Agnes M., and Woodbridge A. Foster. 1982. "Responsiveness of Female *Aedes Aegypti* (Diptera: Culicidae) to Flower Extracts." *Journal of Medical Entomology* 19 (6): 710–718.

Vinauger, Clément. 2019. "Vector Cognition and Neurobiology." *Current Opinion in Insect Science* 34 (August): 68–72.

Vinauger, Clément, Eleanor K. Lutz, and Jeffrey A. Riffell. 2014. "Olfactory Learning and Memory in the Disease Vector Mosquito *Aedes Aegypti*." *The Journal of Experimental Biology* 217 (Pt 13): 2321–2330.

Vogt, R. G., and L. M. Riddiford. 1981. "Pheromone Binding and Inactivation by Moth Antennae." *Nature* 293 (5828): 161–163.

Vosshall, L. B., H. Amrein, P. S. Morozov, A. Rzhetsky, and R. Axel. 1999. "A Spatial Map of Olfactory Receptor Expression in the *Drosophila* Antenna." *Cell* 96 (5): 725–736.

Vosshall, L. B., A. M. Wong, and R. Axel. 2000. "An Olfactory Sensory Map in the Fly Brain." *Cell* 102 (2): 147–159.

Wang, Jing, Emma J. Murphy, Jay C. Nix, and David N. M. Jones. 2020. "*Aedes Aegypti* Odorant Binding Protein 22 Selectively Binds Fatty Acids through a Conformational Change in Its C-Terminal Tail." *Scientific Reports* 10 (1): 3300.

Wang, Lei, Weibo Xie, Ying Chen, et al. 2010. "A Dynamic Gene Expression Atlas Covering the Entire Life Cycle of Rice." *The Plant Journal: For Cell and Molecular Biology* 61 (5): 752–766.

Wang, Qian, Hisashi Fujioka, and Victor Nussenzweig. 2005. "Exit of *Plasmodium* Sporozoites from Oocysts Is an Active Process That Involves the Circumsporozoite Protein." *PLoS Pathogens* 1 (1): e9.

Wang, Xiaofei, Yifan Zhai, and Hao Zheng. 2024. "Deciphering the Cellular Heterogeneity of the Insect Brain with Single-Cell RNA Sequencing." *Insect Science* 31 (2): 314–327.

Wang, Yupu, Meike Lobb-Rabe, James Ashley, et al. 2022. "Systematic Expression Profiling of Dpr and DIP Genes Reveals Cell Surface Codes in Drosophila Larval Motor and Sensory Neurons." *Development (Cambridge, England)* 149 (10): dev200355.

Wekesa, J. W., R. S. Copeland, and R. W. Mwangi. 1992. "Effect of *Plasmodium Falciparum* on Blood Feeding Behavior of Naturally Infected *Anopheles* Mosquitoes in Western Kenya." *The American Journal of Tropical Medicine and Hygiene* 47 (4): 484–488.

Werling, Kristine, W. Robert Shaw, Maurice A. Itoe, et al. 2019. "Steroid Hormone Function Controls Non-Competitive *Plasmodium* Development in *Anopheles*." *Cell*

177 (2): 315–325.e14.

Wesołowska, W., and T. Wesołowski. 2014. “Do *Leucochloridium* sporocysts Manipulate the Behaviour of Their Snail Hosts?” *Journal of Zoology (London, England: 1987)* 292 (3): 151–155.

Whitfield, Charles W., Anne-Marie Cziko, and Gene E. Robinson. 2003. “Gene Expression Profiles in the Brain Predict Behavior in Individual Honey Bees.” *Science (New York, N.Y.)* 302 (5643): 296–299.

Williams, Craig R., Katherine J. Leach, Natasha J. Wilson, and Veronica R. Swart. 2008. “The Allee Effect in Site Choice Behaviour of Egg-Laying Dengue Vector Mosquitoes.” *Tropical Biomedicine* 25 (2): 140–144.

Winding, Michael, Benjamin D. Pedigo, Christopher L. Barnes, et al. 2023. “The Connectome of an Insect Brain.” *Science* 379 (6636): eadd9330.

Winkler, Bente, Dominik Funke, Billel Benmimoun, et al. 2021. “Brain Inflammation Triggers Macrophage Invasion across the Blood-Brain Barrier in *Drosophila* during Pupal Stages.” *Science Advances* 7 (44): eabh0050.

Wolff, Gabriella H., and Jeffrey A. Riffell. 2018. “Olfaction, Experience and Neural Mechanisms Underlying Mosquito Host Preference.” *The Journal of Experimental Biology* 221 (Pt 4). https://doi.org/10.1242/jeb.157131.

Wong, Jacklyn, Amy C. Morrison, Steven T. Stoddard, et al. 2012. “Linking Oviposition Site Choice to Offspring Fitness in *Aedes Aegypti*: Consequences for Targeted Larval Control of Dengue Vectors.” *PLoS Neglected Tropical Diseases* 6 (5): e1632.

Wong, Jacklyn, Steven T. Stoddard, Helvio Astete, Amy C. Morrison, and Thomas W. Scott. 2011. “Oviposition Site Selection by the Dengue Vector *Aedes Aegypti* and Its Implications for Dengue Control.” *PLoS Neglected Tropical Diseases* 5 (4): e1015.

World Health Organization. 2024a. “World Health Statistics 2024: Monitoring Health for the SDGs, Sustainable Development Goals. Geneva: World Health Organization; 2024. Licence: CC BY-NC-SA 3.0 IGO.” Preprint.

World Health Organization. 2024b. “World Malaria Report 2024: Addressing Inequity in the Global Malaria Response. Geneva: World Health Organization; 2024. Licence: CC BY-NC-SA 3.0 IGO.” Preprint.

World Health Organization. n.d. Accessed July 1, 2025. https://www.who.int/teams/global-malaria-programme/prevention/vector-control.

Woyessa, Delelegn, and Delenasaw Yewhalaw. 2025. “*Anopheles* Mosquito Fauna, Blood Meal Sources and Transmission Intensity from High and Moderate Malaria Endemic Areas of Ethiopia.” *Scientific Reports* 15 (1): 10636.

Yadati, Tulasi, Tom Houben, Albert Bitorina, and Ronit Shiri-Sverdlov. 2020. “The Ins and Outs of Cathepsins: Physiological Function and Role in Disease Management.” *Cells (Basel, Switzerland)* 9 (7): 1679.

Yan, Yan, Elaine Cheung, Lisa H. Verzier, et al. 2024. “Mapping Plasmodium Transitions and Interactions in the Anopheles Female.” In *bioRxiv*. November 13.

https://doi.org/10.1101/2024.11.12.623125.

Yao, Zizhen, Cindy T. J. van Velthoven, Michael Kunst, et al. 2023. "A High-Resolution Transcriptomic and Spatial Atlas of Cell Types in the Whole Mouse Brain." *Nature* 624 (7991): 317–332.

Yin, Jun, Hsueh-Ling Chen, Anna Grigsby-Brown, et al. 2024. "Glia-Derived Secretory Fatty Acid Binding Protein *Obp44a* Regulates Lipid Storage and Efflux in the Developing *Drosophila* Brain." *bioRxiv.org: The Preprint Server for Biology*, ahead of print, April 11. https://doi.org/10.1101/2024.04.10.588417.

Yin, Jun, Emma Spillman, Ethan S. Cheng, et al. 2021. "Brain-Specific Lipoprotein Receptors Interact with Astrocyte Derived Apolipoprotein and Mediate Neuron-Glia Lipid Shuttling." *Nature Communications* 12 (1): 2408.

Younger, M., N. Didkovsky, V. Danan, and N. Renier. 2014. "Female *Aedes Aegypti* Brain." Mosquitobrains.org. www.mosquitobrains.org.

Yuval, B., and A. Bouskila. 1993. "Temporal Dynamics of Mating and Predation in Mosquito Swarms." *Oecologia* 95 (1): 65–69.

Zdobnov, Evgeny M., Christian von Mering, Ivica Letunic, et al. 2002. "Comparative Genome and Proteome Analysis of *Anopheles Gambiae* and *Drosophila Melanogaster*." *Science (New York, N.Y.)* 298 (5591): 149–159.

Zhang, Wenxin, Liangliang Wang, Yinjiao Zhao, et al. 2022. "Single-Cell Transcriptomic Analysis of Honeybee Brains Identifies Vitellogenin as Caste Differentiation-Related Factor." *iScience* 25 (7): 104643.

Zhao, Zhilei, and Carolyn S. McBride. 2020. "Evolution of Olfactory Circuits in Insects." *Journal of Comparative Physiology. A, Neuroethology, Sensory, Neural, and Behavioral Physiology* 206 (3): 353–367.

Zhao, Zhilei, Jessica L. Zung, Annika Hinze, et al. 2022. "Mosquito Brains Encode Unique Features of Human Odour to Drive Host Seeking." *Nature* 605 (7911): 706–712.

Zheng, Grace X. Y., Jessica M. Terry, Phillip Belgrader, et al. 2017. "Massively Parallel Digital Transcriptional Profiling of Single Cells." *Nature Communications* 8 (January): 14049.

Zhou, Mingmin, Nannan Chen, Jingsong Tian, et al. 2019. "Suppression of GABAergic Neurons through D2-like Receptor Secures Efficient Conditioning in *Drosophila* Aversive Olfactory Learning." *Proceedings of the National Academy of Sciences of the United States of America* 116 (11): 5118–5125.

Zhu, Feng, Hong Zheng, Suilin Chen, et al. 2022. "Malaria Oocysts Require Circumsporozoite Protein to Evade Mosquito Immunity." *Nature Communications* 13 (1): 3208.

Ziegenhain, Christoph, Beate Vieth, Swati Parekh, et al. 2017. "Comparative Analysis of Single-Cell RNA Sequencing Methods." *Molecular Cell* 65 (4): 631–643.e4.

Zsemlye, J. L., R. G. Hancock, and W. A. Foster. 2005. "Analysis of a Complex Vertical Copulatory-Courtship Display in the Yellow Fever Vector *Sabethes Chloropterus*." *Medical and Veterinary Entomology* 19 (3): 276–285.